

PERFORMANCE ENHANCEMENT OF A COAL CLASSIFIER

Thesis submitted for the degree of

Doctor of Philosophy

at the University of Leicester

by

Norasikin Mat Isa

Department of Engineering

University of Leicester

October 2012

Norasikin Mat Isa

Performance Enhancement of a Coal Classifier

Abstract

World energy demand is increasing relentlessly. The total global energy demand in 2030 is projected to be 50–60% above the current rate of energy consumption (IEA, 2008). Existing developed economies and fast-growing ones like China and India rely heavily on fossil fuels as a source of energy. Coal is still a key element in the energy mix for the world's leading economies, and around 30% of all CO₂ emissions come from the combustion of fossil fuels for electricity generation (IEA, 2008). Therefore, there is a need for clean coal technology to reduce the negative effect of the combustion. The coal particle size is critical to cleaner combustion; the classifier is responsible for that.

The present work details an investigation into improving the performance of coal classifiers. The particular area of focus is to find the optimum design parameters by looking at the effects and influences of key classifier parameters towards the classifier performance. The use of ineffective classifier parameters, especially the vane angle and inlet velocity, reduces the performance of the classifiers where an inappropriate size of particle is being released. This contributes to a reduction in overall efficiency of the coal power plant and contributes to the formation of NO_x gases during fuel burning.

The performance of the classifier in terms of flow and particle distribution is the focus of the analysis. The work within this research study employs the Computational Fluid Dynamics (CFD) technique, which is a very effective, non-intrusive, virtual modelling technique with powerful visualisation capabilities. However, the importance of the experimental appreciation of the classifier is not neglected.

Experiments were carried out to provide a tool for validating the CFD propositions. A one-third scale test facility that mimics an industrial air classifier has been carefully constructed in order to provide experimental data for the further understanding of the coal classification process.

The outcome of this research work provides a guideline for selecting suitable parameters for specific classifier design and application.

Acknowledgements

I would like to express my sincere gratitude to my supervisor, Professor Abdelwahab Aroussi, for his support, ideas, guidance and encouragement throughout my research study. I would like to thank all those that have helped me in this work especially to Dr. Chris Coats and Mr Alan Wale for their generous assistance during this time. Grateful acknowledgement is also made to my friends and colleagues at the University of Leicester, for their ideas and support. I also would like to thank my family for their inseparable support and prayers. Lastly, I would like to thank my sponsors Universiti Tun Hussien Onn (UTHM) and the Government of Malaysia.

Table of Contents

| | |
|---|-----------|
| Abstract | ii |
| Acknowledgements | iii |
| Table of Contents | iv |
| List of Figures | ix |
| List of Tables | xvi |
| Abbreviations | xvii |
| | |
| CHAPTER ONE: INTRODUCTION | 1 |
| 1.1 Problem Definition | 5 |
| 1.2 Aims and Objectives | 6 |
| 1.3 Methodology | 7 |
| 1.4 Thesis Layout | 8 |
| | |
| CHAPTER TWO: LITERATURE REVIEW | 9 |
| 2.1 Coal | 10 |
| 2.1.1 Carbon Cycle | 12 |
| 2.1.2 Environmental Pollutants | 13 |
| 2.2 Coal-Fired Power Plants Technologies | 14 |
| 2.3 Separation Techniques | 18 |
| 2.4 Coal Classification | 21 |
| 2.4.1 Types of Air Classifier | 24 |

| | | |
|---|--|-----------|
| 2.4.1.1 | <i>Static Classifiers</i> | 24 |
| 2.4.1.2 | <i>Dynamic Classifiers</i> | 27 |
| 2.4.2 | Performance of the Air Classifier | 29 |
| 2.5 | Principles of Gas-Solid Flows | 32 |
| 2.5.1 | Size and Properties of Particles | 32 |
| 2.5.2 | Particle Fluid Interaction | 34 |
| 2.5.3 | Particle–Particle Interaction | 35 |
| 2.5.4 | Particle-Wall Interaction | 36 |
| 2.5.5 | Dynamics of the Particulate Phase | 36 |
| 2.5.5.1 | <i>Dynamics Analysis of Particle in Axial Direction</i> | 37 |
| 2.5.5.2 | <i>Dynamics Analysis of Particle in Radial Direction</i> | 41 |
| 2.6 | Related Studies | 43 |
| 2.7 | Conclusion | 45 |
| CHAPTER THREE: EXPERIMENTAL RIG DESIGN | | 46 |
| 3.1 | The Design of a Scaled Classifier Model | 46 |
| 3.2 | Design Candidates | 47 |
| 3.3 | The Model Classifier | 49 |
| 3.3.1 | Classifier Body | 52 |
| 3.3.2 | The Classifier System | 52 |
| 3.3.3 | Classifier Air Flow | 54 |
| 3.3.4 | Particle Feeder | 55 |
| 3.3.5 | The Particle Outlet | 56 |
| 3.3.6 | The Cyclone | 57 |

| | | |
|--|---|-----------|
| 3.3.7 | The Filter | 58 |
| 3.4 | Air Velocity Measurement | 58 |
| 3.4.1 | Five Hole Pitot Tube | 62 |
| 3.4.2 | Air flow measurement | 63 |
| 3.5 | Tuft Visualisation | 65 |
| 3.6 | Particulate Phase Experiment | 66 |
| 3.7 | Determination of Particle Size Distribution | 68 |
| 3.7.1 | Feed Materials | 69 |
| 3.7.2 | Particle Characteristics | 69 |
| 3.8 | Characterisation of One-Third Scale Facility | 70 |
| 3.8.1 | Scaling Criteria | 70 |
| 3.8.2 | Dynamics Similarity | 71 |
| 3.8.3 | Air Speed Characteristics | 72 |
| 3.9 | Error Analysis | 72 |
| 3.9.1 | Error in Air Velocity | 73 |
| 3.9.2 | Error in Particles Measurement | 73 |
| CHAPTER FOUR: MODEL FORMULATION FOR CFD | | 74 |
| 4.1 | The Structure of CFD | 75 |
| 4.1.1 | Pre-Processing | 76 |
| 4.1.2 | Processing (Solver) | 77 |
| 4.1.3 | Post processing | 79 |
| 4.2 | FLUENT | 79 |
| 4.2.1 | Computational Geometry | 79 |
| 4.2.2 | Boundary Conditions | 81 |

| | | |
|--|---|------------|
| 4.2.3 | Governing Equation | 82 |
| 4.2.4 | Turbulence Modelling | 83 |
| 4.2.5 | Solid Phase Modelling | 85 |
| 4.2.6 | The SIMPLE Algorithm | 86 |
| 4.3 | Classifier Model Setup | 88 |
| 4.4 | Conclusion | 101 |
| CHAPTER FIVE: NUMERICAL ANALYSIS AND DISCUSSION | | 102 |
| 5.1 | Air Flow Distribution Analysis | 103 |
| 5.1.1 | General Velocity Profile Inside the Classifier | 104 |
| 5.1.2 | Effects of Varying the Inlet Velocity | 109 |
| | <i>5.1.2.1 Velocity Profile Outside the Separation Area</i> | 109 |
| | <i>5.1.2.2 Velocity Profile Inside the Separation Area</i> | 117 |
| 5.1.3 | Effects of Varying the Vane Angle | 120 |
| | <i>5.1.3.1 Velocity Profile Outside the Separation Area</i> | 121 |
| | <i>5.1.3.2 Velocity Profile Inside the Separation Area</i> | 128 |
| 5.1.4 | Effects of Varying the Outlet Position | 130 |
| | <i>5.1.4.1 Velocity Profile Outside the Separation Area</i> | 131 |
| | <i>5.1.4.2 Velocity Profile Inside the Separation Area</i> | 135 |
| 5.2 | Particles Distribution Analysis | 139 |
| 5.2.1 | Effect of the Velocity Inlet | 139 |
| 5.2.2 | Effect of Vane Angle | 143 |
| 5.2.3 | Effect of Outlet Position | 146 |
| 5.3 | Particles Residence Time | 151 |
| 5.4 | Design Parameter Look-up Table | 155 |

| | | |
|--|----------------------------------|------------|
| 5.5 | Conclusion | 160 |
| CHAPTER SIX: VALIDATION OF THE SIMULATION | | 161 |
| 6.1 | CFD Setup | 161 |
| 6.1.1 | Grid Independency Study | 164 |
| 6.2 | Experimental Setup | 168 |
| 6.3 | Validation of CFD | 169 |
| 6.3.1 | Quantitative Validation | 169 |
| 6.3.1.1 | <i>Velocity Flow Field</i> | 169 |
| 6.3.1.2 | <i>Particle Distribution</i> | 176 |
| 6.3.2 | Flow Visualisation | 178 |
| 6.4 | Conclusion | 179 |
| CHAPTER SEVEN: CONCLUSIONS | | 181 |
| 7.1 | Contribution to Knowledge | 182 |
| 7.2 | Future Directions | 183 |
| References | | 185 |
| Appendices | | 191 |

List of Figures

| | |
|-------------|--|
| Figure 1.1 | Annual electricity net generation in the world |
| Figure 1.2 | World electricity generations by fuel |
| Figure 1.3 | Simple diagram of coal power station |
| Figure 1.4 | A pulveriser |
| Figure 1.5 | Methodology flow chart |
| Figure 2.1 | Fuel mix for electricity supplied in 2010 |
| Figure 2.2 | Primary energy demand of fuels by 2020 |
| Figure 2.3 | The carbon cycle |
| Figure 2.4 | Coal-fired power plants route to CO ₂ reduction |
| Figure 2.5 | PF-based plants |
| Figure 2.6 | Four types of separation techniques |
| Figure 2.7 | Alpine Multiplex Zig-zag Classifier and its zig-zag classifier principle |
| Figure 2.8 | Fluidised bed classifiers |
| Figure 2.9 | Vertical spindle coal mill static classifier |
| Figure 2.10 | Rotating wheel air classifier |
| Figure 2.11 | Dynamic classifier from Foster Wheeler |
| Figure 2.12 | Feret's diameter |
| Figure 2.13 | Rough wall particles collision |
| Figure 2.14 | Forces acting on coal particle in axial motion |
| Figure 2.15 | Forces acting on coal particle in radial motion |
| Figure 3.1 | Static blades classifier with fins |
| Figure 3.2 | Classifier with rotating vane |
| Figure 3.3 | Old classifier designs |
| Figure 3.4 | Cyclone air classifier |
| Figure 3.5 | A 3-D illustration of the built model classifier |
| Figure 3.6 | The actual built model classifier |

| | |
|-------------|--|
| Figure 3.7 | Classifier housing body |
| Figure 3.8 | Separation cone and vanes |
| Figure 3.9 | Mechanism for controlling the vane angle |
| Figure 3.10 | The blower fan (below) and its electric controller (above) |
| Figure 3.11 | The blower fan calibration graph |
| Figure 3.12 | Particle feeder |
| Figure 3.13 | Particle feeder calibration graph |
| Figure 3.14 | Particle outlet |
| Figure 3.15 | The outlet cyclone |
| Figure 3.16 | The air filter for the clean air from the cyclone |
| Figure 3.17 | Velocity measurements at the inlet |
| Figure 3.18 | Schematic diagram for air measurement |
| Figure 3.19 | The measurement locations |
| Figure 3.20 | The experimental setup |
| Figure 3.21 | Velocity measurement procedures |
| Figure 3.22 | Five hole Pitot Tube |
| Figure 3.23 | LabVIEW program block |
| Figure 3.24 | Front panel GUI |
| Figure 3.25 | Flow visualisation using tuft |
| Figure 3.26 | Schematic diagram of the particulate experiment setup |
| Figure 3.27 | Particulate phase experiment procedure |
| Figure 3.28 | New standard grade filite (200 x magnifications) |
| Figure 3.29 | Used standard grade filite (100 x magnifications) |
| Figure 4.1 | Computational grid layout |
| Figure 4.2 | Unstructured mesh for inlet plane |
| Figure 4.3 | Unstructured mesh for outlet plane |
| Figure 4.4 | A converged primary phase case |
| Figure 4.5 | A converged particulate phase case |
| Figure 4.6 | CFD simulation flowchart |

| | |
|-------------|---|
| Figure 5.1 | The classifier and axial level analysed |
| Figure 5.2 | Vane angles (left) and outlet positions locations being analysed |
| Figure 5.3 | Air flow inside the classifier |
| Figure 5.4 | Planes examined in initial velocity profile analysis |
| Figure 5.5 | Axial velocity profiles at Level A with various inlet velocities |
| Figure 5.6 | Axial velocity profiles at Level B with various inlet velocities |
| Figure 5.7 | Axial velocity profiles at Level C with various inlet velocities |
| Figure 5.8 | Axial velocity profiles at Level D with various inlet velocities |
| Figure 5.9 | Axial velocity profiles at Level A using 30° vane angle |
| Figure 5.10 | Axial velocity profiles at Level A using 45° vane angle |
| Figure 5.11 | Axial velocity profiles at Level A using 60° vane angle |
| Figure 5.12 | Axial velocity profiles outside separation area at Level A for various inlet velocities (30° vane angle) |
| Figure 5.13 | Axial velocity profiles outside separation area at Level B for various inlet velocities (30° vane angle) |
| Figure 5.14 | Axial velocity profiles outside separation area at Level C for various inlet velocities (30° vane angle) |
| Figure 5.15 | Axial velocity profiles outside separation area at Level D for various inlet velocities (30° vane angle) |
| Figure 5.16 | Radial velocity profiles outside separation area at Level A for various inlet velocities (30° vane angle) |
| Figure 5.17 | Radial velocity profiles outside separation area at Level B for various inlet velocities (30° vane angle) |
| Figure 5.18 | Radial velocity profiles outside separation area at Level C for various inlet velocities (30° vane angle) |
| Figure 5.19 | Radial velocity profiles outside separation area at Level D for various inlet velocities (30° vane angle) |
| Figure 5.20 | Tangential velocity profiles outside separation area at Level A for various inlet velocities (30° vane angle) |

- Figure 5.21 Tangential velocity profiles outside separation area at Level B for various inlet velocities (30° vane angle)
- Figure 5.22 Tangential velocity profiles outside separation area at Level C for various inlet velocities (30° vane angle)
- Figure 5.23 Tangential velocity profiles outside separation area at Level D for various inlet velocities (30° vane angle)
- Figure 5.24 Axial velocity profiles inside separation area at lower region (Level B) for various inlet velocities (30° vane angle)
- Figure 5.25 Axial velocity profiles inside separation area at upper region (Level C) for various inlet velocities (30° vane angle)
- Figure 5.26 Axial velocity profiles inside vortex finder (Level D) for various inlet velocities with outlet Position 1 (30° vane angle)
- Figure 5.27 Air velocity contour for various vane angles at position1 with 13 m/s inlet velocity
- Figure 5.28 Axial velocity profiles outside separation area at Level A for various vane angles (13 m/s inlet velocity)
- Figure 5.29 Axial velocity profiles outside separation area at Level B for various vane angles (13 m/s inlet velocity)
- Figure 5.30 Axial velocity profiles outside separation area at Level C for various vane angles (13 m/s inlet velocity)
- Figure 5.31 Axial velocity profiles outside separation area at Level D for various vane angles (13 m/s inlet velocity)
- Figure 5.32 Radial velocity profiles outside separation area at Level A for various vane angles (13 m/s inlet velocity)
- Figure 5.33 Radial velocity profiles outside separation area at Level B for various vane angles (13 m/s inlet velocity)
- Figure 5.34 Radial velocity profiles outside separation area at Level C for various vane angles (13 m/s inlet velocity)
- Figure 5.35 Radial velocity profiles outside separation area at Level D for various vane angles (13 m/s inlet velocity)
- Figure 5.36 Tangential velocity profiles outside separation area at Level A for various vane angles (13 m/s inlet velocity)
- Figure 5.37 Tangential velocity profiles outside separation area at Level B for various vane angles (13 m/s inlet velocity)

| | |
|-------------|--|
| Figure 5.38 | Tangential velocity profiles outside separation area at Level C for various vane angles (13 m/s inlet velocity) |
| Figure 5.39 | Tangential velocity profiles outside separation area at Level D for various vane angles (13 m/s inlet velocity) |
| Figure 5.40 | Axial velocity profiles inside separation area at lower region (Level B) for various vane angles (13 m/s inlet velocity) |
| Figure 5.41 | Axial velocity profiles inside separation area at upper region (Level C) for various vane angles (13 m/s inlet velocity) |
| Figure 5.42 | Axial velocity profiles inside vortex finder (Level D) for various vane angles with outlet Position 1 (13m/s inlet velocity) |
| Figure 5.43 | Pressure contour for 30° vane angles at various position with 13m/s inlet velocity |
| Figure 5.44 | Axial velocity profiles outside separation area for various outlet positions (lower region, Level B) |
| Figure 5.45 | Axial velocity profiles outside separation area for various outlet positions (upper region, Level D) |
| Figure 5.46 | Radial velocity profiles outside separation area for various outlet positions (lower region, Level B) |
| Figure 5.47 | Radial velocity profiles outside separation area for various outlet positions (upper region, Level D) |
| Figure 5.48 | Tangential velocity profiles outside separation area for various outlet positions (lower region, Level B) |
| Figure 5.49 | Tangential velocity profiles outside separation area for various outlet positions (upper region, Level D) |
| Figure 5.50 | Axial velocity profiles inside separation area for various outlet positions (lower region, Level B) |
| Figure 5.51 | Axial velocity profiles inside separation area for various outlet positions (upper region, Level D) |
| Figure 5.52 | Axial velocity profiles inside vortex finder for various outlet positions (30° vane angle, 13m/s inlet velocity) |
| Figure 5.53 | Axial velocity profiles inside vortex finder for various outlet positions (45° vane angle, 13m/s inlet velocity) |
| Figure 5.54 | Axial velocity profiles inside vortex finder for various outlet positions (60° vane angle, 13m/s inlet velocity) |

| | |
|-------------|---|
| Figure 5.55 | Particle cumulative size distributions for 30° vane angle at Position 1 |
| Figure 5.56 | Particle size at 40, 60 and 80% of cumulative distribution for 30° vane angle at outlet position 1 |
| Figure 5.57 | Particle cumulative size distributions for 45° vane angle at Position 3 |
| Figure 5.58 | Particle cumulative size distributions for 45° vane angle at Position 4 |
| Figure 5.59 | Particle size at 40, 60 and 80% of cumulative distribution for 45° vane angle at outlet position 4 |
| Figure 5.60 | Particle cumulative size distributions for 60° vane angle at Position 4 |
| Figure 5.61 | Particle cumulative size distributions at Position 1 with 13 m/s inlet velocity |
| Figure 5.62 | Particle cumulative size distributions at Position 1 with 20 m/s inlet velocity |
| Figure 5.63 | Particle size at 40, 60 and 80% of cumulative distribution for 20 m/s inlet velocity at outlet position 3 |
| Figure 5.64 | Particle size at 40, 60 and 80% of cumulative distribution for 30 m/s inlet velocity at outlet position 4 |
| Figure 5.65 | Particle cumulative size distributions at 13 m/s inlet velocity for 30° vane angle |
| Figure 5.66 | Particle cumulative size distributions at 20 m/s inlet velocity for 30° vane angle |
| Figure 5.67 | Particle cumulative size distributions at 30 m/s inlet velocity for 30° vane angle |
| Figure 5.68 | Particle cumulative size distributions at 13 m/s inlet velocity for 45° vane angle |
| Figure 5.69 | Particle cumulative size distributions at 20 m/s inlet velocity for 45° vane angle |
| Figure 5.70 | Particle cumulative size distributions at 13 m/s inlet velocity for 60° vane angle |
| Figure 5.71 | Particle cumulative size distributions at 20 m/s inlet velocity for 60° vane angle |
| Figure 5.72 | Particle tracks of 5 μm particle using outlet Position 1 and Position 3 |

| | |
|-------------|---|
| Figure 5.73 | Residence time for various velocity with 30° vane angle at outlet position 1 |
| Figure 5.74 | The effect of vane angle on particles residence time at outlet position 2 with 13 m/s inlet velocity. |
| Figure 5.75 | The effect of outlet position on particles residence time at 60° vane angle with 30 m/s inlet velocity. |
| Figure 6.1 | Axial velocity profile comparison between 2.4 million and 3.4 million mesh sizes |
| Figure 6.2 | Radial velocity profile comparison between 2.4 million and 3.4 million mesh sizes |
| Figure 6.3 | Tangential velocity profile comparison between 2.4 million and 3.4 million mesh sizes |
| Figure 6.4 | The measurement locations |
| Figure 6.5 | Comparison of the experiment, Rke and RSM axial velocity profiles at different heights in the classifier |
| Figure 6.6 | Comparison of the experiment, Rke and RSM radial velocity profiles at different heights inside the classifier |
| Figure 6.7 | Comparison of the experiment, Rke and RSM tangential velocity profiles at different heights in the classifier |
| Figure 6.8 | Particles cumulative volume distribution |
| Figure 6.9 | Particles cumulative size distribution |
| Figure 6.10 | Particles size 40, 50, 60, 70 and 80 % of cumulative distribution |
| Figure 6.11 | Air velocity flow field from the simulation and experimental visualisations |

List of Tables

| | |
|------------|---|
| Table 3.1 | Comparison of scaling criteria for 1/3 scale facility |
| Table 4.1 | Particles distributions used for the fluent modelling |
| Table 4.2 | Simulation conditions |
| Table 5.1 | Particle residence time for 30° vane angle at outlet position 1 |
| Table 5.2 | Particle residence time for 13 m/s for various vane angles at outlet position 1 |
| Table 5.3 | Parameter look-up table for 30° vane angle and 13m/s inlet velocity |
| Table 5.4 | Parameter look-up table for 30° vane angle and 20m/s inlet velocity |
| Table 5.5 | Parameter look-up table for 30° vane angle and 30m/s inlet velocity |
| Table 5.6 | Parameter look-up table for 45° vane angle and 13m/s inlet velocity |
| Table 5.7 | Parameter look-up table for 45° vane angle and 20m/s inlet velocity |
| Table 5.8 | Parameter look-up table for 45° vane angle and 30m/s inlet velocity |
| Table 5.9 | Parameter look-up table for 60° vane angle and 13m/s inlet velocity |
| Table 5.10 | Parameter look-up table for 60° vane angle and 20m/s inlet velocity |
| Table 5.11 | Parameter look-up table for 60° vane angle and 30m/s inlet velocity |
| Table 6.1 | CFD and experimental results for each velocity components |
| Table 6.2 | Deviation result for experimental result and CFD |

Abbreviations

| | |
|-----------------|--|
| CFD | Computer Fluid Dynamics |
| DECC | Department of Energy and Climate Change |
| DTI | Department of Trade and Industry |
| IEA | International Energy Agency |
| NO _x | Nitrogen Oxide |
| CO ₂ | Carbon Dioxide |
| SO _x | Sulphur Oxide |
| SO ₃ | Sulphur Trioxide |
| SO ₂ | Sulphur Dioxide |
| ZET | Zero Emission Technology |
| WCI | World Coal Institute |
| PF | Pulverised Fuel |
| LHV | Lower Heating Value |
| DAS | Data Acquisition System |
| SEM | Scanning Electron Microscope |
| PDEs | Partial Differential Equations |
| CAD | Computer Aided Design |
| RSM | Reynold Stress Model |
| RNG | Re-Normalisation Group |
| PRESTO | Pressure Staggering Option |
| SIMPLE | Semi-Implicit Method for Pressure-Linked Equations |
| Re | Reynold Number |
| St | Stoke Number |
| D_H | Hydraulic Diameter |
| RANS | Reynolds-Averaged Navier-Stokes |

CHAPTER ONE: INTRODUCTION

This thesis describes a study scrutinising the performance of a pulverised coal classifier for a coal fired power stations. The aim is to improve efficiency and to reduce harmful emissions through particle size control downstream of the mill and upstream of the boiler.

World energy demand is increasing relentlessly and is expected to double by 2050 (WEC, 2007). Equally, the demand in electricity is increasing at a similar rate. The fuels that provide the required electricity are predominantly the fossil type (Figure 1.1). Of the fossil fuel mix, coal is still the second fuel after oil for electricity generation (Figure 1.2). Therefore, clean coal technologies are needed to reduce the harmful emissions from coal-fired power plants. Figure 1.3 illustrates the general principle of a coal power station. In its operation, the coal is first crushed in the crush mill (1) or, as it is specifically known, the pulveriser. The crushed coal is then blown in a stream of air (2) into a large boiler (3). The coal is burned so that the water inside the boiler produces a large amount of steam, which is used to turn the turbine (4). The turbine is coupled to a generator (5), which is connected to the step-up transformer. To increase the power station efficiency, the steam is cooled in a condenser (6). The waste heat is carried out via the cooling tower (7), where it returns as cool water (8) to be used in the boiler again.

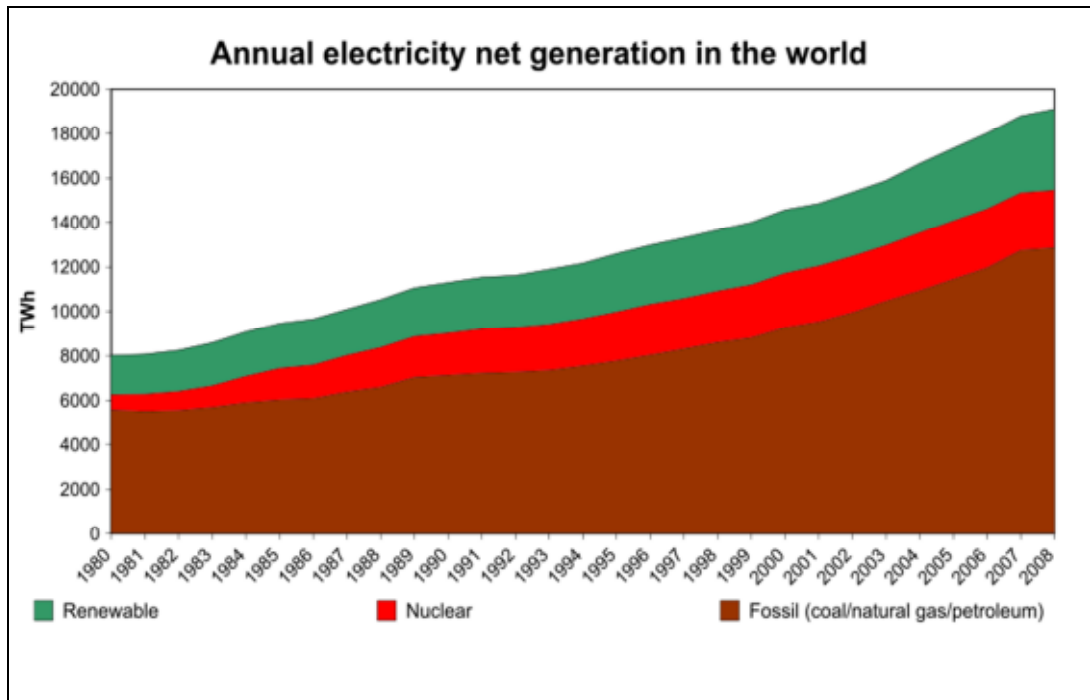


Figure 1.1: Annual electricity net generation in the world

[<http://www.eia.gov/countries/data.cfm> EIA]

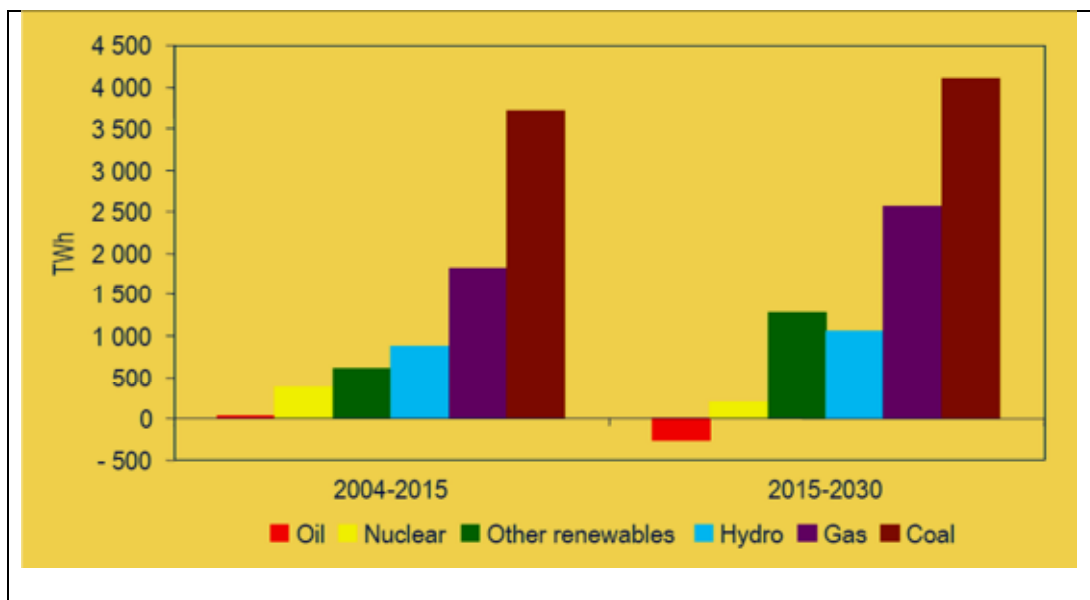


Figure 1.2: World electricity generation by fuel

[<http://www.eia.gov/countries/data.cfm> EIA]

In this study, the area of interest is the coal classifiers. These vital components of

the classifier, centrifugal action forces the coal outwards to the grinding ring (3), where it is pulverised between the rings and grinding roller. Grinding load, transmitted from the tension rods through the loading frame to the roller assemblies, holds the rollers in contact with the grinding ring. The rollers adjust vertically as the depth of the coal load increases or decreases. A nozzle ring on the outside perimeter of the grinding ring feeds primary air to the pulveriser (classifier). Pyrites and tramp metal fall through the nozzle ring openings to be scraped into a rejects hopper. A stream of low-velocity air (4) carries the particles of pulverised coal upwards, where they enter the classifier inlet vanes (6). Fine particles travel to the burners (7) in the primary air stream, but the larger, heavier particles are returned to the grinding zone for further pulverisation.

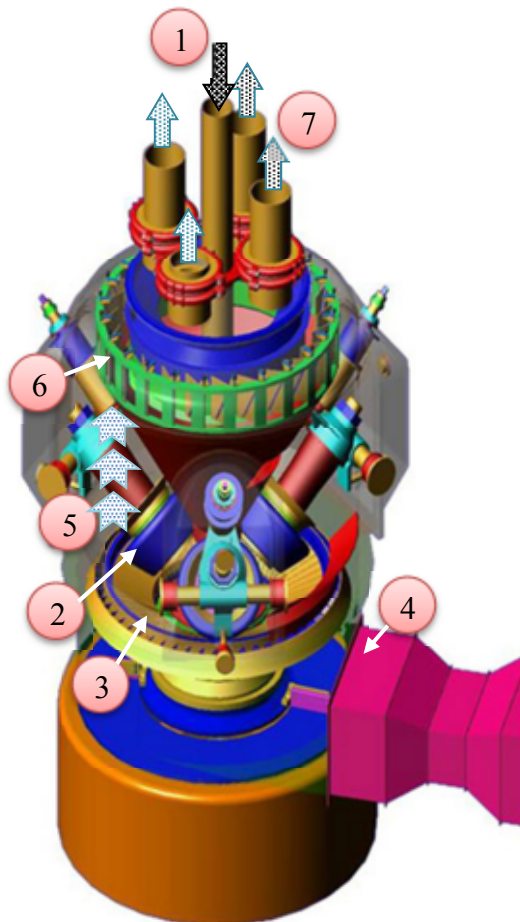


Figure 1.4: A pulveriser [www.innovativecombustion.com]

The study aims to enhance the performance of present coal classifiers. The efficiency of the combustion process in coal-fired power stations depends greatly on the efficiency of the classifier and the fuel distribution network. The latter and the furnace require finer particles for optimum performance. This study, therefore, initially scrutinises the dynamics and the fluid motion prevailing in coal classifiers. These were carried out through a combination of computational predictions using CFD and experiments with a model scale classifier. The work is then progressed to a parametric study of the classifier features. The work was completed with parameters that control the performance of the classifier identified.

1.1 Problem Definition

The primary problems that this work addresses are:

- The lack of knowledge of power stations regarding two phase gas-solid flows.
- Erosion and distribution anomalies due to uncontrollable particle size distribution downstream of the mill.
- Fuel balancing problems at fuel pipes splitters.
- Poor control of low NO_x burners due to inadequate particle size, which results in inefficient burning of the coal and high emissions.

In order to address these problems, which must be overcome, close scrutiny of the classifier performance is required, including all the particle size control factors.

The study includes:

- Vary the inlet velocities and obtain data of particulate mass flow rate and separation efficiency by measuring outlet particle size.
- Vary the vane angles at each inlet speed and obtain the same particulate data.
- Vary the outlet positions as a function of the above parameters.
- Examine the geometrical features effect on the classifier performance.

1.2 Aims and Objectives

The overall aim of the study is to enhance the performance of coal classification in coal-fired power plants. The most important feature is particle size control, hence the controlling parameters that affect the particle size. To this end, the research presented aims to reduce emissions from conventional coal-fired power stations and lengthen their operating life.

In order to achieve this, this work aims to:

- Improve particle separation efficiency or sharpness of cut. This was attained by a geometric parametric study on the design features.
- Understand the effect of the operating parameters/variables (inlet flow rate, vane angles, inlet flow symmetry, swirl number/intensity) on the separation efficiency or sharpness of cut, and develop appropriate correlations.
- Characterise the air distribution inside the original classifier without any physical modifications applied to it.

- Characterise the air distribution inside the classifier with the modifications designed to affect its performance fully implemented.

1.3 Methodology

The work conducted involves experimental and computational analysis of the classifier performance and a parametric study into the main features that control particle size discrimination. The flowchart of the work through this PhD is shown in Figure 1.5.

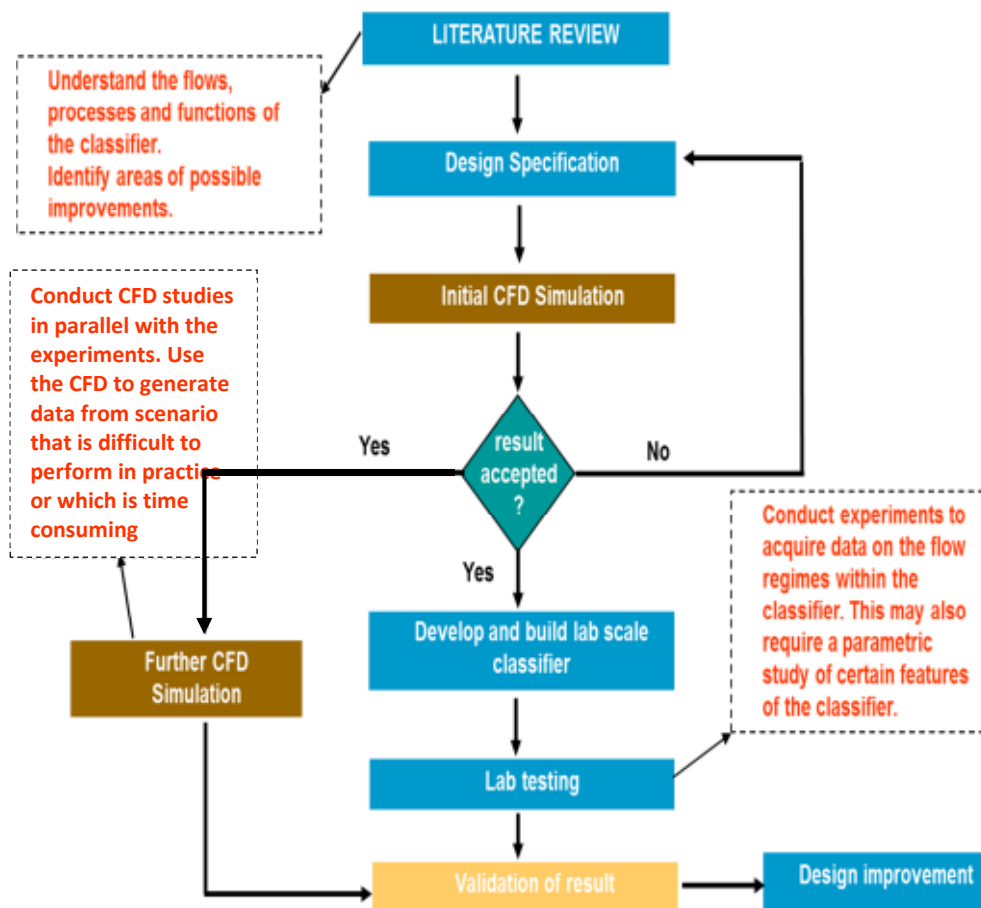


Figure 1.5: Methodology flow chart

1.4 Thesis Layout

The thesis is organised within seven chapters as follows:

Chapter 2 - gives a detailed review of relevant literature and research studies that have been previously carried out in the field of coal classification and two phase flow, looking at both computational and experimental work.

Chapter 3 - describes the experimental rig, techniques and tools used in this research, including a review of the test facilities, procedures and instrumentation.

Chapter 4 - gives a summary of the CFD code, program and set-up for the computational work carried out.

Chapter 5 - details the 3-D computational results obtained and discusses the results.

Chapter 6 - exhibits the data obtained from the experimental testing on the one-third scale test facility. The data from the experiment is used to validate the CFD simulation. Tests for grid independence and validation against experimental data are carried out before parametric testing of devices is reported.

Chapter 7 - discusses the conclusions reached by the present work and gives suggestions of the direction that further work should take.

CHAPTER TWO: LITERATURE REVIEW

To the present day, coal remains one of the principal energy sources used for electricity generation. The rise of gas prices over recent years has led to a preference for coal. In 2009, coal supplied 28% of electricity in the UK (DECC Energy Statistic, 2011) (Figure 2.1). Due to its advantages in terms of availability, affordability and role in stabilising energy markets, coal is anticipated to remain as a primary source of electricity generation. By 2020, coal is expected to remain the provider of the majority of UK energy needs (DTI, 2007) (Figure 2.2). Coal is also projected to play a major role in the global energy system, with more than 20% shares in primary energy and up to 40% in electricity production by 2030 (IEA, 2007).

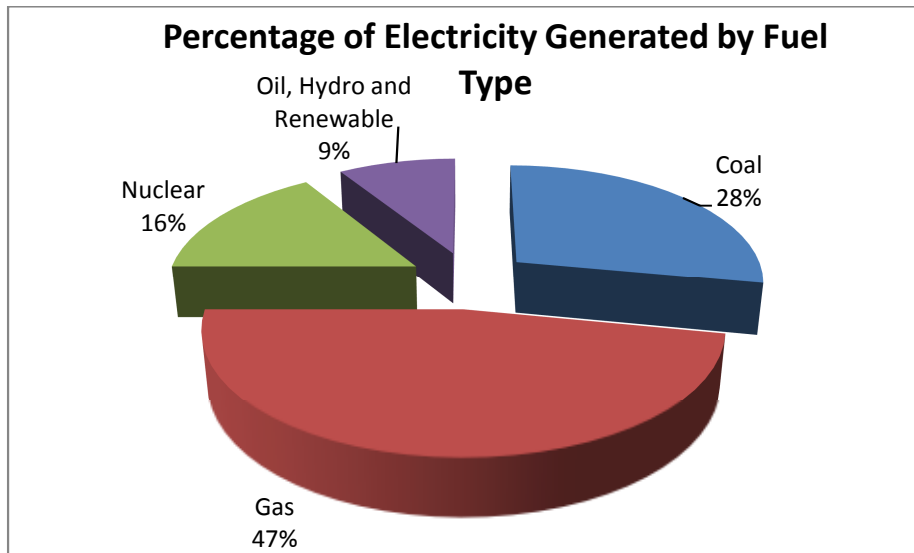


Figure 2.1: Fuel mix for electricity supplied in 2010 (DECC Energy Statistic, 2011)

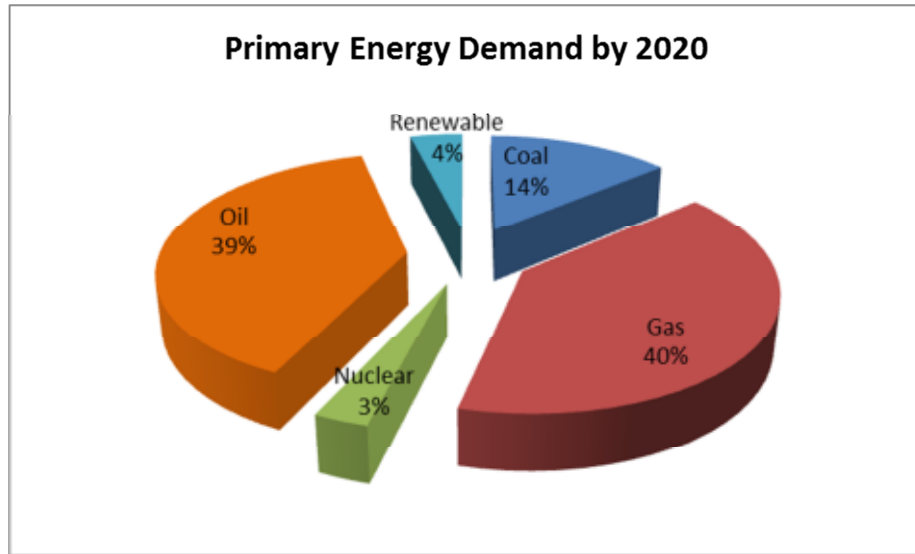


Figure 2.2: Primary energy demand of fuels by 2020 (DTI 2007)

Despite being used widely as a power generator, coal however, when burned, creates the most pollution of all fossil fuels. The coal industry uses the term "clean coal" to describe technologies designed to enhance both the efficiency and the environmental acceptability of coal extraction, preparation and use, with no specific quantitative limits on any emissions, particularly carbon dioxide. Coal-fired power plants emit a large amount of hazardous pollutants. Power stations now have limits on NO_x, SO₃ (the chemicals primarily responsible for acid rain) and CO₂, following the Kyoto treaty in 1997. Increasingly stringent emission regulations have encouraged considerable research and development in optimising combustion conditions (Aroussi, 2006).

2.1 Coal as Fuel

Coal is a fossil fuel created from the remains of plants that lived and died around 100 to 400 million years ago, when parts of the earth were covered with huge swamp-like forests. It is classified as a non-renewable energy source because it

takes millions of years to form (NEED, 2011). Since various plants grew more intensively in different areas of the world and pressure effects were not the same during the coalification process, samples of coal from different regions will be different.

Coal can be broken down into four main types, based upon the amount of pressure and heat that was used to create the coal over millions of years in the earth and also by the amount of carbon that is in the coal. The four main types of coal are:

i. Anthracite

Anthracite has the highest concentration of carbon (85–97% carbon) and has a slightly lower heating rate than bituminous coal.

ii. Bituminous

Bituminous coal contains 45–86% carbon and has a high heating value. For this reason it is a very important fossil fuel for the steel and iron industries and is widely used to generate electricity. It is a highly abundant form of coal and was formed 100–300 million years ago.

iii. Subbituminous

Subbituminous coal will typically contain 35–45% carbon and has a slightly higher heat rating than that of lignite coal. Again, subbituminous is an abundant form of coal and it is thought to have been formed 100 million years ago.

iv. Lignite

Lignite coal will typically contain 25–35% carbon and has the lowest coal energy rating. The reason for this is that deposits of lignite are relatively young so they have not been subjected to extreme heat and pressure over the long periods of time that other forms of coal have; as such, this type of coal is quite brittle and moist.

In general, the energy rank of a type of coal will be dependent on the heat and pressure that it has withstood over the years, so the higher the pressure and heat it has withstood and the longer it has withstood it, the greater the heating rank it will be.

2.1.1 Carbon Cycle

The carbon cycle is an intricately controlled system on which all carbon life forms and plants heavily rely. Respiration and the burning of coal transfers carbon in the earth's crust into the atmosphere as carbon dioxide (CO₂), while plants take CO₂ from the atmosphere and store carbon in the earth's crust, as shown in Figure 2.3.

The cycle of CO₂ is not balanced. The CO₂ content of the atmosphere is gradually and steadily increasing. As a greenhouse gas, CO₂ is contributing to global warming, which is estimated to raise the average temperatures of the world.

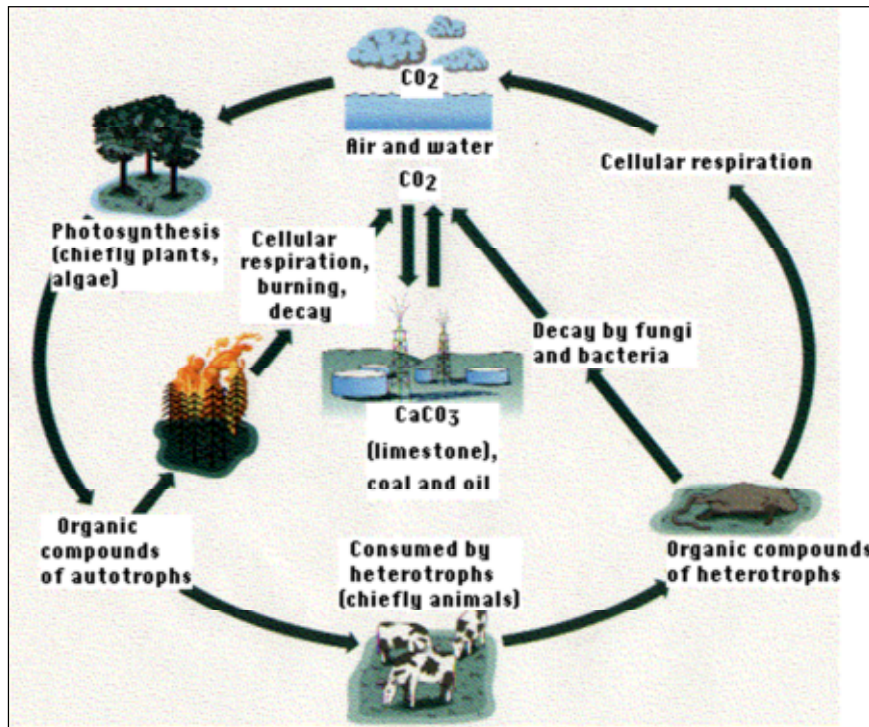


Figure Error! No text of specified style in document..3: The carbon cycle

(Kimbal J. website)

2.1.2 Environmental Pollutants

The NO_x and SO_2 emissions are also damaging the environment. The emissions of sulphur oxides are dependent on the sulphur content of the particular coal and can be successfully removed from the flue gases of power stations. The formation of oxides of nitrogen occurs with an excess of oxygen in a combustion process and is more difficult to remove

New low NO_x technologies, providing an oxygen lean burn process, and coal re-burn systems combined with reduction of NO_x by hydrocarbons and flue gas clean-up can reduce NO_x emissions by up to 90% (IEA Clean Coal Centre website and Hampartsoumian, 2003).

2.2 Coal-Fired Power Plants Technologies

Coal plays an important role in ensuring secure, reliable and affordable energy supplies throughout the world, and it is continuously predicted to be a globally leading source of power generation for the foreseeable future. However, its environmental performance needs to improve if coal is to continue to make an important contribution. Currently, coal-fired power plants are claimed to be the main culprit for the extensive release of CO₂. The enhancement of coal-fired power plants is believed to be the best option to substantially mitigate the CO₂ emissions (IEA, 2004; WCI, 2005).

The prospects of development and commercialisation of clean coal technologies (for example, advanced technologies and improved plant efficiency) together with near Zero Emission Technologies (ZET) over the next two decades are seen to be promising for abating CO₂ emissions (IEA, 2007). Figure 2.4 shows the route to reducing CO₂ emissions. In the interim, improving the efficiency of existing coal-fired power plants (for example, Pulverised Fuel-based plants) is a cost-effective way of limiting the growth of CO₂ emissions. Generally, Pulverised Fuel (PF) plants are widely employed all over the world, hence abating CO₂ emissions from such plants is going to be worthwhile.

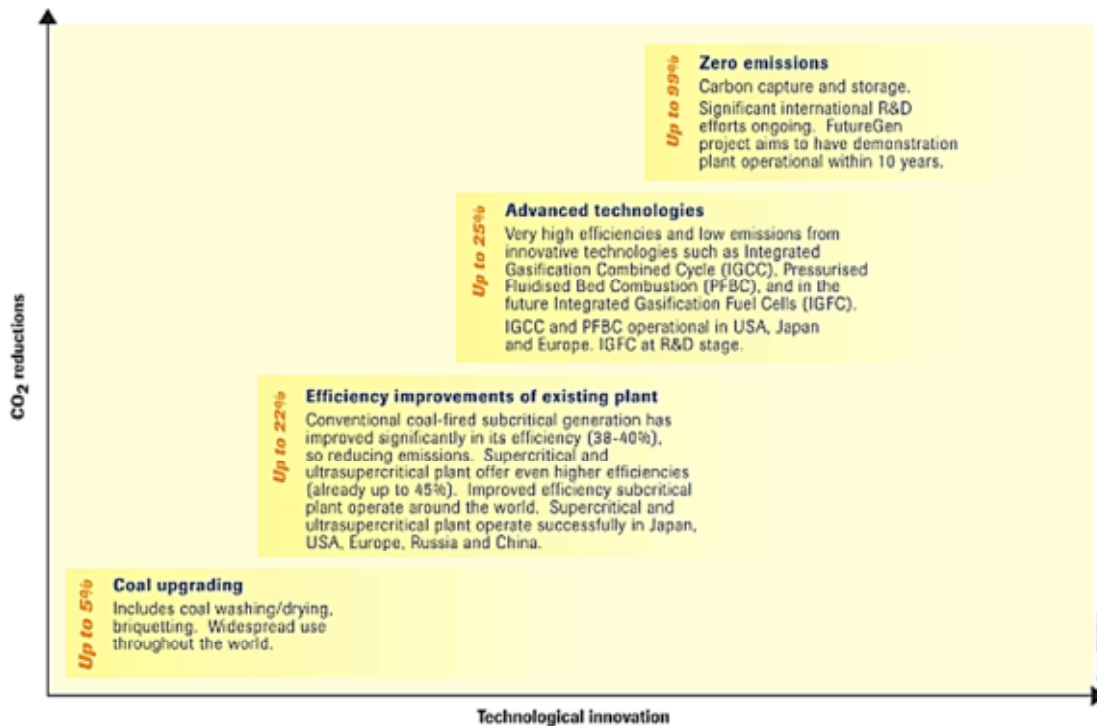


Figure 2.4: Coal-fired power plants route to CO₂ reduction (WCI, 2005)

Most of the existing coal-fired power plants today are based on PF plants that have been used for over 60 years and, in terms of overall numbers and generating capacity, they dominate the global market (IEA, 2003b). Figure 2.5 illustrates the mechanism of PF-based plants. In PF-based plants, coal is pulverised into a fine powder, which increases the surface area and allows it to burn more quickly. The fine powder is combusted in a high temperature furnace to heat water and produce steam to drive steam turbines.

Over the years, many advances have been made with PF-based plants, including environmentally focused measures to minimise emissions of SO_x and NO_x, as well as applications of advanced steam cycles that allow greater plant efficiency. PF-based plants are characterised by overall thermal efficiency of up to roughly

36% Lower Heating Value (LHV) (for example, sub-critical steam cycle), whereas plants with higher steam temperatures and pressures can attain up to some 45% (for example, in super-critical steam cycle) (IEA, 2003b) and even up to 50% for ultra-supercritical (USC) power plants (WCI, 2005).

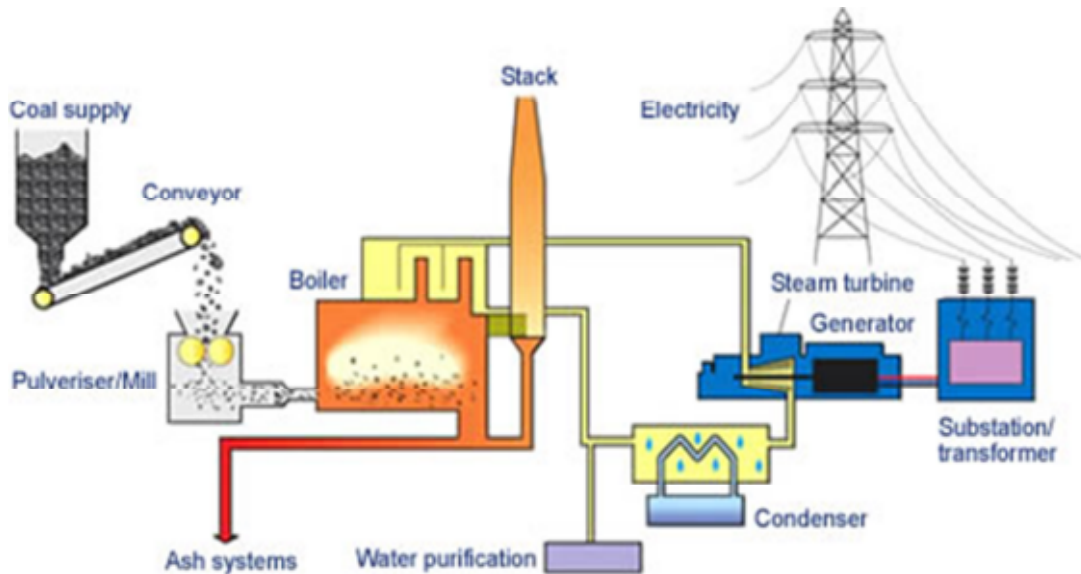


Figure 2.5: PF-based plants (WCI, 2005)

Currently, many countries put significant efforts into improving the efficiency of PF-based plants by producing a lean burnout. Obtaining a lean burnout of a coal depends on many factors. For a given coal, the quantity of larger-sized (coal particles) fractions used has a major effect on combustion. A finer size of coal particles helps increase the power generation efficiency. Therefore, this helps to generate more megawatts of electricity from the same amount of fuel. This indirectly results in lower power costs and a reduction in greenhouse gas emissions.

Classifiers are normally used in coal-fuel power plants in order to ensure that the optimum size of coal powder for burning is below a threshold of around 75 microns. In addition to optimising combustion, coal classification helps reduce sulphur dioxide and nitrogen oxide emissions.

Classifier design is a constantly changing industry, which is based heavily on the advanced retrofitting of coal power stations to improve efficiency and research into developing more efficient and cleaner stations. This makes the study of PF an exciting and cutting-edge area of research, as it is constantly changing and leading to the development of devices that are turned into working devices for companies to use.

Whilst Pulverised Fuel (PF) may be seen as a dirty fuel and more at home in the industrial revolution than in the 21st century, PF is being touted by the government. In addition, a Department of Trade and Industry (DTI) report states that PF will still be a major contributor of the future energy production in this country and can satisfy its energy requirements as far into the future as 2030 (DTI, 2007).

Pulverised Fuel is the term used for any fuel source that is ground or otherwise reduced to a powder for combustion. Whilst the most common example is coal in coal-fired power stations, paper, bio-mass and wood chips are amongst the various fuels that are pulverised for use in combustion.

The use of other fuels is important, as using renewable sources of PF (such as

biomass) is one of the many ways of slowly moving away from dependency on fossil fuels as power source. The percentage of other fuels added to pulverised coal is considered, including the increased possibility of localised mill combustion (mill pops) due to the increased percentage of volatiles in the pulverised fuel. The use of biomass as PF is important, as, in relation to the carbon cycle, no new carbon is being released into the atmosphere. New biomass will need to be produced to replace that which is being used in combustion.

The decline in use of PF is not linked to lack of fuel, but to self-imposed emission targets put in place by the Kyoto Agreement, and the cost in comparison to constructing gas-fired power stations of similar sizes. If current power stations can be cost effectively retro-fitted to increase efficiency and reduce CO₂ emissions, then PF-fired power stations are likely to remain in place.

The efforts undertaken for this thesis focus towards the goal of increasing the efficiency of PF-fired power stations are not only in terms of efficient fuel utilisation, but also in abiding by the emission efficiency targets imposed by the government in United Kingdom. The specific area of efficiency tackled is the effect of changing various classifier parameters on the performance of the classifier. These include the effect of changing the classifier's blades angle, blow ratio and the outlet size. The data is generated by experimental and computational means, depicting the fluid behaviour within the classifier.

2.3 Separation Techniques

The separation of particles from the air stream can be either counter-current or cross-current. In counter-current classifiers, particles are separated from the fluid in the opposite direction to the main flow. In cross-current classifiers, particles are removed perpendicular to the main flow. Particle separation is usually driven by gravity or inertial forces, like centrifugal forces, which are due to the angular momentum of the flow. As centrifugal acceleration can be much stronger than gravitational acceleration at high tangential velocities, centrifugal classifiers are able to remove smaller particles from the flow than gravity classifiers. In general, counter-current classifiers can provide smaller-cut sizes than cross-current classifiers, with the counter-current centrifugal classifier providing the smallest cut sizes.

The separation mechanism is the element that makes one classifier design different from the other. According to Shapiro and Galperin (2004), and Rumpf (1975), separation techniques can be classified into four different methods, which can be described as follows:

- i. Gravitational counter-current – in this separation technique, particles experience the downward pull of gravity and the uplift due to airflow. The gravitational force (from particle's weight) and drag forces act in opposite directions. Coarse particles, having larger terminal settling velocity than air flow velocity, move downwards and fine particles rise with the stream.
- ii. Gravitational cross-current – in this separation technique, horizontal airflow carries particles until they drop or are carried through the

outlet. In practice, a horizontal current entering the separation chamber expands within it and converges towards the outlet. Particles fed in the chamber will accelerate horizontally by the drag force. Separation occurs due to particles' vertical motion across the air stream. Each particle falls at its own terminal settling velocity. Particles are graded within the separating chamber; with coarse particles close to the inlet and finer particles closer to the outlet (i.e. coarse particles will end at the bottom of the chamber, while fine particles will be carried by the air flow through the outlet).

- iii. Centrifugal counter-current – this technique is distinguished by the flat air vortex generated in a cylindrical chamber with tangential inlet and central outlet. Airflow is fed tangentially into a cylindrical or cone-shaped chamber forming a vortex. Vortex air rotates and flows radially towards the inner chamber. Coarse particles are thrown outwards and migrate to the outlet at the base. Fine particles are entrained in the airflow and migrate to a central outlet. The radial air motion provides the particles' separation track.
- iv. Centrifugal cross-current – in this separation technique, an air vortex is created in a cylindrical chamber with the inlet and outlet placed on opposite sides of the chamber. Particles enter with the air stream through whirl blades, which create a swivel flow. Particles will rotate while travelling radially towards the chamber walls, with velocities depending on their sizes. Larger particles arrive at the wall faster, while smaller particles make it further along the axial direction. Coarse

particles report to the lower outlet and fine particles are entrained in the airflow and migrate to an upper outlet.

These separation techniques are illustrated by Shapiro and Galperin (2004), as shown in Figure 2.6.

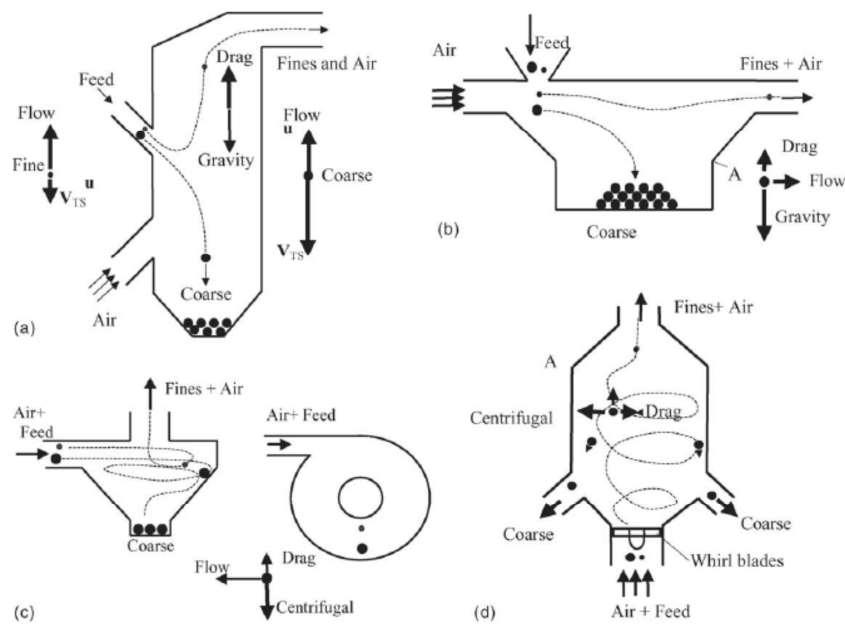


Figure 2.6: Four types of separation techniques: (a) gravitational counter-current, (b) gravitational cross-current, (c) centrifugal counter-current and (d) centrifugal cross-current (Shapiro & Galperin, 2004)

2.4 Coal Classification

Coal classification begins with a coal pulveriser. Coal pulverisation occurs in four stages. The first stage is the drying of raw coal, which is done by using hot air from the heaters; the surface area of coal increases during this stage and exposes fresh coal to the air entrainment to evaporate moisture. The second stage is grinding. Raw coal is fed through a central coal inlet at the top of the pulveriser

and falls due to gravity onto the rotating grinding table. There are three basic types of grinding:

- i. Impaction- where the material is hit or impacted by outside force
- ii. Crushing- where material is forced between two fixed objects
- iii. Attribution- where material is ground by rubbing or friction

During the third stage, circulation, primary air that enters the mill through an aerodynamically ported nozzle circulates coal through the pulveriser. Air circulation is also important in allowing for the removal of heavy materials, such as pyrites and extraneous metal. The final stage is classification; this is a closely controlled three-stage process in the pulveriser, capable of producing finer coal for improved combustion and emission control (Harding, 2003).

During the first stage of classification, fine particles in the housing are carried upwards within the air stream and courser particles fall back to the table for regrinding. It is in the second stage of classification that the velocity in the upper housing decreases and larger particles are dropped out. Only particles fine enough to be entrained in the stream of low-velocity air are carried to the classifier. The final stage of classification takes place in the classifier section at the top of the pulveriser.

A classifier is designed to segregate fine particles from coarse ones. They are mainly used to produce particles in a limited size range. Classifiers use either air or fluid motion to carry coal. However, the air classifier is more commonly used

in the coal industrial application, which uses pneumatics to transport coal in their system. Air classification offers separation by particle density and diameter into the required fractions. It depends on three main factors: (i) velocity of the primary air, (ii) close adjustment of the classifier vanes and (iii) the cyclonic action of the primary air/coal mixture provided by the pulveriser. These factors indirectly determine the classifier geometry. Only particles that are fine enough will be transported to the burners, while coarse ones fall back to the grinding table for regrinding (Carol, 2009).

Several experiments have been carried out to provide a better understanding of coal classification, there are three main factors that should be consciously addressed to optimise the pulveriser at its best condition (Shah, 2009):

- i. Uniform coal mass flow rate to balance air/fuel ratio, which leads to complete combustion.
- ii. Classifier efficiency: more particles will return to the grinder section if the efficiency drops and this will increase the regrinding cost.
- iii. Maximum escaping particle size: if coarse particles escape, combustion will be incomplete and this will lead to reduction in power station efficiency.

An experiment was carried out by Shah (2009) to see the effects of vane settings of the classifier; it was discovered that an optimisation of the vane settings should be decided by interlinking the above three parameters. An experiment was carried out at vane settings 45,55,65 and 100% to find out the impact on the above three

parameters; according to Shah (2009), 65% vane angle was the optimum setting that showed closest uniformity, 60% classifying efficiency and 70% passing 75 μ m sieve.

2.4.1 Types of Air Classifier

Generally, air classifiers are divided into two categories: static and dynamic. Static classifiers are always associated with gravitational separation techniques, while dynamic classifiers are normally of centrifugal.

In many cases, replacing a pulveriser's static classifier with a dynamic classifier improves the unit's grinding performance, reducing the level of unburned carbon in the coal in the process (Storm, 2007).

2.4.1.1 Static Classifiers

Static classifiers consist of air flowing through a separating chamber with product outlets for the coarse and fine particles. There are no moving components in the separation chamber (static). Static classifiers are typically limited to coarse classification with cut sizes between the ranges of 212 micron to 1.7 mm. However, it is possible to have a cut size of up to 75 microns. Early classifiers consisted of vertical chambers with an upward-moving airflow (also known as winnowing machines) that use the gravitational cross-current principle (Figure 2.6b). However, these types of classifiers experienced poor separation efficiency.

Cascade air classifiers are a development of the vertical classifiers, with varieties such as the zig-zag (Figure 2.7) and shelf classifier. Separation efficiency of this type of classifier is improved by disturbing the flow of material as it falls through

the chamber. The existence of air vortexes in the chamber improves the separation.

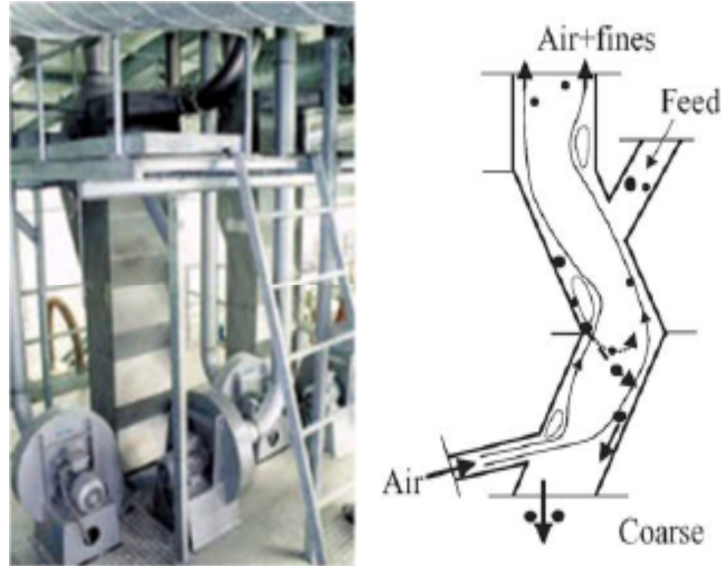


Figure 2.7: Alpine® Multiplex Zig-zag Classifier¹ and its Zig-zag classifier principle (Shapiro & Galperin, 2004)

Fluidised bed static classifiers employ the gravitational counter-current principle. The fluidised state is formed by forcing air up through a bed of feed material with the fine particles breaking away. Coarse particles remain at the bottom of the separator and are removed through the outlet. Fluidised bed classifiers have higher recoveries of fine particles than other classifiers. This is because of the longer residence time in the separator. Fluidised bed classifiers also have the sharpest separation of the static classifiers. Cut points are viable in the size range of 50 microns to 1 mm. Figure 2.8 shows several types of fluidised bed classifier.

¹ Alpine® Multiplex Zig-zag Classifier is a product of Hosokawa Micron Group.

Some static classifiers were designed to have blades, vanes and/or fins, which show some advantages over the rest by having a more delicate adjustment for the air flow motion within the classifier. An example of this type of classifier is shown in Figure 2.9.

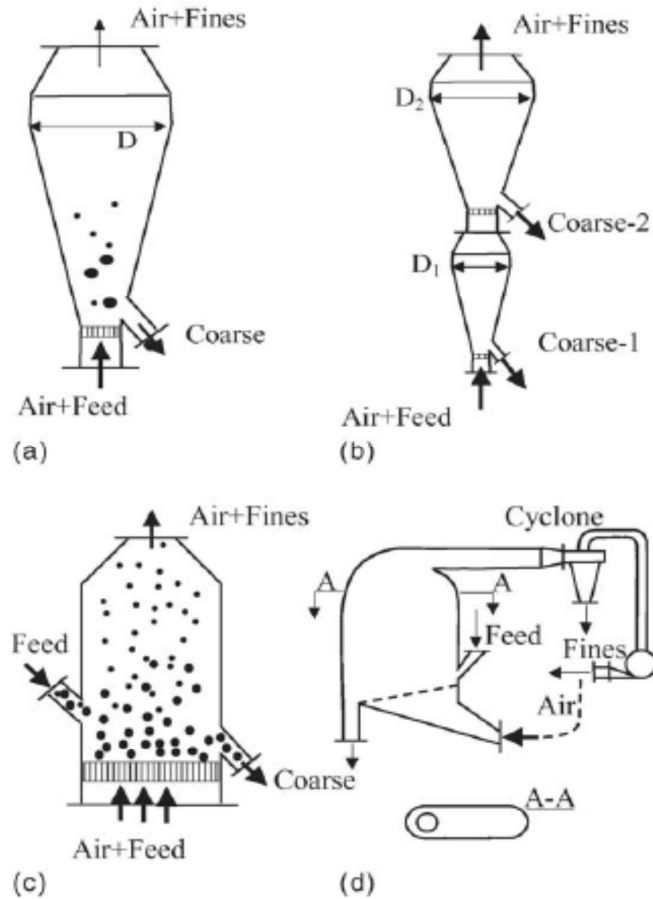


Figure 2.8: Fluidised bed classifiers: (a) single-stage, (b) two-stage, (c) and (d) continuous operation (Shapiro & Galperin, 2004).

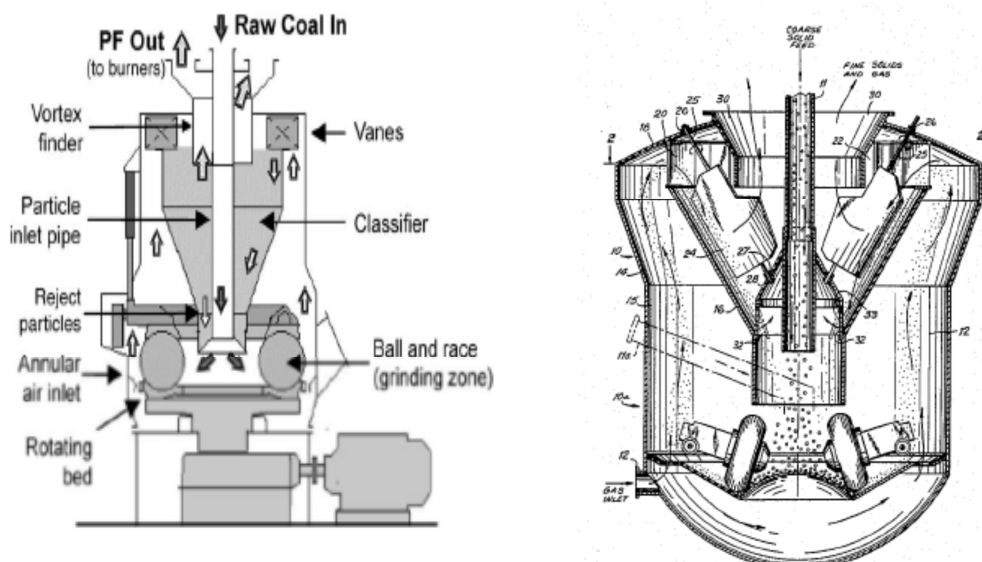


Figure 2.9: Vertical spindle coal mill static classifier (Parham & Easson, 2003).

2.4.1.2 Dynamic Classifiers

Dynamic classifiers usually consist of conical separation chambers that act as a cyclone to create vortices inside the chambers. They generally employ the centrifugal counter-current principle. However, some air classifiers of this type utilise a blend of both gravitational and centrifugal separation. Dynamic classifiers have been recognised as providing finer separations in comparison to static classifiers. They provide a greater degree of cut point control and higher recoveries. Classifiers employing centrifugal force can achieve separation cut points in the range of 5 to 100 microns. The efficiency of dynamic air classifiers is influenced by several factors such as centrifugal force, drag factor, particle concentration and air flow conditions (Galk, 1999).

Vortex air classifiers typically consist of single or double cones. Stationary inclined vanes or adjustable blades are used to create a vortex in the airflow. The feed is entrained in the airflow and introduced to the separator via a tangential inlet into the top of the chamber or an inlet at the base of the chamber. When single cone is used, coarse classification will be delivered, whereas double cones can be used to remove finer materials. A rotating wheel classifier is shown in Figure 2.10 (Karunakumari *et al.* 2005), an example of a vortex dynamic air classifier.

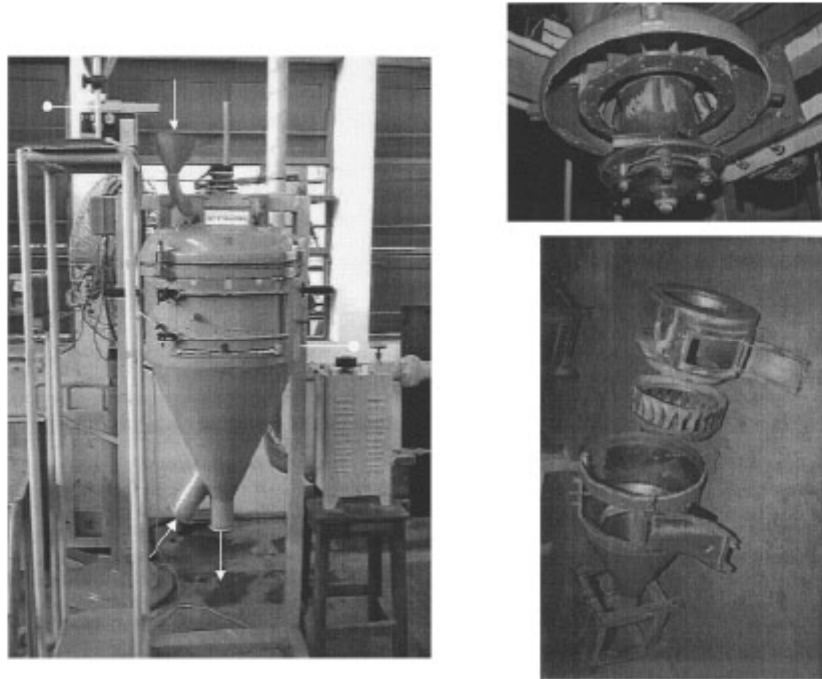


Figure 2.10: Rotating wheel air classifier (Karunakumari *et al.* 2005)

Another type of dynamic classifier is the rotor classifier. Rotor classifiers contain rotating blades that create cyclonic air circulation within the separator. The rotors are mounted on vertical or horizontal shafts. The speed of rotation and airflow velocity are the main factors that determine the cut size in this type of classifier. The rotor classifiers have a high volume throughput. However, controlling the desired cut point is difficult. Figure 2.11 shows an example of rotor type classifiers.

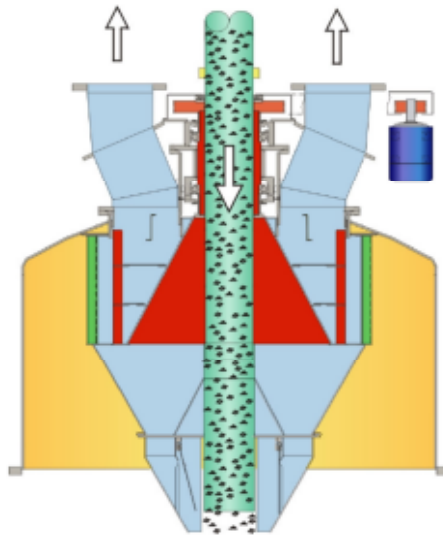


Figure 2.11: Dynamic classifier from Foster Wheeler (Foster Wheeler, 2003)

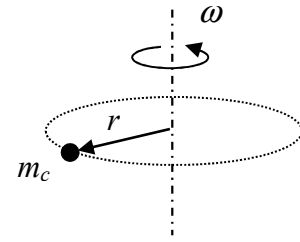
2.4.2 Performance of the Air Classifier

The efficiency of coal classification is influenced by several parameters such as centrifugal force, drag force, particle concentration and flow conditions at the inlet and outlet (Galk, 1999).

Separation is typically measured by efficiency, defined as the fraction of particles of a given size (d) in the feed reporting to the coarse fraction. In coal classification, two dominant forces to be considered are the centrifugal force and the air drag force (Kolacz, 2002). In a dynamic classifier, centrifugal force is the result of the rotational motion of classifier rotor. The air drag forces results from the exposure of coal particles during the transport of the coal materials.

Mathematically, the centrifugal force, F_c , acting on the coal particle (which is assumed to be spherical), can be defined by:

$$\begin{aligned}
F_c &= m_c * \omega^2 r \\
&= (V_c * \rho_c) * \omega^2 * r \\
&= [(4/3 * \pi * r_c^3) * \rho_c] * \omega^2 * r \\
&= \frac{4\pi * r_c^3 * \rho_c * \omega^2 * r}{3}
\end{aligned}$$



(2.1)

where,

V_c – volume of coal particle

ρ_c – density of coal

m_c – mass of coal particle

ω – angular velocity

r – rotor radius

r_c – radius of coal particle

The air drag force, F_D , can be derived from the formula:

$$\begin{aligned}
F_D &= c_d * \rho_a * A_c * u_a^2 / 2 \\
&= c_d * \rho_a * \pi * r_c^2 * u_a^2 / 2
\end{aligned}$$

(2.2)

where,

c_d – drag coefficient

ρ_a – air density (fluid density)

A_c – cross-sectional area of coal particle

r_c – radius of coal particle

u_a – air velocity

Principally, in a balanced condition where the centrifugal force is equal to the drag force (neglecting the buoyant force),² the cut size (d_{50}) of a dynamic classifier can be formulated as follows:

$$r_c = \frac{3 * c_d * \rho_a * u_a^2}{8 * \rho_c * r * \omega^2}$$

i.e.
$$d_{50} = \frac{3 * c_d * \rho_a * u_a^2}{4 * \rho_c * r * \omega^2}$$

From the formula, it is shown that the cut size (d_{50}) depends on air velocity and rotor speed (square in function).

As mentioned previously, additional parameters such as particle concentration, particle shape and flow conditions at the inlet and outlet areas influence the efficiency of coal classifiers. Due to these various random factors, some fine particles are separated with the coarse products and vice versa. The quality of the products can be defined by the proportion of expected particles, which is known as size selectivity or grade efficiency (S_d). The proportion of coarse particles in the coarse product is known as fractional cleanness. Alternatively, the proportion of unwanted particles, such as fine particles in the coarse product, is known as fractional dirtiness. For proper classification, S_d should be low for small particles and high for large particles (Karunakumari, 2005; AIChE, 1993).

Another process factor is sharpness of separation (β), which is the ratio between the mass of any fraction in a product and in the feed. This describes the

² In radial motion the buoyant force is relatively small.

effectiveness of a given classification. For example, 90% efficiency ($\beta = 0.9$) would relate to 90% of the mass of fine particles in the feed reporting to the fines product.

2.5 Principles of Gas-Solid Flows

The most important fundamental and physical concept for the separation of the solid particles and the gas flow is to grasp the behaviour of the motion of sub-micron particles, fine particles and coarse particles.

The three vital characteristics of an individual particle are its composition, size and shape. Composition determines properties such as density and conductivity, provided that the particle is completely uniform. In many cases, however, the particle is porous or consists of a continuous matrix, in which is a distribution of small particles of a second material. Particle size is important as it affects the surface per unit volume and the rate at which a particle will settle in a fluid. A particle shape may be regular, such as spherical or cubic, or it may be irregular, for example, like a piece of broken glass. Regular shapes can be precisely defined by mathematical equations. Irregular shapes cannot, and the properties of irregular particles are usually expressed in terms of the particular characteristics of a regular-shaped particle.

2.5.1 Size and Properties of Particles

The simplest shape of a particle is the sphere. Due to its symmetry, questions of orientation do not have to be considered, since the particle looks exactly the same from every direction and behaves in the same manner as a fluid, heedless of its

orientation. No other particle has this characteristic. Frequently, the size of a particle of irregular shape is defined in terms of the size of an equivalent sphere. However, the particle is represented by a sphere of different size according to the properties selected. Some of the important properties of equivalent spheres are:

- i. The sphere has the same volume as the particle.
- ii. The sphere has the same surface area as the particle.
- iii. The sphere has the same surface area per unit volume as the particle.
- iv. The sphere has the same area as the particle when projected onto a plane perpendicular to its direction of motion.
- v. The sphere has the same projected area as the particle, as viewed from above, when lying in its position of maximum stability, such as on a microscope slide.
- vi. The sphere will manage to pass through the same size of square aperture as the particle on a screen.
- vii. The sphere has the same settling velocity as the particle in a specified fluid.

Several definitions depend on the measurement of a particle in a particular orientation.

Thus Feret's statistical diameter is the mean distance apart between two parallel lines that are tangential to the particle in a randomly fixed direction, heedless of each particle's orientation when coming up for inspection. This is shown in Figure 2.12.

A measure of particle shape that is frequently used is the sphericity, ψ , defined as:

$$\psi = \frac{\text{surface area of a sphere the same volume as the particle}}{\text{particle's surface area}}$$

Another method of indicating shape is to use the factor by which the cube of the size of the particle must be multiplied to give the volume. In this case, the particle size is usually defined by method (e).

Other properties of the particle that may be of importance are whether it is crystalline or amorphous, whether it is porous and what the properties of its surface are, including roughness and presence of adsorbed films.

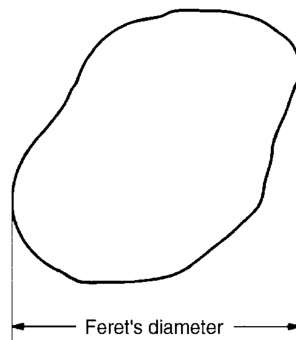


Figure 2.12: Feret's diameter

2.5.2 Particle Fluid Interaction

Particle's trajectories are heavily affected by interactions with the air, which transports them as they travel through pneumatic conveying pipelines. As the particles are given energy by the air, the energy of the air is lessened. This leads to two things; the first is that the pressure drops severely in the whole system, and

the second is a reduction of turbulence in localised regions. Smaller particles are more effective in reducing the turbulence energy because larger particles disregard the turbulence fluctuations and their trajectories are not affected (Ljus *et al.* 2002). In fact, larger particles are known to boost turbulence. Irregularly shaped particles reduce the intensity of turbulence within the whole pipe, whereas spherical particles increase turbulence intensity at the centre of the pipe while decreasing it by the walls.

The interaction of the fluid on particles is never more at the front than when around bends. This interaction, or lack of, causes roping. If the fluid has a large effect on the particle, it will travel around a 90° bend without having contact with the wall, as in the case of Fokeer's 'Dilute Phase'. For most PF particles, the particle-fluid interaction is not significant enough to result in ropes. The Stokes number is considered so as to predict the scale of the interaction. When the Stokes number is much higher than one ($St \gg 1$) the fluid has less effect on the particle, whereas a Stokes number much lower than one ($St \ll 1$) suggests the opposite.

2.5.3 Particle-Particle Interaction

Understanding the interaction between particles is not easy, especially when it involve a great many of them. It is understood particle-particle interactions involve the transfer of energy between particles and the loss of energy in the form of heat to the surroundings. This eventually decreases the particles' velocity in dense rope region where collisions are more regular (Akilli, 2001).

According to Sommerfeld (2001), particle–particle interactions have a strong influence on density profile, even at low loadings (air fuel ratio of 10 to 1). He and Cartaxo (2001) have successfully generated codes that are able to predict the particles collision process. However, according to Giddings (2004), analysis can still be precise and instructive without modelling the particle interactions.

2.5.4 Particle–Wall Interaction

Rope normally formed on the pipe wall. The understanding of particle–wall collisions, which determines rope dispersion, is very important. Sommerfeld (1999 & 2002) suggests that increasing the pipe’s wall roughness can reduce the horizontal dropout considerably. A rougher wall will create collisions with greater impact angles, as shown in Figure 2.13.

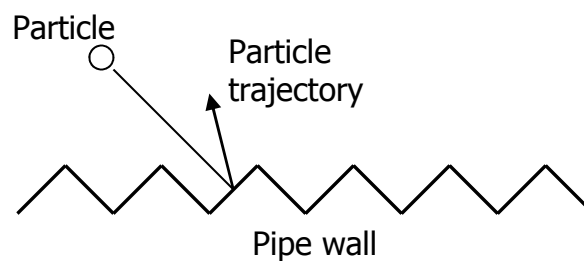


Figure 2.13: Rough wall particles’ collision

2.5.5 Dynamics of the Particulate Phase

Pressure differences across the inlet orifice accelerate the inlet air flow. The fluid enters tangential to the enclosure walls in a slightly upward direction, which then flows radially into the main separation zone. The characteristic of the incoming fluid, together with the geometry of the classifier, creates a strong vortex flow

field. The vortex field has pressure gradients that accelerate the flowing fluid in both axial and radial directions.

Employing the Newton equation of motion, the dynamics of particles moving through fluid can easily be analysed by understanding the forces acting on the particle in both axial and radial directions. The following sections describe the dynamic analysis of the moving particle in axial and radial directions.

2.5.5.1 Dynamics Analysis of Particle in Axial Direction

In the axial direction, the forces acting on the particle are the gravitational force (weight), the buoyant force and the drag force. The buoyant force (F_B) acts in opposition to the gravitational force (W). The drag force (F_D) is the force in the direction of flow exerted by the fluid on the solid, which exists whenever there is relative motion between the particle and the fluid. The forces acting on the particle in axial motion are illustrated in Figure 2.14 below.

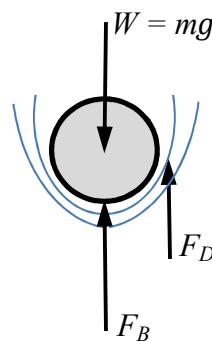


Figure 2.14: Forces acting on coal particle in axial motion

From Newton's Second Law ($\Sigma F = ma$),

$$W - F_B - F_D = ma = m \frac{du_A}{dt} \quad (2.3)$$

In this equation, u_A is the velocity of the particle relative to the fluid and is directed upwards along axial axis, m is particle mass and a is the particle acceleration.

The buoyant force is the product of the mass of the fluid displaced by the particle and the acceleration of the mass in motion (i.e. the gravity). The mass of the fluid displaced by the particle is obtained by considering Archimedes' law,

i.e. $V_f = V_c$

$$\frac{m_f}{\rho_f} = \frac{m_c}{\rho_c}$$

$$m_f = \frac{m_c \rho_f}{\rho_c}$$

where,

V_f – fluid volume

V_c – coal volume

ρ_f – fluid density

ρ_c – coal density

m_f – fluid mass

m_c – coal particle mass

Hence, the buoyant force,

$$F_B = m_f \cdot g$$

$$F_B = \frac{m_c \rho_f}{\rho_c} \cdot g \tag{2.4}$$

Substituting eq. (2.2) and (2.4) into eq. (2.3),

$$m_c \frac{du_A}{dt} = m_c g - \frac{m_c \rho_f}{\rho_c} \cdot g - c_d \rho_f \pi r_c^2 u_A^2 / 2$$

i.e.

$$\begin{aligned} \frac{du_A}{dt} &= g - \frac{\rho_f}{\rho_c} \cdot g - \frac{c_d \rho_f \pi r_c^2 u_A^2}{2m_c} \\ &= g \frac{\rho_c - \rho_f}{\rho_c} - \frac{c_d \rho_f \pi r_c^2 u_A^2}{2m_c} \end{aligned}$$

In gravitational settling, g is constant and the drag always increases with velocity. The acceleration decreases with time and approaches zero. The particle quickly reaches a constant velocity (terminal velocity³), which is the maximum attainable under the circumstances. Thus,

$$\frac{du_A}{dt} = g \frac{\rho_c - \rho_f}{\rho_c} - \frac{c_d \rho_f \pi r_c^2 u_A^2}{2m_c} = 0$$

i.e.

$$u_A^2 = \frac{2g(\rho_c - \rho_f)m_c}{c_d \rho_c \rho_f \pi r_c^2}$$

Assuming the coal particles are spheres of diameter D_c , the coal mass,

$$\begin{aligned} m_c &= \rho_c V_c \\ &= \rho_c \frac{4}{3} \pi \left(\frac{D_c}{2}\right)^3 \\ &= \rho_c \pi \left(\frac{D_c^3}{6}\right) \end{aligned}$$

³ At one point, coal particle of one particular diameter will stop accelerating altogether and continue to fall at a constant speed, which is its terminal velocity. In axial motion, higher terminal velocity results in the particle reaching the classifier bed more quickly.

Hence,

$$\begin{aligned}
 u_A^2 &= \frac{2g(\rho_c - \rho_f)\rho_c\pi\left(\frac{D_c^3}{6}\right)}{c_d\rho_c\rho_f\pi\left(\frac{D_c^2}{4}\right)} \\
 &= \frac{4g(\rho_c - \rho_f)D_c}{3c_d\rho_f} \tag{2.5}
 \end{aligned}$$

Drag coefficient, c_d is a function of Reynolds number. Reynolds number is formulated as,

$$Re = \frac{u_A\rho_f D_c}{\mu}$$

where μ is fluid kinematic viscosity. For Stokes flow (low Reynolds number),

$$\begin{aligned}
 c_d &= 24/Re \\
 &= \frac{24\mu}{u_A\rho_f D_c} \tag{2.6}
 \end{aligned}$$

Substituting eq. (2.5) into eq. (2.6), the axial terminal velocity for any coal particle diameter can be obtained,

$$\begin{aligned}
 u_A^2 &= \frac{4g(\rho_c - \rho_f)D_c}{3\left(\frac{24\mu}{u_A\rho_f D_c}\right)\rho_f} \\
 u_A &= \frac{g(\rho_c - \rho_f)D_c^2}{18\mu} \tag{2.7}
 \end{aligned}$$

2.5.5.2 Dynamic Analysis of Particle in Radial Direction

In the radial direction, the forces acting on the particle are the centrifugal force (due to angular speed), the radial buoyant force and the drag force. The forces acting on the particle in radial motion are illustrated in Figure 2.15 below.

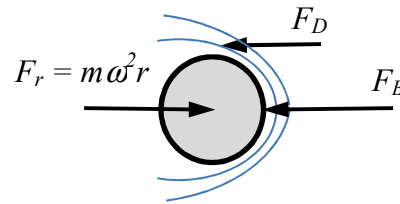


Figure 2.15: Forces acting on coal particle in radial motion

Applying Newton's Second Law,

$$F_r - F_B - F_D = ma = m \frac{du_R}{dt} \quad (2.8)$$

In this equation, u_R is the velocity of the particle relative to the fluid and is directed outwardly along the radial axis.

In the radial motion, the buoyant force is the product of the mass of the fluid displaced by the particle and the acceleration of the mass due to rotational motion ($\omega^2 r$). Once again, through consideration of the Archimedes' principle, the mass of the fluid displaced by the particle can be obtained,

i.e.
$$m_f = \frac{m_p \rho_f}{\rho_c}$$

The buoyant force,

$$F_B = \frac{m_c \rho_f}{\rho_c} \cdot \omega^2 r \quad (2.9)$$

where r is the distance from the center of classifier.

Substituting eq. (2.2) and (2.9) into eq. (2.8),

$$m_c \frac{du_R}{dt} = m_c \omega^2 r - \frac{m_c \rho_f}{\rho_c} \cdot g - c_d \rho_f \pi r_c^2 u_R^2 / 2$$

$$\text{i.e.} \quad \frac{du_R}{dt} = \omega^2 r \frac{\rho_c - \rho_f}{\rho_c} - \frac{c_d \rho_f \pi r_c^2 u_R^2}{2m_c}$$

In the motion resulting from the centrifugal force, the angular velocity depends on the radius and the acceleration is not constant. However du/dt is normally small and can be neglected; the radial terminal velocity can be formulated as follows,

$$\frac{du_R}{dt} = \omega^2 r \frac{\rho_c - \rho_f}{\rho_c} - \frac{c_d \rho_f \pi r_c^2 u_R^2}{2m_c} = 0$$

$$\text{i.e.} \quad u_R^2 = \frac{2\omega^2 r (\rho_c - \rho_f) m_c}{c_d \rho_c \rho_f \pi r_c^2}$$

With the assumption that coal particles are spheres,

$$u_R^2 = \frac{4\omega^2 r (\rho_c - \rho_f) D_c}{3c_d \rho_f} \quad (2.10)$$

Hence, the radial terminal velocity for a particular coal particle diameter is,

$$u_R = \frac{\omega^2 r(\rho_c - \rho_f) D_c^2}{18\mu} \quad (2.11)$$

In this section, the axial and radial terminal velocities have been formulated. With respect to this, the information regarding axial, radial and tangential velocities inside the classifier (i.e. velocity profiles) helps to provide a better prediction of the particle motion inside the classifier. In general, if the axial velocity is greater than the axial terminal velocity of a particle, the particle will move upwards. A large radial velocity (larger than the radial terminal velocity) will assist the particle to move towards the classifier core. Meanwhile, the tangential velocity determines the magnitude of the angular speed (ω), which indirectly influences the magnitude of the radial terminal velocity.

2.6 Related Studies

Due to the cost, time consumed and difficulties in organising laboratory and/or simulation study, research on classifiers is not very prevalent. To date, no researcher has completed a comprehensive study on classifier performance that is able to relate classifier performances with the effect of exploiting various classifier parameters. This section will look into a few researches that have been carried out by some researchers.

Parham (2003), for example, conducted research into the flow visualisation on a reduced scaled model to provide data for improving separation particles using Laser Doppler Anemometry Measurement. The study found that the effect of varying the inlet vane angle within the range of industrially useful principally

affected only the tangential velocity magnitude. No conclusions were provided as to the other effects of vane angle on other velocity components.

Similar work by Karunakumari *et al.* (2005) was conducted experimentally as well as numerically. However, their work places emphasis more on visualising the flow pattern rather than the velocity profile inside the classifier. Thus, the research does not provide a significant conclusion between flow distribution and particle distribution. Furthermore, the vane parameters studied were limited to radial (90°) and angular (0°) vanes only, which are not common in coal power plant applications.

To evaluate the uniform flow rate and desired size fraction at the outlet, Shah (2009) carried out a numerical study for different vane settings. The study focused only on the effect of vane angle on particle size, without considering the flow distribution and its effect. Results indicate that the optimum opening for the vanes is 65% for selected utility, which leads to closest uniformity with 60% classifying efficiency, wherein 70% particles pass through 75 μm sieve.

A study to examine the flow path in the grinding chamber, separator and classifier was carried out by Bhasker (2001). The study was conducted solely through the use of simulation, without any validation. Results from the study did provide valuable insight for designers on optimisation of the components for better efficiency, but no relationship with the particle distribution was documented.

It is also noted that gas-solid flows have been widely researched; there are a great deal of articles on the subject, but there have been few in-depth investigations into coal classifier performance and flow characteristics. Research by Ogawa (1984) and Jordan *et al.* (2003) has proven that there are reasonable agreements between experiment and CFD simulations. With the advancement of microprocessor technology, computational power has reached a level of affordability so that those complex flow situations can be solved using CFD programmes. The simulation output provides a better knowledge of the workability and feasibility of the rig, and also supplies useful guidance in finalising the design. Any disagreement or failure in the model simulation indicates that the design is not able to perform within predetermined working conditions and is not appropriate for manufacture. Thus, modifications of the design have to be carried out.

Although there are some other researches being conducted on classifiers, most of the classifiers being studied are not related to coal power plant application. This study focuses on the effects of varying vane angles, inlet velocity and outlet positions on the classification of particles within a lab-sized classifier.

2.7 Conclusion

In this chapter, an introduction to the problems regarding the use of coal, the classifier technology and the theories related to classifier's particles reactions and flow dynamics has been presented. The intention is to give readers an introduction to, and some basic information regarding, the field, as well as closely allied theory. This will help to better understand the work presented in the later chapter.

CHAPTER THREE: EXPERIMENTAL RIG DESIGN

This chapter describes the experimental rig used in this study. Experimental work was carried out on the test rig at the University of Leicester.

The rig was built to be capable of modelling the fuel loading conditions of a coal-fired power plant. The effects on the controlled parameters can be tested accurately on the scaled rig and are comparable to an actual scale classifier.

The first section of the chapter gives a description of the rig and its function. The second section provides the details of the experiment instrumentation. The third section contains information on the particles selected for the experiment. The fourth section explains the dynamic similarity of the one-third scaled rig.

3.1 The Design of a Scaled Classifier Model

A one-third scale test facility was used in this work and was constructed at the University of Leicester. The rig was designed to mimic an industrial air classifier. It was used to provide experimental data for the further understanding of the coal classification process, the engineered improvements to the classifier and, hence, the classification process.

The rig is a scaled down version of an industrial air classifier with a static blade configuration to reduce mechanical failure. It was designed with a clear body for

ease of monitoring the flow. Removable parts were used to allow an interchangeable variety of the classifying properties, as well as for the purpose of maintenance simplicity.

The main objective of the model-scaled classifier is to reduce the size of a current working classifier to a laboratory size, in order to ease the study of the airflow inside the classifier. Overall, the design has to meet the following objectives:

- good optical access
- static blades to reduce the risk of mechanical failure
- detachable parts for ease of maintenance and implementation of new concepts
- controllable vane angle for varying classification properties

3.2 Design Candidates

The final design of the model classifier was decided based upon evaluation of existing patents and designs. Figure 3.1 through to Figure 3.4 are examples of the design candidates.

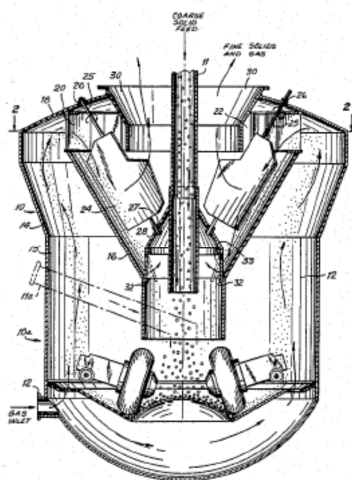


Figure 3.1: Static blades classifier with fins (Diggins, 1985)

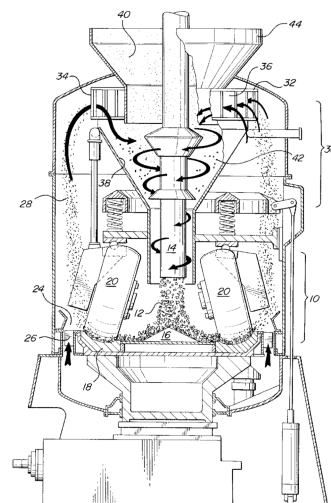


Figure 3.2: Classifier with rotating vane (Nardi, 1999)

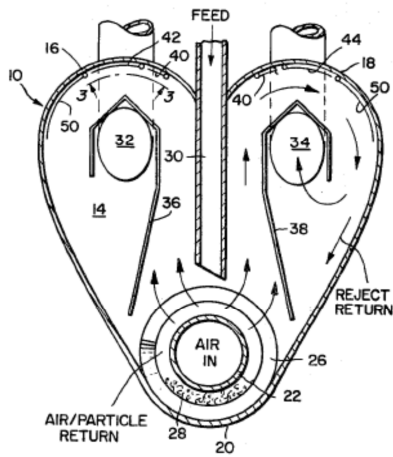


Figure 3.3: Old classifier design
(Trozzi, 1984)

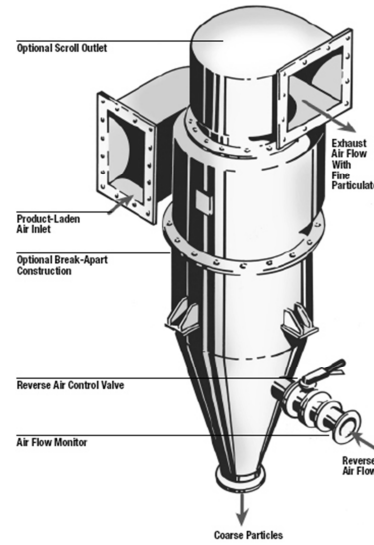


Figure 3.4: Cyclone air classifier
(Northland, 2007)

From the design candidates, the classifier's aerodynamic properties were fully realised and a suitable design was selected from the list of working classifiers. The initial design was decided after choosing from a list of working models. The rig was first verified and then passed on for a detailed design. Below are the features chosen and considered for the design:

- Basic static blade classifier offers the basic concept design for the model-scaled classifier
- Cyclone air classifiers offer the small-scale requirement for the design
- A classifier with vanes was chosen because it has an advantage over the rest in that it has a more delicate adjustment for the air flow motion within the classifier
- Modifications completed on the existing design:
 - Scaled down to a laboratory size

- Smaller sections for inter-changeability
- See-through body for observation
- Ability to change vane angle to give different results
- Ease of access for cleaning and maintenance purposes
- Miller or pulveriser was omitted as there will be no milling
- Air blower was connected to generate air flow
- A custom feeder used to feed in particles
- Cyclone with collection hopper was fitted to the outlet pipe to help with air and particle separation
- Air filter was connected to cyclone to make sure no particles are released to the air

3.3 The Model Classifier

Figure 3.5 shows a 3-D illustration of the built model classifier, while Figure 3.6 demonstrates the actual system. Features of the classifier include the cone, the vanes, a particle feeder, an outlet, a cyclone, an air filter and a tangential air inlet.

The laboratory scale model is about a third of the size of a typical classifier. Its design was created based upon the design of the vertical spindle mill static classifier with one outlet. The outer diameter of the model is 1.2m, the diameter of the classifier cone at the outer flange is 790mm and the diameter of the inner pipe is 150mm. The classifier cone is set at an angle of 70°. As the model was designed to simulate only the aerodynamic features of a coal mill, the grinding bed and related components (of a pulveriser system) are not required, and thus are not included. Perspex and polycarbonate sheets acted as the window to provide

optical access, as it is uneconomical to fabricate a full transparent model of this scale.

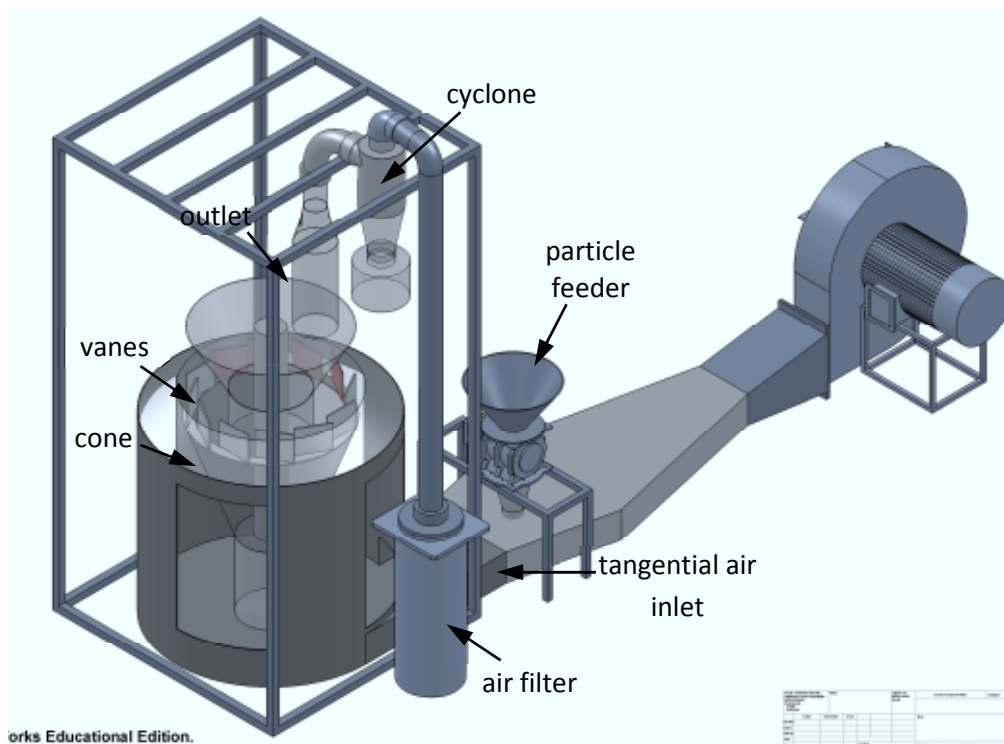


Figure 3.5: A 3-D illustration of the built model classifier

The model operates under positive pressure, thus the air is blown by a centrifugal fan through the inlet. In a two-phase configuration (gas-particle), glass particles are injected through the feeder in front of the fan, which sweeps the particles along. The air particles exit through the outlet (in both single- and two-phase configurations) into a single 200mm-diameter pipe that connects the model to the fan. The classifier consists of twelve vanes 150mm in height and 180mm in width; flat panels pivoted at the top and bottom on a pitch circle diameter of 790mm. The top of the vanes are fitted into the upper cover and the vane angle control mechanism, in order to allow the vane angle to be controlled and set to the desired

angle. The following sections provide the details of each component of the model classifier.

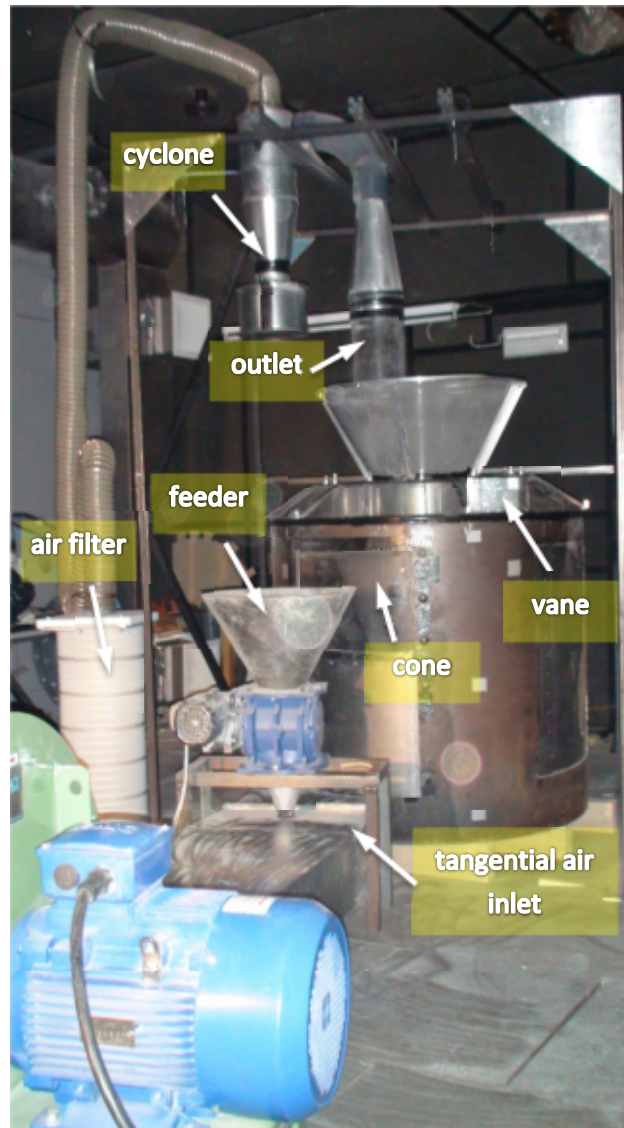


Figure 3.6: The actual built model classifier

3.3.1 Classifier Housing Body

The classifier body was designed to enable users to view the airflow patterns inside the classifier; hence, Perspex is used as an enclosure. Figure 3.7 shows the classifier housing body.



Figure 3.7: Classifier housing body

3.3.2 The Classifier System

The main part of the classifier system is the cone and vane (Figure 3.8) within the centre core. The vane angle, relative to the radial line through the central axis, can be varied from 0° to 90° . Increasing the vane angle is likely to increase the particle separation efficiency of the classifier (Parham, 2003). The vanes are designed to channel the air, together with the particles, into the centre core and create a cyclonic effect inside the cone. Heavier particles will flow deeper into the centre core, while lighter particles will flow upwards together with the air.

Velocity of the cyclone flow can be varied by adjusting the angle of the vanes.

Figure 3.9 shows the control mechanism that assists the change of the vane angle.

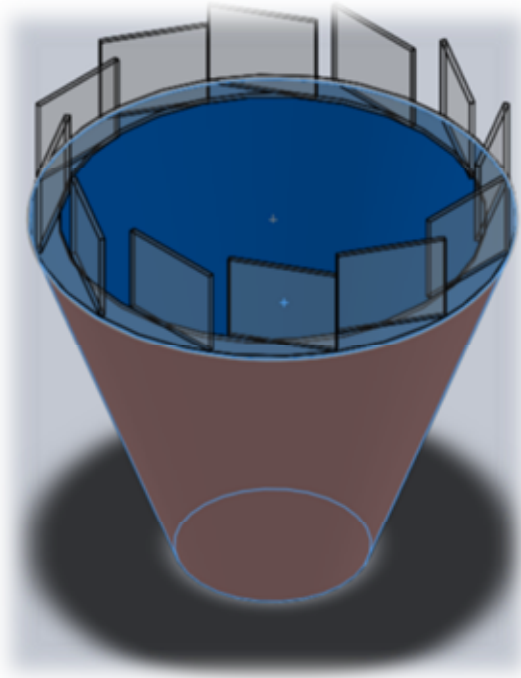


Figure 3.8: Separation cone and vanes

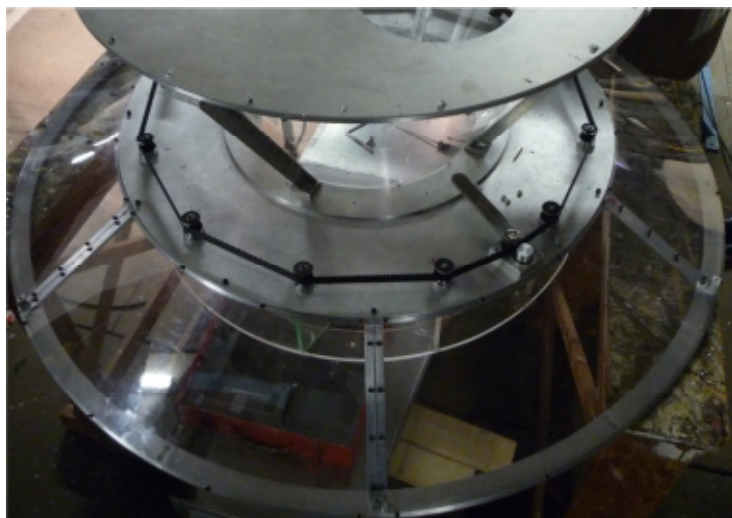


Figure 3.9: Mechanism for controlling the vane angle

3.3.3 Classifier Air Flow

Air is induced into the system through the side of the classifier (tangential air inlet). A blower is used to blow the air into the system as well as thrust the flow to the outer ring of the inner body to simulate air flow in an industrial classifier. The tangential air inlet creates swirl flow and mimics the function of the grinder, as it was omitted in the design. Figure 3.10 shows the blower fan. The fan is electrically controlled by utilising a frequency controller.



Figure 3.10: The blower fan (below) and its frequency controller (above)

The calibration of the blower fan is illustrated in the graph shown in Figure 3.11.

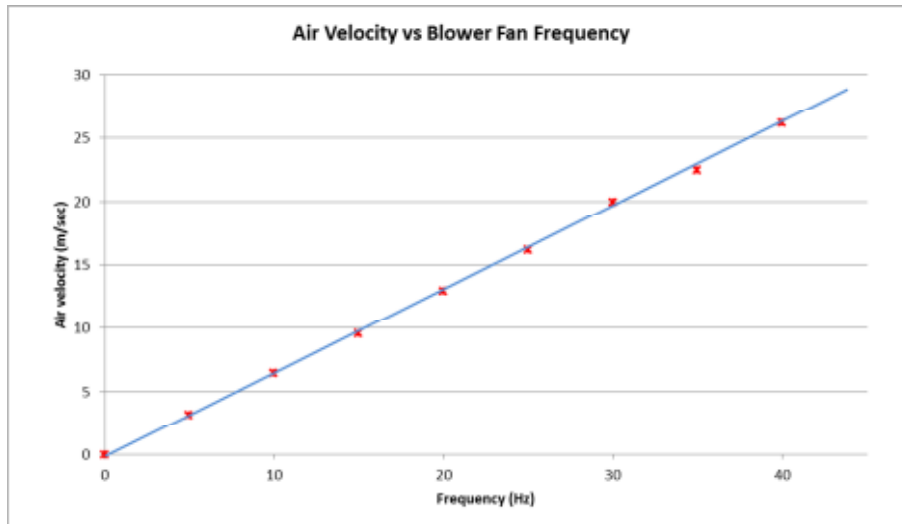


Figure 3.11: The blower fan calibration graph

3.3.4 Particle Feeder

The rotary feeder shown in Figure 3.12 controls the volume of powder feed rate into the system. The motor speed is set at the controller. Figure 3.13 shows the calibration graph of the particle feeder.



Figure 3.12: Particle feeder

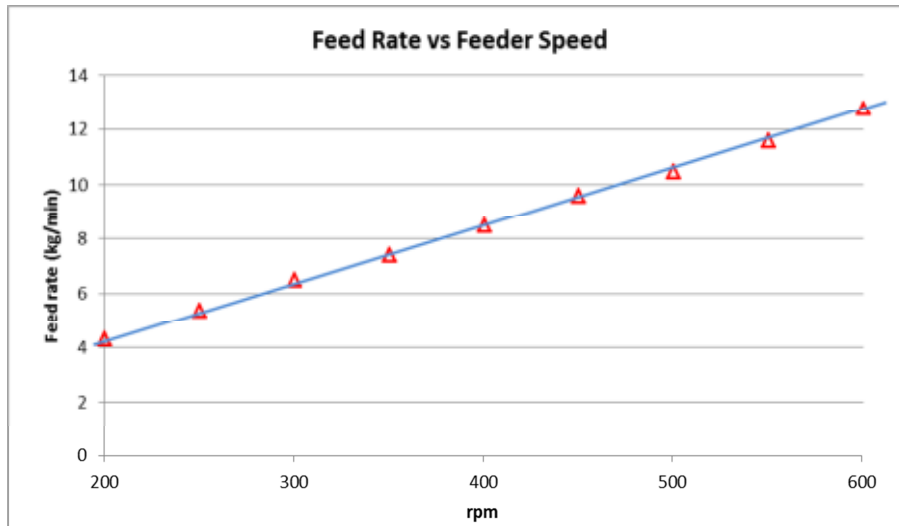


Figure 3.13: Particle feeder calibration graph

3.3.5 The Particle Outlet

Figure 3.14 shows the rig cover with the particle outlet. The cover helps to hold the centre unit in place. It also acts as a channel for heavy particles to flow downstream and influence the desired flow characteristics.

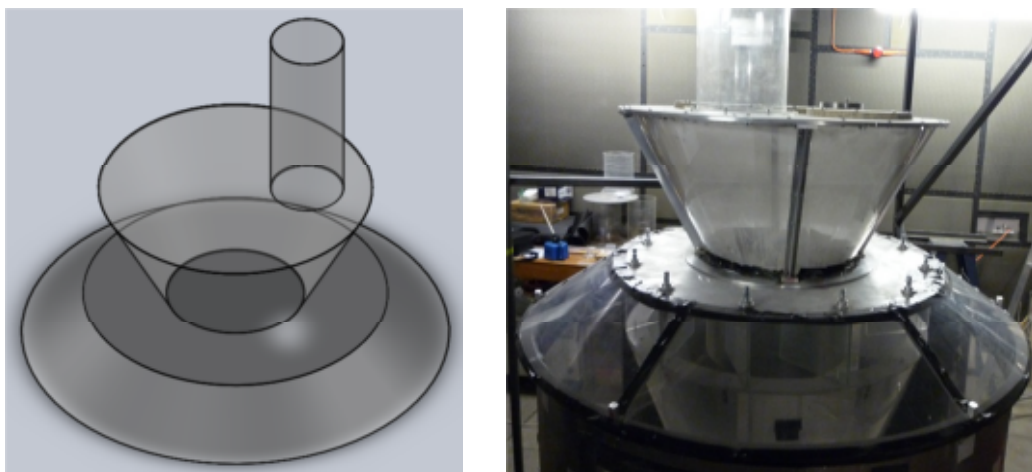


Figure 3.14: Particle outlet

3.3.6 The Cyclone

Cyclonic separation was used to remove the particles from the air through vortex separation. Figure 3.15 shows the cyclone used in the model classifier. Rotational effects and gravitational force separate the mixture of solids and fluids. The mixture of Fillite and air entered the cyclone from the outlet of the model classifier. The incoming air-particle mixture entered the cyclone and was forced around the system, forming a vortex. As the larger particles were pushed outside by centrifugal forces, the smaller particles stayed at the centre of the vortex.

At the bottom of the cyclone, the larger particles fell into a hopper attached underneath the cyclone. This hopper is removable. The air at the middle exited through the gas outlet tube at the top. This outlet tube is more commonly known as a vortex finder. As the air rushed up the centre of the system, it picked up the smaller particles and removed them. The particles trapped in the hopper were then weighed.

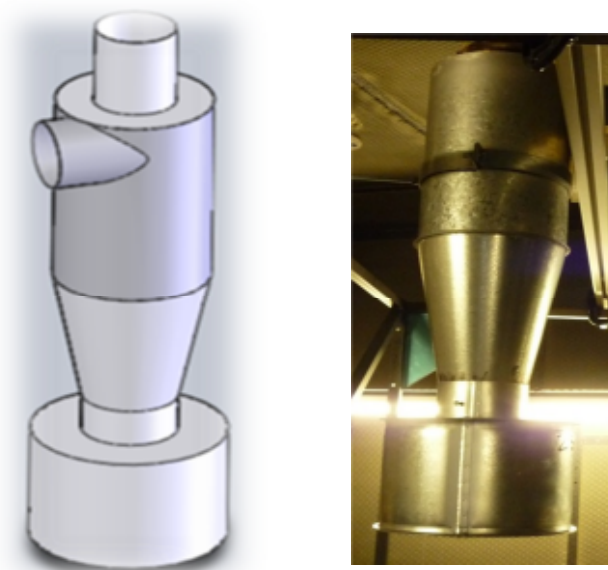


Figure 3.15: The outlet cyclone

3.3.7 The Filter

A particulate air filter is a device that removes solid particulates from the air. The air filter is used to maintain air quality in the laboratory. The filter is connected to the cyclone. The air released from the cyclone is filtered before escaping. Figure 3.16 shows the filter used to filter the air released from the cyclone.



Figure 3.16: The air filter for the clean air from the cyclone

3.4 Air Velocity Measurement

As mentioned in Section 3.3.4, the motor speed is set at the frequency controller. From the calibration graph, it was found that a 20Hz on the display will produce an air velocity of approximately 13m/s. Before each test was started, velocity measurements were taken using a pitot tube at the location across the pipe between the main body and the blower. Figure 3.17 shows the set up.

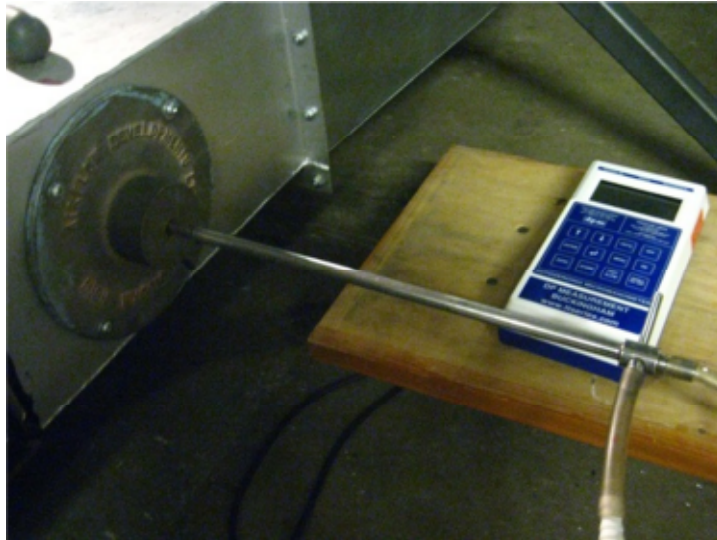


Figure 3.17: Velocity measurement at the inlet

Prior to running the experiment with particles, air velocity was also measured. The test rig was run without any particles being fed. The readings were taken to see the flow behaviour inside the model classifier.

Figure 3.18 shows a schematic diagram of the air velocity measurement conducted using the pitot tube. The velocity measurements were taken at four axial locations between the inlet and outlets. Figure 3.19 illustrates the measurements locations. For validation purposes, the velocities are measured along lines A, B, C and D, shown in the figure.

The purpose of conducting this study is to investigate the flow structure of the dominant velocity component at the annular region between the enclosure and central cone. This is the transportation region where the coal-particle flow is directed into the main separation region (cone) via guide vanes before reaching the outlets. Gravitational separation is also expected to occur in this zone, as

heavier particles will fall back down to the floor or grinding bed. The preliminary tests also involve study into the effect of the radial guide vane angles on the inlet flow to the centrifugal separation zone.

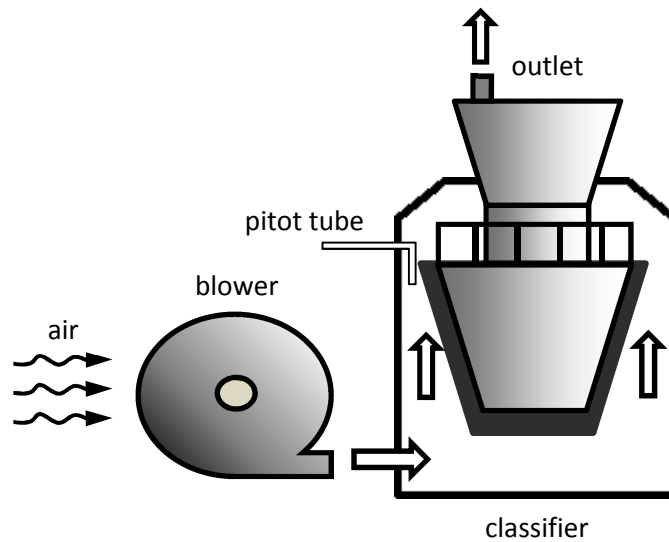


Figure 3.18: Schematic diagram for air measurement

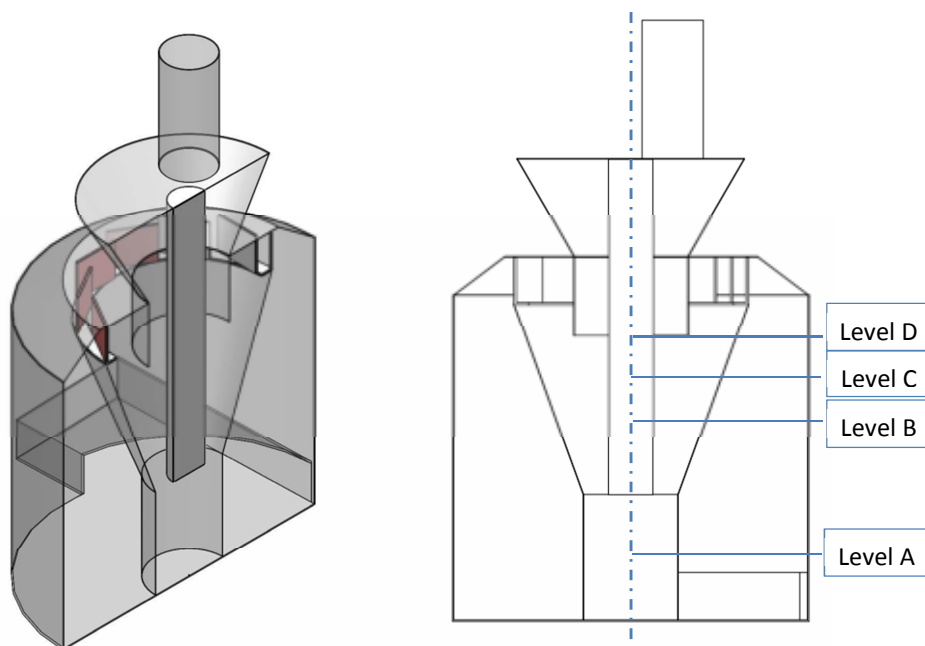


Figure 3.19: The measurement locations

The geometrically similar model to the Babcock 10E mill was designed and the dynamic non-dimensional numbers, such as the swirl, Reynolds, Stokes and

Froude numbers, were made comparable to the real coal classifier cases. Figure 3.20 shows the experimental setup, while Figure 3.21 shows the flowchart for air velocity measurement.

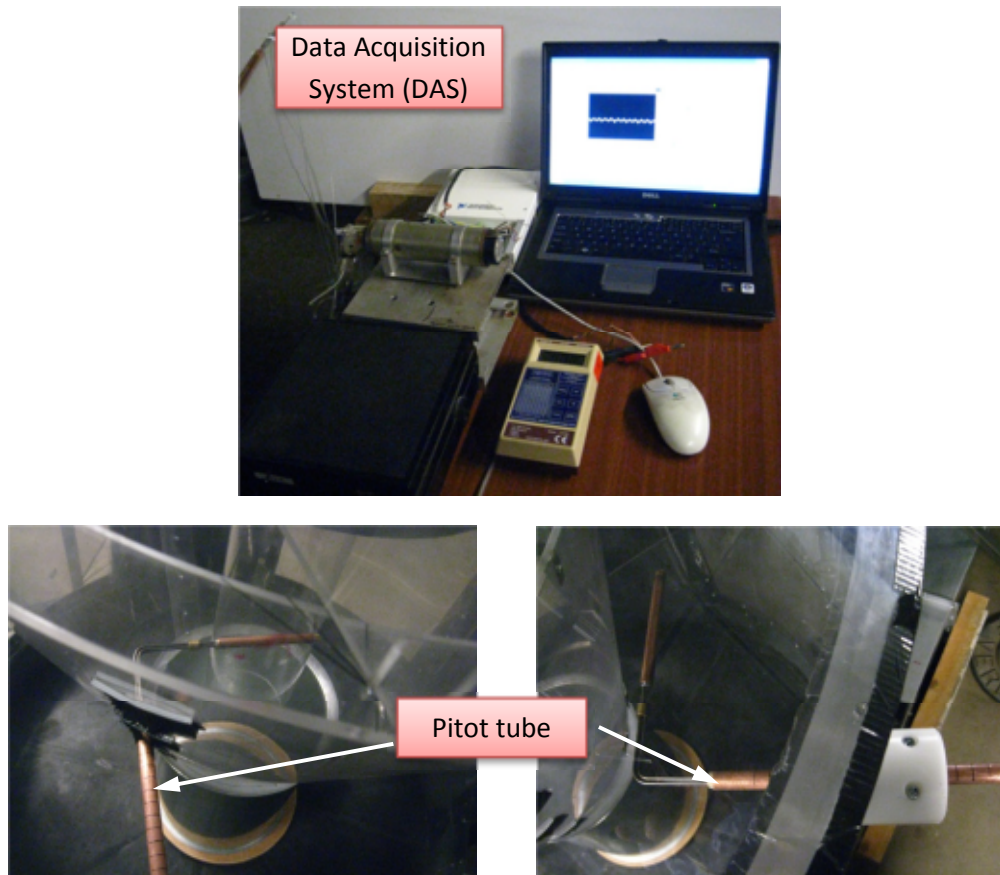


Figure 3.20: The experimental setup

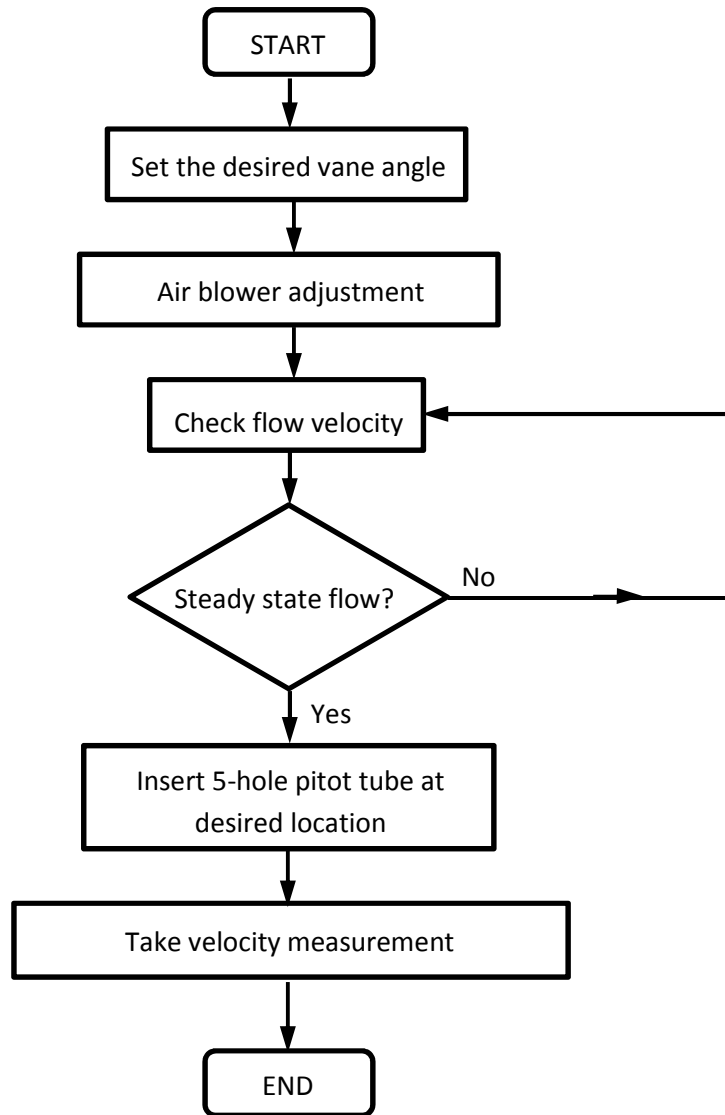


Figure 3.21: Velocity measurement procedure

3.4.1 Five-Hole Pitot Tube

The air velocity measurement was taken in order to determine the axial, radial and tangential velocity components inside the classifier model. The measurement was completed using a five-hole pitot tube mounted in such a way that it lay directly to the direction of the airflow. All holes were situated on the tip of an extended probe head. One hole was at the precise center of the head, while the remaining four were oriented at 45° angles in each compass direction, adjacent to the center hole, as shown in Figure 3.22. The pitot tube was held using an external

positioning flange mounting plate. Once the tube was adjusted to an appropriate depth, a smaller hex tightening bush was used to lock its position. All the data acquired were compared against the calibration data provided in order to get the velocity component.

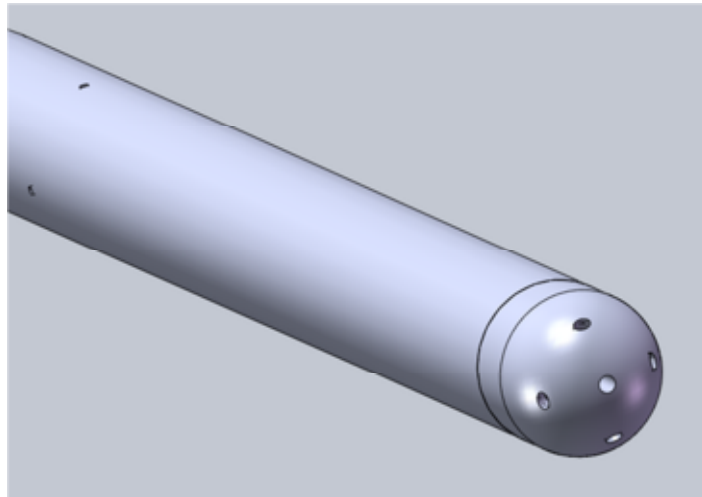


Figure 3.22: Five-hole pitot tube

3.4.2 Air Flow Measurement

To assist the collection and processing of experimental data, LabVIEW software was used. LabVIEW is powerful software for developing a PC-based Data Acquisition System (DAS). As opposed to a text-based language, LabVIEW uses a graphical programming language where the user creates programs in block diagram form. The software allows the creation of a front panel Graphical User Interface (GUI) for DAS instrumentation. The system converts voltages to the corresponding units, displays the graphs on the monitor and writes them to a MS Excel file.

The PC-based DAS was used to read each of the six input air measurement data from the five holes in the pitot tube. The five-hole pitot tube was connected to a scanni-valve, which enabled one pressure reading to sequentially measure a number of different taps. The LabVIEW program took one hundred samples of data a second from each input and presented an average voltage over that time.

3.5 Tuft Visualisation

Additional qualitative data was taken inside the model to establish the flow patterns. Flow visualisation using tufts was performed inside the model classifier. Figure 3.25 shows a picture of the image acquired during the laser flow visualisation using tuft inside the model classifier.

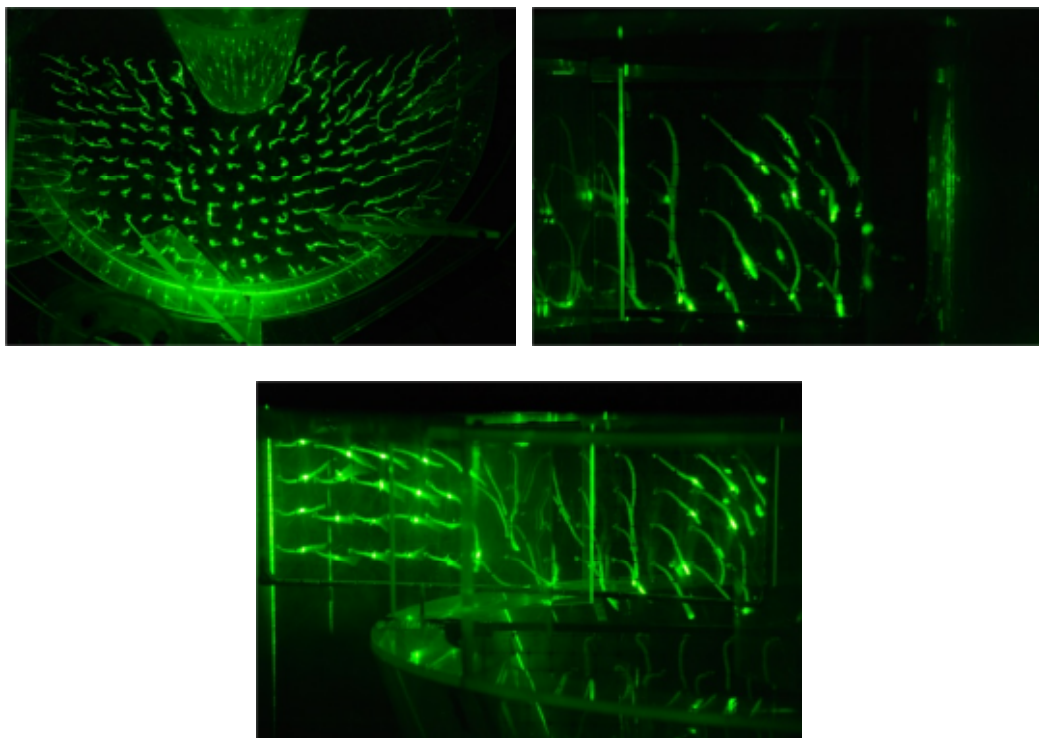


Figure 3.25: Flow visualisation using tuft

Flow visualisation was performed in several areas to help to understand the flow field. Light yellow-coloured polyester tufts were used, along with a continuous pulse laser for better visualisation. Black mesh with an area of 2cm x 2cm was used to attach small pieces of tuft (about 4–6cm apart) uniformly over the area of interest. A hand-held Canon digital camcorder was used to record the images.

3.6 Particulate Phase Experiment

The particulate phase experimental setup and flowchart are shown in Figure 3.26 and Figure 3.27 respectively. The air is supplied to the classifier by a positive displacement-type blower through a channel that is 500mm in width and 170mm in height.

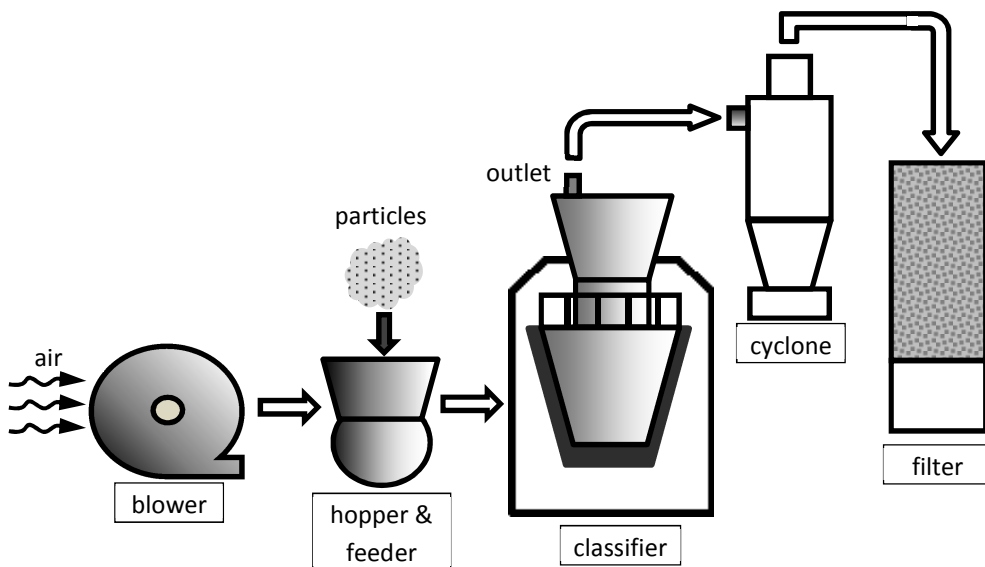


Figure 3.26: Schematic diagram of the particulate experiment setup

The blower provided a constant air flow rate. The air was fed with particles as it passed through the rotary feeder. The air-particle mixture was then fed into the classifier. The air blew the particles firstly to the outer body and then to the classifying area through the guide vanes. Fine particles left through the top of the

classifier together with the air to the cyclone. Heavier particles dropped to the bottom as the coarse fraction and were collected in a sealed drum. Air released from the cyclone was filtered using an air filter, to make sure that only clean air is released to the atmosphere.

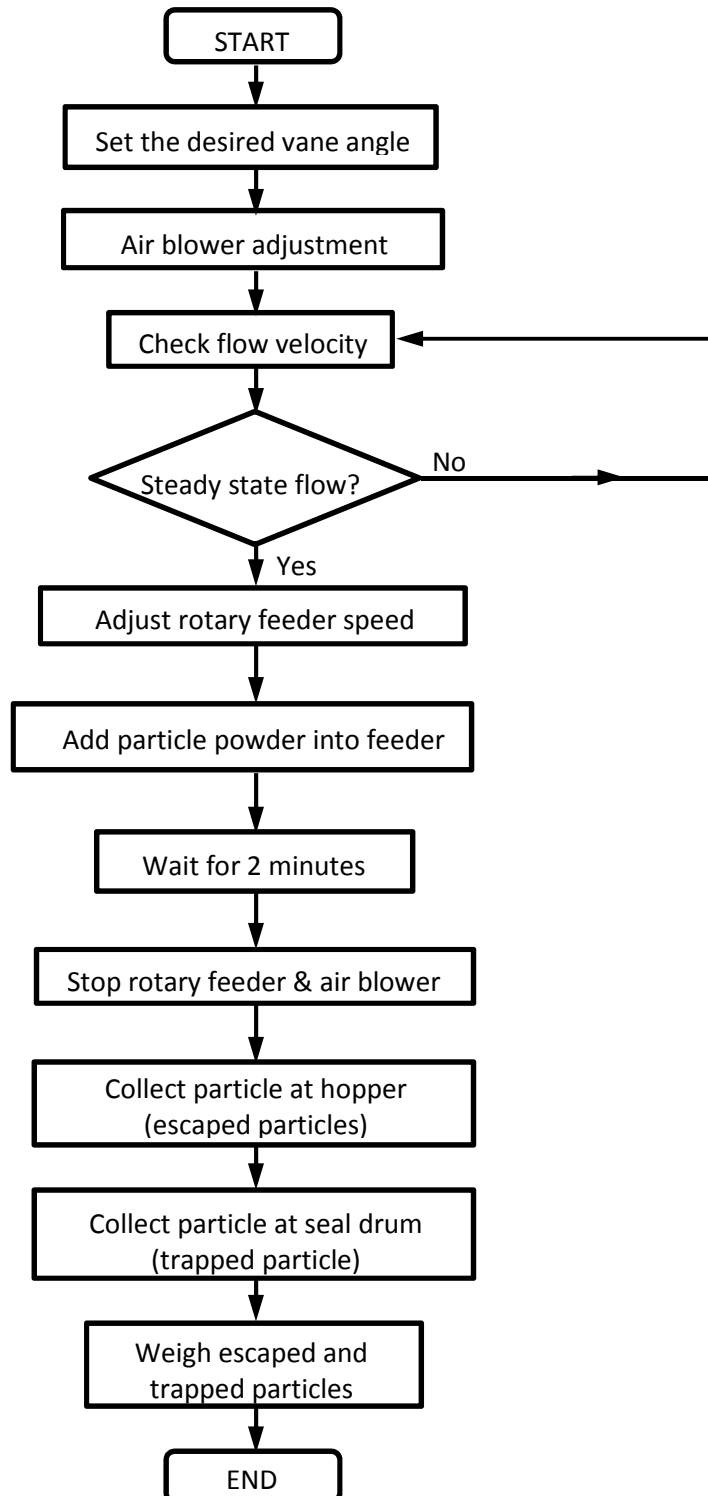


Figure 3.27: Particulate phase experiment procedures

Before conducting the experiment, the downstream and upstream air flow rates of the classifier were measured. The flow rate was initially measured using the pitot tube, and later with a vane anemometer. The flow rate measured using the pitot tube was in agreement with that measured by the vane anemometer.

The particles fed into the hopper were weighed, as well as the particles trapped in the cyclone, in order to acquire the percentage of particles leaving the classifier.

The experiments were conducted only when the system had reached its steady state. The run time began when the screw feeder was turned on, which was after starting the air flow, accelerating the disks up to the required rpm and the air phase reaching its steady state. This typically takes around two minutes.

3.7 Determination of Particle Size Distribution

The cyclone hopper was weighed before and after each experiment conducted. This was to attain the mass of fine and coarse fractions (m_{ff} and m_{fc}) separated by the classifier. The two fractions were split and riffled to obtain a representative sample for analysis of size distribution. Samples were analysed using the Scanning Electron Microscope (SEM) at the Material Lab, University of Leicester. This instrument measures particle size by light diffraction. From the intensity and angular distribution of light scattered, the SEM determined the fraction of each particle's diameter. At least five samples from each fraction were measured.

3.7.1 Feed Materials

In the experiment, particles of hollow silicate glass known as Fillite are used. They are spherical in shape, hard and inert. In terms of chemical composition, Fillite consists of approximately 65% Silica (SiO₂) and 35% Alumina (Al₂O₃); it is easily broken into smaller particles. This hollow spherical material was chosen because of its large mean diameters, which allow better scaling according to the Stoke number. Furthermore, Fillite is non-explodable and not poisonous or an irritant to the skin.

3.7.2 Particle Characteristics

The Scanning Electron Microscope (SEM) was used to assist with Fillite characterisation for Particle Size Distribution analysis. The analysis was crucial in the modelling of the for CFD investigation. Figure 3.28 and Figure 3.29 show the SEM image of the unused and used Fillite. The unused particles were initially spherical in shape, but starting losing their shape after more than fifteen runs. Thus, both used and unused particles will have different Stokes numbers. In order to maintain an average Stokes number, fresh unused particles were employed in each experiment.

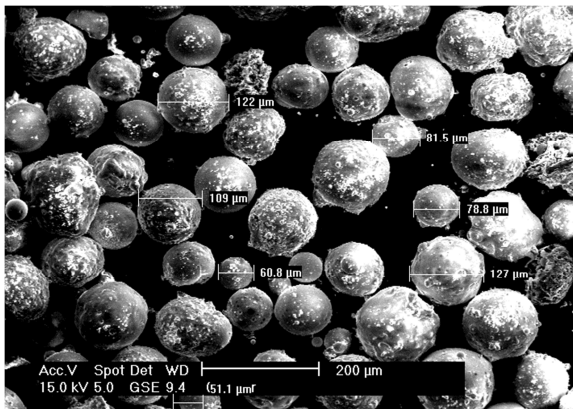


Figure 3.28 New standard grade fillite
(200 x magnifications)

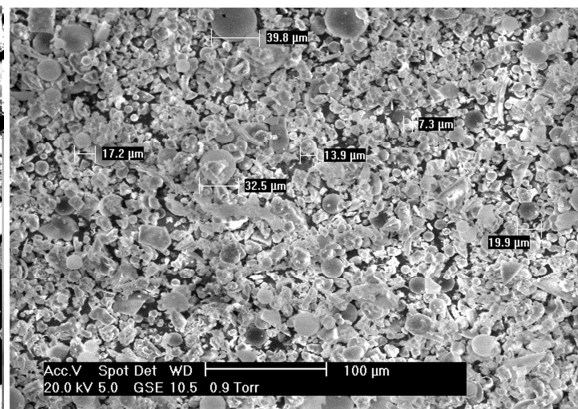


Figure 3.29 Used standard grade fillite
(100 x magnifications)

With the assistance of the SEM facility, unused particles were run through the system and samples were taken from the hopper after each run. The test was run with a sufficiently small mass of powder so that all could be retained in the weigh hopper.

3.8 Characterisation of One-Third Scale Facility

In order to promote accurate measurement and testing using the one-third scale facility, careful considerations were taken in calibrating various control and measurement devices, designing the tests and analysing of the results. This section elaborates on the characteristics of the facility being considered.

3.8.1 Scaling Criteria

In scaling down the test subject, it is vital that the scaled facility strictly match the Froude and Stokes numbers. Table 3.1 shows the comparison between typical UK power station classifier characteristics compared to the one-third scale facility. It should be noted that the Stoke number with a closely matched Froude number of the same magnitude is considered agreeable. Meanwhile, the Reynolds number of both actual and scale facility are in the turbulent regime.

Table 3.1: Comparison of scaling criteria for one-third scale facility

| | UK Power Station | Test Facility |
|----------|------------------|---------------|
| Stokes | 0.01 | 0.07 |
| Reynolds | 240000 | 400000 |

3.8.2 Dynamics Similarity

Laboratory experiments must be conducted on correctly scaled rigs. It is inconceivable to always construct test rigs at full scale, but a scale model has to be able to produce useful results. MacPhail (1983) points out that the size of a test rig is not important, but more the matching of key dimensionless numbers in order to obtain dynamic similarity. This means preserving all the relevant dimensionless numbers, which in this case are the Reynolds number (Re) and Stokes number (St).

Reynolds Number - The Reynolds number (Re) is described as the ratio of inertial to viscous forces. The Reynolds expression is:

$$Re = \frac{vD}{u}$$

Where u =kinematic viscosity (m^2/s), v =conveyance velocity (m/s) and D =pipe diameter (m). The turbulence region is considered to be when $Re > 2300$ (Massey, 1998). As long as the Reynolds number is well into the turbulent regime it is not important to pay close attention to its value (MacPhail, 1983).

Stokes Number - The Stokes Number is described as the ratio of the particle inertial force to the drag force on the particle. The Stokes expression is:

$$St = \frac{\rho_p d^2 v}{\mu D}$$

Where ρ_p =particle density (kg/m^3) and d =particle diameter (m).

Since the Reynolds number of a typical power station is of the order of 10^6 , it is not possible to match this constant. It can, however, be considered matched if it is within the turbulent regime. The Stokes number is considered vital for the accurate experimental modelling, but the Froude number is generally considered less important unless particulate deposition is the focus of the study.

It is also necessary to consider the scaling of the particles and wall roughness to accurately mimic collisions.

3.8.3 Air Speed Characteristics

Ideally, the fan speed should be the same for each test. However, differences in the pressure drop of the rig between tests result in velocity differences. As the fan speed is set in the control area, it is difficult to maintain the same fan speed accurately. To overcome this, the fan was allowed to run for a few minutes before a test was conducted.

3.9 Error Analysis

Experimental work, even when carried out to the highest standard, contains inherent errors due to uncertainties in all measurement techniques. The test facility used represents a system of uncertainties too complex to analyse in full, but a few key elements are discussed here. Key values output by the rig and used in results are:

1. Air speed velocity blown into the test rig.
2. Particles' size measurement.

3.9.1 Error in Air Velocity

The air velocity is calculated according to the pressure drop across the classifier body. The air velocity can be influenced by vibrations, temperature effects and static pressure. The measurement point can also contribute to the error as the pitot tube traverse is done manually.

3.9.2 Error in Particles Measurement

The mass of powder in the hoppers is weight, and the Scanning Electron Microscope (SEM) was used to measure the particles' size in the hopper. For spherical particles, size is defined by diameter. However, the particles' shape can sometimes be irregular. Therefore, characterisation of particle size must also include information on the type of diameter measured, as well as information on particle shape. Malvern Instrument's Morphologi software provides the perfect complement to SEM imaging with its advanced, dedicated image analysis software. Unfortunately, the Malvern Instrument was unavailable.

In order to maintain consistency between tests, the weigh hoppers were emptied prior to each test so that the same, albeit small, non-linearity is repeated. The cyclones in the facility also induce an error in their efficiency, which is circa 95%. In addition, particles that break up during a test run will be small and also add to the inefficiency of the cyclones. It is impossible to place an actual value on this, but it is estimated to be worth a further 1% inefficiency, bringing the total inefficiency to 6%.

CHAPTER FOUR: MODEL FORMULATION FOR CFD

This chapter describes the Computational Fluid Dynamics (CFD) method that investigates the air flow and the two-phase (gas-solid) flow inside the classifier. The numerical simulations were performed using the commercial software FLUENT 6.3 available at the University of Leicester. CFD is the analysis of systems involving fluid flow, heat transfer and associated phenomena such as particle tracking. The technique is very powerful and extends to a wide range of industrial and research applications. In this study, CFD is used mainly as a predictive tool for classifying behaviour and development.

CFD is concerned with the obtaining of numerical solutions to fluid flow problems through the use of computers. The rise in technological advancements has enabled CFD to obtain solutions to many flow problems, including those which are compressible or incompressible, laminar or turbulent, chemically reacting or non-reacting flows.

The governing equations for the fluid flow are as follows:

- the continuity (conservation of mass)
- the Navier-Stokes (balance of momentum)
- the energy (conservation of energy) equations

These equations are what form a system of coupled non-linear Partial Differential Equations (PDEs). The fluid flow equations are commonly not amenable to the

attainment of the solution through the analytical method, due to the coupled nature of the equations and the presence of non-linear terms. Closed form analytical solutions are usually possible only under circumstances wherein these PDEs be made linear, either because non-linear terms naturally drop out (as for parallel flows or flows that are inviscid and irrotational everywhere) or due to the non-linear terms being smaller compared to other terms, to the point that they are neglected (for example, creeping flows and small amplitude sloshing of liquid). In the circumstance that the non-linearities in the governing PDEs cannot be neglected (which occurs frequently for most engineering flows), numerical methods must be employed to obtain solutions.

4.1 The Structure of CFD

Formulating the flow problem is the first step of the CFD process. This starts with identification of the analysis objective and planning methods in order to achieve the objective. The geometry of the subject and the operating conditions must also be considered in the CFD simulation process.

As proposed by Menter *et al.* (2002), the first step in CFD analysis is to define the target variables. Variables that are demonstrative of the goals of the simulation, and those that can be compared with the corresponding experiments, should be included. Further criteria are:

- Sensitivity to numerical treatment and resolution
- Computation with existing post-processing tools
- Computation inside the solver are ideally displayed during run-time

The first point is vital, as the target variables should be indicative of the numerical errors and uncertainties. The following two points simplify the definition and the monitoring of the variables, which is especially important for the judgment of iterative convergence. The general process for performing a CFD analysis is outlined below.

4.1.1 Pre-Processing

The geometry of the flow to be analysed requires modelling. This normally involves modelling the geometry using the CAD software package. Simplifications and approximations of the geometry may be required to allow an analysis with a reasonable attempt. The finite flow domain for the flow to be simulated also needs to be decided. Portions of the boundary of the flow domain correspond to the surface of the body geometry. Other surfaces are free boundaries, over which the flow enters or leaves. As a means of providing input for the grid generation, the geometry and flow domain are modelled while taking into account the structure and topology of the grid generation.

The next step is establishing the boundary and initial conditions. As the finite flow domain is specified, physical conditions are required on the boundaries of the flow domain. The simulation typically starts with an initial solution and acts upon an iterative method to achieve a final flow field solution.

Following this, the grids are generated. The flow domain is discretised into a grid. The process of grid generation involves, firstly, defining the structure and

topology, and then generating a grid on that topology. Currently, all cases involve multi-block, unstructured grids. The grid (especially the boundaries) should exhibit high grid quality by measures of orthogonality, relative grid spacing and grid skewness. The maximum spacing should be consistent with the desired resolution of important features. The next step is establishing the simulation strategy. The strategy for performing the simulation involves selecting the simulation model, such as the choice of turbulent model, and the choice of algorithms.

The last step for pre-processing is establishing the input parameters and files. CFD codes generally require that input data files be created, listing the value of the input parameters and consisting of the necessary approach. Different boundary conditions require different specification data, thus selection should be undertaken carefully. A grid file containing the grid and boundary condition information is generally required. It is vital for the files for the grid and initial flow solution to be generated.

4.1.2 Processing (Solver)

The solver is the most important measure of CFD; it is the steps of calculation that are carried out in an iterative manner until a result of sufficient accuracy is achieved. Among other equations, the primary flow calculations are discretised from the Navier-Stokes equations.

The Navier-Stokes equations can explain and solve the full 3-D nature of fluid flow, taking into consideration viscosity, laminar and turbulent flow in an

infinitesimally small volume. The first approximation to the calculation is that each cell in the mesh is considered to be very small, it being clear when this is not the case, and cells may be 40mm across in large meshes. Further assumptions are made to the flow conditions, making the Navier-Stokes equations more manageable and, by time averaging and ignoring instantaneous fluctuations, it may be possible to reach a solution.

The information to run the model is contained in the 'case' file; for the models dealt with in this work it includes:

i. Turbulent model.

Fluent has many models. Each model formulates different assumptions and approximations to the flow regime. Selecting the correct one for the geometry is essential and requires understanding of flow.

ii. Boundary conditions.

Known input data can be imposed on the inlet(s) with the outlet being left with few or no restrictions to allow the iteration to provide data.

iii. Secondary Phase Injections.

Specific to two-phase flow, particulate properties, injections points and loadings are inputted.

iv. Solution method.

This includes under relaxation factors and the accuracy required in the solution.

The iteration is converged at the point that either the user considers the residuals to have reached a suitably low level or the residuals show that they will not go any lower.

4.1.3 Post-Processing

Post-processing the simulation is to display the results. Post-processing involves extracting the desired flow properties from the computed flow field and making comparisons of the results. The computed flow properties are compared to the results from analytic, computational or experimental studies to establish the validity of the computed results.

In fluent, there is a post-processor capable of interpreting the data provided to display flow fields, patterns and quantitative data. Data can also be extracted, and Excel is used to manipulate and display numerical data.

4.2 FLUENT

4.2.1 Computational Geometry

The computational grid is a discretised representation of the geometry of interest. It should provide an adequate resolution of the geometry and the expected flow features. The grid's cells should be arranged in such a way as to minimise discretisation errors. Before the grid generation is initiated, the geometry has to be created or imported from CAD data or other geometry representations. The correct coordinate system is used. The geometry must not over-simplify as this will cause a problems. The location of boundary conditions also needs to be

concentrated upon. This point of the computational domain has to capture relevant flow and geometrical features.

As the CAD data is the source of the geometry, this data should be checked scrupulously. It is vital for CAD data to be frequently adapted or cleaned before being used for mesh generation. Closed 3-D volumes (solids) are necessary for mesh generation, and CAD data may not always be the primary source. Thus, the CAD data has to be modified. However, these changes to the geometry must be done carefully so that the computed flow is not influenced.

The flow domain is subdivided into a large number of elements or control volumes. In each computational cell, the model equations are solved. This yields the discrete distributions of mass, momentum and energy. The number of cells in the mesh should be sufficient to obtain an adequate resolution of the flow geometry and the flow phenomena in the domain. As the number of elements is proportional to storage requirements and computing time, many 3-D problems require a compromise between the desired accuracy of the numerical result and the number of cells. The available cells need to be distributed in a manner that minimises discretisation errors.

In areas where local details are needed, local grid refinement is used to capture fine geometrical details. If grid refinement is used, the additional grid points should lie on the original boundary geometry and not simply be a linear interpolation of more grid points on the original coarse grid.

If the target variables of a turbulent flow simulation include wall values, like wall heat fluxes or wall temperatures, the choice of the wall model and the corresponding grid resolution can have a large effect on the results. Wall functions of this kind are used for all RANS turbulence models. The choice of the wall model has a direct influence on the mesh design.

Hex elements are the most efficient elements from a numerical point of view. They require the least memory and computing time per element. They can be adapted to shear layers (long and thin), for instance in the vicinity of walls. However, generation of hex meshes in complex geometries often requires a large manual and cognitive effort. Therefore, use of tetrahedral meshes is a viable alternative.

A grid dependence and sensitivity study should always be performed to analyse the suitability of the mesh and to provide an estimate of the numerical error of the results. At least two (or better, three) grids with significantly different mesh sizes should be employed.

4.2.2 Boundary Conditions

The computational domain normally contains only a part of the interested body. Therefore, the choice of the position of the boundaries of the computational domain influences the results. This influence definitely adds to the uncertainty of the simulation results, but it can also lead to errors if the choice is inadequate. The influence of the flow and dispersion within the computational domain is taken into account with the prescription of the behaviour of the flow variables at the

boundaries. For the boundaries through which the flow enters the computational domain, complete information on all flow variables is necessary. Sometimes an approximation of some or all flow variables at the inflow boundaries adds to the uncertainty of the numerical results needed. This is also the case for the choice of the boundary conditions at solid walls. Here, the prescribed roughness and the chosen wall functions are especially important. For boundary layer flows, the roughness at the ground has to be chosen in accordance with the prescribed inflow profile of the velocity. Knowledge of the geometrical details is required for defining the computational domain in which the flow and dispersion field shall be computed.

4.2.3 Governing Equation

This section looks on the governing equation involved. They are described as follows:

Continuity Equation

$$\frac{\partial \rho}{\partial t} + \nabla \cdot (\rho \mathbf{V}) = 0 \quad (4.1)$$

Conservation of Momentum Equations (in three dimensions)

$$\frac{\partial(\rho u)}{\partial t} + \nabla \cdot (\rho u \mathbf{V}) = -\frac{\partial p}{\partial x} + \frac{\partial \tau_{xx}}{\partial x} + \frac{\partial \tau_{yx}}{\partial y} + \frac{\partial \tau_{zx}}{\partial z} + \rho f_x \quad (4.2)$$

$$\frac{\partial(\rho v)}{\partial t} + \nabla \cdot (\rho v \mathbf{V}) = -\frac{\partial p}{\partial y} + \frac{\partial \tau_{xy}}{\partial x} + \frac{\partial \tau_{yy}}{\partial y} + \frac{\partial \tau_{zy}}{\partial z} + \rho f_y \quad (4.3)$$

$$\frac{\partial(\rho w)}{\partial t} + \nabla \cdot (\rho w \mathbf{V}) = -\frac{\partial p}{\partial z} + \frac{\partial \tau_{xz}}{\partial x} + \frac{\partial \tau_{yz}}{\partial y} + \frac{\partial \tau_{zz}}{\partial z} + \rho f_z \quad (4.4)$$

Conservation of Energy Equations (in three dimensions)

$$\begin{aligned}
\frac{\partial}{\partial t} \left[\rho \left(e + \frac{V^2}{2} \right) \right] + \nabla \cdot \left[\rho \left(e + \frac{V^2}{2} \mathbf{V} \right) \right] &= \rho \dot{q} + \frac{\partial}{\partial x} \left(k \frac{\partial T}{\partial x} \right) + \frac{\partial}{\partial y} \left(k \frac{\partial T}{\partial y} \right) \\
+ \frac{\partial}{\partial z} \left(k \frac{\partial T}{\partial z} \right) - \frac{\partial(u\rho)}{\partial x} - \frac{\partial(v\rho)}{\partial y} - \frac{\partial(w\rho)}{\partial z} + \frac{\partial(u\tau_{xx})}{\partial x} + \frac{\partial(u\tau_{yx})}{\partial y} + \frac{\partial(u\tau_{zx})}{\partial z} \\
+ \frac{\partial(v\tau_{xy})}{\partial x} + \frac{\partial(v\tau_{yy})}{\partial y} + \frac{\partial(v\tau_{zy})}{\partial z} + \frac{\partial(w\tau_{xz})}{\partial x} + \frac{\partial(w\tau_{yz})}{\partial y} + \frac{\partial(w\tau_{zz})}{\partial z} + \rho \mathbf{f} \cdot \mathbf{V}
\end{aligned} \tag{4.5}$$

4.2.4 Turbulence Modelling

Choosing the correct turbulence model can have a great effect on the result. It is important to study which model is most competent for the current scenario. Some powerful industrial computers are now capable of carrying out DNS and LES, in which all the turbulent scales are mathematically solved, but this requires a large computing power. Fluent provides a number of turbulent models that use approximation and prediction to provide quick solutions with a good level of accuracy.

k-ε model

The k-ε is a two-equation model consisting of differential equations and constants determined from experimental data. The dependent variables in the pair of differential equations are the turbulent energy, k, and the dissipation rate of the turbulent energy, ε. The k-ε model is able to study both near-wall and free-shear flows and is considered to be the simplest turbulence model able to do this.

Realizable k-ε Model

The realizable k-ε model is a relatively recent development and differs from the standard k-ε model in two important ways:

- The realizable k- ϵ model contains a new formulation for the turbulent viscosity.
- A new transport equation for the dissipation rate, ϵ , has been derived from an exact equation for the transport of the mean-square vorticity fluctuation.

“Realizable” here can be defined as the model that satisfies certain mathematical constraints on the Reynolds stresses, in correspondence with the physics of turbulent flows. Both the standard k- ϵ model and the RNG k- ϵ model are not realizable.

The realizable k- ϵ model more accurately predicts the spreading rate of both planar and round jets. It can provide an excellent performance for flows involving rotation, boundary layers under strong adverse pressure gradients, separation and recirculation.

Both the realizable and RNG k- ϵ models have shown significant progress over the standard k- ϵ model, where the flow features include strong streamline curvature, vortices and rotation. The model is still relatively new, thus the instances in which the realizable k- ϵ model consistently outperforms the RNG model cannot be pinpointed. Nevertheless, research shows that the realizable model presents the best performance of all the k- ϵ model versions for several validations of separated flows and flows with complex secondary flow features. Hence, the k- ϵ model is extensively employed and accepted as a powerful classifier modelling tool.

Reynolds Stress Model (RSM)

The RSM calculates the individual Reynolds stresses by solving the transport equations. The Reynolds stresses are components of the conservation of momentum equation and the transport equations, which are derived from the conservation equations. Solving the seven equations within the RSM results in a more computationally challenging solution, with run-times up to 30% longer than for the k- ϵ model. Very similar pressure and velocity flow fields are calculated by each of the models. Rotating flow is effectively captured with both models, presenting almost identical velocity vector fields. As a result, the less computationally intensive k- ϵ model is preferred for this work.

4.2.5 Solid Phase Modelling

It is vital for the solid phase behaviour to be correctly modelled in this study. There are two routes to solid phase modelling: Lagrangian and Eulerian.

Lagrangian involves tracking a set of packages that signify the mass of the flow. These packages are assigned a size and density and are affected by the flow. The mass is then split up into discrete elements, referred to as discrete phase modelling. Lagrangian tracking tends to be good for relatively dilute flows.

Eulerian tracking introduces the solid phase as another fluid, given all the properties of that substance. The mass is consequently treated as a continuous phase, referred to as continuous phase modelling. As opposed to Lagrangian, Eulerian tracking tends to be good for relatively dense flows.

For the current work, Lagrangian tracking was used, as most of the cases run were comparably dilute. Whilst there is an issue with Lagrangian tracking not modelling particle-particle interactions, it was considered to be the most efficient model in terms of time and computational power.

In FLUENT, injections are set up to model the solid flow using the Lagrangian model. The type of injection can be tailored to represent a great many different flow types. The injection conditions used for the purposes of this work tend to be injected as a surface (usually the velocity inlet).

4.2.6 The SIMPLE Algorithm

In FLUENT, the equations of motion are integrated and discretised over control volumes or cells, in order to obtain algebraic equations of conservation of mass and momentum for each cell. These equations are linearised implicitly to solve for the unknown quantities, so that a given quantity is determined for all cells simultaneously.

The equations are solved using the segregated solver. With this solver, the momentum equations are solved sequentially. Then, from a pressure-correction equation derived from the continuity equation, corrections to the pressure and velocities are calculated to satisfy the continuity equation. Finally, the k and ϵ equations are solved. This process is continued until the solution has converged to a specified limit.

Pressures at cell faces are required to solve the discretised momentum equations. As FLUENT stores values at cell centres, the face value must be interpolated from

the cell centre. The PRESTO (Pressure Staggering Option) discretisation scheme has been chosen to interpolate pressure at faces centres from cell centres, because it gives the best predictions for rotating flows. PRESTO is similar to the staggered grid schemes given by Patankar (1980).

By default, FLUENT stores discrete values for fluid properties at cell centres; when face values of a cell are required, the value is interpolated from the cell centre. This is accomplished by using an upwind scheme. Upwinding is the process of deriving the face value of a cell from quantities "upwind" of the cell, relative to the direction of the flow velocity.

FLUENT presents several upwind schemes: the first-order upwind scheme and the second-order upwind scheme. Face centre values for velocities and turbulence quantities are computed using the second-order upwind scheme (Barth & Jespersen, 1989). "Upwind" means the face centre values are interpolated from cell centre values of the cell upstream, or "upwind" of the face, relative to the normal velocity. The second-order upwind works by using the Taylor series to apply a gradient throughout the cell, based on the surrounding cells. Hence, the face value of a cell will be calculated based on the two cells that form the face. The second-order upwind solutions tend to be more computationally intense and more accurate than first-order upwind solutions. All cases used in this thesis use the second-order upwind scheme.

4.3 Classifier Model Setup

This section describes the various elements of the Gambit and Fluent operations, in order to create a reliable and consistent CFD model. The components of the model are considered in chronological order of setup, with a description of the decision made for each part and with sensitivity studies used where necessary.

Meshing Regime

The model was meshed using a tetrahedral meshing scheme with 2.4 million cells. Figure 4.1 shows the computational grid. The grid resolution was restricted due to computational cost. However, a sizing function was applied to the inlet, outlet and vane faces, consequently refining the mesh size in these zones as they are a major point of interest.

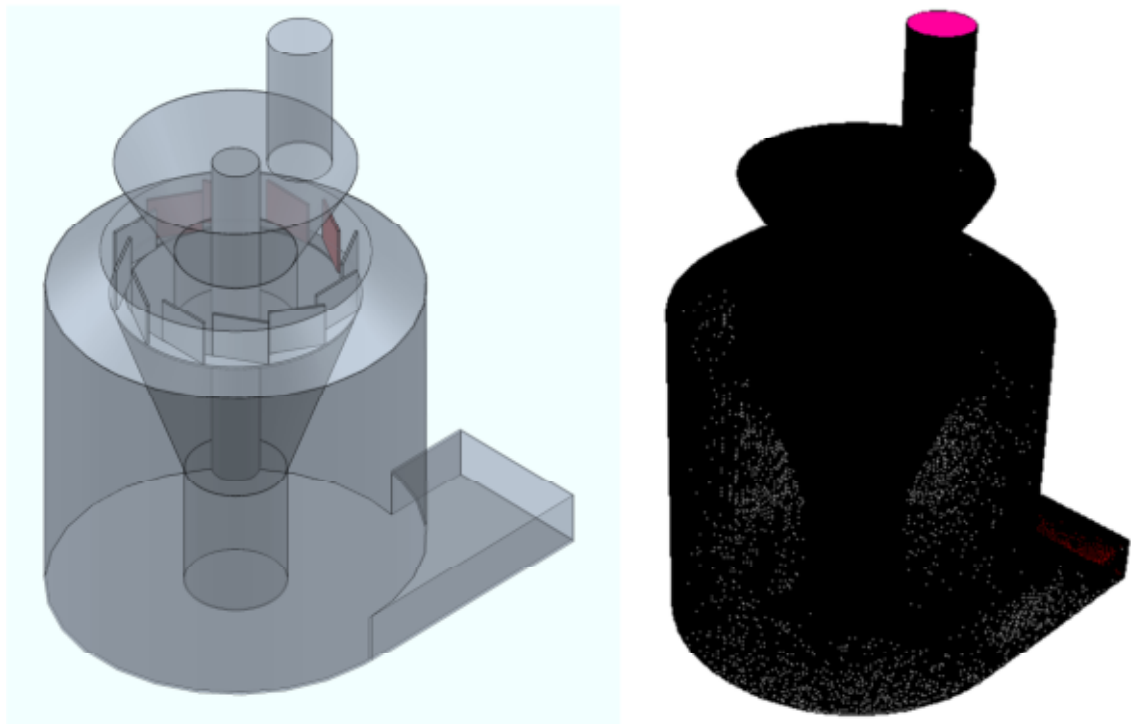


Figure 4.1: Computational grid layout

A mesh size was applied with a growth rate of 1.5 and maximum size of 40. The mesh qualities are lower or equal to 0.4 for more than 90% of the control volumes. The mesh quality was evaluated using the EquiAngle Skew criterion. Hence, the overall mesh qualities are considered satisfactory.

Cell Size

Grid independence checking should be carried out on all geometries to ensure the correct cell size is used. But in this work, checking each geometry would be very time consuming, so it was decided that grid independence should be carried out on one of the geometry only.

Importing the Mesh

The file output by Gambit is of the form *.msh. This file is imported directly into Fluent and is saved as a *.cas file. The mesh is checked for errors both automatically and manually. In addition, the model also needed to be scaled, as Solidworks work in millimetres while Fluent in metres.

Selection of Turbulence Model

The turbulence flow is a very complicated flow to model. Selecting the right model can effects the result. So, it is important to research which model is most suited to the current scenario.

The gas phase turbulence quantities were predicted using the realisable k- ϵ model. This model more accurately predicts the performance for flows involving rotation, boundary layers under strong adverse pressure gradients, separation and

recirculation. In the vicinity of the wall, the turbulence becomes more complex because of the no-slip conditions there. In the near-wall zone, the velocity and other transport properties vary rapidly within a short distance from the wall. In order to predict the rapid variation in this region, excellent grid resolution is required.

Initial studies have shown that, of all the k- ϵ model versions, the best results are acquired from realizable model for several validations of separated flows and flows with complex secondary flow features. Hence, the k- ϵ model is used and accepted as a powerful tool for modelling the classifier.

Selection of Particle Model

The particulate phase was treated by the Lagrangian approach. In this model, the particles are grouped in so called "parcels", a collection of particles with the same properties. The parcels are introduced at a finite number of starting locations at the inlet cross-section and move simultaneously through the flow field. In every given time step, their positions and velocities were calculated according to the forces acting on the particle and using Newton's Second Law.

The interaction between these eddies and the particles were taken into account by a stochastic procedure. It was assumed that the turbulence was isotropic and that the instantaneous fluid velocity component was sampled from a Gaussian velocity distribution. The instantaneous fluid velocity was assumed to influence the particle motion.

Particle-wall collisions were modelled as having a value of 0.01–0.3 in all the calculations, depending on the material of the classifier model. Particle-particle collisions were neglected in this study. This is a good assumption for dilute gas-particle flows.

Setup of Particulate Injections

This study selected the Lagrangian model as the method most appropriate for particle tracking. The particles were injected from cell faces on the inlet to model the real-life scenario. The injection was set up with inert particles of anthracite.

Drag Law

There is a choice of spherical or non-spherical drag laws. The spherical considers all particles as perfect spheres, while the non-spherical introduces a shape factor as defined by the equation (4.5) below.

$$\phi = \frac{s}{S} \tag{4.6}$$

Where ‘s’ is the surface area of a sphere having the same volume as the particle and ‘S’ is the actual surface area of the particle.

By applying a shape factor of less than one, the particles are considered to have, relative to the particle volume, a greater surface area, specifying a flatter shape with a quicker response time. Raw Fillite particles are spherical so the spherical drag law is suitable. While it is not ideal to consider all particles to have the same shape factor, as they would not have this in real life, it was the response time of the particles that this researcher was trying to reduce, so a shape factor of 0.5 was applied.

Particle Size

The variety of particle sizes modelled is the basis of the success of a CFD study. Table 4.1 shows the summary of particle injections. A uniform distribution was used to investigate the particulate phase.

Table 4.1: Particles distributions used for the fluent modelling

| | Fillite SG 500 |
|-----------------------------------|------------------------|
| Min. Diameter (m) | 1×10^{-6} |
| Max. Diameter (m) | 90×10^{-6} |
| Mean Diameter (m) | 45.05×10^{-6} |
| Number of Particle Diameters used | 19 |

The anthracites used in the CFD studies with the values input to the Fluent injections panel for each size. The injections consisted of nineteen different particle diameters sampled by Fluent from equally spaced points.

Boundary Conditions

In the simulation of the model classifier, the geometrical structure and dimensions, as well as operating conditions, were kept the same as in the actual system. The boundary conditions and the fluid and solid properties had to be specified. The air inlet was modelled as a velocity inlet boundary condition of 13m/s. Details on simulation conditions with the respective boundary condition case are listed in Table 4.2.

Specification of the inlet and outlet conditions provides flow through the system and must be realistic.

Table 4.2: Simulation conditions

| Description | Value | Comment |
|---|--|---|
| Operating gas velocity • 3 inlet velocities Gas density, ρ_g Gas viscosity, μ_g | 13/20/30 (m/sec) 1.225 kg/m ³ 1.789 kg/ms | tangential inlet air |
| Particle density, ρ_s Particle diameter, d_s | 1700 kg/m ³ 1–90 μm | Anthracite Particle size was injected in each case |
| Solver | 3-D, double precision, steady, realisable $k-\varepsilon$ model | |
| Multiphase Model | Discrete Phase Model (DPM), two phases | |
| Viscous Model | Turbulent Model | |
| Boundary Conditions • Inlet • Outlet | Various inlet velocities for different cases Pressure outlet is P atm | |

Inlets

When modelling the classifier, the air inlet was modelled from the tangential inlet at the bottom of the mill. In all cases, Velocity Inlets were specified. The Inlet velocities were 13m/s, 20m/s and 30m/s. Figure 4.2 shows the meshed inlet of the model.

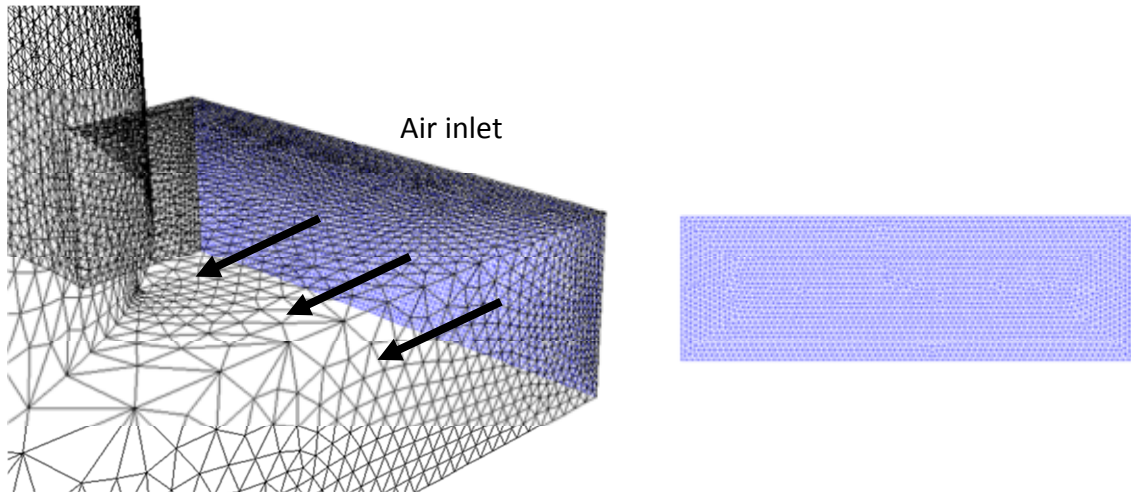


Figure 4.2: Unstructured mesh for inlet plane

Along with a specification of inlet velocity, Fluent also requires users to input the Turbulence Intensity [equation (4.6)] and Hydraulic diameter, which for this study is the width of the pipe.

$$I = 0.16(\text{Re}_{D_H})^{-\frac{1}{8}} \quad (4.7)$$

where,

D_H is the Hydraulic diameter

Outlets

Pressure outlets allow the system to reach its own solution to the flow rates on each of the outlets and were therefore used here. The outlet was modelled as a pressure outlet of 1.01325 bar (atmospheric pressure). In order to minimise convergence difficulties, realistic values for backflow quantities were entered. Air was taken as the fluid domain. From the literature search (Bernardo, 2006), these

boundary conditions are one of the most common conditions used and also provide most reasonable results. Figure 4.3 shows the unstructured grid at the outlet.

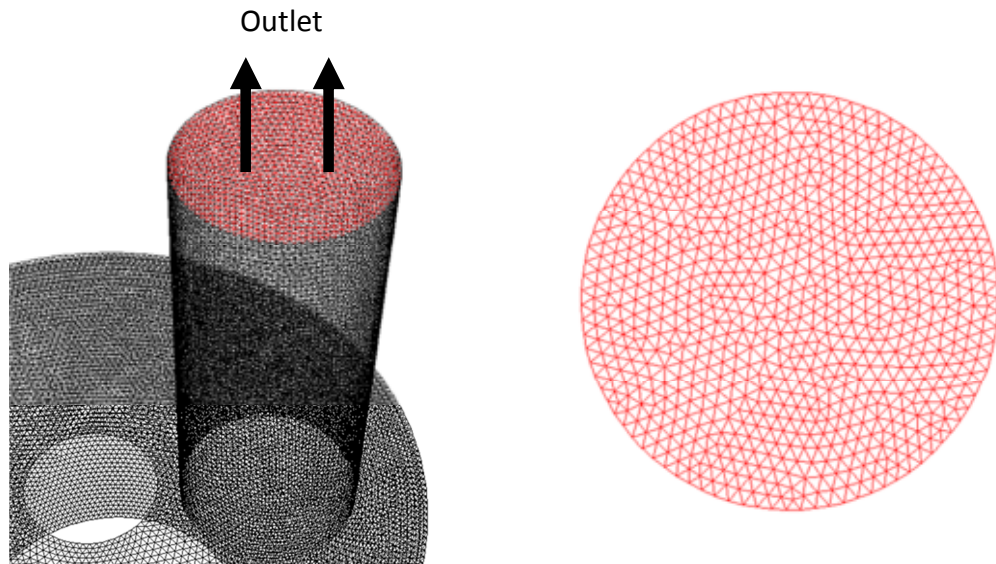


Figure 4.3: Unstructured mesh for outlet plane

Wall Conditions

In order to predict the boundary layer, standard wall conditions were used. This setting applies the boundary layer up to a maximum distance into one cell-size pipe. A sensitivity study is carried out to confirm the correct meshing due to the significance of mesh size (Section 0). Boundary layer meshing would more precisely model the boundary layer, but an abundance of cells are required and this would have been too computationally demanding. The prominent boundary conditions are the wall roughness height and the wall reflection coefficients for the particle phase. As to model the inelastic particle-wall collisions, reflection coefficients of 0.1 tangentially and 0.5 normally are used – as according to the

work of Giddings (2003). The roughness height is set to a realistic value of 0.0001m for one-third and full-scale models.

Simulation Criteria

Double precision solver was used to perform the simulations so as to capture the small gradients and minimise round-off error. In order to simulate the turbulent flow in the classifier, segregated implicit solver and Reynolds-Averaged Navier-Stokes (RANS) Equations Models with standard wall treatment were applied. A standard discretisation scheme was used for the continuity equation. A second-order upwind scheme was selected for the discretisation of the momentum equations, the turbulence kinetic energy equation and the turbulence dissipation rate equation to reduce numerical diffusion. Subsequently, the SIMPLE algorithm was employed to decipher the pressure-velocity coupling algorithms. All the default values for under-relaxation factors were applied, with the exception of the turbulence kinetic energy and dissipation rate. The governing equations for flow, turbulence and energy were solved iteratively until convergence was obtained.

Convergence Criteria

The convergence criterion was set to 10^{-6} for all variables. A solution was considered converged when the scaled residuals had dropped six orders of magnitude for all simulated variables and when the conservation of overall mass balance through domain boundary exceeded 99%. Typical compute times of about three (3) days were consumed for each case (the PC used was Intel Quad Core 2.66GHz, 4.00 GB of RAM).

The purpose of numerical method was to provide the solution to a differential equation at a number of discrete points in the calculation domain. The exact mathematical solution to the coupled partial differential equations defining fluid flow behaviour is not commonly attainable. Therefore, it was essential for this study to employ numerical methods that might supply a result approximately similar to the real solution. It was assumed that the increase in grid points would influence the approximation to be closer to the real solution.

A critical issue in discretising the convection-diffusion equations was the formulation of suitable expressions for the values of the transported property cell faces when accounting for the convective contribution in the equation. All the finite volume schemes available described the effects of simultaneous convection and diffusion by means of discretised equations whose coefficients were weighted combinations of the convective mass flux per unit area, F and the diffusion conductance, D . Discretisation schemes that possess conservativeness, boundedness and transportiveness give physically realistic results and stable iterative solutions.

To judge the convergence of the solution in this study, the ideal method was to set a point for the iterations to finish according to the residuals' size. The accuracy of this method aside, a better way would be to observe the residuals in graphical format and allow a reduction in the residuals to the point at which they tail off, as shown in Figure 4.4.

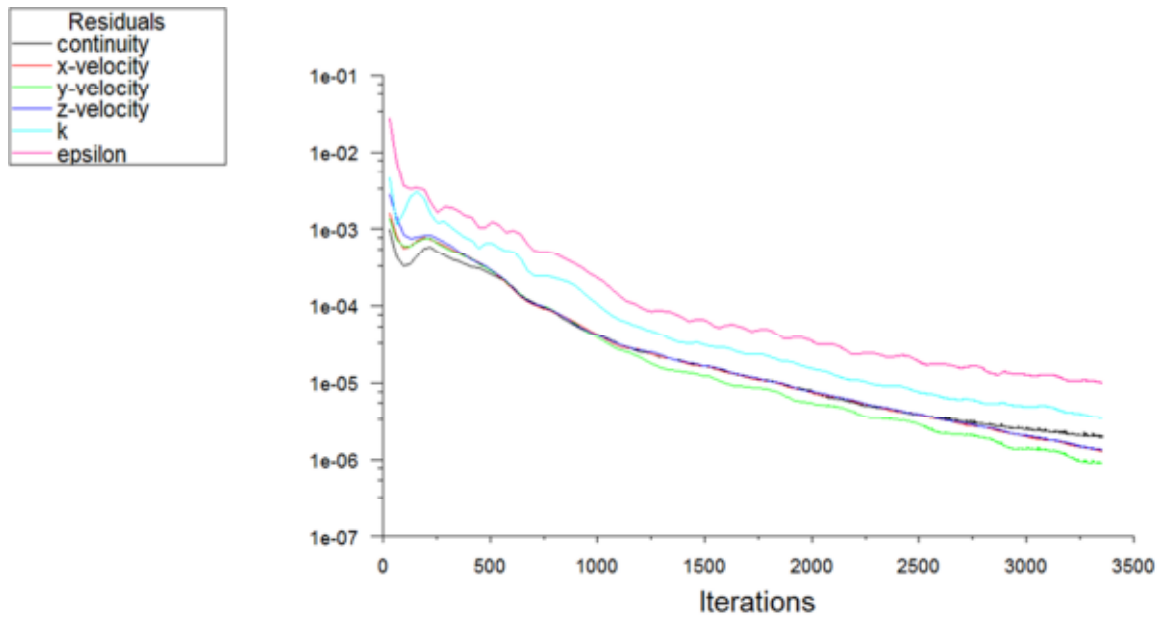


Figure 4.4: A Converged primary phase case.

Discrete Phase

On convergence of the primary phase, the discrete phase was introduced to the solution and a second convergence needed to be reached. It is important to obtain a coupled solution and this is achieved by injecting a stream of particles into the primary phase a number of times and at intervals, each time allowing the primary phase to adjust before the residuals appear, as in Figure 4.5. Further to this, either pressures or velocities can be plotted in another window, at a point of interest in the flow, in order to be completely confident of a solution.

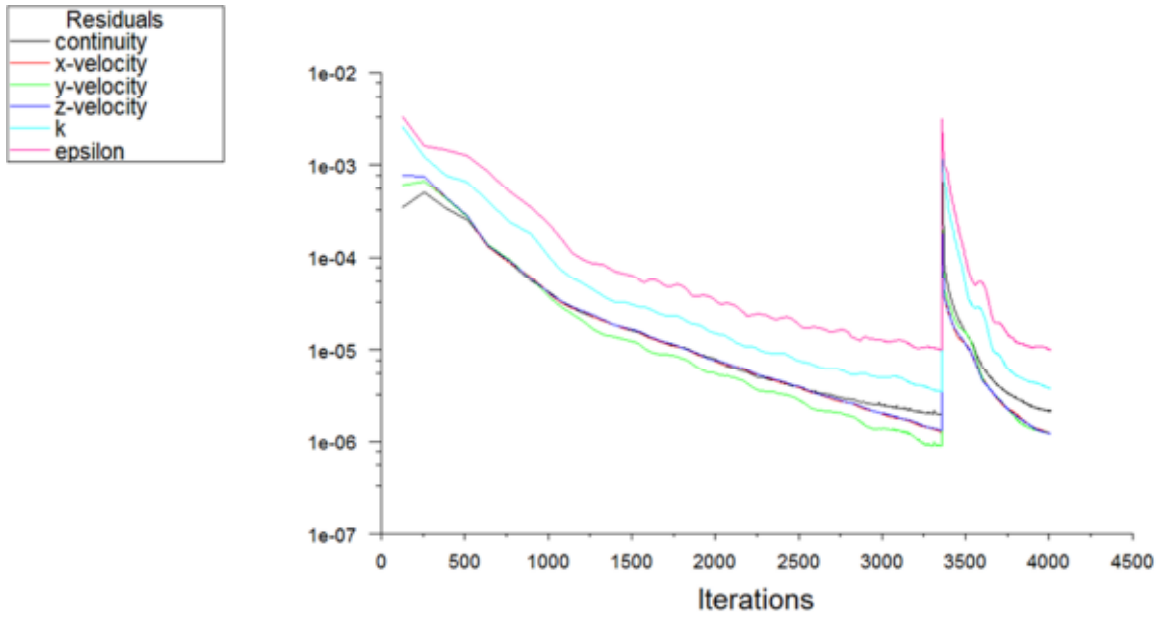


Figure 4.5: A Converged particulate phase case

The flowchart in Figure 4.6 illustrates the CFD simulation process.

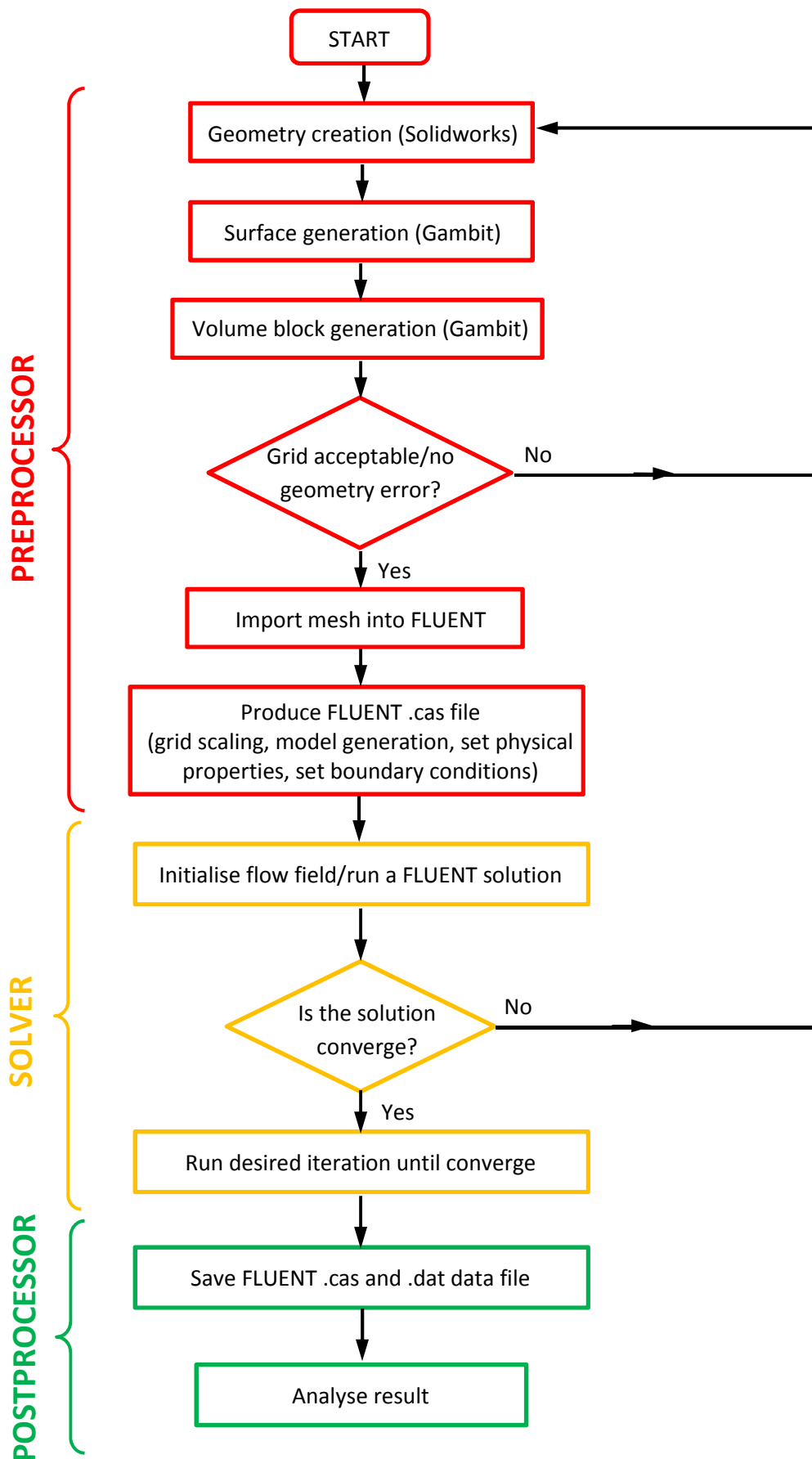


Figure 4.6: CFD simulation flowchart

4.4 Conclusion

This chapter has provided insight on how the Computational Fluid Dynamics (CFD) method being used to investigate the air flow and particle flow inside the classifier under study. Detailed descriptions on how the classifier was modelled and the steps taken to minimise simulation errors were elaborated upon.

CHAPTER FIVE: NUMERICAL ANALYSIS AND DISCUSSION

The main advantage of using CFD is its capability to effectively simulate the flow of the air which is the particulate carrier fluid and an essential element for the combustion process downstream travels through the classifier. This chapter gives an evaluation of the air flow (axial, radial and tangential velocities) and the transportation of coal particles inside the classifier.

The chapter starts by looking at the effect of the inlet velocities and vane angles on the velocity profile outside and inside the separation area in the classifier followed by studying the effect of varying the outlet location and particle distribution evaluation. To help understand the analysis better, the illustration of the classifier is shown again in Figure 5.1. Four axial regions were analyzed which are named Level A to Level D. The four outlet locations (Position 1 to Position 4) and the vane angles are shown in Figure 5.2.

Since the CFD simulation provides a lot of information from the variation of several classifiers' parameters, only the influential results are presented and discussed in this chapter. The focus of these investigations is to identify the parameters that could enhance the performance of the classifier.

This chapter builds on the CFD set up in the CFD methodology chapter (Chapter Four). In order to investigate all possible factors that may affect the classifier

performance, parameters such as the inlet velocity, the vane angle and the position of the outlet have been varied. The aim of these test cases is to get an insight of the effect of vane angle, inlet velocity and the outlet position on the classifier performance.

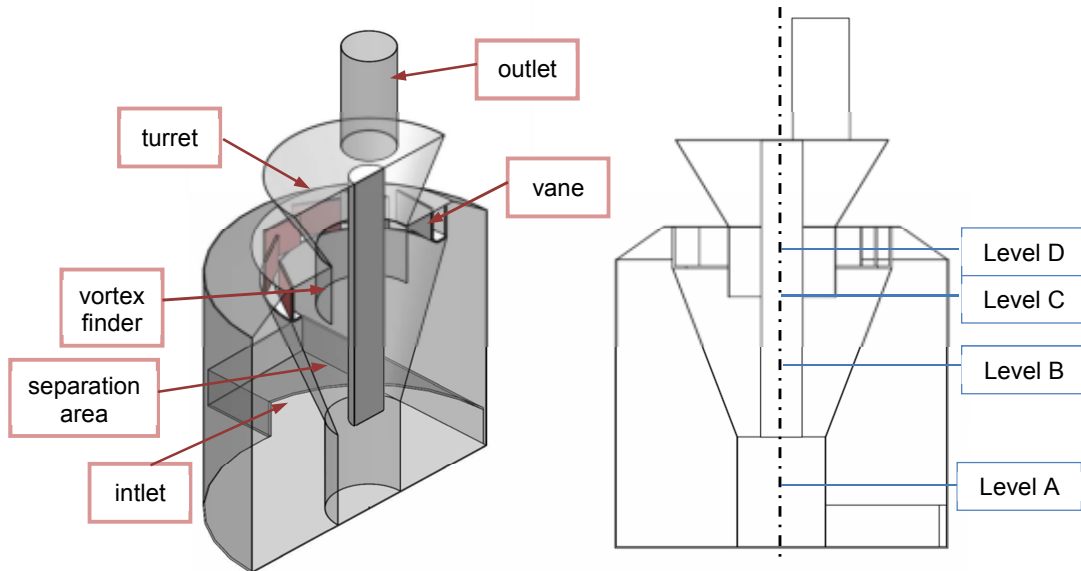


Figure 5.1: The classifier and axial level analysed

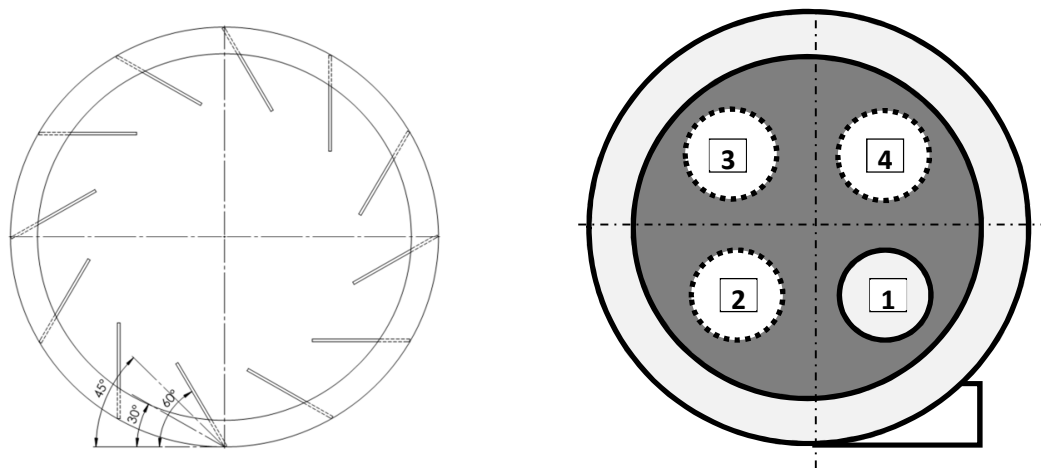


Figure 5.2: Vane angles (left) and outlet positions locations being analysed

5.1 Air Flow Distribution Analysis

Air (with coal particles) enters tangentially near the bottom of the classifier into the area outside the classifier's separation (cone) area. The air then travels

upwards, in a spiral motion, and enters the separation area through the vanes. The evaluation of the velocity profiles for the axial, radial and tangential velocity components is important because the flow structure indirectly determine the separation of coarse and fine particles by moving the particles upwards (axially) and radially into the separation area via the vanes into the conically shaped particulate classification zone. Figure 5.3 shows the air flow inside the classifier body. It shows the flow travel towards the outlet after tracing its path around the classifier body.

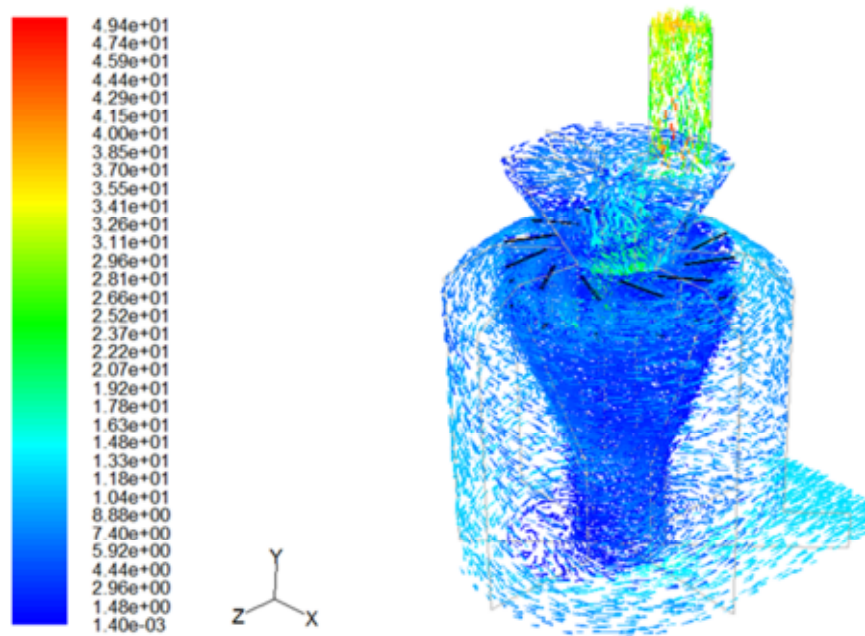


Figure 5.3 Air flow inside the classifier

5.1.1 General Velocity Profile Inside the Classifier

Before the comprehensive velocity analysis is conducted, the general features of the velocity profile inside and around the classifier were assessed. The velocity profiles at four different planes as shown in Figure 5.4 were analyzed. This is to determine which area (i.e. plane) is the most influential.

The axial velocity analysis at the selected planes was conducted in order to determine whether the coal particles are able to move upwards. Figures 5.5 to 5.8 show the axial velocity profiles outside the separation area at Level A to Level D.

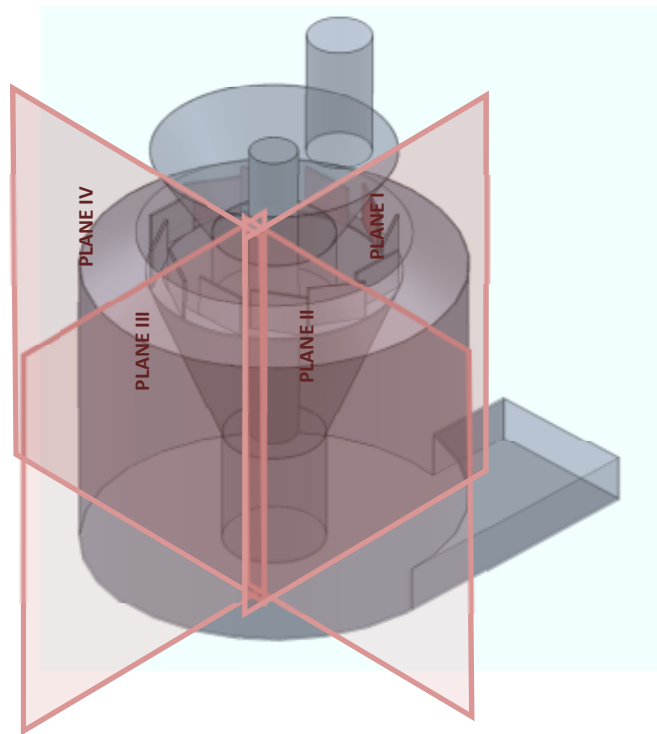


Figure 5.4: Planes examined in initial velocity profile analysis

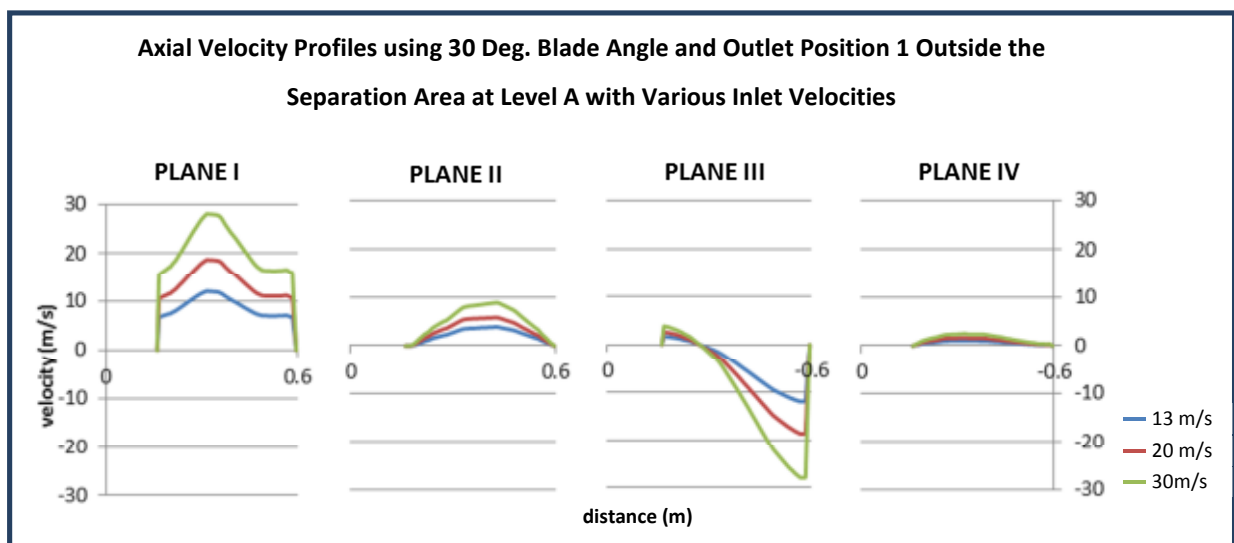


Figure 5.5: Axial velocity profiles at Level A with various inlet velocities

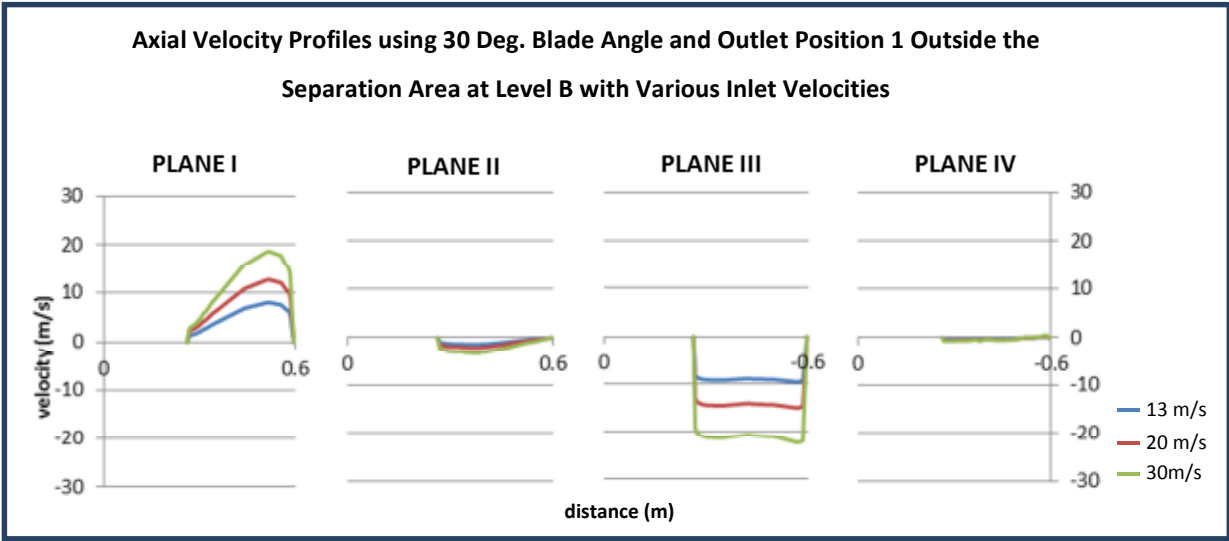


Figure 5.6: Axial velocity profile at Level B with various inlet velocities

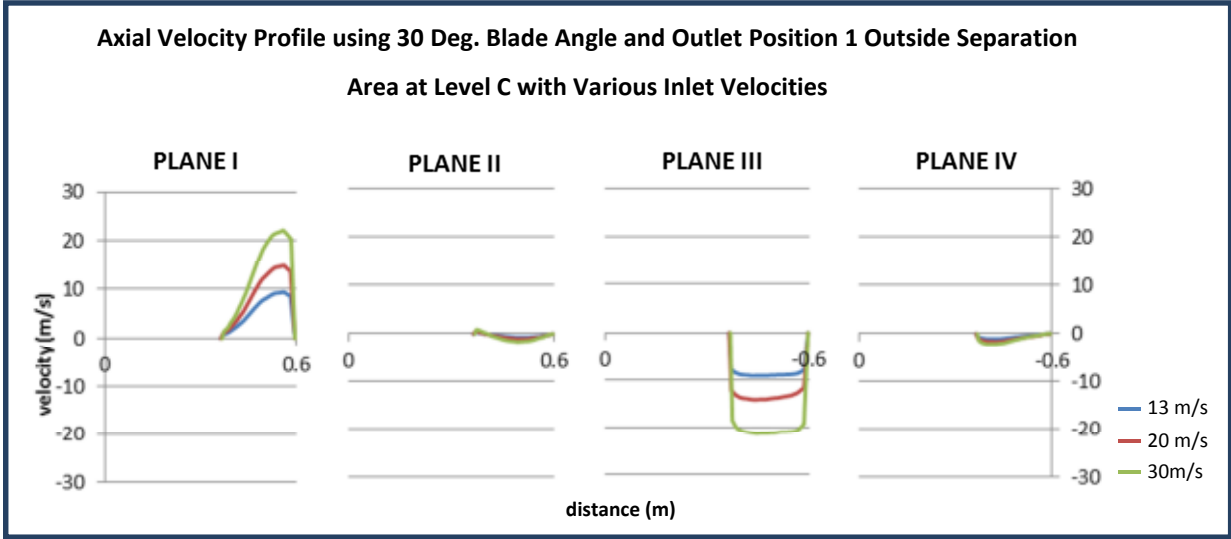


Figure 5.7: Axial velocity profiles at Level C with various inlet velocities

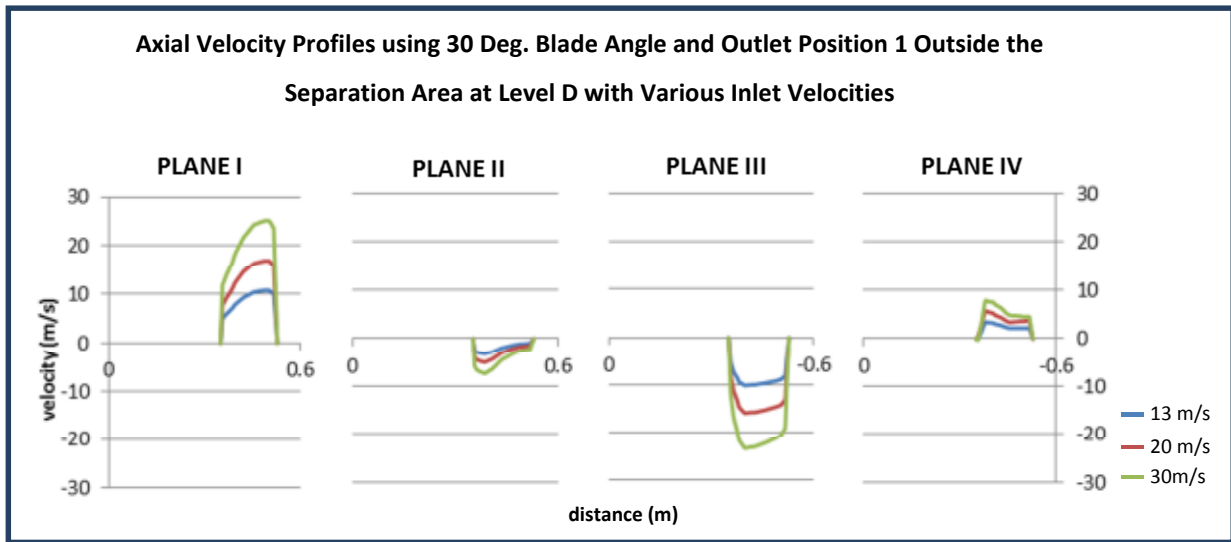


Figure 5.8: Axial velocity profiles at Level D with various inlet velocities

The occurrence of swirl can be observed clearly at all level of the classifier. The swirl begins with a large upward velocity in Plane I, reduces its speed in Plane II and then moves downwards with an increase velocity in Plane III. The swirl reduces its speed again in Plane IV and it repeats at all levels of the classifier. The trend of the swirl is found to be the same for all inlet velocities (13m/s, 20m/s and 30m/s). Figure 5.9 to Figure 5.11 compare the velocity profiles for different vane angles which show similar swirling trends.

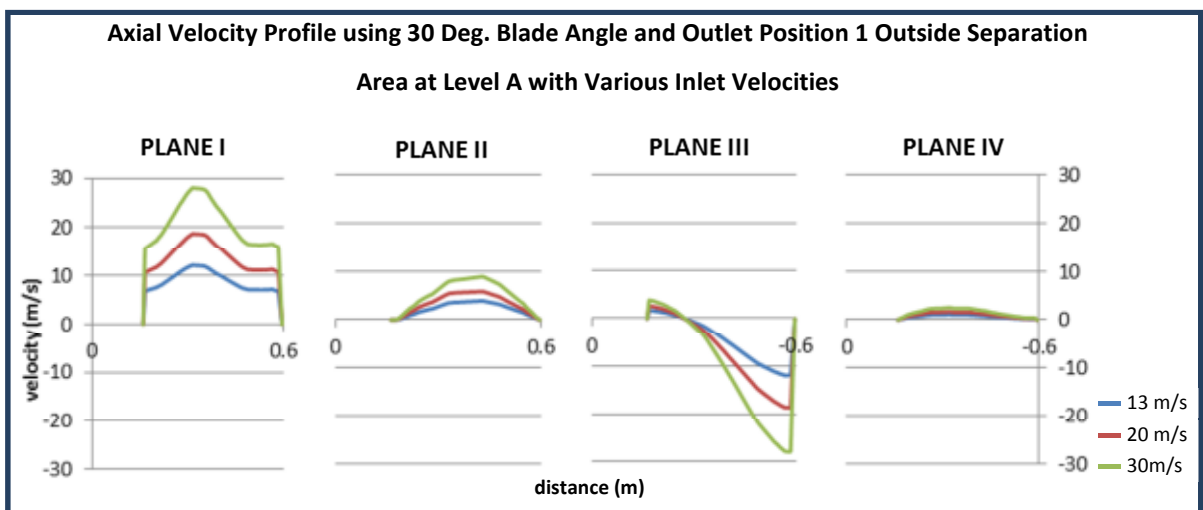


Figure 5.9: Axial velocity profile at Level A using 30° vane angle

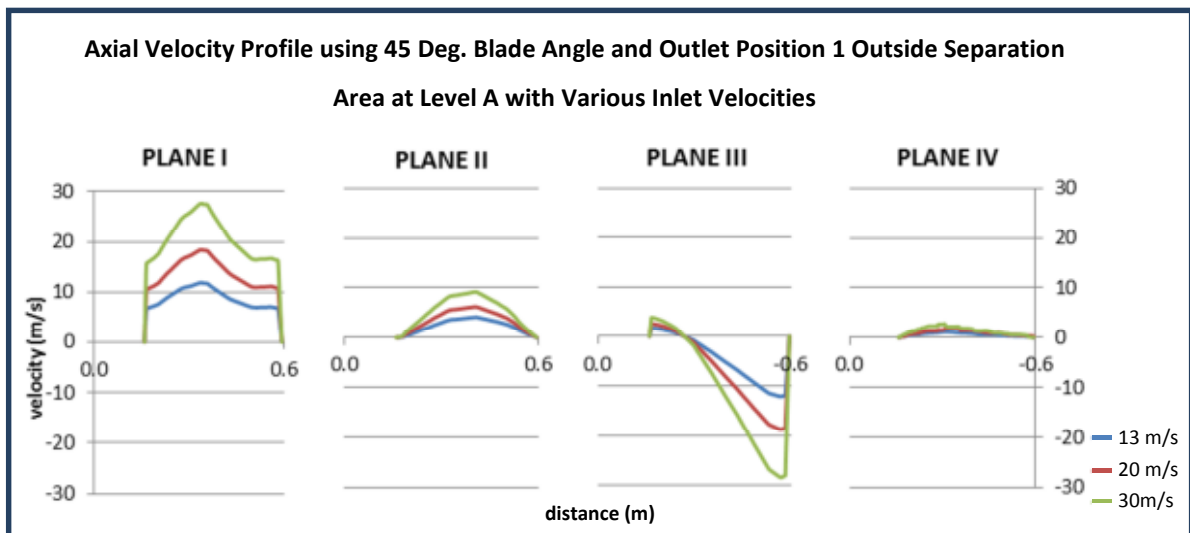


Figure 5.10: Axial velocity profile at Level A using 45° vane angle

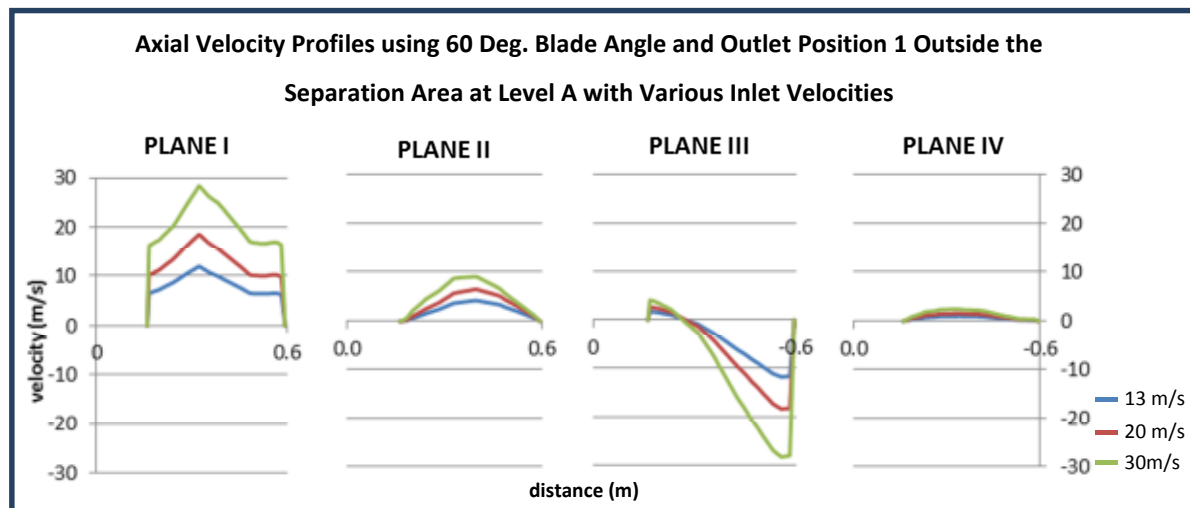


Figure 5.11: Axial velocity profile at Level A using 60° vane angle

From this initial axial velocities analysis it can be concluded that the most important plane to be evaluated is Plane I. The particles will move upwards at this plane area as it has the largest positive axial velocity. Further analyses which include the radial and tangential velocity components on this plane will be the focus of discussion in the following sections. Furthermore, this initial result also has been the basis why experiment data were collected at the similar area.

Experimental analysis (experimental validation) is discussed in the following chapter.

5.1.2 Effects of Varying the Inlet Velocity

In this section the effects of varying the inlet velocity on air flow outside and inside the separation area, and inside the vortex finder will be discussed.

5.1.2.1 Velocity Profile Outside the Separation Area

Figure 5.12 to Figure 5.15 show the axial velocity profiles outside the separation area for inlet velocities 13m/s, 20m/s and 30m/s at Level A through D. The vane angle is 30° and the outlet is at Position 1.

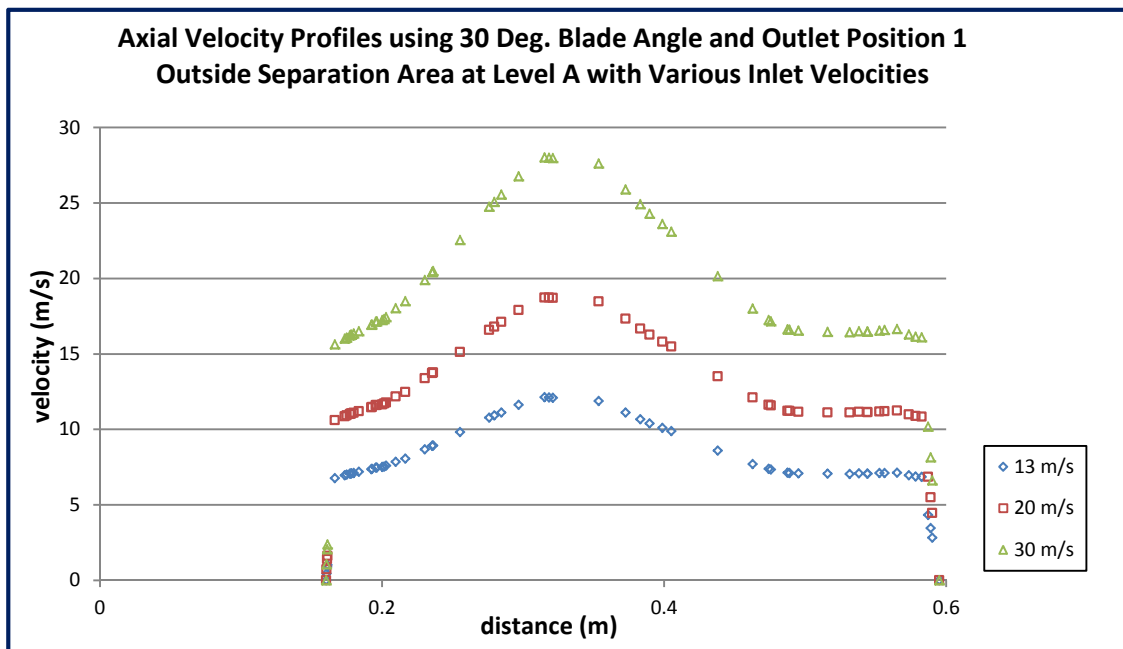


Figure 5.12: Axial velocity profiles outside separation area at Level A for various inlet velocities (30° vane angle)

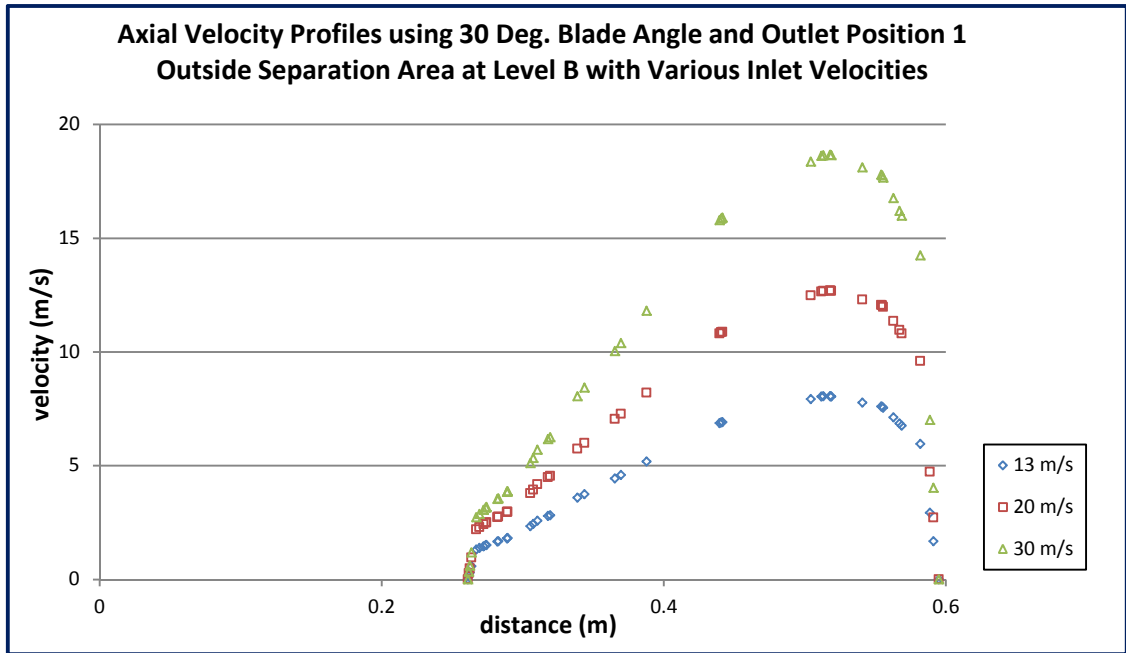


Figure 5.13: Axial velocity profiles outside separation area at Level B for various inlet velocities (30° vane angle)

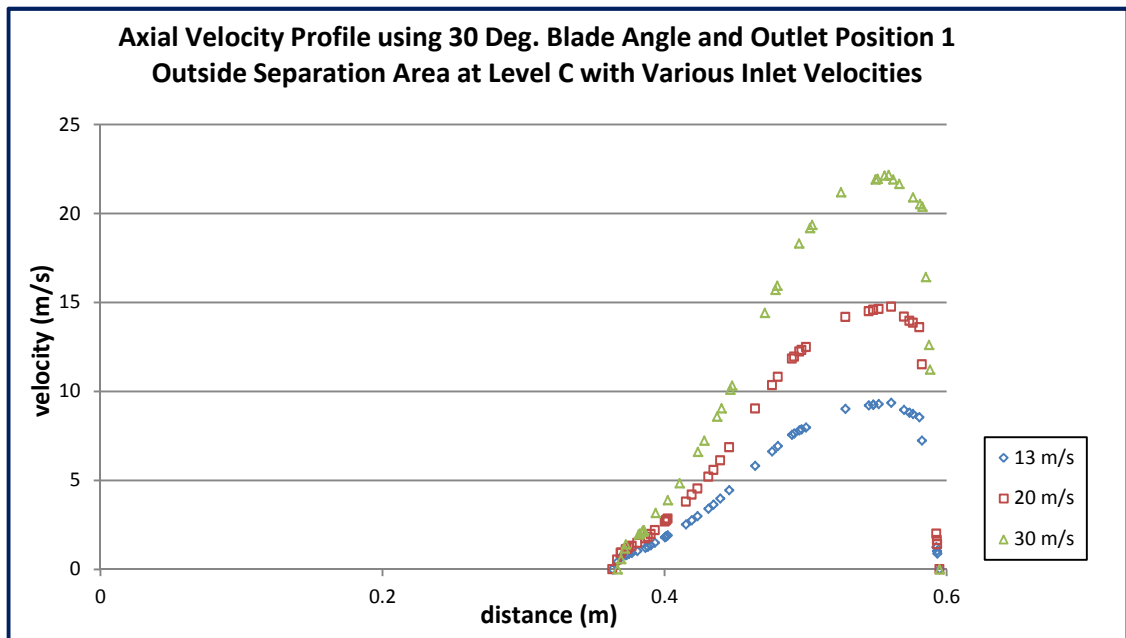


Figure 5.14: Axial velocity profile outside separation area at Level C for various inlet velocities (30° vane angle)

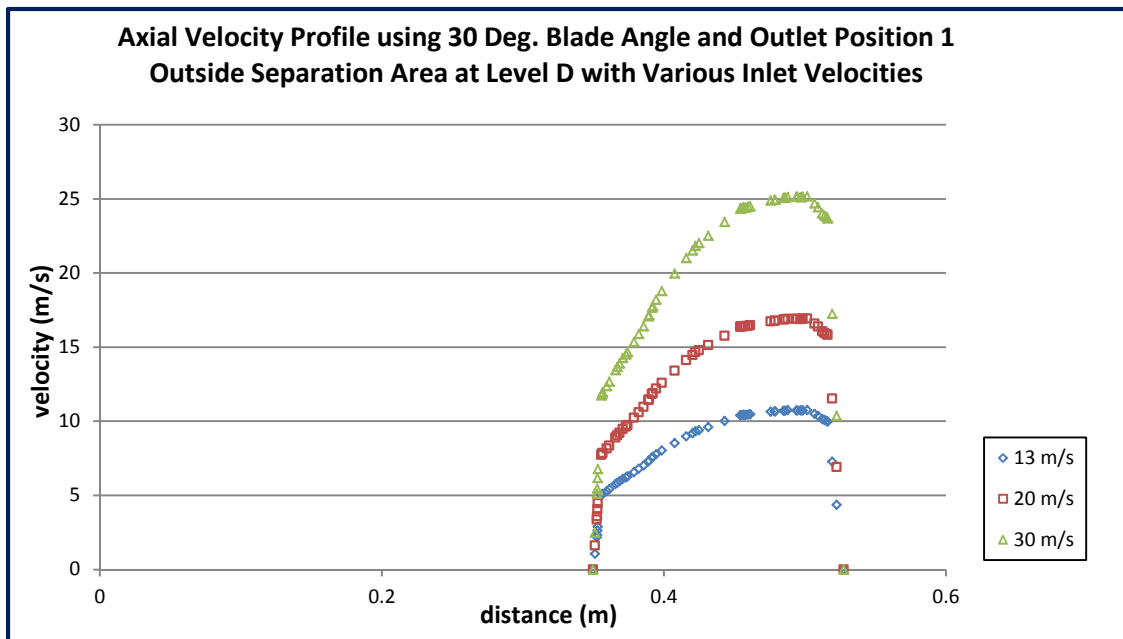


Figure 5.15: Axial velocity profile outside separation area at Level D for various inlet velocities (30° vane angle)

From the graphs, it can be noted that higher inlet velocity contributes to higher axial velocity at each level outside the separation area of the classifier. The axial velocity magnitude is at its highest at Level A and slightly reduced when it reaches Level B. The axial velocity magnitude then rise back when it reaches Level C and towards the vane area at Level D.

The transportation of coal particles upwards is dependent on the axial velocity. From the results it shows that higher axial velocity can be achieved by increasing the inlet velocity. This indirectly determines which particle size will move upwards or downwards. Higher axial velocity allows larger particle to be carried upwards. The effects of varying the inlet velocity for vane angles 45° and 60° are found to give similar results. The graphs are not presented here but are incorporated in Appendix I.

Figure 5.16 to Figure 5.19 show the radial velocity profiles outside the separation area for inlet velocities 13m/s, 20m/s and 30m/s at Level A through D. The vane angle is 30° and the outlet is at Position 1.

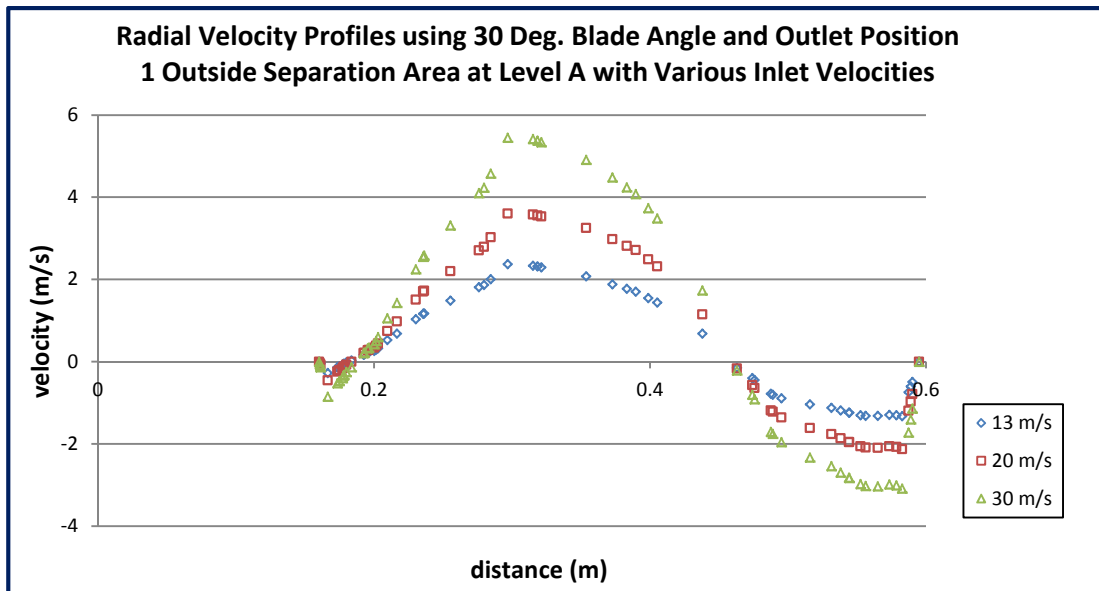


Figure 5.16: Radial velocity profile outside separation area at Level A for various inlet velocities (30° vane angle)

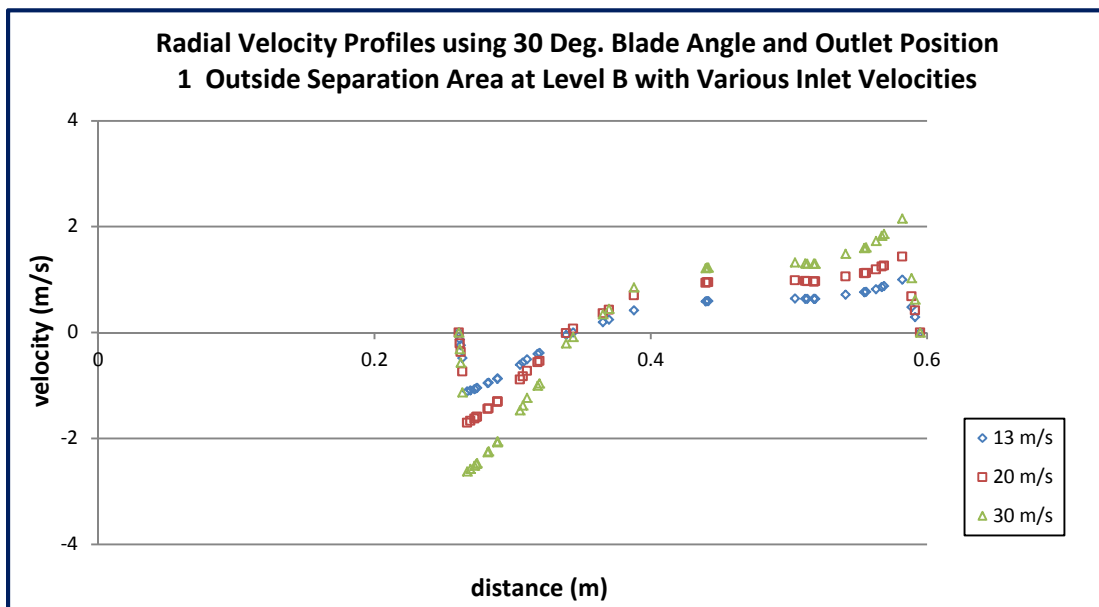


Figure 5.17: Radial velocity profiles outside separation area at Level B for various inlet velocities (30° vane angle)

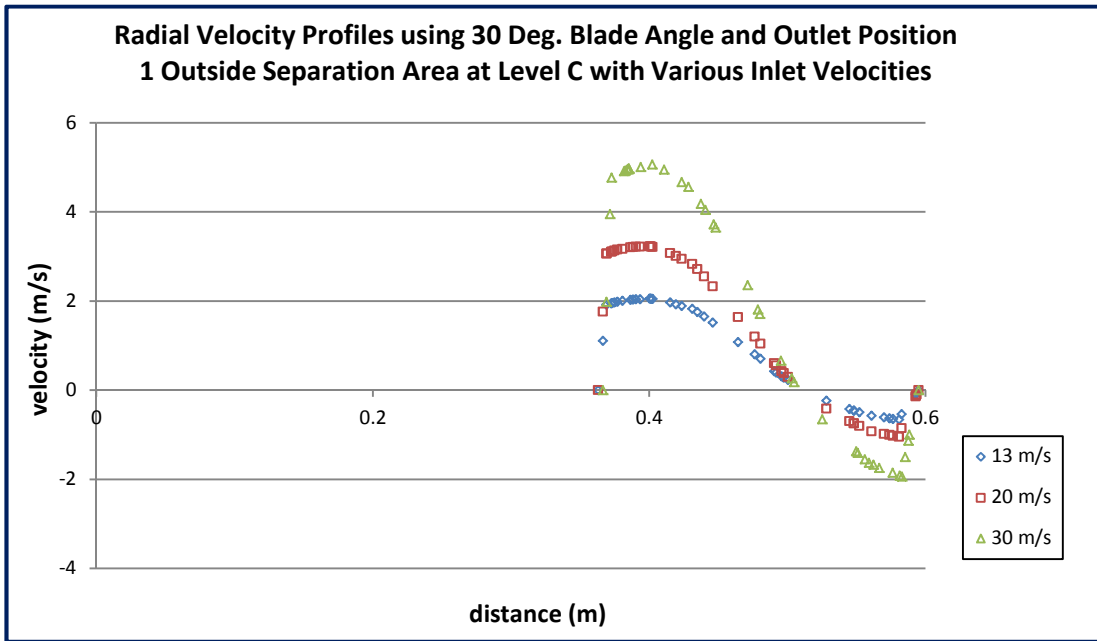


Figure 5.18: Radial velocity profiles outside separation area at Level C for various inlet velocities (30° vane angle)

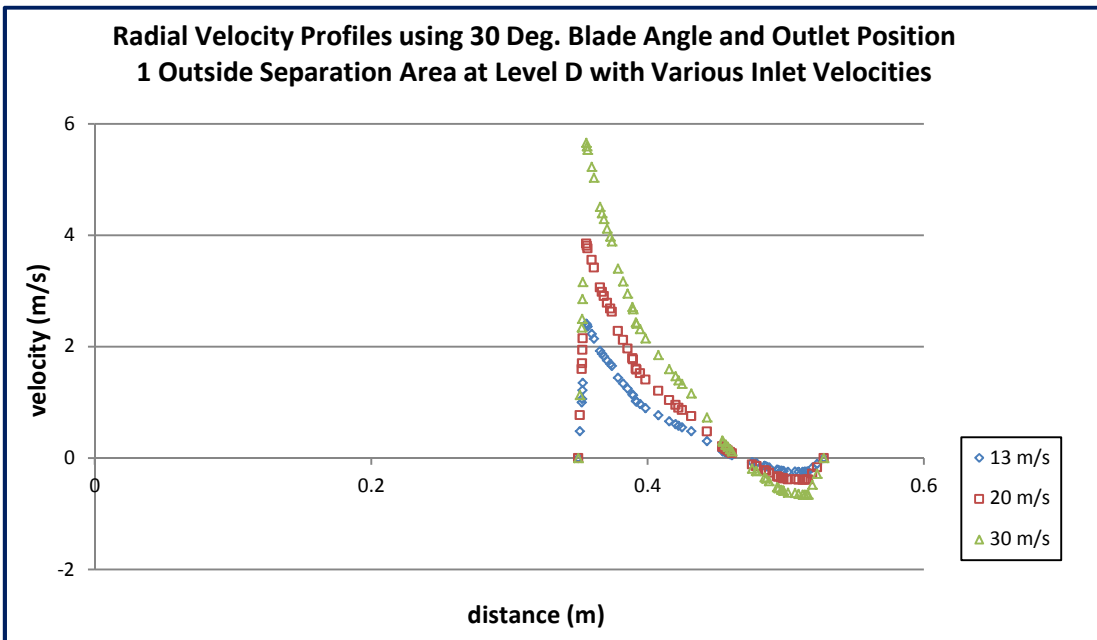


Figure 5.19: Radial velocity profiles outside separation area at Level D for various inlet velocities (30° vane angle)

From the graphs, it can be seen that all graphs are divided into two segments; positive and negative value. Positive values indicate the radial velocity is directed towards the core of the classifier meanwhile negative values indicate the radial velocity is directed towards the wall.

At Level A, the radial velocity is at its highest. The division of the two segments is nearly symmetry with the segment towards the classifier core has positive radial velocity while the segment towards the wall has negative radial velocity. With the high radial magnitude, this will help to push large particle towards the classifier walls.

At Level B, the division is opposite but with small magnitude. This phenomenon helps the smaller particles stay at the center of the area which indirectly helps them to be easily pushed upwards. At level C and D which are near to the top of the classifier, the segment with positive radial velocity is larger than the one with negative values. The positive segment is close to the core while the negative segment is towards the wall. This phenomenon assists the particles move easily into the separation area through the vanes especially at Level D. Furthermore the positive radial velocity magnitudes near the vane area (at Level D) are relatively large. This will expedite further the radial motion of the particle into the separation area.

In the graphs, it is apparent that increasing the inlet velocity increases the radial velocity magnitude. A larger radial velocity will push large particles to the wall

and also will allow the particle move faster radially. A fast radial movement at the top of the classifier will reduce the resident time of the escaped particles.

The effects of varying the inlet velocity for vane angles 45° and 60° offer quite similar results. The graphs are presented in Appendix I.

The tangential velocity profiles at Level A to Level D outside the separation area are presented in Figure 5.20 through Figure 5.23. Tangential velocity contributes to angular velocity ($v_{\text{tangential}} = \omega r$) of the flow inside the classifier. The angular velocity determines the magnitude of the centrifugal force acting on the particle. Higher centrifugal force pushes the particle towards the outside wall.

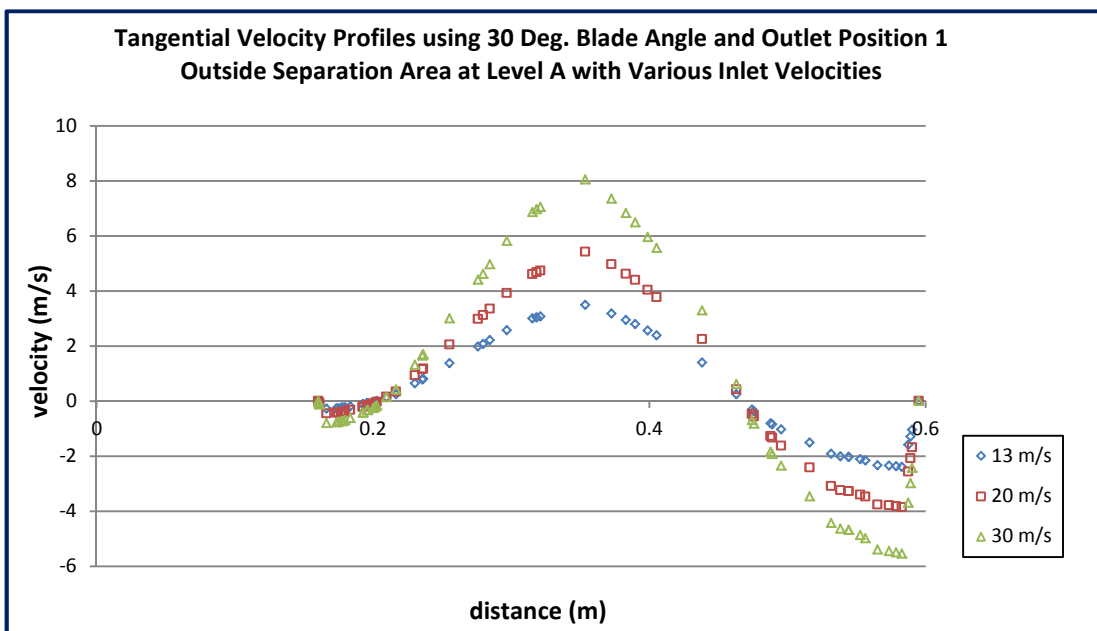


Figure 5.20: Tangential velocity profiles outside separation area at Level A for various inlet velocities (30° vane angle)

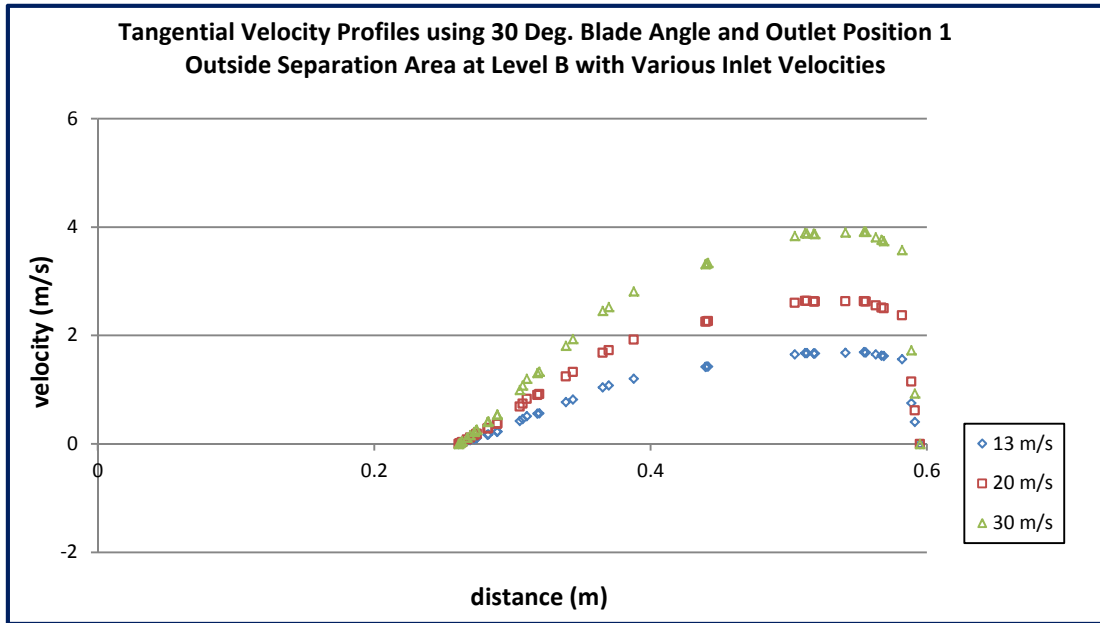


Figure 5.21: Tangential velocity profiles outside separation area at Level B for various inlet velocities (30° vane angle)

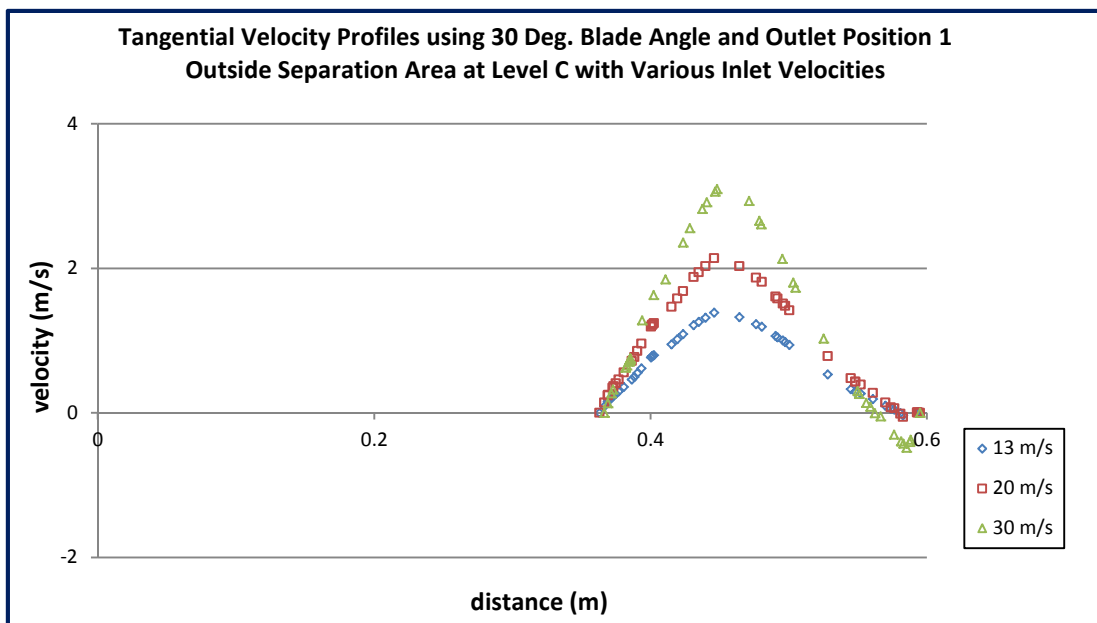


Figure 5.22: Tangential velocity profiles outside separation area at Level C for various inlet velocities (30° vane angle)

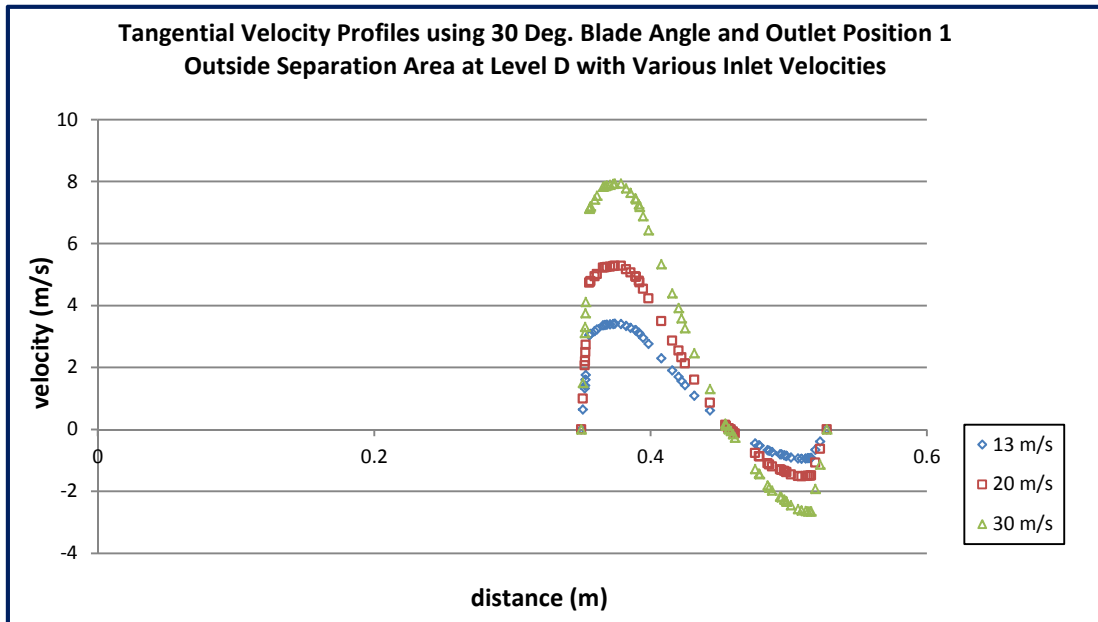


Figure 5.23: Tangential velocity profiles outside separation area at Level D for various inlet velocities (30° vane angle)

From the graphs it can be seen that the tangential velocity is at its highest at Level A and reduces dramatically at Level B. The velocity increases slightly at Level C and Level D. It can also be seen that higher inlet speed will contribute higher tangential velocity. Small tangential velocity decreases the resistance of the particles moving towards the core which is much needed at the upper level. It should be noted that the direction of the tangential velocities have no substantial effects on the particle motion. Appendix I presents the effects of varying the inlet velocity of vane angles 45° and 60° on the tangential velocity. There are no significant different in the results.

5.1.2.2 Velocity Profile Inside the Separation Area

Inside the separation area only the axial velocity profiles were analyzed. In the separation area what is of interest is how quick the particles can be released

through the outlet. Thus, radial and tangential velocity components are insignificant (Parham, 2003).

Figure 5.24 and 5.25 show the axial velocity profiles at the lower (Level B) and upper (Level C) region of the separation area. The axial velocity magnitudes inside the separation area are larger (more than double) compared to outside the separation area at the same axial level. This can be observed by comparing the graphs in Figure 5.13 with Figure 5.24 and Figure 5.14 with Figure 5.25. These shows that a particular size of particle that is able to go inside the separation area will definitely escaped through the outlet.

The inlet velocity has also been observed to have significant influence on the axial velocity inside the separation area. Higher inlet velocity contributes to higher axial velocity inside the area. Thus, the inlet velocity indirectly determines the residence time of the particle inside the classifier.

At Level C (upper region of the separation area), higher velocities magnitudes occur under the vortex finder while the velocity magnitude are almost constant around the vane area. This shows that vortex finder (towards the outlet) helps to increase the axial velocity magnitude.

Further axial velocity analyses inside the vortex finder are presented in Figure 5.26. The figure illustrates the axial velocity profile inside the vortex finder (at Level D) for outlet Position 1. The vane angle is 30° . The axial velocity inside the vortex finder is higher near the wall. This suggests the particles moves upward

close to the wall into the turret. Changing the inlet velocity has direct influence to the axial velocity in the vortex finder where higher inlet velocity results in higher axial velocity.

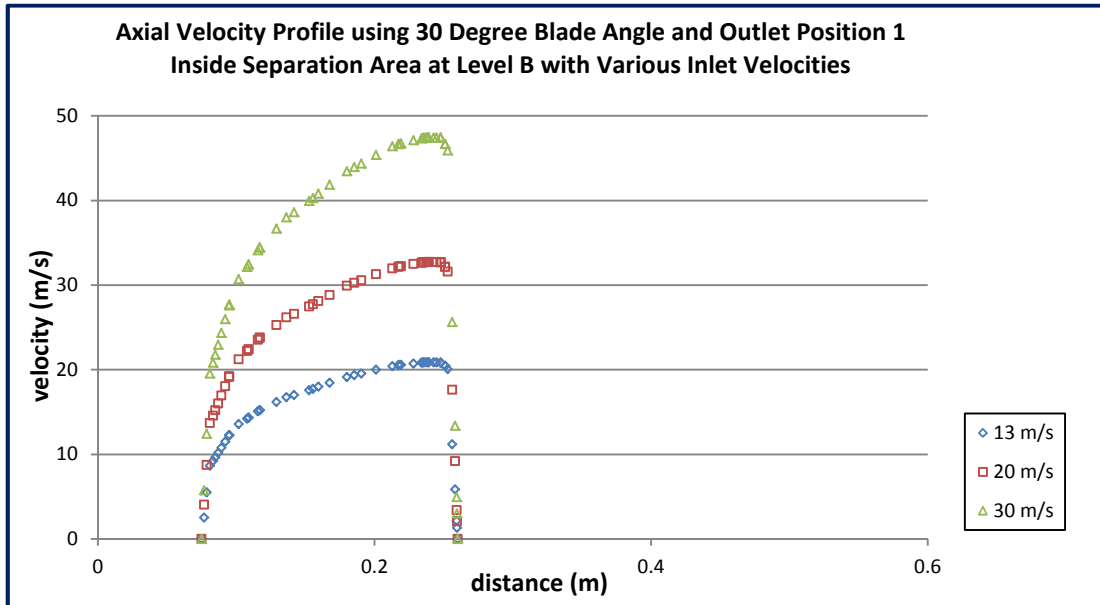


Figure 5.24: Axial velocity profiles inside separation area at lower region (Level B) for various inlet velocities (30° vane angle)

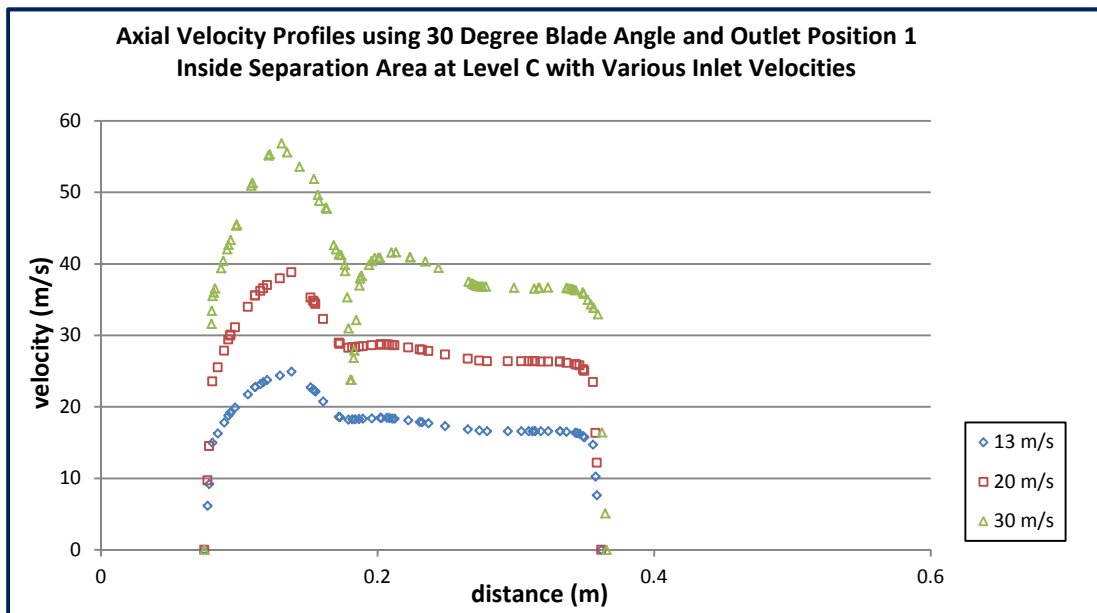


Figure 5.25: Axial velocity profiles inside separation area at upper region (Level C) for various inlet velocities (30° vane angle)

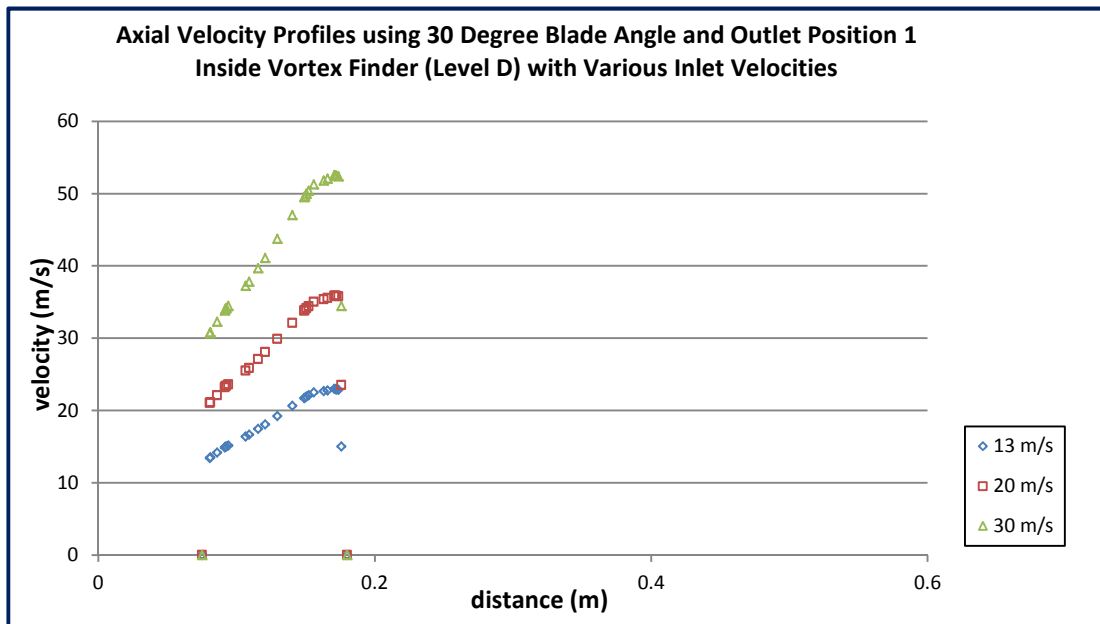


Figure 5.26: Axial velocity profiles inside vortex finder (Level D) for various inlet velocities with outlet Position 1 (30° vane angle)

Similar velocity patterns inside the separation area and vortex finder were also observed for classifier with vane angle 45° and 60°. Graphs in Appendix II provide the results for 45° and 60° vane angles which are comparable to the 30° vane angle results described above.

5.1.3 Effects of Varying the Vane Angle

In this section, the effects of varying the vane angle on air flow outside and inside the separation area, and inside the vortex finder will be discussed. Vane angles evaluated are 30°, 45° and 60°.

Figure 5.27 shows initial observation of the axial, radial and tangential velocity distributions for vane angle 30°, 45° and 60°. The figures show that the vane angle has considerable influence on the air velocity flow field. Different vane

setting develops different velocity contour. In the classifier, vane is used to channel air with particle into the centre core. It creates a cyclonic effect on entry inside the cone. This helps heavier particle to flow deeper into the centre core while lighter particle will flow upstream with the air. Thus, the effect of varying the vane angle is observed to be very important in the analysis of the classifier performance. A more thorough analysis on the effect of varying the vane angle had been conducted and is presented in the following sections.

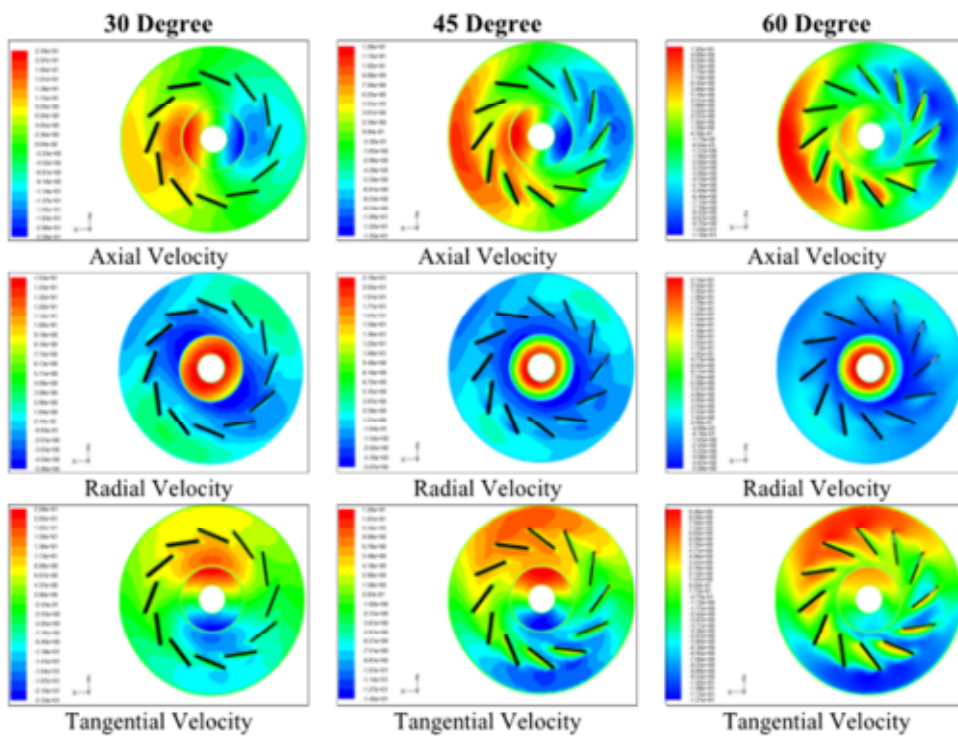


Figure 5.27: Air velocity contour for various vane angles at position1 with 13 m/s inlet velocity

5.1.3.1 Velocity Profile Outside the Separation Area

The axial velocity profiles for various vane angles with inlet speed of 13 m/s at Level A through Level D are presented in Figure 5.28 to 5.31 below. The graphs show that varying the vane angle does not have any effect on the axial velocity outside the separation area. The axial velocity profiles are all the same at all level

in the area. Similar results were found for inlet velocity of 20m/s and 30m/s which are included in Appendix III.

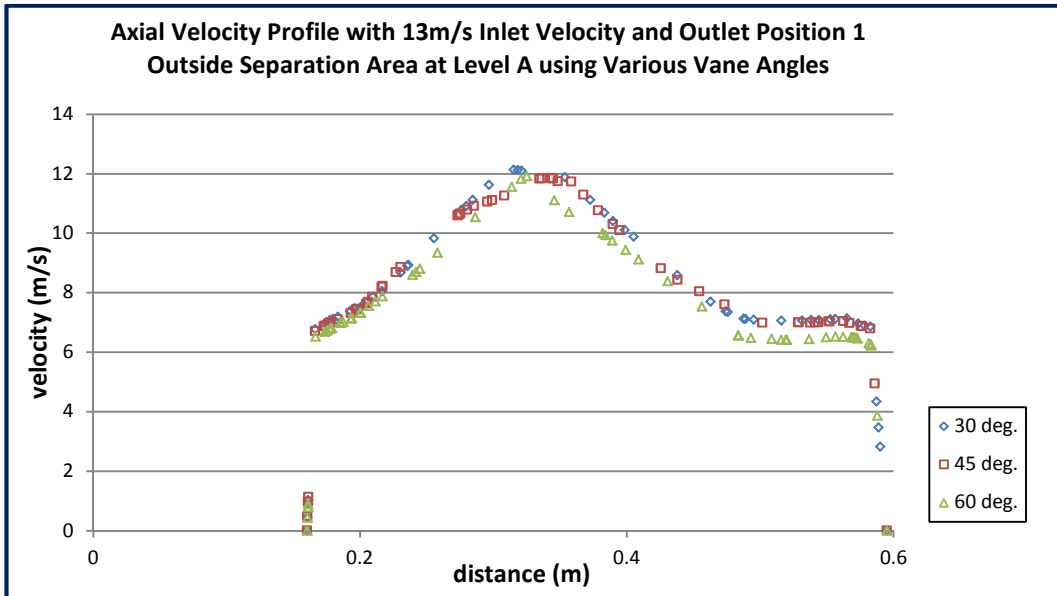


Figure 5.28: Axial velocity profiles outside separation area at Level A for various vane angles (13 m/s inlet velocity)

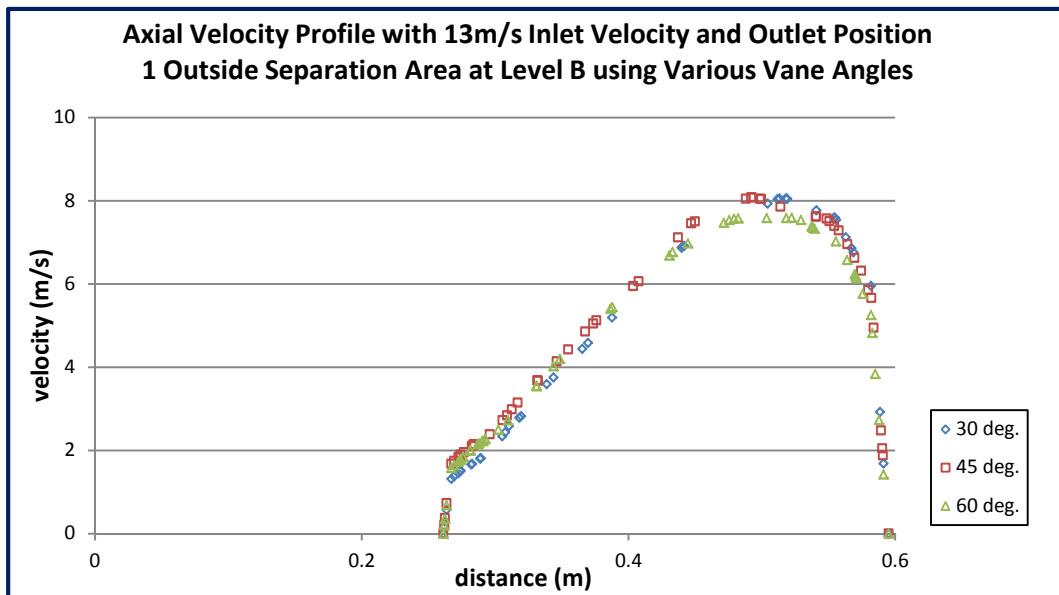


Figure 5.29: Axial velocity profiles outside separation area at Level B for various vane angles (13m/s inlet velocity)

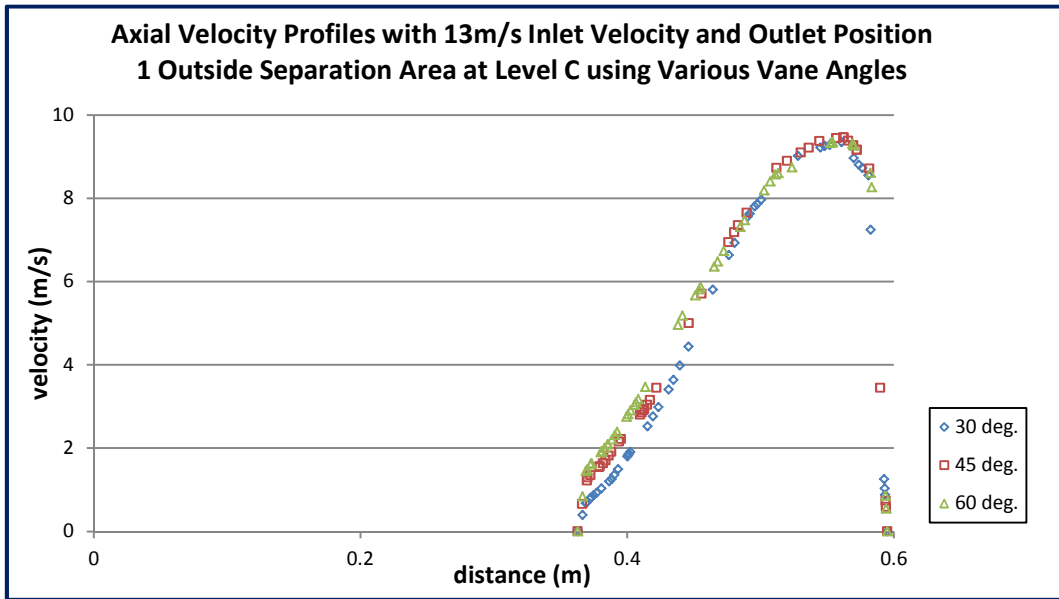


Figure 5.30: Axial velocity profiles outside separation area at Level C for various vane angles (13m/s inlet velocity)

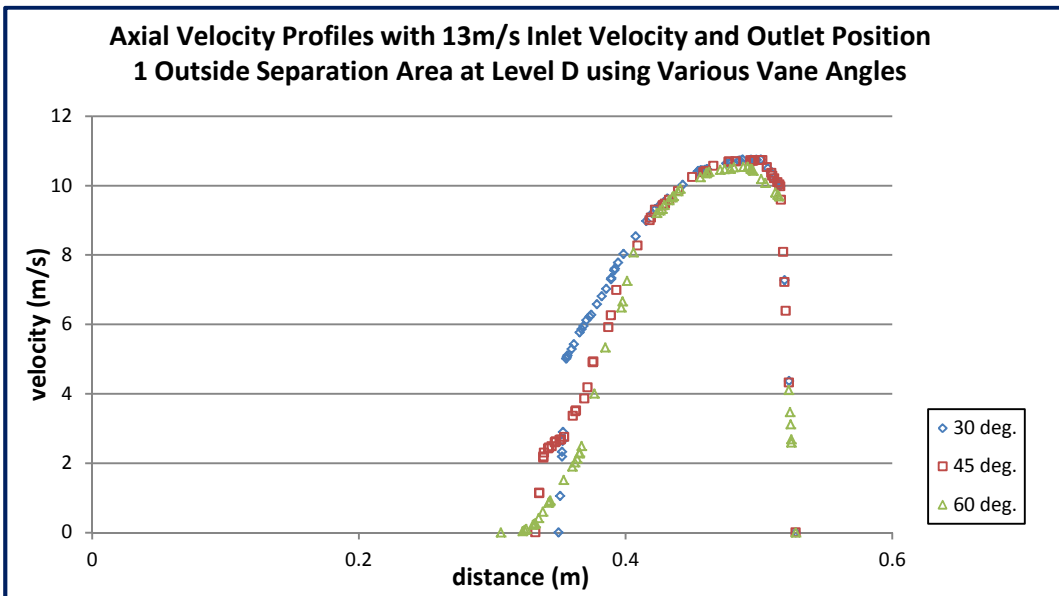


Figure 5.31: Axial velocity profiles outside separation area at Level D for various vane angles (13m/s inlet velocity)

Meanwhile Figure 5.32 through Figure 5.35 show the radial velocity profiles for various vane angles with inlet speed of 13 m/s at Level A through Level D. Varying the vane angle does not influence the radial velocity at Level A, Level B and Level C. But, at Level D which is near the vane area, it can be observed that smaller vane angle provide higher radial velocity for a same inlet velocity. Since the radial velocity profiles have positive values, it can be concluded that using smaller vane angles will improve the flowing of particles into the separation area.

The radial velocity profiles developed from varying vane angles for 20m/s and 30m/s inlet velocities also conform to the results described above. These are illustrated in the graphs in Appendix III.

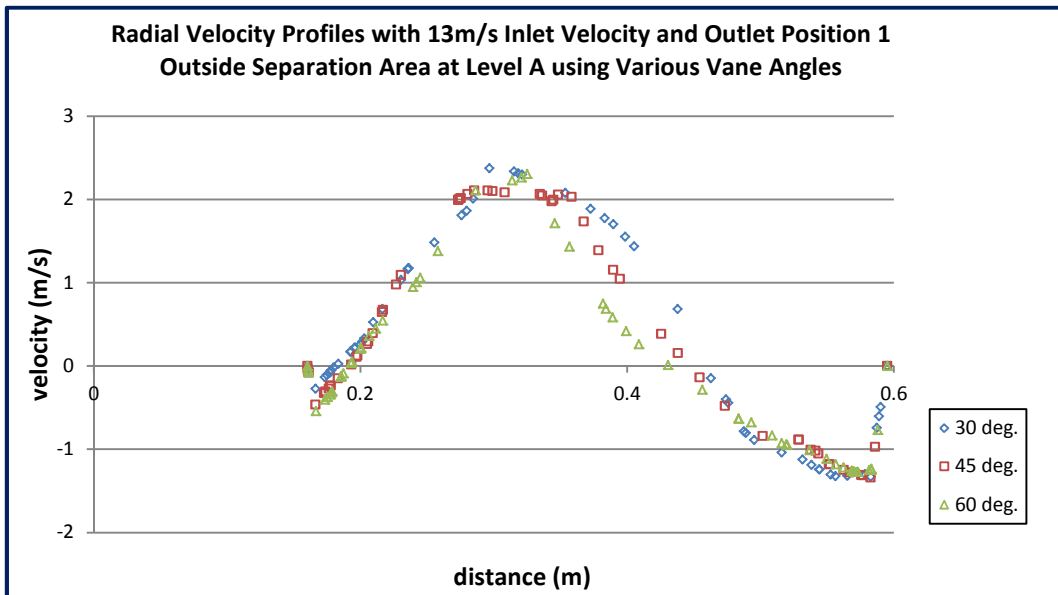


Figure 5.32: Radial velocity profiles outside separation area at Level A for various vane angles (13m/s inlet velocity)

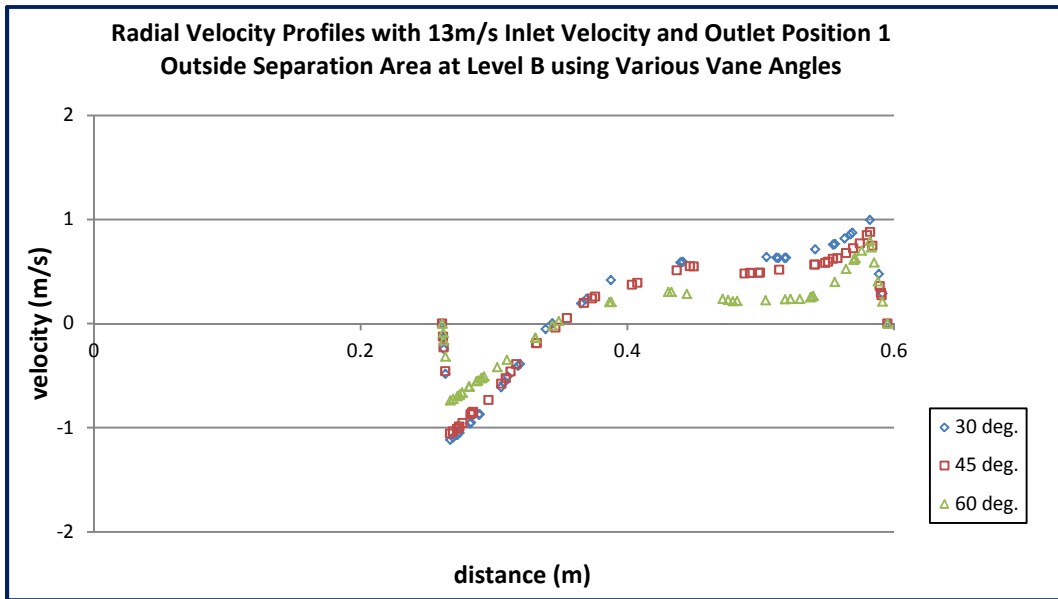


Figure 5.33: Radial velocity profiles outside separation area at Level B for various vane angles (13m/s inlet velocity)

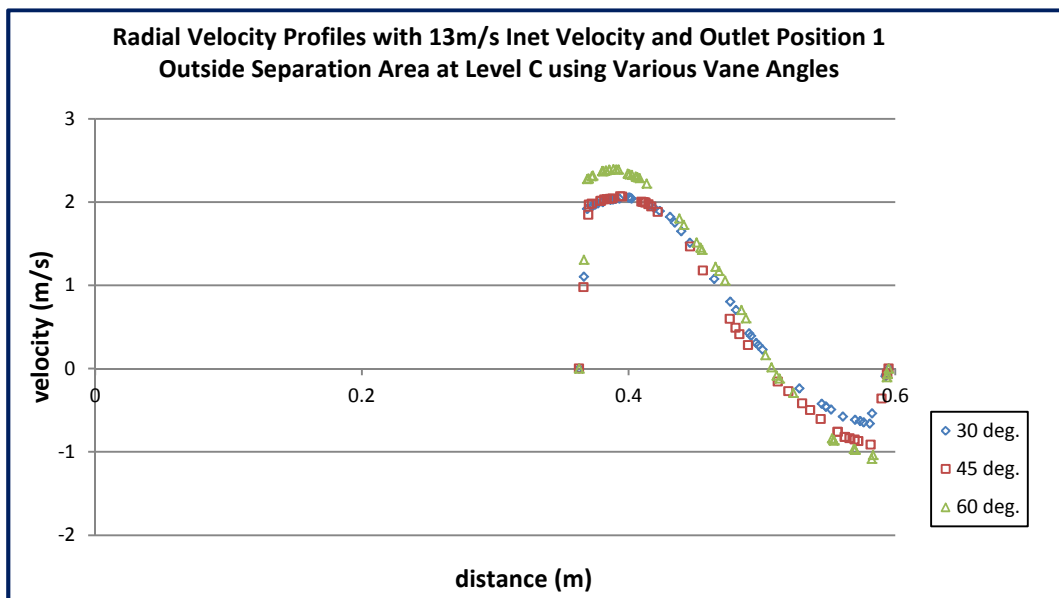


Figure 5.34: Radial velocity profiles outside separation area at Level C for various vane angles (13m/s inlet velocity)

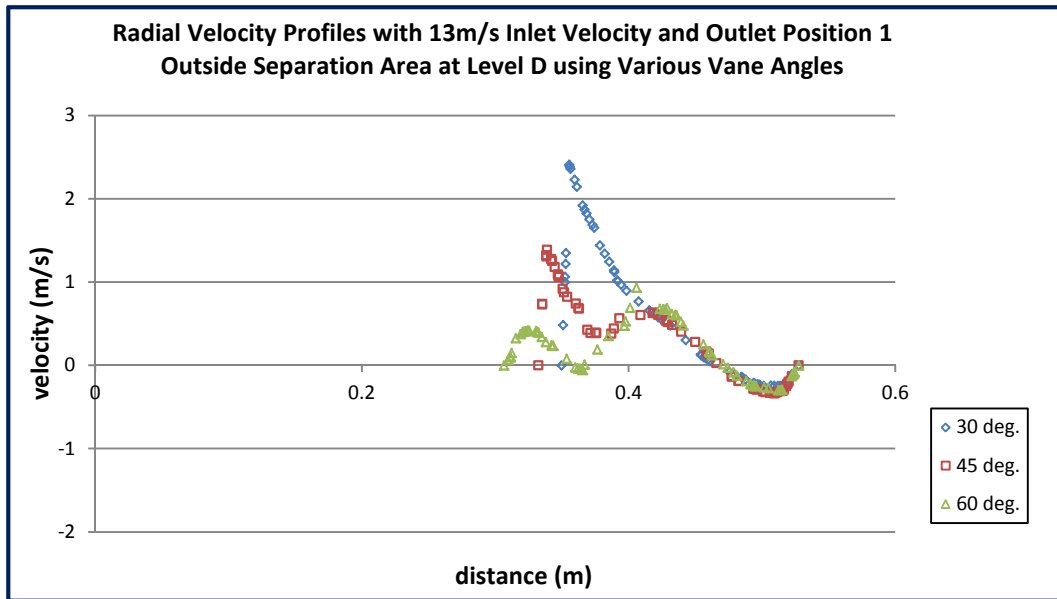


Figure 5.35: Radial velocity profiles outside separation area at Level D for various vane angles (13 m/s inlet velocity)

Figure 5.36 through Figure 5.39 show the tangential velocity profiles resulting from varying the vane angles. The tangential velocity magnitudes do not show much difference at Level A outside the separation area. The magnitudes are increased by the reduction of the vane angle at Level B, Level C and Level D. The increments become more apparent at the higher level. The increase of the tangential velocity magnitude increases the centrifugal force which is the resistance to the particles radial motion. It can be concluded that although smaller vane angle provide better radial flow at the higher level outside the separation area, but, the centrifugal force is also higher.

Similar results were also observed for other inlet velocities (20m/s and 30m/s) which are shown in Appendix III.

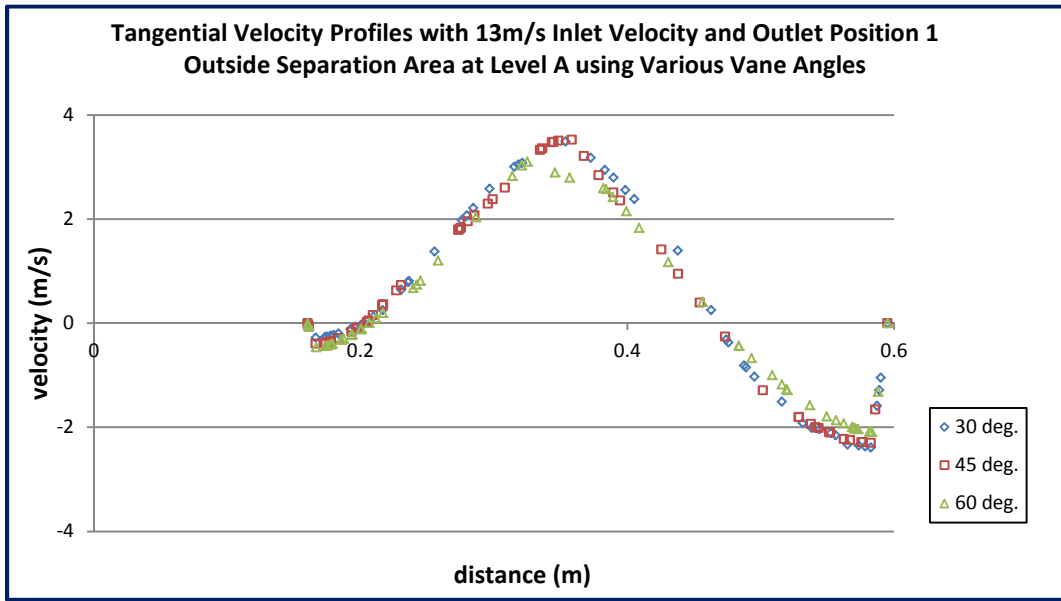


Figure 5.36: Tangential velocity profiles outside separation area at Level A for various vane angles (13m/s inlet velocity)

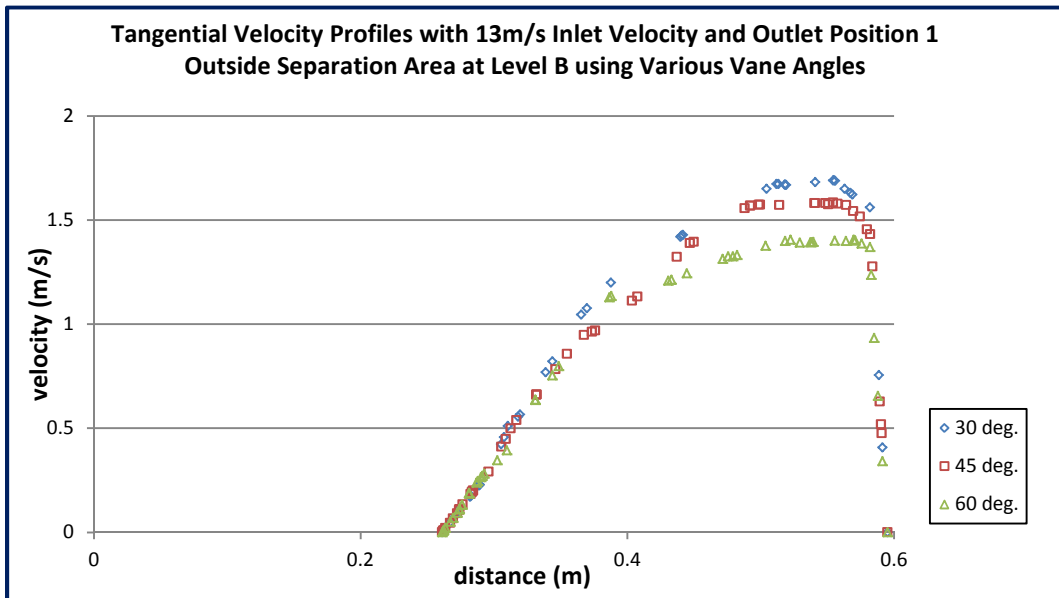


Figure 5.37: Tangential velocity profiles outside separation area at Level B for various vane angles (13m/s inlet velocity)

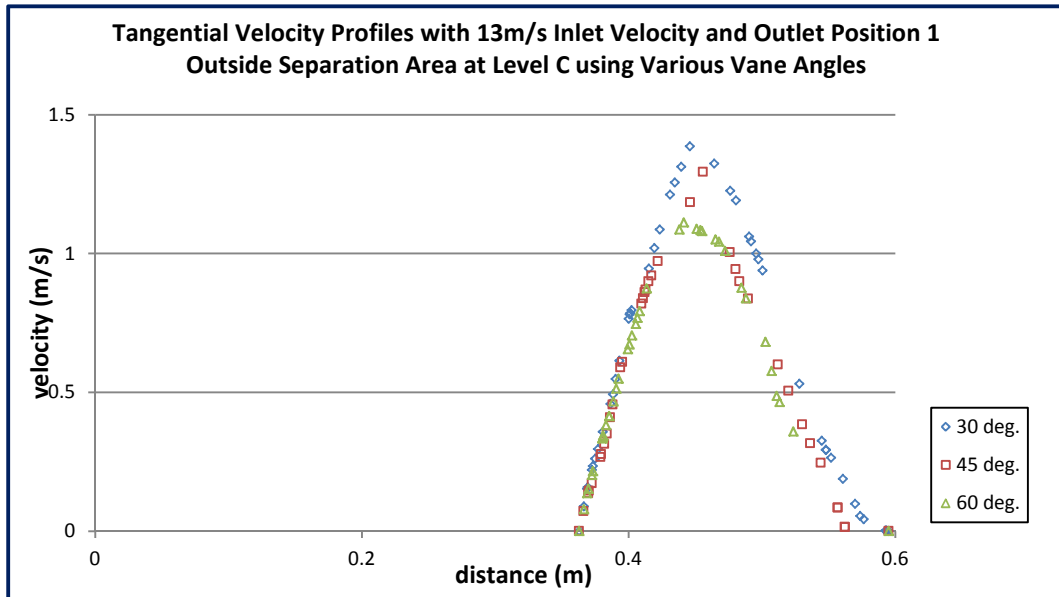


Figure 5.38: Tangential velocity profiles outside separation area at Level C for various vane angles (13m/s inlet velocity)

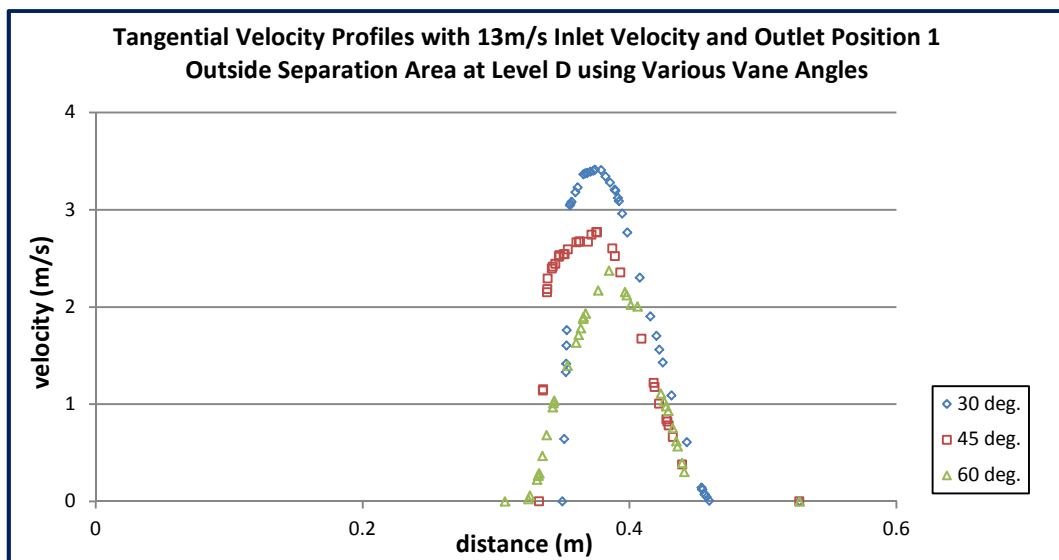


Figure 5.39: Tangential velocity profiles outside separation area at Level D for various vane angles (13m/s inlet velocity)

5.1.3.2 Velocity Profile Inside the Separation Area

In previous section (Section 5.1.3.1), it was observed that varying the vane angles show no effect on the axial velocity profiles outside the separation area. However, inside the separation area, the vane angle has significant influence on the axial

velocity. It is apparent that smaller vane angle increases the magnitude of axial velocity in both lower and upper region of the separation area. This can be observed from Figure 5.40 and 5.41 which show the axial velocity profiles at the lower (Level B) and upper (Level C) region of the separation area for various vane angles with 13 m/s inlet velocity. High axial velocity magnitude helps better upwards transportation of coal particles. Appendix IV shows the axial velocity profiles inside separation area for 20m/s and 30m/s inlet velocities resulting from varying the vane angles. The profiles imitate the results for 13m/s inlet velocity described above.

Figure 5.42 shows the axial velocity profiles inside the vortex finder (at Level D) for outlet Position 1. Changing the vane angle influences the axial velocity in the vortex finder where smaller vane angle results in higher axial velocity. This is also true for other inlet velocities which are shown in Appendix IV.

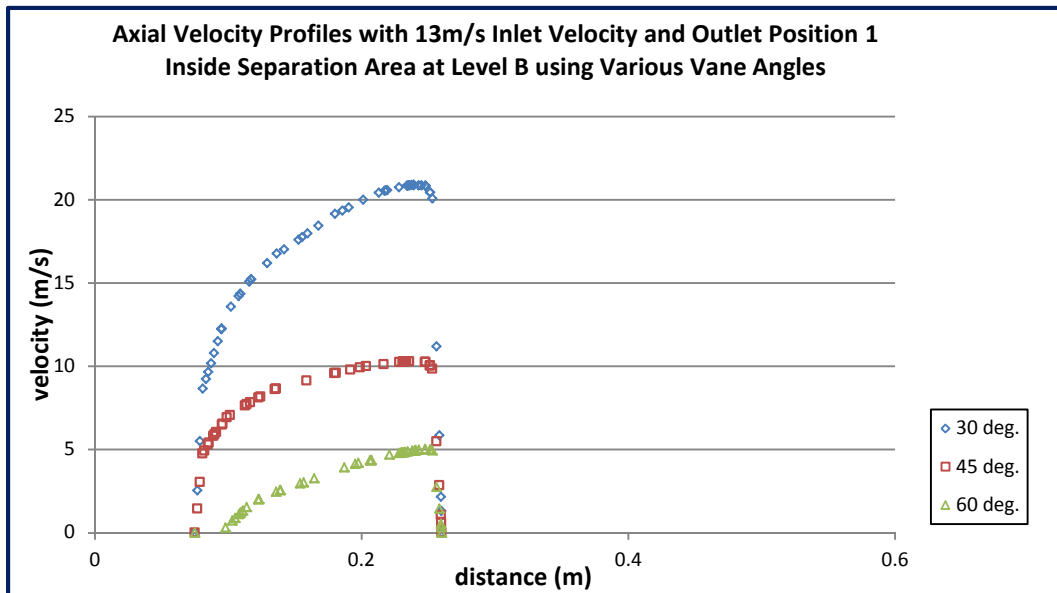


Figure 5.40: Axial velocity profiles inside separation area at lower region (Level B) for various vane angles (13m/s inlet velocity)

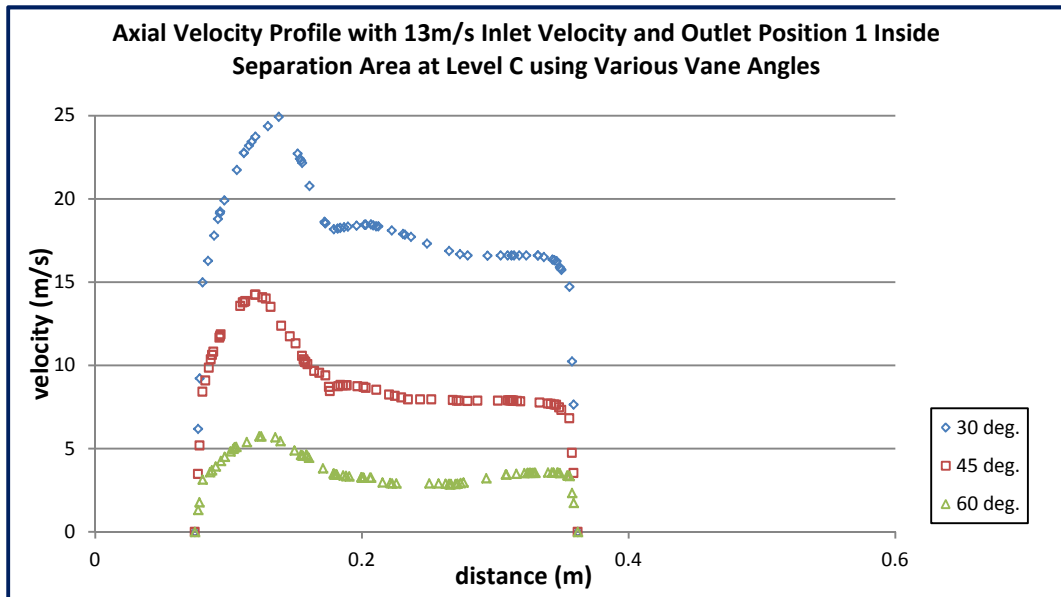


Figure 5.41: Axial velocity profiles inside separation area at upper region (Level C) for various vane angles (13m/s inlet velocity)

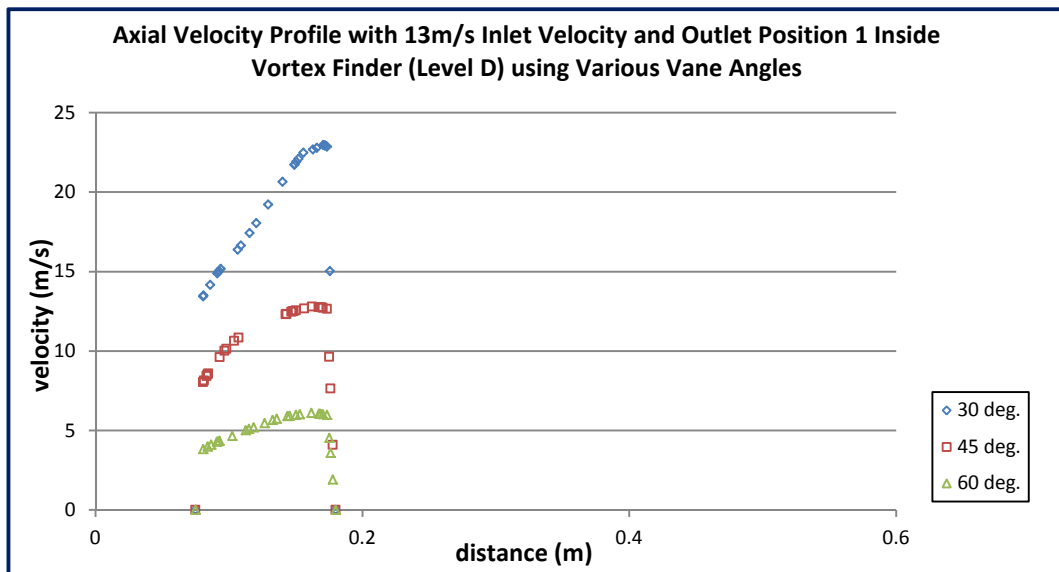


Figure 5.42: Axial velocity profiles inside vortex finder (Level D) for various vane angles with outlet Position 1 (13m/s inlet velocity)

5.1.4 Effects of Varying the Outlet Position

Analyses were also conducted to find the effect of varying the outlet positions of the classifier. Both outside and inside the separation area together with the vortex finder area were analyzed

Figure 5.43 shows the effect of varying outlet positions on pressure distribution inside the classifier at 30° vane angle with 15 m/s inlet velocity. The difference between the pressure contours is not apparent. From this initial observation, it can be concluded that varying the outlet positions have not much impact on the classifier performance. However, velocity profile analysis was performed to confirm the finding. The following sections describe the velocity profile analysis.

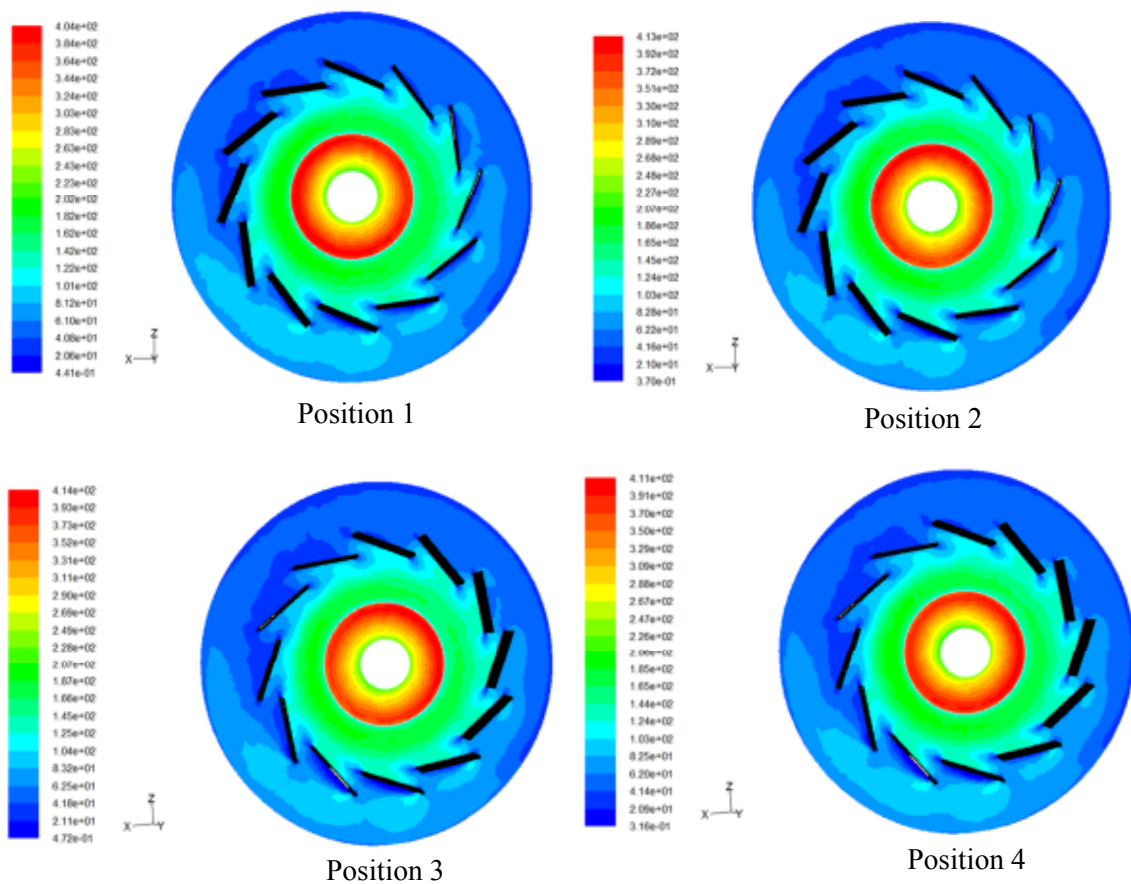


Figure 5.43: Pressure contour for 30° vane angles at various position with 13m/s inlet velocity

5.1.4.1 Velocity Profile Outside the Separation Area

Figure 5.44 to Figure 5.49 shows the axial, radial and tangential velocity profiles outside the separation area for the four outlet positions. Both lower and upper

regions (Level B and Level D) were analyzed. The vane angle is 30° and inlet velocity is 13m/s.

Outlet position is an opening at the upper level of the classifier where the coal particles are released. The positions of the outlet are as illustrated in Figure 5.2. The study is to determine whether the location of the outlet has any influence on the classifier performance.

It was found that the location of the outlet does not have any influence on all the three velocity components in both lower and upper region outside the separation area. Similar results were also established for all variation of inlet velocities and vane angles which are shown in Appendix V.

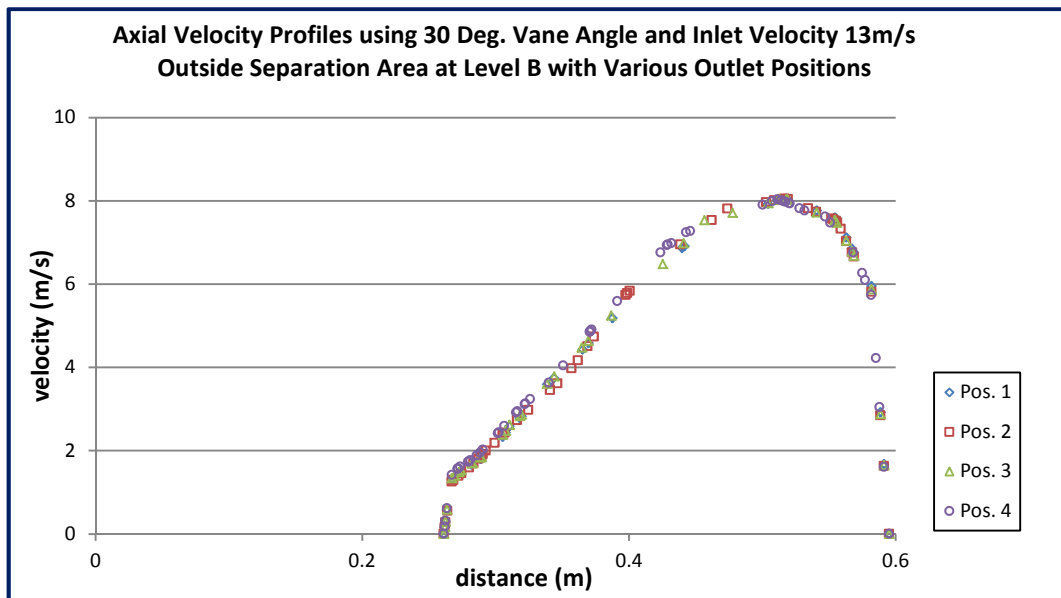


Figure 5.44: Axial velocity profiles outside separation area for various outlet positions (lower region, Level B)

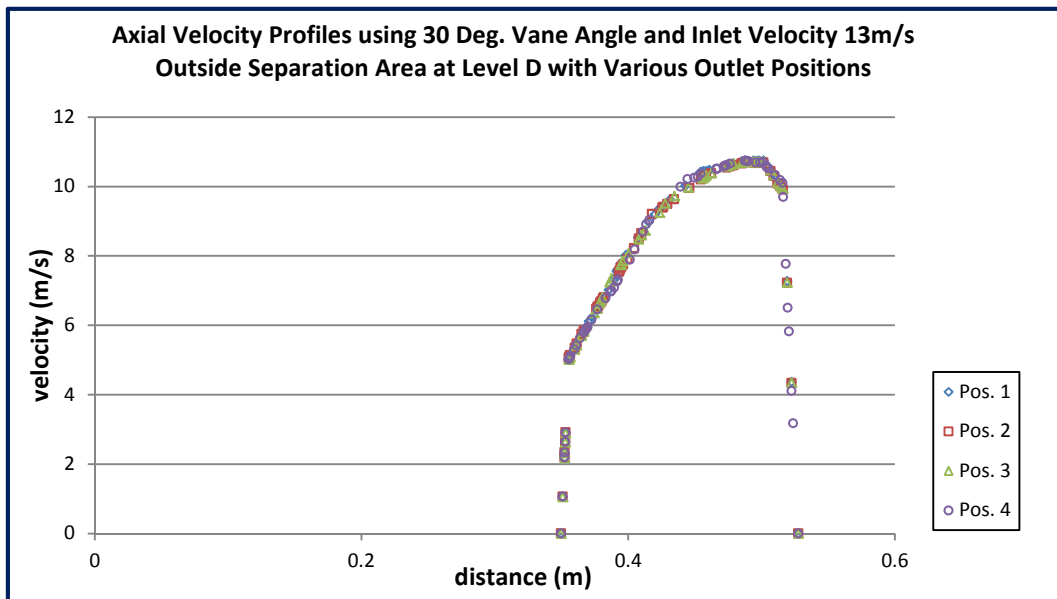


Figure 5.45: Axial velocity profiles outside separation area for various outlet positions (upper region, Level D)

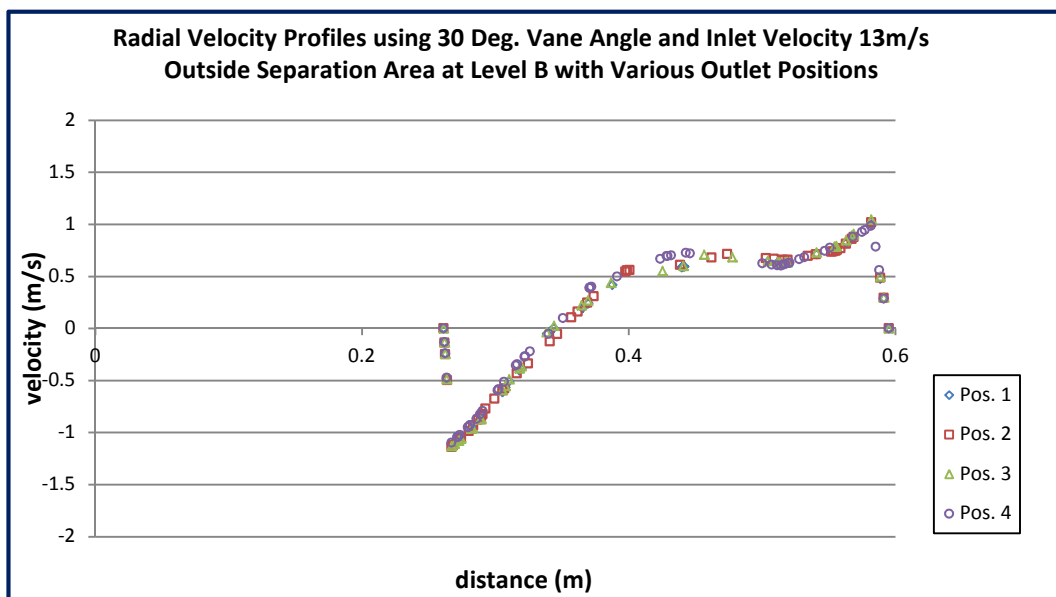


Figure 5.46: Radial velocity profiles outside separation area for various outlet positions (lower region, Level B)

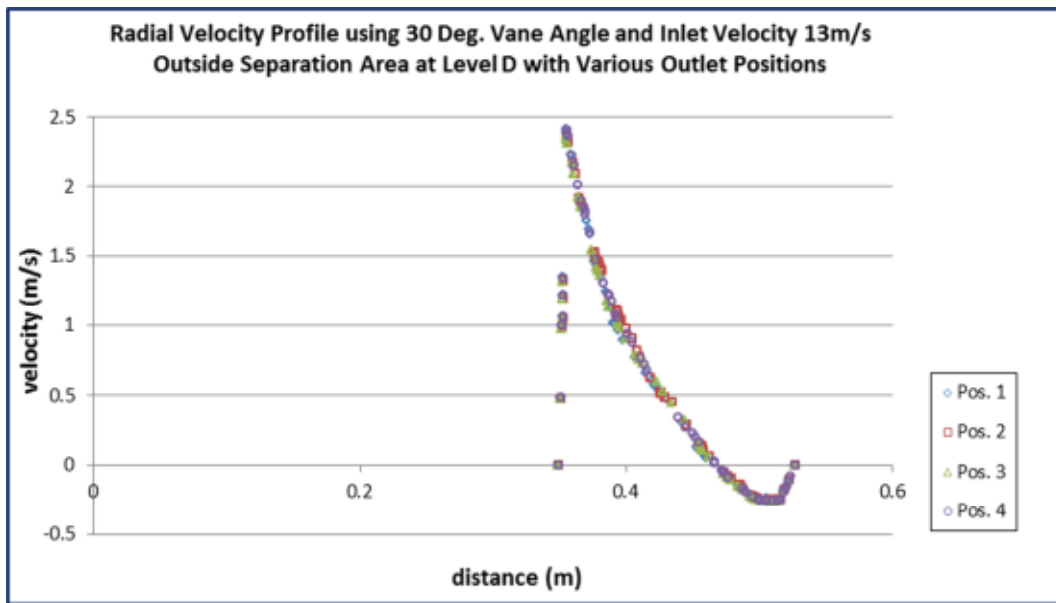


Figure 5.47: Radial velocity profiles outside separation area for various outlet positions (upper region, Level D)

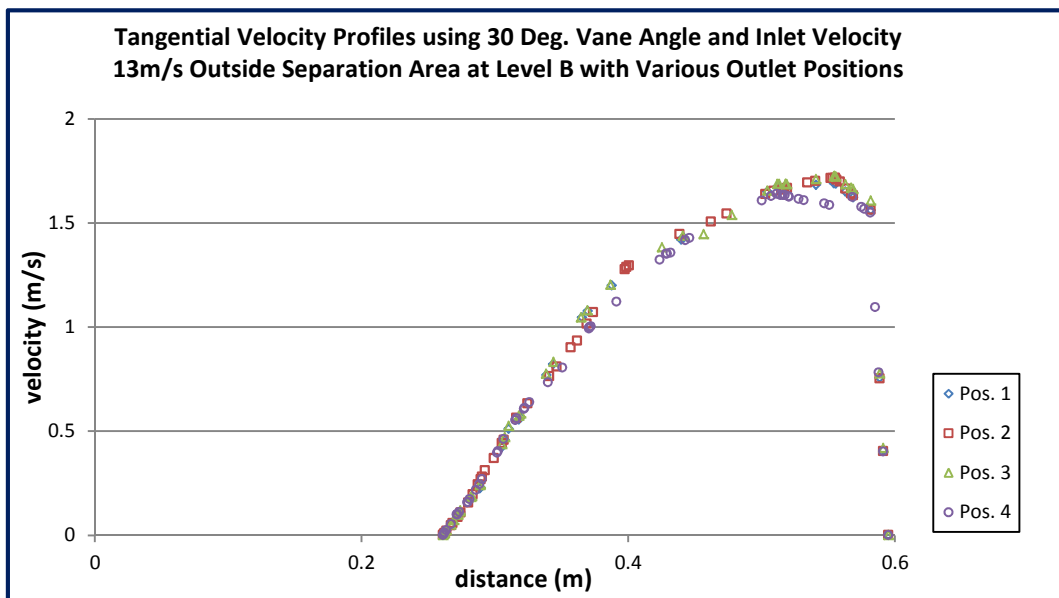


Figure 5.48: Tangential velocity profiles outside separation area for various outlet positions (lower region, Level B)

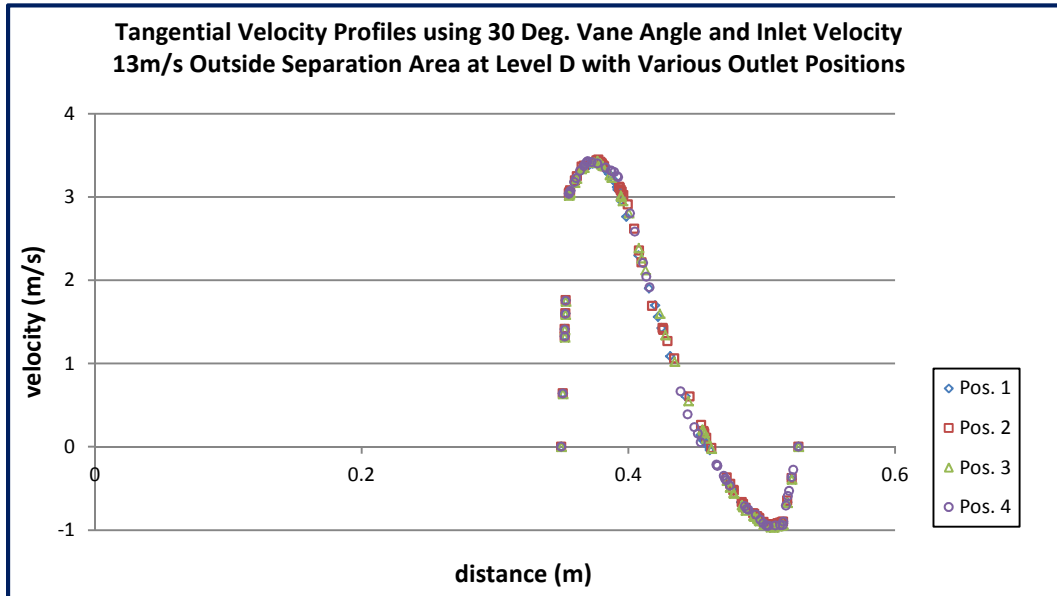


Figure 5.49: Tangential velocity profiles outside separation area for various outlet positions (upper region, Level D)

5.1.4.2 Velocity Profile Inside the Separation Area

Axial profiles inside the separation area for the four different outlet position are shown in Figure 5.50 and Figure 5.51. Both lower and upper regions (Level B and Level D) were analyzed. The vane angle is 30° and inlet velocity is 13 m/s. It can be observed that the location of outlet does not influence the axial velocity inside the separation area. Similar results were also observed for all variation of inlet velocities and vane angles which are shown in Appendix VI.

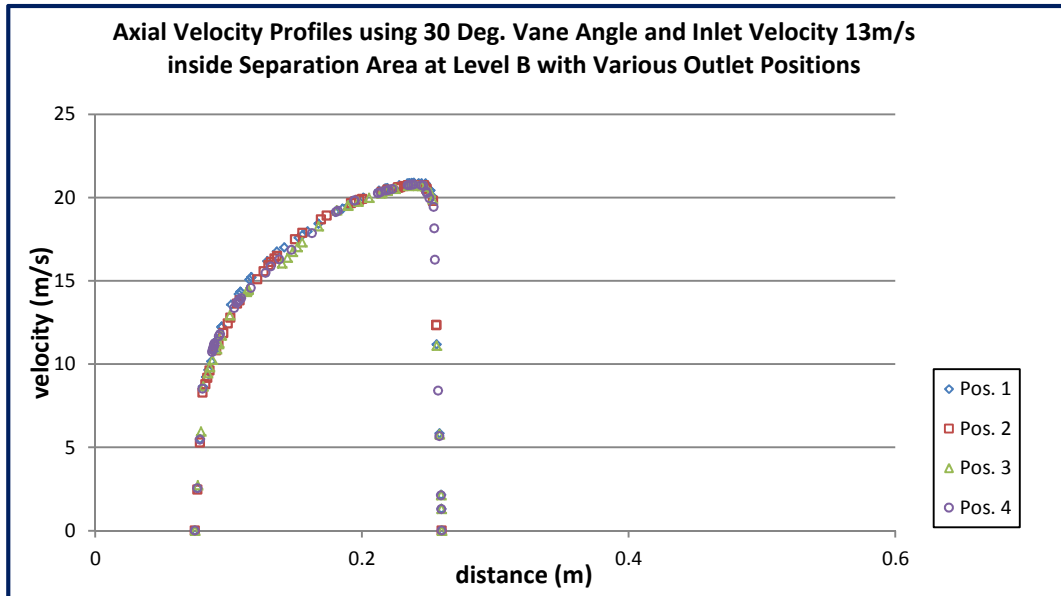


Figure 5.50: Axial velocity profiles inside separation area for various outlet positions (lower region, Level B)

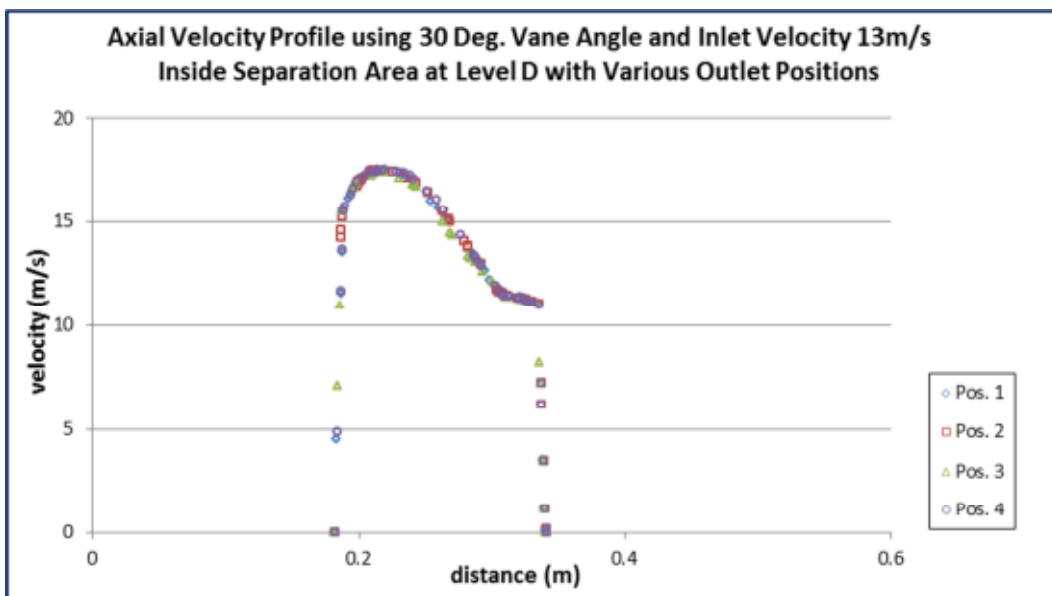


Figure 5.51: Axial velocity profiles inside separation area for various outlet positions (upper region, Level D)

Figure 5.52 to Figure 5.54 shows axial velocity profile inside the vortex finder (Level D) for different outlet locations with inlet velocity 13m/s. The vane angles are 30°, 45° and 60°.

From the figures it can be observed, that is no influence of outlet position on axial velocity inside the vortex finder for 30° vane angle. However, if 45° or 60° vane angle is used, selecting the appropriate outlet location will increase the axial velocity. From graph in Figure 5.53 for the 45° vane angle, Position 2 is found to provide the highest axial velocity followed by Position 3 and Position 1. However, for vane angle 60° (Figure 5.54), axial velocity for Position 2 and Position 3 are almost the same profile with their magnitudes higher than Position 1 and Position 4. The magnitude for Position 4 is slighter higher than Position 1.

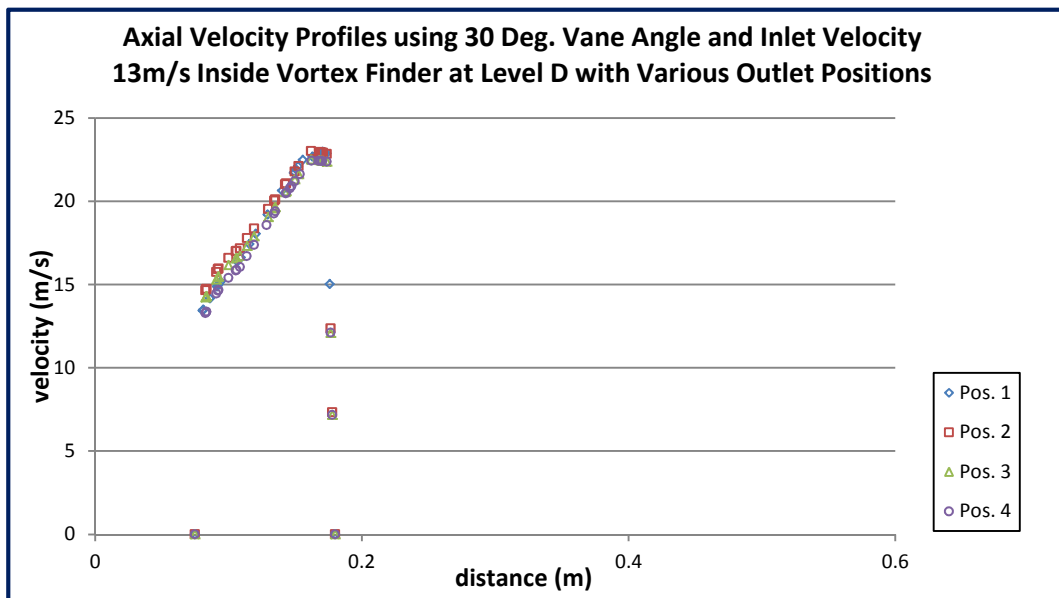


Figure 5.52: Axial velocity profiles inside vortex finder for various outlet positions (30° vane angle, 13m/s inlet velocity)

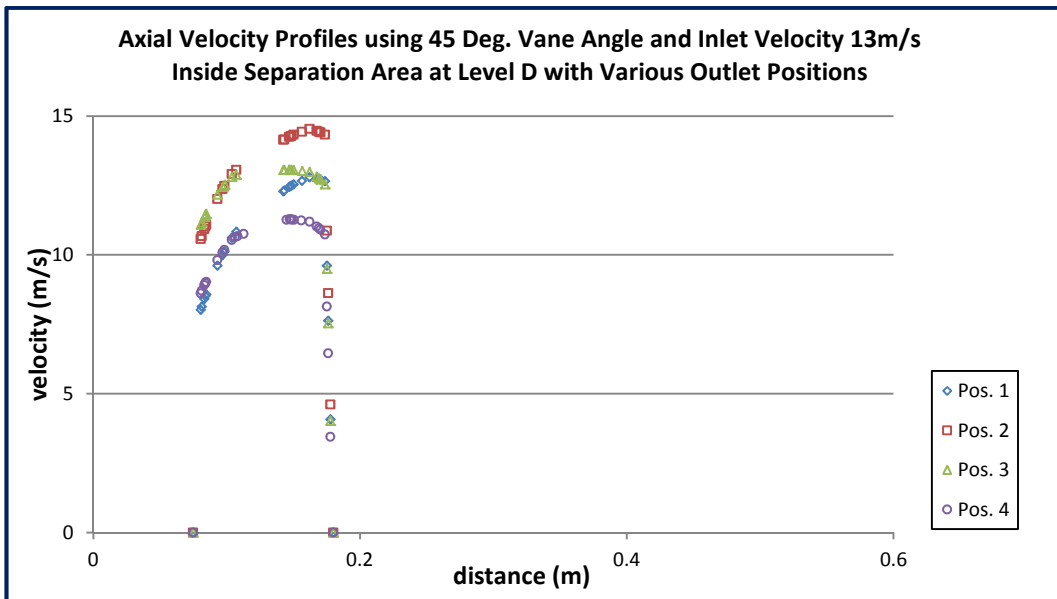


Figure 5.53: Axial velocity profiles inside vortex finder for various outlet positions (45° vane angle, 13m/s inlet velocity)

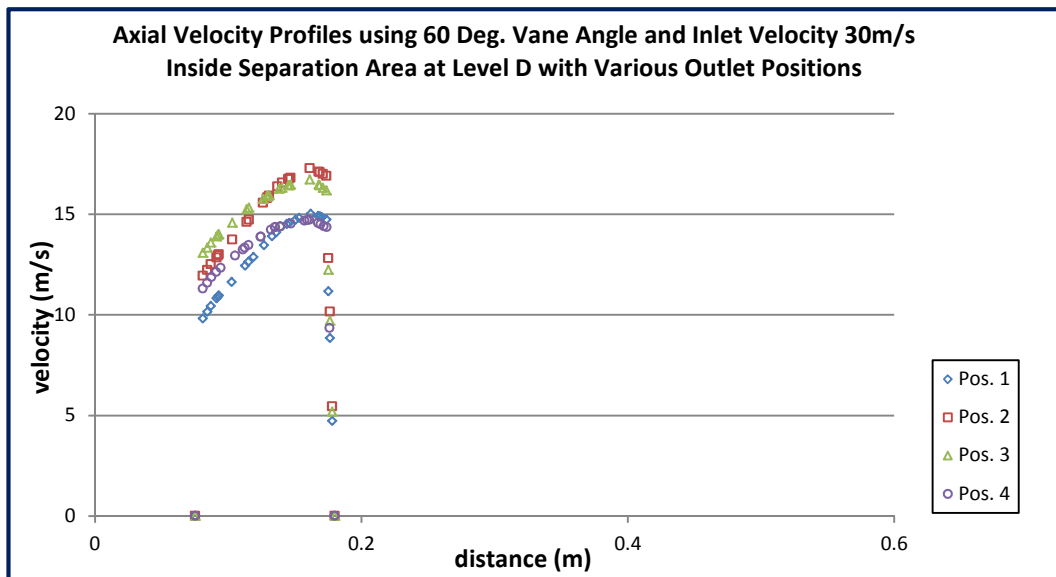


Figure 5.54: Axial velocity profiles inside vortex finder for various outlet positions (60° vane angle, 13m/s inlet velocity)

It can be concluded that placing the outlet at Position 2 may help to increase the axial velocity inside the vortex finder. Identical results were also observed for 20m/s and 30m/s inlet velocities which are included in Appendix VI.

5.2 Particles Distribution Analysis

Subsequent to seeing the effect of changing the parameters on the air flow, the effect of particles distribution were studied. This section is an extension of the previous section, which is it employs stochastic tracking which allows individual paths of particles to be plotted and give a better representation of the split over a period of time.

5.2.1 Effect of the Inlet Velocity

Three different inlet velocity, 13 m/s, 20 m/s and 30 m/s have been selected for evaluation. Thirty six (36) test cases; with various outlet position and the vane angle of 30°, 45° and 60°, were conducted for each velocity on the model classifier design.

For each test case, a variation of particle sizes (between 1 to 90 microns) was used. The variation of parameters and particle sizes helps to visualise the effect of the inlet velocity on the percentage of escaped particles. However, to have a better understanding of the effect of the inlet velocity, data from each test cases were extracted and presented in graphical form.

Figure 5.55 and Figure 5.56 show the effect of changing the inlet velocity on the distribution of escaped particle for various particle sizes and the particle size at 40, 60 and 80% of cumulative distribution for 30° vane angle at outlet Position 1.

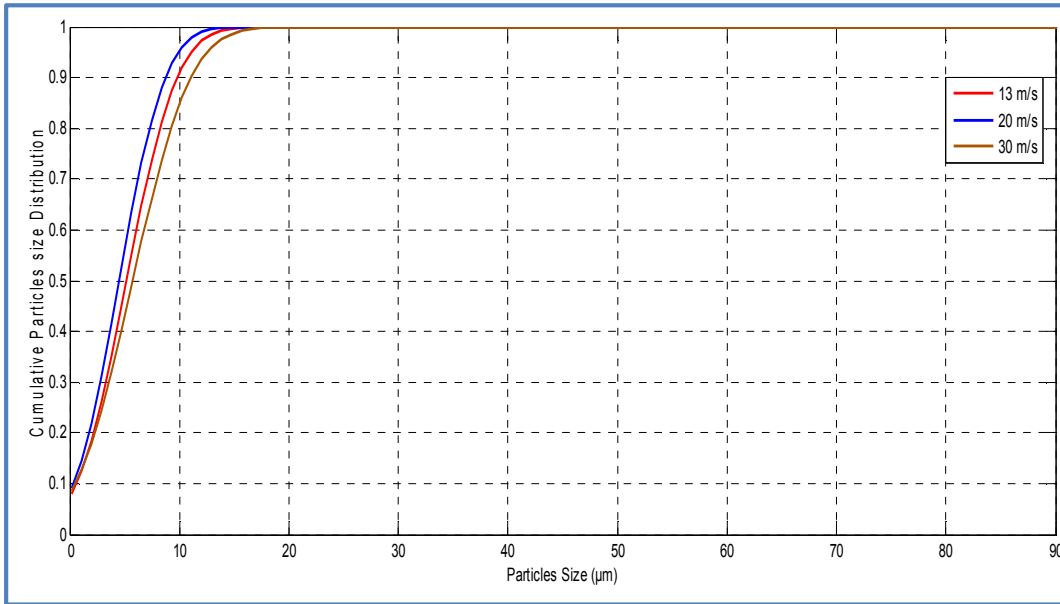


Figure 5.55: Particle cumulative size distribution for 30° vane angle at Position 1

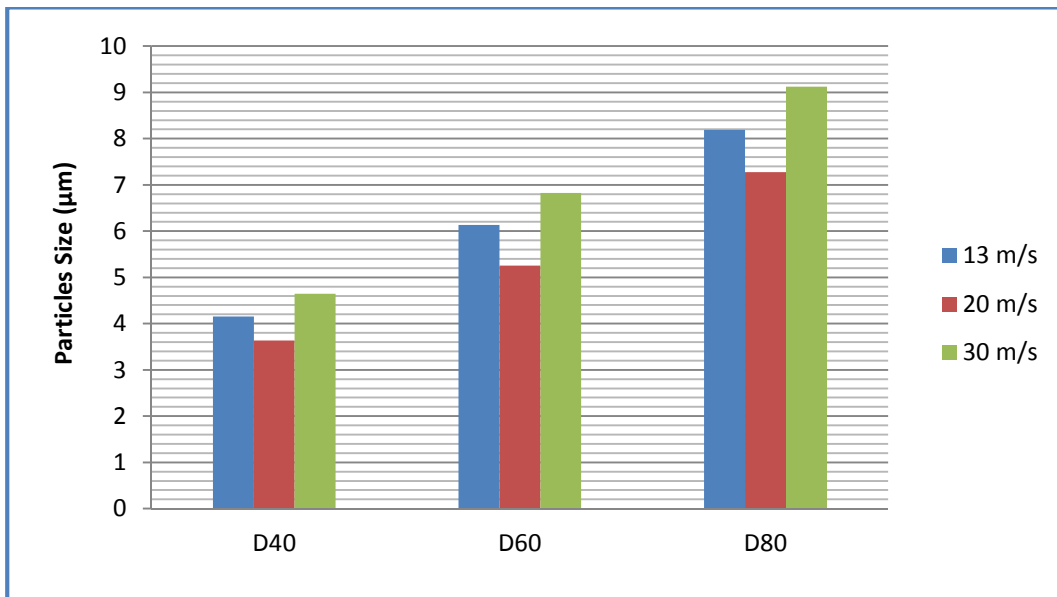


Figure 5.56: Particle size at 40, 60 and 80% of cumulative distribution for 30° vane angle at outlet Position 1

The graphs show that changing the inlet velocity has impact on the particle distribution. The same trend applies to all the outlet positions. At inlet velocity 30m/s, more particles escaped and least particle escaped for inlet velocity 20m/s.

The value of D40, D60 and D80 for the 30m/s and 20m/s indicates the same conclusion. This is true for all outlet positions for 30° vane angles.

Figure 5.57 through Figure 5.59 shows the results for vane angle of 45°. The figures show that the inlet velocity has greater effect on the escaped particles. Figure 5.57 and Figure 5.58 show that increasing the inlet velocity will cause coarse particles remain in the classifier of 45° vane angle. Figure 5.59 shows that changing the inlet velocity for 45° vane angle at Position 4 give a distinctive effect than other outlet positions to the particles escaped. Particle of size 25 microns and larger will not escaped. For small particle sizes, for example 1 micron, almost all particles will escape regardless of the input velocity. However, for the coarsest particle 90 microns; were not escaped.

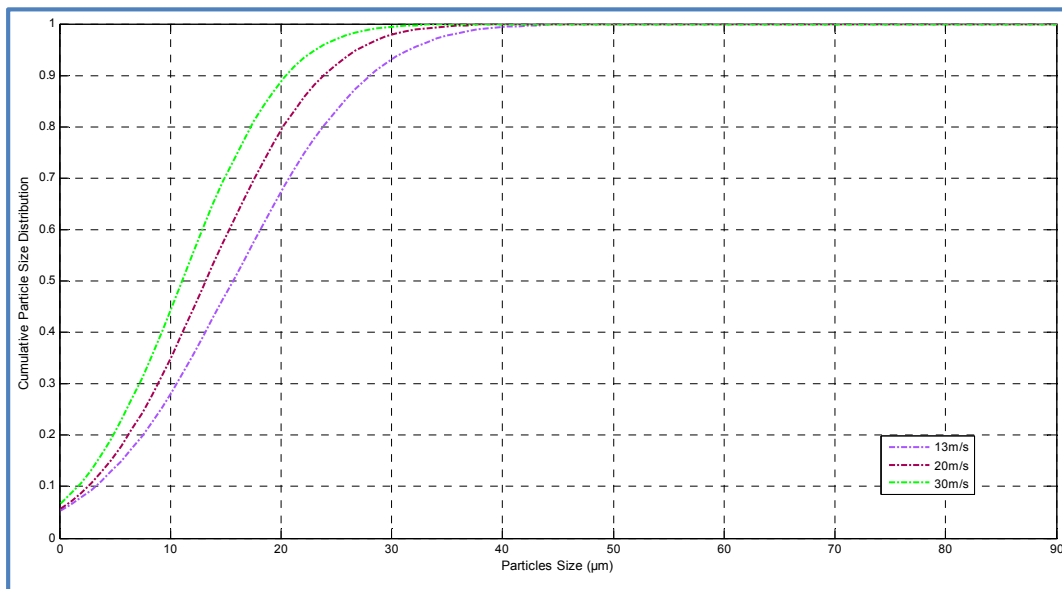


Figure 5.57: Particle cumulative size distribution for 45° vane angle at Position 3

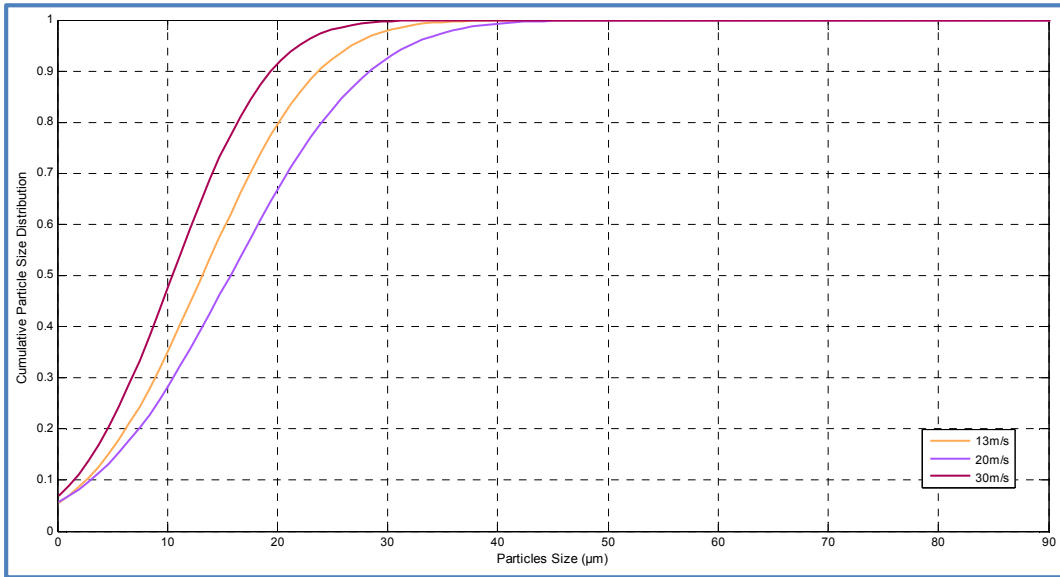


Figure 5.58: Particle cumulative size distribution for 45° vane angle at Position 4

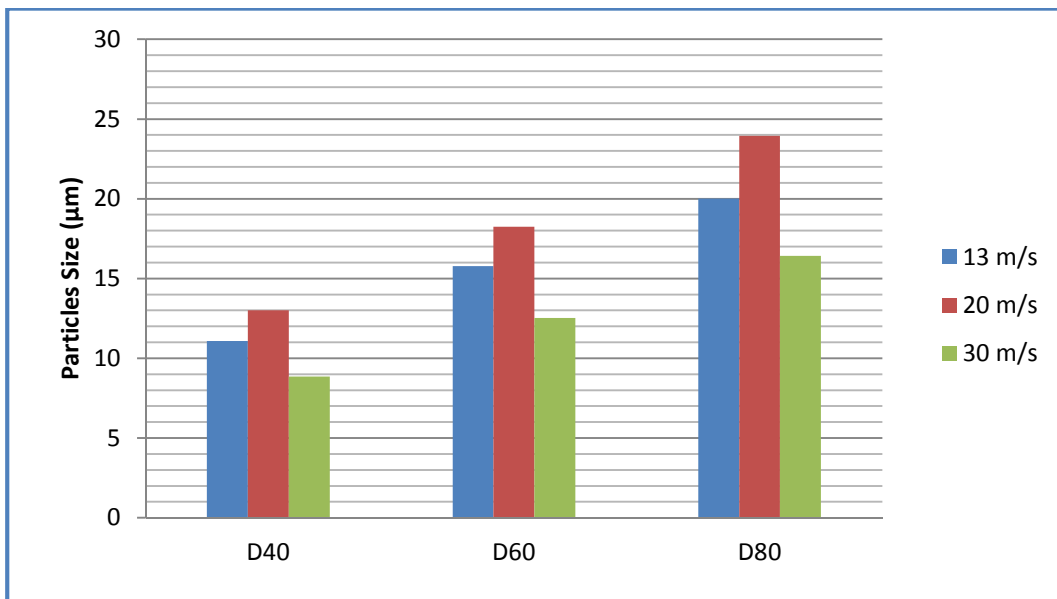


Figure 5.59: Particle size at 40, 60 and 80% of cumulative distribution for 45° vane angle at outlet Position 4

Figure 5.60 below indicates that increasing the inlet velocity has effect on the percentage of escaped particles of 60° vane angle at outlet Position 4. For 13m/s inlet velocity, particles greater than 60 microns will be trapped inside the

classifier while particles with size less than 60 microns escaped. For all outlet positions at the 60° vane angle yielded similar result.

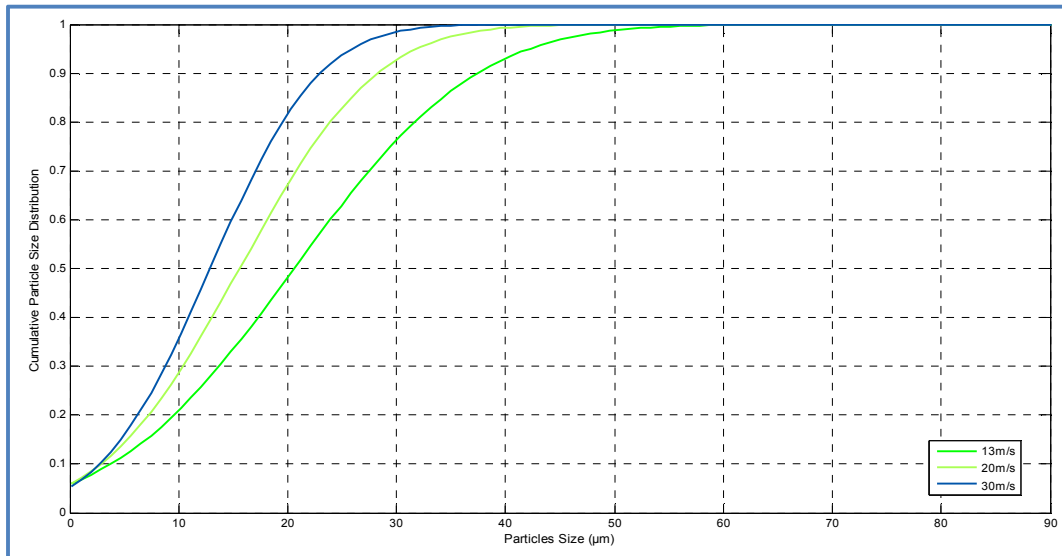


Figure 5.60: Particle cumulative size distribution for 60° vane angle at Position 4

From the CFD investigation into the effect of varying the inlet velocity it can be seen that the inlet velocity can influence the size of particles escaped. However, the results provide no certain conclusions on the optimum classifier parameter. Beside the shortcoming, the results can still be used as a guide for selecting the appropriate parameters for the desired escaped particles size.

5.2.2 Effect of Vane Angle

To further evaluate the proposed approach, classifier with various vane angles were simulated. Another thirty six (36) test cases have been performed to evaluate the effect of changing the vane angle on the classifier performance.

Vane angle of 30°, 45° and 60° have been selected for evaluation. Simulations conducted on the inlet velocity of 13m/s, 20m/s and 30 m/s with outlet positions from 1 to 4.

Results show that the vane angle plays a role in determining the sizes of the particles released. By changing the vane angle, the particle size being released from the classifier can be controlled. Figure 5.61 to Figure 5.64 show the same repetition for the entire velocities and outlet positions. It is observed that by varying the vane angle the particle size leaving the classifier is also shifted. The vane angle of 60° shows that coarser particles also leave the classifier. This can be seen clearly through the figures. Size of particle escaped increases with the increase of vane angle.

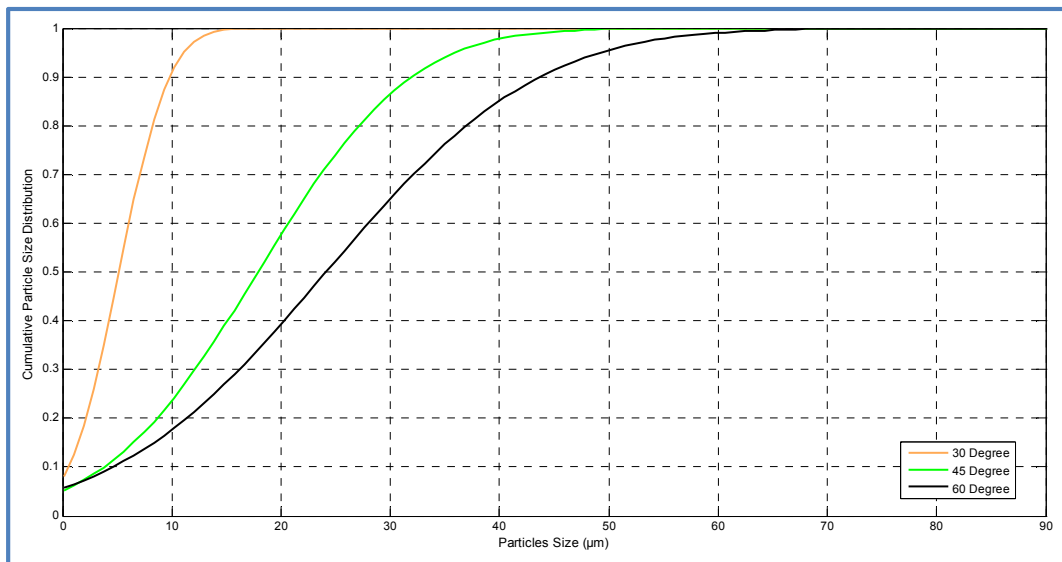


Figure 5.61: Particle cumulative size distribution at Position 1 with 13m/s inlet velocity

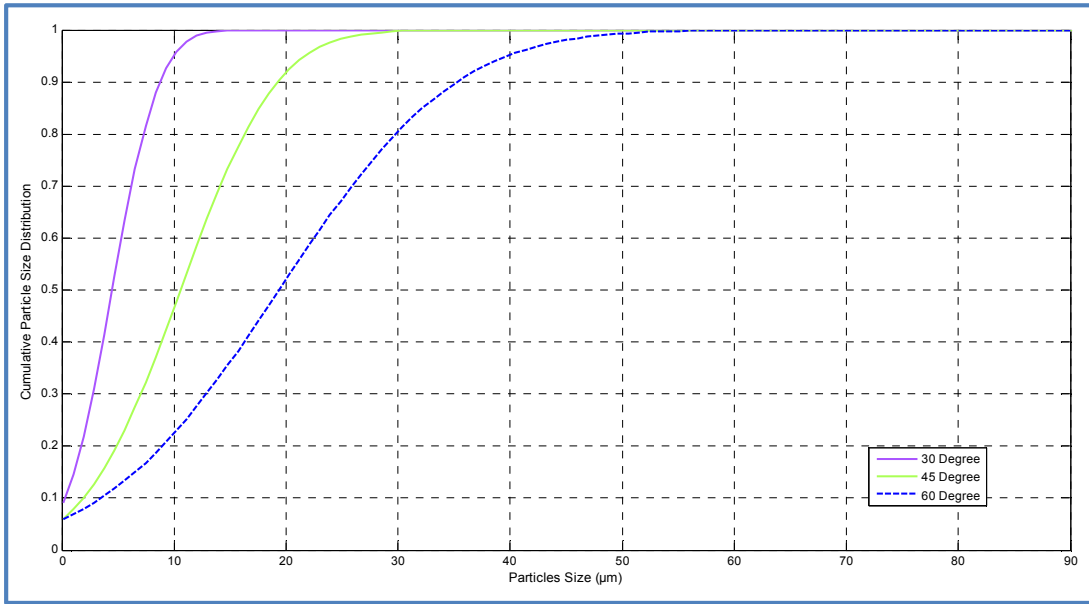


Figure 5.62: Particle cumulative size distribution at Position 1 with 20m/s inlet velocity

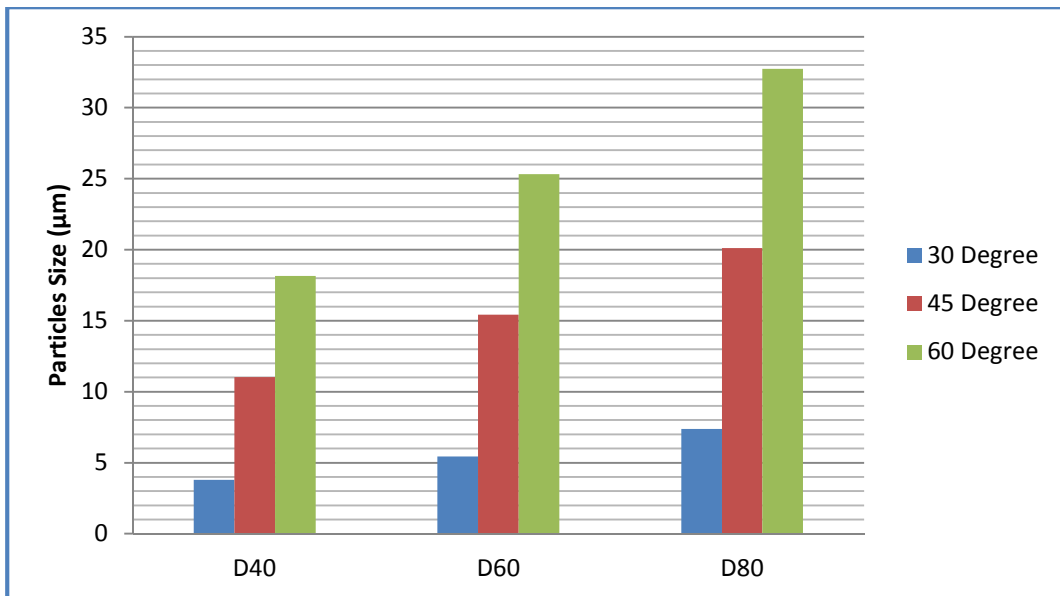


Figure 5.63: Particle size at 40, 60 and 80% of cumulative distribution for 20m/s inlet velocity at outlet Position 3

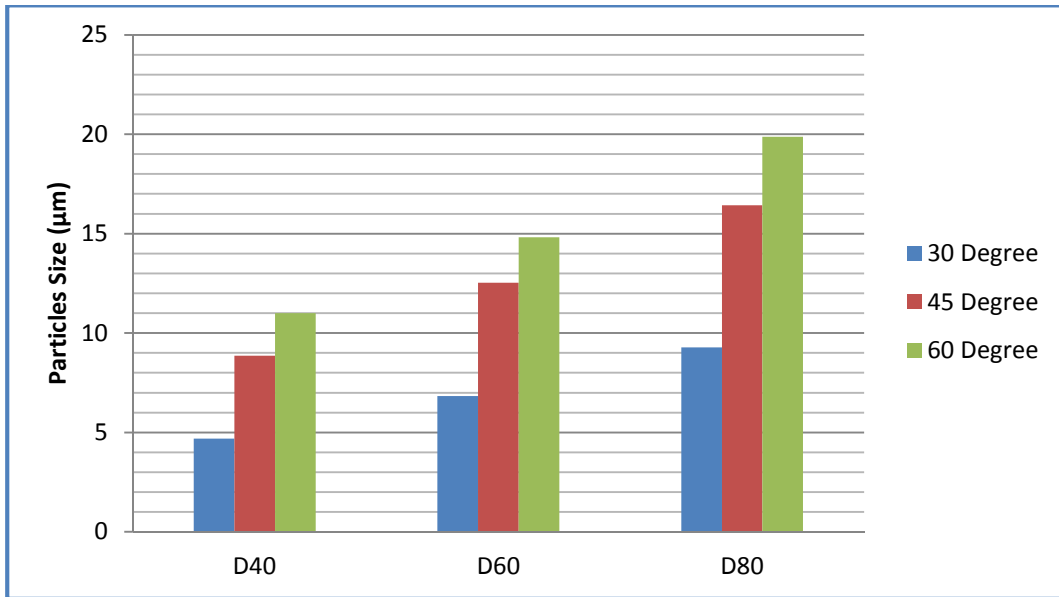


Figure 5.64: Particle size at 40, 60 and 80% of cumulative distribution for 30m/s inlet velocity at outlet Position 4

From the analysis it shows that particle size increases with the increase of vane angle. This is true for all inlet velocities and outlet positions.

5.2.3 Effect of Outlet Position

The third parameter being considered is the effect of outlet positions to particle escaped. Location of the outlet positions is as shown in Figure 5.2. The investigations are conducted on inlet velocity of 13m/s, 20m/s and 30m/s with 30°, 45° and 60° vane angles. Thirty six (36) cases have been carried out for this investigation.

Figure 5.65 through Figure 5.67 show that 30° vane angle suggest similar results for all outlet positions.

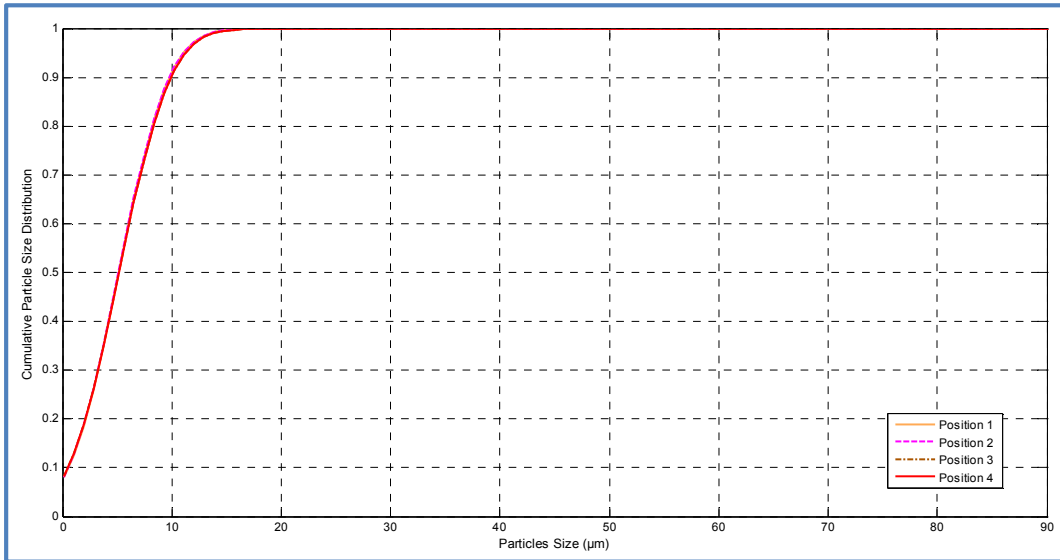


Figure 5.65: Particle cumulative size distribution at 13m/s inlet velocity for 30° vane angle

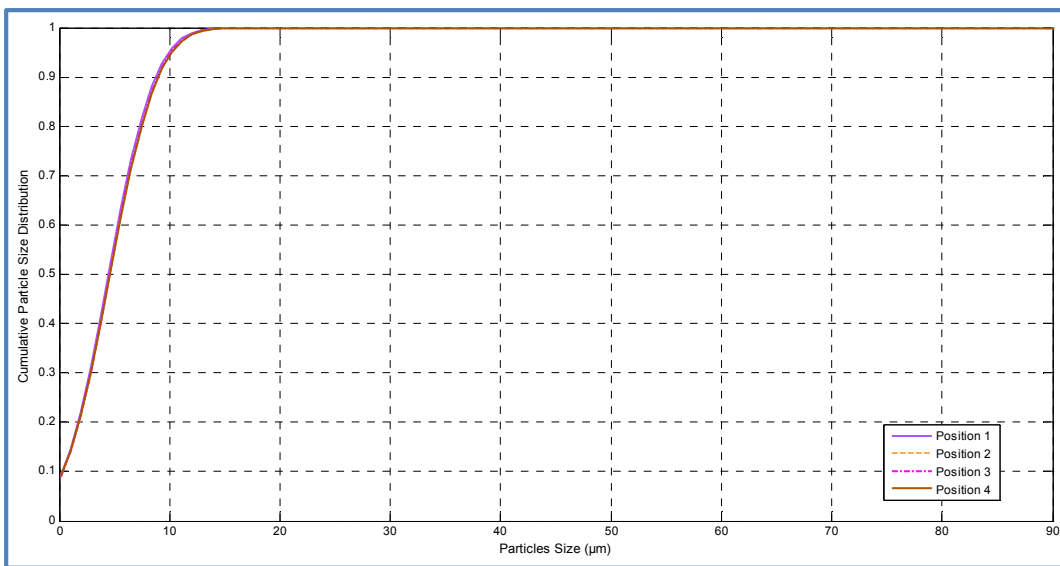


Figure 5.66: Particle cumulative size distribution at 20m/s inlet velocity for 30° vane angle

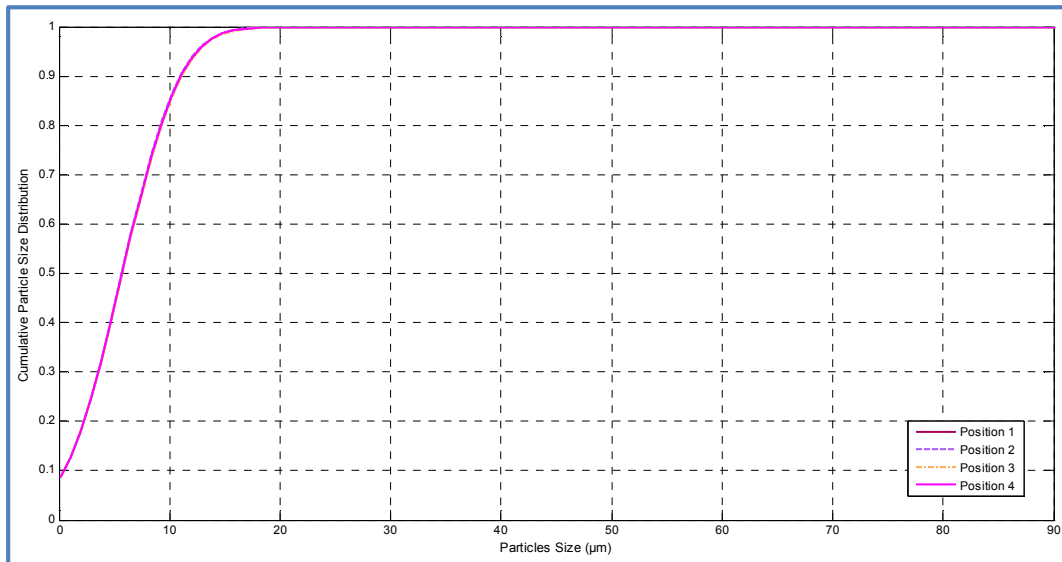


Figure 5.67: Particle cumulative size distribution at 30 m/s inlet velocity for 30° vane angle

The graphs clearly show that by changing the outlet positions it does not affect the escaped particles from the classifier. However, vane angle 45° show mixed result. For inlet velocity of 30m/s, outlet position had no effect on particles escaped. At inlet velocity of 13 m/s, Position 1 shows better particles distribution compared to Position 4. Size of the particles that escaped was more variation. Particles size of 50 microns and below were found escaped. Whereas only particles of size 35 micron and below escape from outlet Position 4. However, with inlet velocity of 20m/s shows the opposite result. This can be seen in Figure 5.68 and Figure 5.69 below.

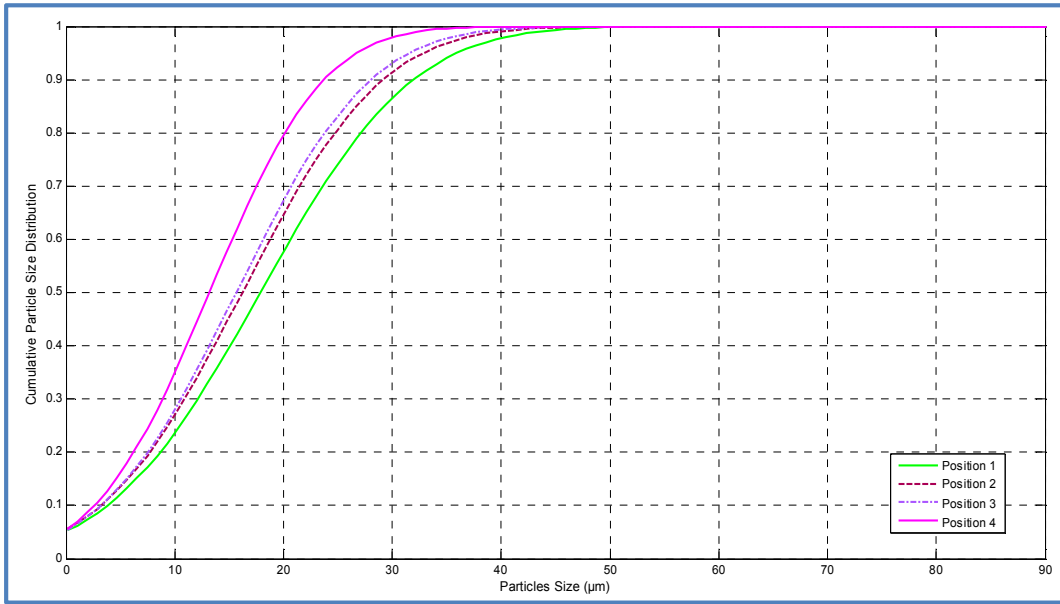


Figure 5.68: Particle cumulative size distribution at 13 m/s inlet velocity for 45° vane angle

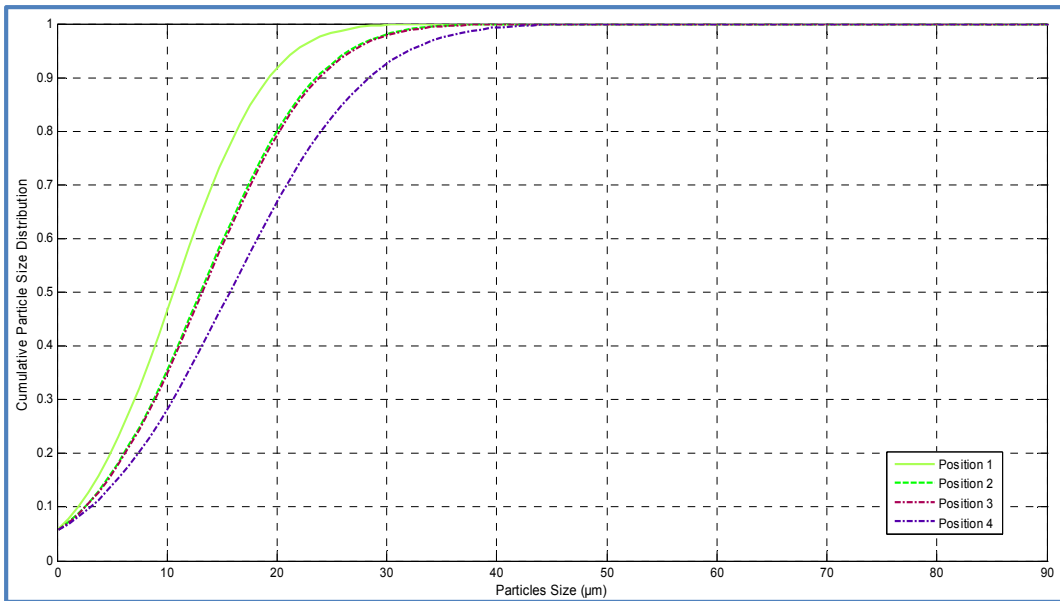


Figure 5.69: Particle cumulative size distribution at 20 m/s inlet velocity for 45° vane angle

Vane angle 60° also shows mixed result. For inlet velocity 30m/s, outlet positions had no effect on particles escaped. At inlet velocity of 13m/s, Position 1 shows the

better particles distribution of all outlet positions. The size of particles escaped was also more variation. Particles of size 60 microns and below are escaped. For inlet velocity of 20m/s, the particles distributions are good for Position 1 and Position 2. Figure 5.70 and Figure 5.71 below represent the results mentioned.

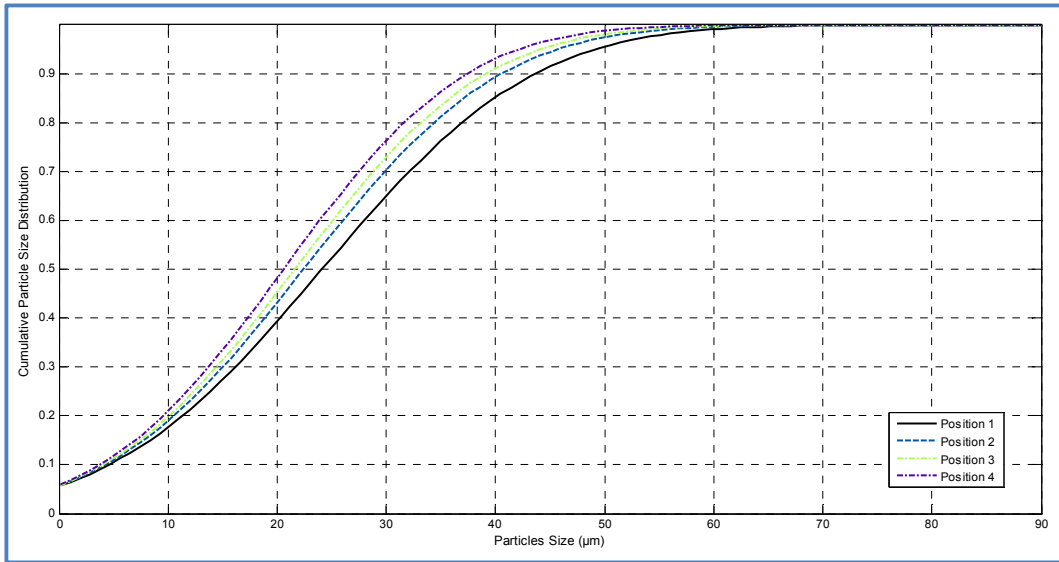


Figure 5.70: Particle cumulative size distribution at 13m/s inlet velocity for 60° vane angle

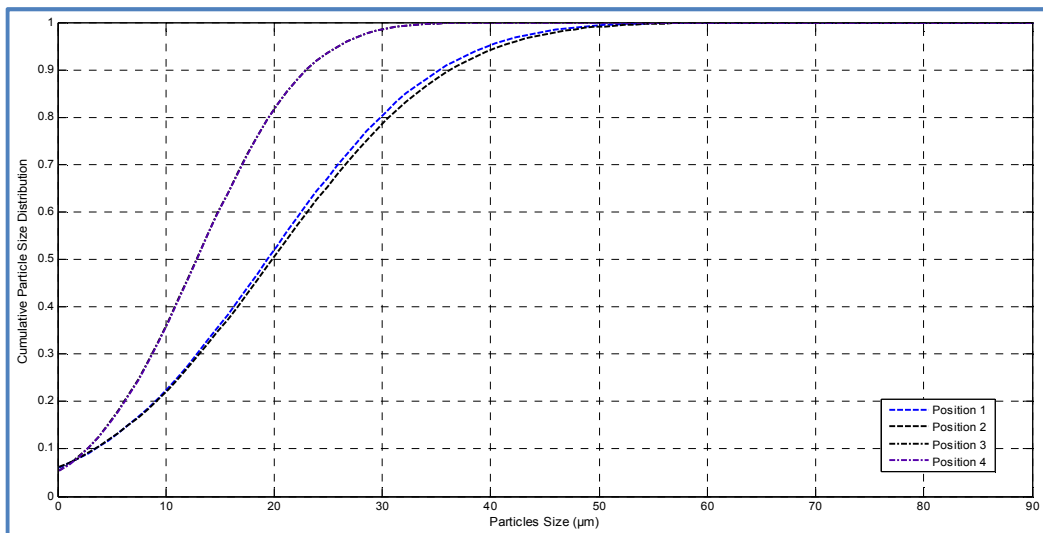


Figure 5.71: Particle cumulative size distribution at 20m/s inlet velocity for 60° vane angle

It was expected that changing the outlet positions will have no effect on the classifier performance. However, CFD has the tendency to overestimate particle motion, as it does not take into account particle-particle interactions.

5.3 Particles Residence Time

Residence time inside for the classifier model has been considered as a factor that can be seen to determine classifier performance. It is the average amount of time that a particle spends in the system. The residence time is a representation of how long it takes for the particles to significantly travel to the outlet.

Figure 5.72 shows the particles track for 5 μm particle size for outlet Position 1 and Position 3. It is clearly seen that the particles travel towards the outlet after tracing its path around the classifier body.

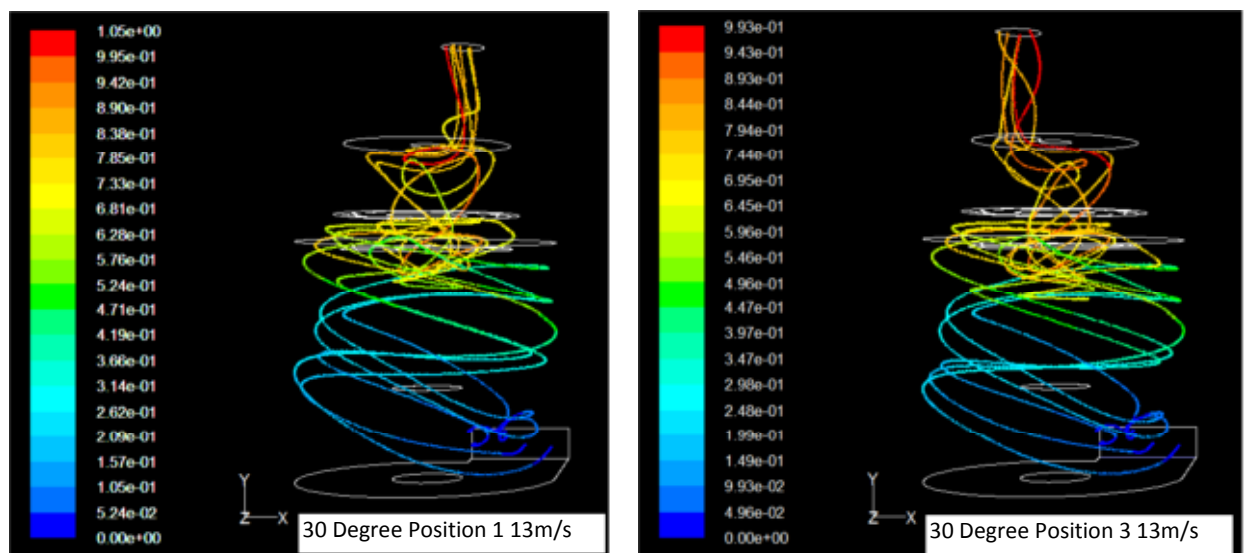


Figure 5.72: Particle tracks of 5 μm particle using outlet Position 1 and Position 3

Table 5.1 present the residence time for 30° vane angle at outlet Position 1 with inlet velocity of 13m/s, 20m/s and 30m/s. From the table it shows that inlet velocity influence the residence time. Figure 5.73 also shows the same conclusion.

Table 5.1: Particle Residence Time for 30° vane angle at outlet Position 1

| 30 DEGREE | | | |
|--------------------------------|-----------------------|-----------------------|-----------------------|
| Particles Size (microns) | Position 1 | | |
| | 13 m/s | 20 m/s | 30 m/s |
| | Residence Time (s) | Residence Time (s) | Residence Time (s) |
| 1 | 1.26 | 0.82 | 0.66 |
| 5 | 1.71 | 1.30 | 1.27 |
| 10 | 2.19 | 1.28 | 1.73 |
| 15 | 1.41 | 0 | 1.50 |
| 20 | 0 | 0 | 1.11 |
| 25 | 0 | 0 | 0 |
| 30 | 0 | 0 | 0 |
| 35 | 0 | 0 | 0 |

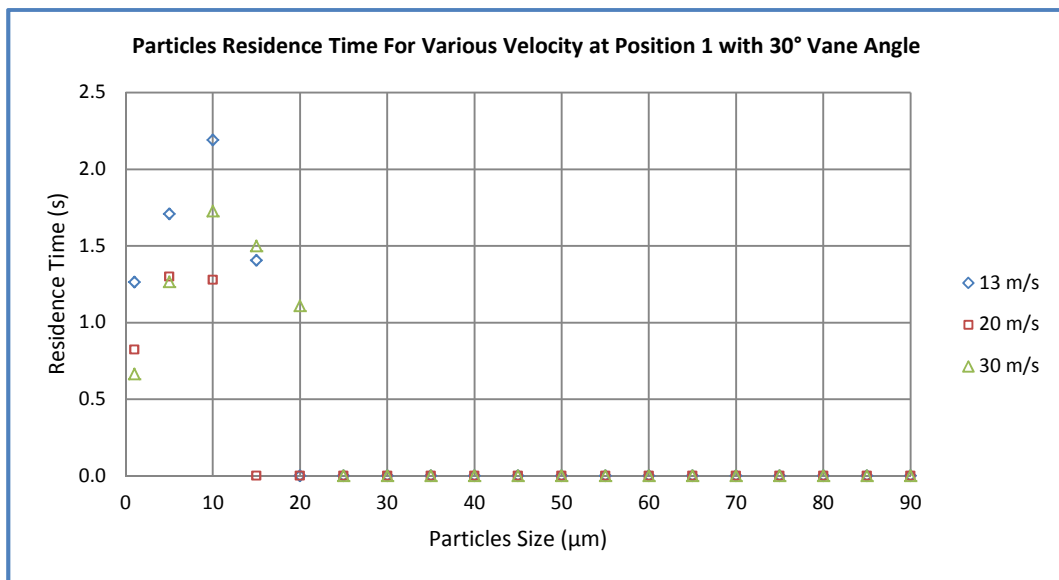


Figure 5.73: Residence time for various velocities with 30° vane angle at outlet Position 1

The residence time in the model classifier depends on the flow conditions inside the classifier. The residence time decreases if the inlet velocity increased. This parameter has a significant influence as the enclosure air velocity needs to be higher than the suspension velocity to prevent the particle to drop. The effect of inlet velocity for all cases showed similar results. The results are shown in Appendix VII.

Particles' residence time is also affected by the vane angle. Analysis of the effect of vane angle on the particles residence time can be seen in Table 5 .2. This is also illustrated by Figure 5.74. From the analysis, vane angle 30° has the lowest residence time compared to other vane angles. This analysis also confirmed by the analysis of the air velocity in Section 5.1. This conclusion has also been agreed by the work done by Shah (2009).

Table 5.2: Particle Residence Time for 13m/s for various vane angles at outlet
Position 1

| 13 m/s | | | |
|--------------------------|--------------------|--------------------|--------------------|
| Particles Size (microns) | Position 1 | | |
| | 30 Degree | 45 Degree | 60 Degree |
| | Residence Time (s) | Residence Time (s) | Residence Time (s) |
| 1 | 1.26 | 1.47 | 2.22 |
| 5 | 1.71 | 1.85 | 3.02 |
| 10 | 2.19 | 2.87 | 2.78 |
| 15 | 1.41 | 2 | 2.67 |
| 20 | 0 | 2 | 2.15 |
| 25 | 0 | 3 | 2 |
| 30 | 0 | 2.55 | 2.335 |
| 35 | 0 | 4.325 | 3.907 |
| 40 | 0 | 0 | 1.783 |
| 45 | 0 | 0 | 1.995 |
| 50 | 0 | 0 | 3.071 |
| 55 | 0 | 0 | 1.166 |

The effect of changing the vane angle for all cases indicated similar results. These are included in Appendix VII.

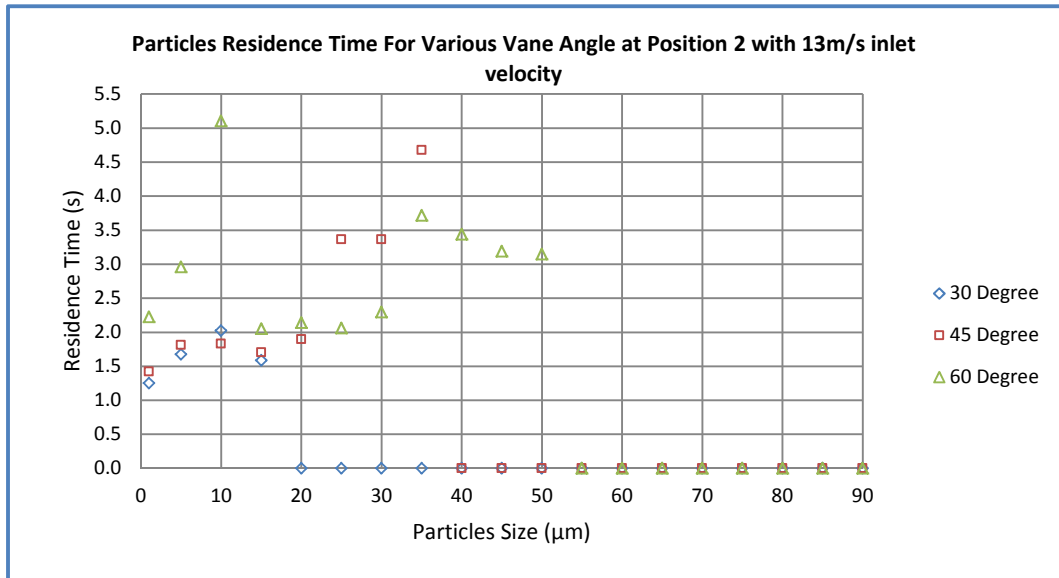


Figure 5.74: The effect of vane angle on particles residence time at outlet position 2 with 13 m/s inlet velocity.

Figure 5.75 shows the effect of outlet positions on particles residence time at 60° vane angle with 30 m/s inlet velocity. Outlet positions can be concluded have not much impact on the particle residence time.

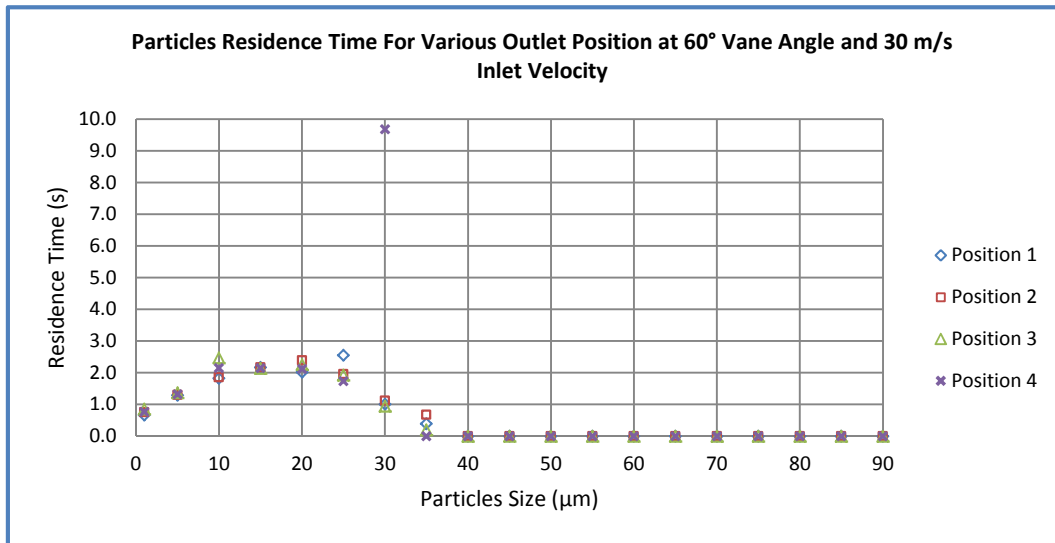


Figure 5.75: The effect of outlet position on particles residence time at 60° vane angle with 30 m/s inlet velocity.

5.4 Design Parameter Look-up Table

From the velocity analysis (Section 5.1) and particle distribution analysis (Section 5.2), they have shown that CFD is a very useful tool for giving an insight of the influences and effects of certain parameters on the classifier behaviour. The analysis also shown that classifier is highly non-linear system which difficult to predict its behaviour if more than one parameter is changed.

However, from CFD analyses, the end results from the combination of parameter manipulation can be compiled as look-up table which can assist the operator of dynamic classifier determine the appropriate settings to achieve the desired output performance. A set of look-up table compiled from this research with the assist of CFD analysis are shown in Table 5.3 through Table 5.11 below.

Table 5.3: Parameter look-up table for 30° vane angle and 13m/s inlet velocity

| 30 DEGREE | | | | | | | | | | | | |
|----------------------------|------------|-------------|--------------------|------------|-------------|--------------------|------------|-------------|--------------------|------------|-------------|--------------------|
| Partides Size (microns) | 13 m/s | | | | | | | | | | | |
| | Position 1 | | | Position 2 | | | Position 3 | | | Position 4 | | |
| | Escaped | Escaped (%) | Residence Time (s) | Escaped | Escaped (%) | Residence Time (s) | Escaped | Escaped (%) | Residence Time (s) | Escaped | Escaped (%) | Residence Time (s) |
| 1 | 3719 | 73.94 | 1.26 | 3344 | 73.17 | 1.25 | 3719 | 73.94 | 1.26 | 3774 | 75.03 | 1.27 |
| 5 | 4242 | 84.33 | 1.71 | 3871 | 84.70 | 1.68 | 4203 | 83.56 | 1.78 | 4237 | 84.23 | 1.75 |
| 10 | 3263 | 64.87 | 2.19 | 2790 | 61.05 | 2.02 | 3123 | 62.09 | 2.12 | 3195 | 63.52 | 2.21 |
| 15 | 45 | 0.89 | 1.41 | 70 | 1.39 | 1.59 | 138 | 2.74 | 1.78 | 133 | 2.64 | 1.93 |
| 20 | 0 | 0 | - | 0 | 0 | - | 0 | 0 | - | 0 | 0 | - |
| 25 | 0 | 0 | - | 0 | 0 | - | 0 | 0 | - | 0 | 0 | - |
| 30 | 0 | 0 | - | 0 | 0 | - | 0 | 0 | - | 0 | 0 | - |
| 35 | 0 | 0 | - | 0 | 0 | - | 0 | 0 | - | 0 | 0 | - |
| 40 | 0 | 0 | - | 0 | 0 | - | 0 | 0 | - | 0 | 0 | - |
| 45 | 0 | 0 | - | 0 | 0 | - | 0 | 0 | - | 0 | 0 | - |
| 50 | 0 | 0 | - | 0 | 0 | - | 0 | 0 | - | 0 | 0 | - |
| 55 | 0 | 0 | - | 0 | 0 | - | 0 | 0 | - | 0 | 0 | - |
| 60 | 0 | 0 | - | 0 | 0 | - | 0 | 0 | - | 0 | 0 | - |
| 65 | 0 | 0 | - | 0 | 0 | - | 0 | 0 | - | 0 | 0 | - |
| 70 | 0 | 0 | - | 0 | 0 | - | 0 | 0 | - | 0 | 0 | - |
| 75 | 0 | 0 | - | 0 | 0 | - | 0 | 0 | - | 0 | 0 | - |
| 80 | 0 | 0 | - | 0 | 0 | - | 0 | 0 | - | 0 | 0 | - |
| 85 | 0 | 0 | - | 0 | 0 | - | 0 | 0 | - | 0 | 0 | - |
| 90 | 0 | 0 | - | 0 | 0 | - | 0 | 0 | - | 0 | 0 | - |

Table 5.4: Parameter look-up table for 30° vane angle and 20m/s inlet velocity

| 30 DEGREE | | | | | | | | | | | | |
|----------------------------|------------|-------------|--------------------|------------|-------------|--------------------|------------|-------------|--------------------|------------|-------------|--------------------|
| Partides Size (microns) | 20 m/s | | | | | | | | | | | |
| | Position 1 | | | Position 2 | | | Position 3 | | | Position 4 | | |
| | Escaped | Escaped (%) | Residence Time (s) | Escaped | Escaped (%) | Residence Time (s) | Escaped | Escaped (%) | Residence Time (s) | Escaped | Escaped (%) | Residence Time (s) |
| 1 | 3735 | 74.25 | 0.82 | 3354 | 73.39 | 0.83 | 3656 | 72.68 | 0.81 | 3752 | 74.59 | 0.82 |
| 5 | 4175 | 83.00 | 1.30 | 3784 | 82.80 | 1.31 | 4133 | 82.17 | 1.31 | 4134 | 82.19 | 1.29 |
| 10 | 1983 | 39.42 | 1.28 | 2008 | 43.94 | 1.40 | 2125 | 42.25 | 1.24 | 2247 | 44.67 | 1.30 |
| 15 | 0 | 0 | - | 0 | 0 | - | 0 | 0 | - | 0 | 0 | - |
| 20 | 0 | 0 | - | 0 | 0 | - | 0 | 0 | - | 0 | 0 | - |
| 25 | 0 | 0 | - | 0 | 0 | - | 0 | 0 | - | 0 | 0 | - |
| 30 | 0 | 0 | - | 0 | 0 | - | 0 | 0 | - | 0 | 0 | - |
| 35 | 0 | 0 | - | 0 | 0 | - | 0 | 0 | - | 0 | 0 | - |
| 40 | 0 | 0 | - | 0 | 0 | - | 0 | 0 | - | 0 | 0 | - |
| 45 | 0 | 0 | - | 0 | 0 | - | 0 | 0 | - | 0 | 0 | - |
| 50 | 0 | 0 | - | 0 | 0 | - | 0 | 0 | - | 0 | 0 | - |
| 55 | 0 | 0 | - | 0 | 0 | - | 0 | 0 | - | 0 | 0 | - |
| 60 | 0 | 0 | - | 0 | 0 | - | 0 | 0 | - | 0 | 0 | - |
| 65 | 0 | 0 | - | 0 | 0 | - | 0 | 0 | - | 0 | 0 | - |
| 70 | 0 | 0 | - | 0 | 0 | - | 0 | 0 | - | 0 | 0 | - |
| 75 | 0 | 0 | - | 0 | 0 | - | 0 | 0 | - | 0 | 0 | - |
| 80 | 0 | 0 | - | 0 | 0 | - | 0 | 0 | - | 0 | 0 | - |
| 85 | 0 | 0 | - | 0 | 0 | - | 0 | 0 | - | 0 | 0 | - |
| 90 | 0 | 0 | - | 0 | 0 | - | 0 | 0 | - | 0 | 0 | - |

Table 5.5: Parameter look-up table for 30° vane angle and 30m/s inlet velocity

| 30 DEGREE | | | | | | | | | | | | |
|--------------------------|------------|-------------|--------------------|------------|-------------|--------------------|------------|-------------|--------------------|------------|-------------|--------------------|
| Particles Size (microns) | 30 m/s | | | | | | | | | | | |
| | Position 1 | | | Position 2 | | | Position 3 | | | Position 4 | | |
| | Escaped | Escaped (%) | Residence Time (s) | Escaped | Escaped (%) | Residence Time (s) | Escaped | Escaped (%) | Residence Time (s) | Escaped | Escaped (%) | Residence Time (s) |
| 1 | 2283 | 45.39 | 0.66 | 2122 | 46.43 | 0.66 | 2355 | 46.82 | 0.70 | 2320 | 46.12 | 0.65 |
| 5 | 3612 | 71.81 | 1.27 | 3301 | 72.23 | 1.20 | 3622 | 72.01 | 1.24 | 3621 | 71.99 | 1.32 |
| 10 | 1843 | 36.64 | 1.73 | 1684 | 36.85 | 0.17 | 1890 | 37.57 | 1.62 | 1875 | 37.28 | 2.11 |
| 15 | 541 | 10.76 | 1.50 | 486 | 10.63 | 1.73 | 580 | 11.53 | 1.45 | 529 | 10.52 | 1.10 |
| 20 | 41 | 0.82 | 1.11 | 27 | 0.59 | 1.03 | 40 | 0.80 | 0.99 | 42 | 0.83 | 1.04 |
| 25 | 0 | 0 | - | 0 | 0 | - | 0 | 0 | - | 1 | 0.02 | 0.86 |
| 30 | 0 | 0 | - | 0 | 0 | - | 0 | 0 | - | 0 | 0 | - |
| 35 | 0 | 0 | - | 0 | 0 | - | 0 | 0 | - | 0 | 0 | - |
| 40 | 0 | 0 | - | 0 | 0 | - | 0 | 0 | - | 0 | 0 | - |
| 45 | 0 | 0 | - | 0 | 0 | - | 0 | 0 | - | 0 | 0 | - |
| 50 | 0 | 0 | - | 0 | 0 | - | 0 | 0 | - | 0 | 0 | - |
| 55 | 0 | 0 | - | 0 | 0 | - | 0 | 0 | - | 0 | 0 | - |
| 60 | 0 | 0 | - | 0 | 0 | - | 0 | 0 | - | 0 | 0 | - |
| 65 | 0 | 0 | - | 0 | 0 | - | 0 | 0 | - | 0 | 0 | - |
| 70 | 0 | 0 | - | 0 | 0 | - | 0 | 0 | - | 0 | 0 | - |
| 75 | 0 | 0 | - | 0 | 0 | - | 0 | 0 | - | 0 | 0 | - |
| 80 | 0 | 0 | - | 0 | 0 | - | 0 | 0 | - | 0 | 0 | - |
| 85 | 0 | 0 | - | 0 | 0 | - | 0 | 0 | - | 0 | 0 | - |
| 90 | 0 | 0 | - | 0 | 0 | - | 0 | 0 | - | 0 | 0 | - |

Table 5.6: Parameter look-up table for 45° vane angle and 13m/s inlet velocity

| 45 DEGREE | | | | | | | | | | | | |
|--------------------------|------------|-------------|--------------------|------------|-------------|--------------------|------------|-------------|--------------------|------------|-------------|--------------------|
| Particles Size (microns) | 13 m/s | | | | | | | | | | | |
| | Position 1 | | | Position 2 | | | Position 3 | | | Position 4 | | |
| | Escaped | Escaped (%) | Residence Time (s) | Escaped | Escaped (%) | Residence Time (s) | Escaped | Escaped (%) | Residence Time (s) | Escaped | Escaped (%) | Residence Time (s) |
| 1 | 4114 | 81.79 | 1.47 | 4256 | 84.61 | 1.42 | 4158 | 82.66 | 1.40 | 4124 | 81.99 | 1.45 |
| 5 | 4627 | 91.99 | 1.85 | 4670 | 92.84 | 1.81 | 4629 | 92.03 | 1.94 | 4602 | 91.49 | 1.83 |
| 10 | 4575 | 90.95 | 2.87 | 4531 | 90.08 | 1.83 | 4571 | 90.87 | 2.77 | 4550 | 90.46 | 1.91 |
| 15 | 4771 | 94.85 | 1.71 | 4800 | 95.43 | 1.70 | 4820 | 95.83 | 1.82 | 4879 | 97.00 | 1.75 |
| 20 | 4972 | 98.85 | 1.98 | 4989 | 99.18 | 1.90 | 4982 | 99.05 | 2.04 | 5005 | 99.50 | 2.42 |
| 25 | 5030 | 100.00 | 3.44 | 5029 | 99.98 | 3.37 | 5030 | 100.00 | 1.99 | 5008 | 99.56 | 3.57 |
| 30 | 5029 | 99.98 | 2.55 | 5029 | 99.98 | 3.37 | 4889 | 97.20 | 3.67 | 0 | 0 | - |
| 35 | 4167 | 82.84 | 4.33 | 965 | 19.18 | 4.68 | 9 | 0.18 | 3.44 | 0 | 0 | - |
| 40 | 0 | 0 | - | 0 | 0 | - | 0 | 0 | - | 0 | 0 | - |
| 45 | 0 | 0 | - | 0 | 0 | - | 0 | 0 | - | 0 | 0 | - |
| 50 | 0 | 0 | - | 0 | 0 | - | 0 | 0 | - | 0 | 0 | - |
| 55 | 0 | 0 | - | 0 | 0 | - | 0 | 0 | - | 0 | 0 | - |
| 60 | 0 | 0 | - | 0 | 0 | - | 0 | 0 | - | 0 | 0 | - |
| 65 | 0 | 0 | - | 0 | 0 | - | 0 | 0 | - | 0 | 0 | - |
| 70 | 0 | 0 | - | 0 | 0 | - | 0 | 0 | - | 0 | 0 | - |
| 75 | 0 | 0 | - | 0 | 0 | - | 0 | 0 | - | 0 | 0 | - |
| 80 | 0 | 0 | - | 0 | 0 | - | 0 | 0 | - | 0 | 0 | - |
| 85 | 0 | 0 | - | 0 | 0 | - | 0 | 0 | - | 0 | 0 | - |
| 90 | 0 | 0 | - | 0 | 0 | - | 0 | 0 | - | 0 | 0 | - |

Table 5.7: Parameter look-up table for 45° vane angle and 20m/s inlet velocity

| 45 DEGREE | | | | | | | | | | | | |
|-----------------------------|------------|-------------|--------------------|------------|-------------|--------------------|------------|-------------|--------------------|-----------|-------------|--------------------|
| Particles Size (microns) | 20 m/s | | | | | | | | | | | |
| | Position 1 | | | Position 2 | | | Position 3 | | | Position4 | | |
| | Escaped | Escaped (%) | Residence Time (s) | Escaped | Escaped (%) | Residence Time (s) | Escaped | Escaped (%) | Residence Time (s) | Escaped | Escaped (%) | Residence Time (s) |
| 1 | 4202 | 83.54 | 0.95 | 4302 | 85.53 | 0.94 | 4199 | 83.48 | 0.92 | 4207 | 83.64 | 1.09 |
| 5 | 4711 | 93.66 | 1.36 | 4725 | 93.94 | 1.37 | 4687 | 93.18 | 1.40 | 4627 | 91.99 | 1.47 |
| 10 | 4652 | 92.49 | 1.14 | 4712 | 93.68 | 1.20 | 4701 | 93.46 | 1.16 | 4431 | 88.09 | 1.10 |
| 15 | 4985 | 99.11 | 1.32 | 4994 | 99.28 | 1.17 | 4982 | 99.05 | 1.23 | 3830 | 76.14 | 1.72 |
| 20 | 5029 | 99.98 | 1.87 | 5030 | 100.00 | 1.90 | 5030 | 100.00 | 1.44 | 4915 | 97.71 | 1.16 |
| 25 | 0 | 0 | - | 4995 | 99.30 | 2.58 | 5030 | 100.00 | 1.44 | 5025 | 99.90 | 1.48 |
| 30 | 0 | 0 | - | 1 | 0.02 | 2.01 | 170 | 3.38 | 2.38 | 5006 | 99.52 | 2.40 |
| 35 | 0 | 0 | - | 0 | 0 | - | 0 | 0 | - | 0 | 0 | - |
| 40 | 0 | 0 | - | 0 | 0 | - | 0 | 0 | - | 0 | 0 | - |
| 45 | 0 | 0 | - | 0 | 0 | - | 0 | 0 | - | 0 | 0 | - |
| 50 | 0 | 0 | - | 0 | 0 | - | 0 | 0 | - | 0 | 0 | - |
| 55 | 0 | 0 | - | 0 | 0 | - | 0 | 0 | - | 0 | 0 | - |
| 60 | 0 | 0 | - | 0 | 0 | - | 0 | 0 | - | 0 | 0 | - |
| 65 | 0 | 0 | - | 0 | 0 | - | 0 | 0 | - | 0 | 0 | - |
| 70 | 0 | 0 | - | 0 | 0 | - | 0 | 0 | - | 0 | 0 | - |
| 75 | 0 | 0 | - | 0 | 0 | - | 0 | 0 | - | 0 | 0 | - |
| 80 | 0 | 0 | - | 0 | 0 | - | 0 | 0 | - | 0 | 0 | - |
| 85 | 0 | 0 | - | 0 | 0 | - | 0 | 0 | - | 0 | 0 | - |
| 90 | 0 | 0 | - | 0 | 0 | - | 0 | 0 | - | 0 | 0 | - |

Table 5.8: Parameter look-up table for 45° vane angle and 30m/s inlet velocity

| 45 DEGREE | | | | | | | | | | | | |
|-----------------------------|------------|-------------|--------------------|------------|-------------|--------------------|------------|-------------|--------------------|-----------|-------------|--------------------|
| Particles Size (microns) | 30 m/s | | | | | | | | | | | |
| | Position 1 | | | Position 2 | | | Position 3 | | | Position4 | | |
| | Escaped | Escaped (%) | Residence Time (s) | Escaped | Escaped (%) | Residence Time (s) | Escaped | Escaped (%) | Residence Time (s) | Escaped | Escaped (%) | Residence Time (s) |
| 1 | 3110 | 61.83 | 0.73 | 3088 | 61.39 | 0.67 | 3108 | 61.79 | 0.64 | 3140 | 62.43 | 0.64 |
| 5 | 4464 | 88.75 | 1.36 | 4481 | 89.09 | 1.28 | 4456 | 88.59 | 1.29 | 4449 | 88.45 | 1.27 |
| 10 | 4371 | 86.90 | 2.17 | 4381 | 87.10 | 2.24 | 4378 | 87.04 | 1.96 | 4305 | 85.59 | 1.88 |
| 15 | 3813 | 75.81 | 1.54 | 3832 | 76.18 | 1.56 | 3750 | 74.55 | 1.27 | 3839 | 76.32 | 1.38 |
| 20 | 2768 | 55.03 | 1.75 | 2835 | 56.36 | 1.40 | 2811 | 55.88 | 1.36 | 2557 | 50.83 | 1.50 |
| 25 | 1238 | 24.61 | 1.47 | 1272 | 25.29 | 1.63 | 1615 | 32.11 | 1.56 | 902 | 17.93 | 1.27 |
| 30 | 203 | 4.04 | 1.28 | 114 | 2.27 | 1.24 | 30 | 0.60 | 1.11 | 45 | 0.89 | 1.05 |
| 35 | 0 | 0 | - | 1 | 0.02 | 0.28 | 0 | 0 | - | 0 | 0 | - |
| 40 | 0 | 0 | - | 0 | 0 | - | 0 | 0 | - | 0 | 0 | - |
| 45 | 0 | 0 | - | 0 | 0 | - | 0 | 0 | - | 0 | 0 | - |
| 50 | 0 | 0 | - | 0 | 0 | - | 0 | 0 | - | 0 | 0 | - |
| 55 | 0 | 0 | - | 0 | 0 | - | 0 | 0 | - | 0 | 0 | - |
| 60 | 0 | 0 | - | 0 | 0 | - | 0 | 0 | - | 0 | 0 | - |
| 65 | 0 | 0 | - | 0 | 0 | - | 0 | 0 | - | 0 | 0 | - |
| 70 | 0 | 0 | - | 0 | 0 | - | 0 | 0 | - | 0 | 0 | - |
| 75 | 0 | 0 | - | 0 | 0 | - | 0 | 0 | - | 0 | 0 | - |
| 80 | 0 | 0 | - | 0 | 0 | - | 0 | 0 | - | 0 | 0 | - |
| 85 | 0 | 0 | - | 0 | 0 | - | 0 | 0 | - | 0 | 0 | - |
| 90 | 0 | 0 | - | 0 | 0 | - | 0 | 0 | - | 0 | 0 | - |

Table 5.9: Parameter look-up table for 60° vane angle and 13m/s inlet velocity

| 60 DEGREE | | | | | | | | | | | | |
|-----------------------------|------------|-------------|--------------------|------------|-------------|--------------------|------------|-------------|--------------------|------------|-------------|--------------------|
| Particles Size (microns) | 13 m/s | | | | | | | | | | | |
| | Position 1 | | | Position 2 | | | Position 3 | | | Position 4 | | |
| | Escaped | Escaped (%) | Residence Time (s) | Escaped | Escaped (%) | Residence Time (s) | Escaped | Escaped (%) | Residence Time (s) | Escaped | Escaped (%) | Residence Time (s) |
| 1 | 4482 | 89.11 | 2.22 | 4455 | 88.57 | 2.23 | 4481 | 89.09 | 1.92 | 4459 | 88.65 | 1.91 |
| 5 | 4890 | 97.22 | 3.02 | 4914 | 97.69 | 2.96 | 4907 | 97.55 | 2.37 | 4901 | 97.44 | 2.46 |
| 10 | 4944 | 98.29 | 2.78 | 4962 | 98.65 | 5.11 | 4987 | 99.15 | 2.20 | 4998 | 99.36 | 5.30 |
| 15 | 4998 | 99.36 | 2.67 | 4998 | 99.36 | 2.05 | 5016 | 99.72 | 1.72 | 5012 | 99.64 | 2.25 |
| 20 | 5024 | 99.88 | 2.15 | 5029 | 99.98 | 2.14 | 5030 | 100.00 | 2.24 | 5030 | 100.00 | 2.44 |
| 25 | 5030 | 100.00 | 2.37 | 5028 | 99.96 | 2.06 | 5030 | 100.00 | 2.33 | 5030 | 100.00 | 2.07 |
| 30 | 5030 | 100.00 | 2.34 | 5030 | 100.00 | 2.30 | 5030 | 100.00 | 3.23 | 5030 | 100.00 | 3.15 |
| 35 | 5027 | 99.94 | 3.91 | 4686 | 93.16 | 3.72 | 4092 | 81.35 | 3.48 | 3823 | 76.00 | 1.80 |
| 40 | 3806 | 75.67 | 1.78 | 3834 | 76.22 | 3.44 | 3818 | 75.90 | 1.97 | 3760 | 74.75 | 1.87 |
| 45 | 3742 | 74.39 | 2.00 | 3770 | 74.95 | 3.19 | 3761 | 74.77 | 2.09 | 2057 | 40.89 | 2.89 |
| 50 | 3671 | 72.98 | 3.07 | 1073 | 21.33 | 3.15 | 24 | 0.48 | 2.37 | 0 | 0 | - |
| 55 | 345 | 6.86 | 1.17 | 0 | 0 | - | 0 | 0 | - | 0 | 0 | - |
| 60 | 0 | 0 | - | 0 | 0 | - | 0 | 0 | - | 0 | 0 | - |
| 65 | 0 | 0 | - | 0 | 0 | - | 0 | 0 | - | 0 | 0 | - |
| 70 | 0 | 0 | - | 0 | 0 | - | 0 | 0 | - | 0 | 0 | - |
| 75 | 0 | 0 | - | 0 | 0 | - | 0 | 0 | - | 0 | 0 | - |
| 80 | 0 | 0 | - | 0 | 0 | - | 0 | 0 | - | 0 | 0 | - |
| 85 | 0 | 0 | - | 0 | 0 | - | 0 | 0 | - | 0 | 0 | - |
| 90 | 0 | 0 | - | 0 | 0 | - | 0 | 0 | - | 0 | 0 | - |

Table 5.10: Parameter look-up table for 60° vane angle and 20m/s inlet velocity

| 60 DEGREE | | | | | | | | | | | | |
|-----------------------------|------------|-------------|--------------------|------------|-------------|--------------------|------------|-------------|--------------------|------------|-------------|--------------------|
| Particles Size (microns) | 20 m/s | | | | | | | | | | | |
| | Position 1 | | | Position 2 | | | Position 3 | | | Position 4 | | |
| | Escaped | Escaped (%) | Residence Time (s) | Escaped | Escaped (%) | Residence Time (s) | Escaped | Escaped (%) | Residence Time (s) | Escaped | Escaped (%) | Residence Time (s) |
| 1 | 4505 | 89.56 | 1.30 | 4512 | 89.70 | 1.36 | 4525 | 89.96 | 2.03 | 4505 | 89.56 | 1.34 |
| 5 | 4922 | 97.85 | 2.26 | 4949 | 98.39 | 1.98 | 4950 | 98.41 | 1.66 | 4965 | 98.71 | 1.65 |
| 10 | 4996 | 99.32 | 4.64 | 5007 | 99.54 | 2.70 | 4987 | 99.15 | 3.31 | 5014 | 99.68 | 3.95 |
| 15 | 5004 | 99.48 | 2.26 | 5022 | 99.84 | 3.43 | 5008 | 99.56 | 1.81 | 5030 | 100.00 | 1.36 |
| 20 | 5030 | 100.00 | 1.35 | 4911 | 97.63 | 1.26 | 4974 | 98.89 | 1.54 | 5030 | 100.00 | 1.44 |
| 25 | 5030 | 100.00 | 1.75 | 4915 | 97.71 | 1.51 | 5030 | 100.00 | 1.39 | 5030 | 100.00 | 1.85 |
| 30 | 4387 | 87.22 | 2.35 | 4266 | 84.81 | 2.31 | 5019 | 99.78 | 2.41 | 4668 | 92.80 | 2.15 |
| 35 | 3919 | 77.91 | 1.27 | 3956 | 78.65 | 2.25 | 3934 | 78.21 | 1.17 | 613 | 12.19 | 1.67 |
| 40 | 3868 | 76.90 | 1.59 | 3902 | 77.57 | 2.10 | 3806 | 75.67 | 1.49 | 0 | 0 | - |
| 45 | 130 | 2.58 | 0.73 | 952 | 18.93 | 1.99 | 3831 | 76.16 | 2.80 | 0 | 0 | - |
| 50 | 0 | 0 | - | 0 | 0 | - | 0 | 0 | - | 0 | 0 | - |
| 55 | 0 | 0 | - | 0 | 0 | - | 0 | 0 | - | 0 | 0 | - |
| 60 | 0 | 0 | - | 0 | 0 | - | 0 | 0 | - | 0 | 0 | - |
| 65 | 0 | 0 | - | 0 | 0 | - | 0 | 0 | - | 0 | 0 | - |
| 70 | 0 | 0 | - | 0 | 0 | - | 0 | 0 | - | 0 | 0 | - |
| 75 | 0 | 0 | - | 0 | 0 | - | 0 | 0 | - | 0 | 0 | - |
| 80 | 0 | 0 | - | 0 | 0 | - | 0 | 0 | - | 0 | 0 | - |
| 85 | 0 | 0 | - | 0 | 0 | - | 0 | 0 | - | 0 | 0 | - |
| 90 | 0 | 0 | - | 0 | 0 | - | 0 | 0 | - | 0 | 0 | - |

Table 5.11: Parameter look-up table for 60° vane angle and 30m/s inlet velocity

| 60 DEGREE | | | | | | | | | | | | |
|-----------------------------|------------|-------------|--------------------|------------|-------------|--------------------|------------|-------------|--------------------|-----------|-------------|--------------------|
| Particles Size (microns) | 30 m/s | | | | | | | | | | | |
| | Position 1 | | | Position 2 | | | Position 3 | | | Position4 | | |
| | Escaped | Escaped (%) | Residence Time (s) | Escaped | Escaped (%) | Residence Time (s) | Escaped | Escaped (%) | Residence Time (s) | Escaped | Escaped (%) | Residence Time (s) |
| 1 | 3239 | 64.39 | 0.66 | 3320 | 66.00 | 0.76 | 3338 | 66.36 | 0.85 | 3287 | 65.35 | 0.77 |
| 5 | 4706 | 93.56 | 1.29 | 4726 | 93.96 | 1.30 | 4702 | 93.48 | 1.37 | 4659 | 92.62 | 1.32 |
| 10 | 4834 | 96.10 | 1.82 | 4849 | 96.40 | 1.86 | 4834 | 96.10 | 2.47 | 4824 | 95.90 | 2.15 |
| 15 | 4728 | 94.00 | 2.17 | 4779 | 95.01 | 2.17 | 4721 | 93.86 | 2.14 | 4763 | 94.69 | 2.15 |
| 20 | 4519 | 89.84 | 2.02 | 4535 | 90.16 | 2.39 | 4526 | 89.98 | 2.26 | 4483 | 89.13 | 2.11 |
| 25 | 3946 | 78.45 | 2.55 | 3839 | 76.32 | 1.96 | 3850 | 76.54 | 1.92 | 3895 | 77.44 | 1.74 |
| 30 | 15 | 0.30 | 1.01 | 18 | 0.36 | 1.12 | 35 | 0.70 | 0.94 | 14 | 0.28 | 9.68 |
| 35 | 1 | 0.02 | 0.39 | 2 | 0.04 | 0.68 | 1 | 0.02 | 0.20 | 0 | 0 | - |
| 40 | 0 | 0 | - | 0 | 0 | - | 0 | 0 | - | 0 | 0 | - |
| 45 | 0 | 0 | - | 0 | 0 | - | 0 | 0 | - | 0 | 0 | - |
| 50 | 0 | 0 | - | 0 | 0 | - | 0 | 0 | - | 0 | 0 | - |
| 55 | 0 | 0 | - | 0 | 0 | - | 0 | 0 | - | 0 | 0 | - |
| 60 | 0 | 0 | - | 0 | 0 | - | 0 | 0 | - | 0 | 0 | - |
| 65 | 0 | 0 | - | 0 | 0 | - | 0 | 0 | - | 0 | 0 | - |
| 70 | 0 | 0 | - | 0 | 0 | - | 0 | 0 | - | 0 | 0 | - |
| 75 | 0 | 0 | - | 0 | 0 | - | 0 | 0 | - | 0 | 0 | - |
| 80 | 0 | 0 | - | 0 | 0 | - | 0 | 0 | - | 0 | 0 | - |
| 85 | 0 | 0 | - | 0 | 0 | - | 0 | 0 | - | 0 | 0 | - |
| 90 | 0 | 0 | - | 0 | 0 | - | 0 | 0 | - | 0 | 0 | - |

5.5 Conclusion

This chapter disclosed an extensive analysis on the flow distribution and particle distribution inside the classifier. The analyses help to generate a look-up table which can assist in determine the most suitable set of parameter for classifier applications.

CHAPTER SIX: VALIDATION OF THE SIMULATION

In this chapter the numerical method used in the simulations was validated. The first section elaborates the pro and cons of several turbulence models under consideration. Results from the simulation models were compared with the experimental in order to choose the best method. The deviation of the selected methodology to the experimental data was then determined to arrive at the average discrepancy. Comparison of flow visualisations between numerical and experimental approaches were presented in the third section. The fourth section described the comparison of the particles' distribution from the simulation and experimental. The agreement between numerical and experimental results validated the numerical method.

6.1 CFD Setup

Governing equations for the steady turbulent 3-D flow were solved numerically under certain boundary conditions for an inlet velocity of 13m/s, corresponding to the inlet Reynolds numbers, Re , of 472163. Therefore, the effects of fluid turbulence (Reynolds number $\left(\frac{\rho UD}{\mu}\right) > 2300$) have to be considered.

The numerical analysis is based on the solution of the Reynolds Averaged Navier-Stokes (RANS) equations. The finite volume method with tetrahedral grid and adaptive time step were the main numerical features of the software. Pressure-velocity coupling used the SIMPLE algorithms. Various turbulence models, including the Reynolds stress model and the Realisable model, were considered as the best candidates for use in this study.

The numerical calculations for the gas phase were performed by solving a set of Reynolds-Averaged Navier-Stokes equations. Reynolds-Averaged Navier-Stokes (RANS) equations models are the most widely taken approach for calculating industrial flows. In this approach, all turbulence scales are modelled. In order to approximate the turbulence scales, the solution variables are decomposed into their mean and fluctuating components and the Reynolds-Averaged Navier-Stokes (RANS) equations are obtained (Patankar, 1972).

From literature searches, two different RANS turbulence models were considered for the present study: Realisable k - ϵ and Reynolds Stress Model (RSM).

The gas phase turbulence quantities were predicted using the Reynolds Stress Model, together with the isotropic eddy viscosity hypothesis, which relates the Reynolds Stress linearly to the mean velocity gradient. In the vicinity of the wall, the turbulence becomes more complex because of the no-slip conditions there. Also in the near-wall zone, the velocity and other transport properties vary rapidly within a short distance from the wall. In order to predict the rapid variation in this

region, very good grid resolution is required, however this does increase the computational time.

The particulate phase was treated by the Lagrangian approach. In this model, the particles are grouped in so called "parcels", a collection of particles with the same properties. The parcels are introduced at a finite number of starting locations at the inlet cross-section and move simultaneously through the flow field. The interaction between these eddies and the particles are taken into account by a stochastic.

Particle-wall collisions were modelled using a coefficient of restitution, having a value of 0.01–0.3 in all the calculations depends on the type of material. The coefficient of restitution is defined as the ratio of the normal velocity component after impact to that before impact. In order to provide data for numerical models, a number of studies have been performed to investigate the collision characteristics of solid particles with a wall. Particle-particle collisions were neglected in this study. This is a good assumption for dilute gas-particle flows.

A total of 52,000 computational particles were tracked throughout the flow domain. Each computational particle (or parcel) carried the same flow rate and was assumed to be spherical. The particle diameters were stochastically sampled using the Rossin Rammler distribution function.

The solution for the system of equations continues until a converged solution is obtained. Converged solutions were assumed to be obtained when the normalised

residuals and the time rate change of the conserved variable had decreased to their minimums and remained unchanged as iterations continued.

6.1.1 Grid Independency Study

Finer mesh does not necessarily lead to accurate results (Thompson, 1985). Therefore, a grid independence study was carried out for two mesh configurations of 2,400,000 and 3,400,000 cells. In the model setup, the standard discretisation scheme was used for the pressure equation, and the second-order upwind discretisation scheme was used for all other equations. The pressure velocity coupling was solved using the SIMPLE (Semi-Implicit Method for Pressure-Linked Equations) algorithm. This model setup was applied to all simulations described in this study unless stated. Figures 6.1 through to Figure 6.3 show the results from the classifier grid independence study. All four axial levels (Level A to Level D), as shown in Figure 5.1, were analysed separately. Axial, radial and tangential velocity profiles of the two mesh configurations were analysed .

The results show that there was no significant difference between the two mesh configurations, as all lines of both configurations overlapped. These indicated that using finer mesh did not improve the model prediction. Thus, meshing with a lower number of mesh cells does not sacrifice accuracy of the solution. Since the Central Processing Unit (CPU) time increases exponentially with the number of grids, the lower mesh cells (2,400,000) were chosen. Less mesh cells reduce the CPU time during CFD simulation, which permits a significant number of cases to be run.

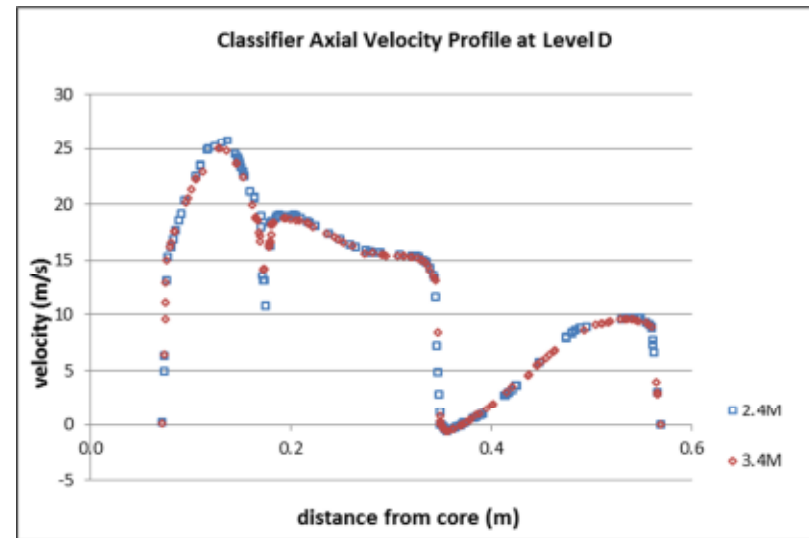
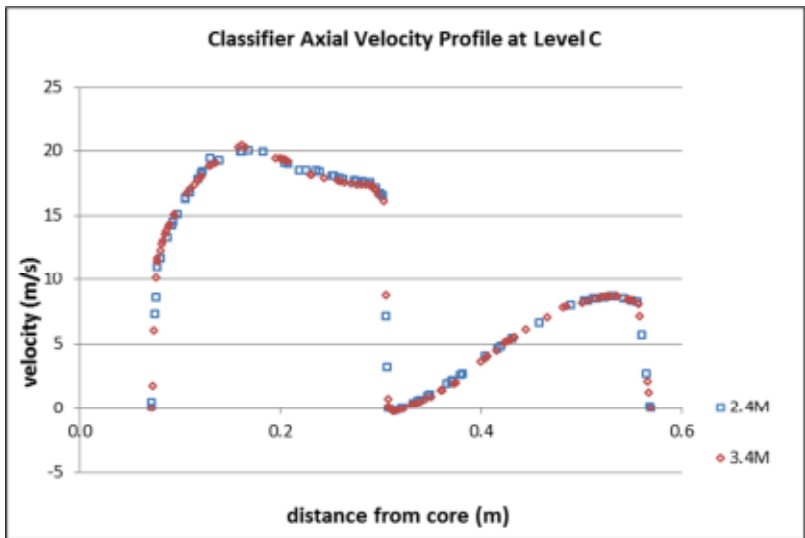
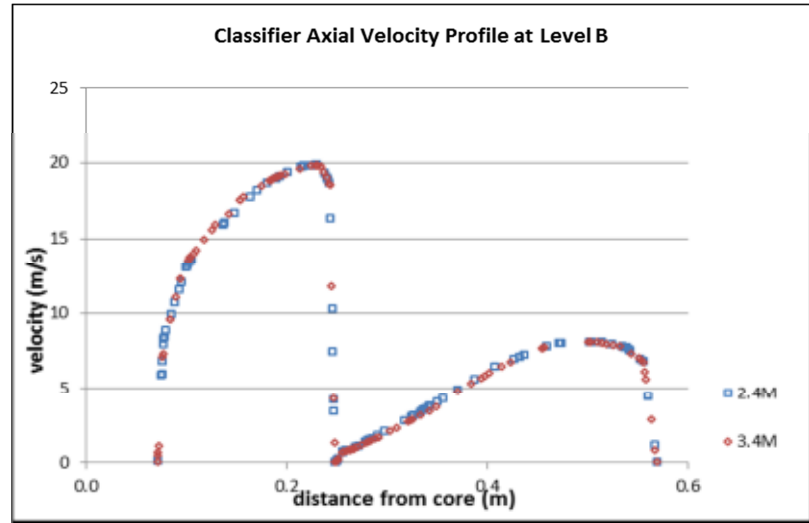
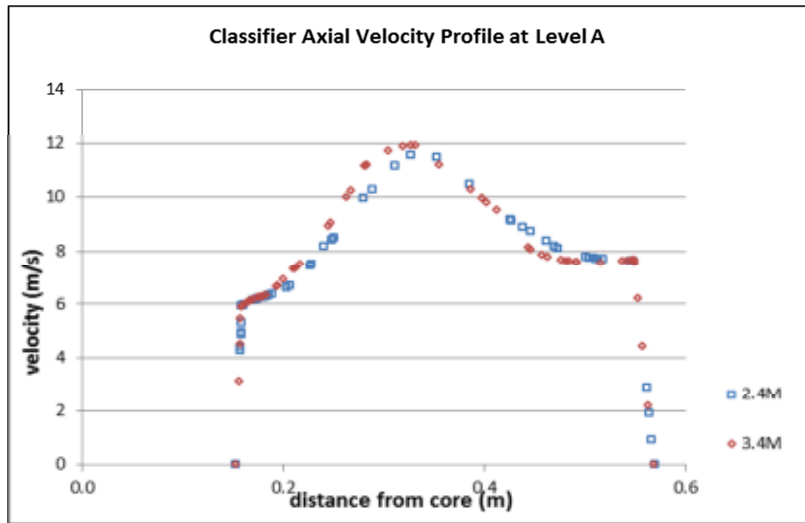


Figure 6.1: Axial velocity profile comparison between 2.4 million and 3.4 million mesh sizes

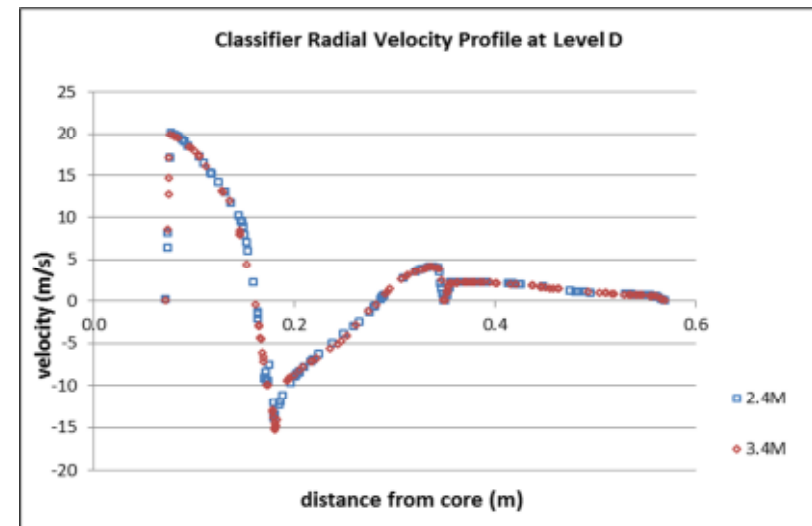
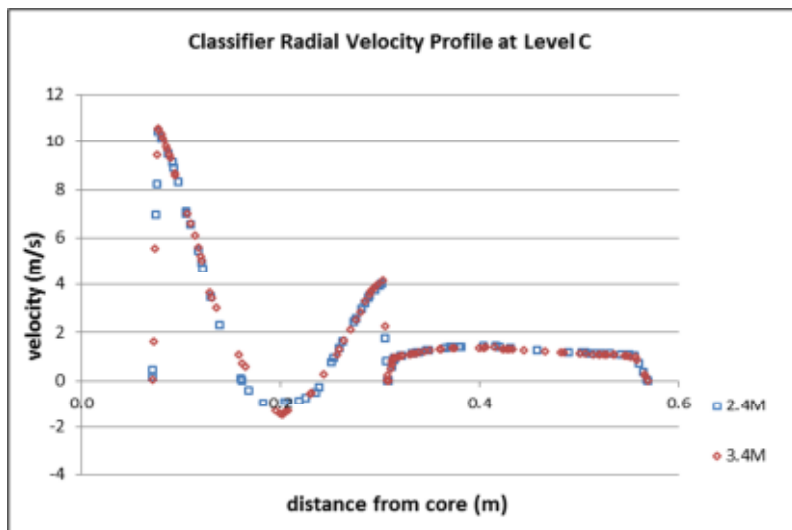
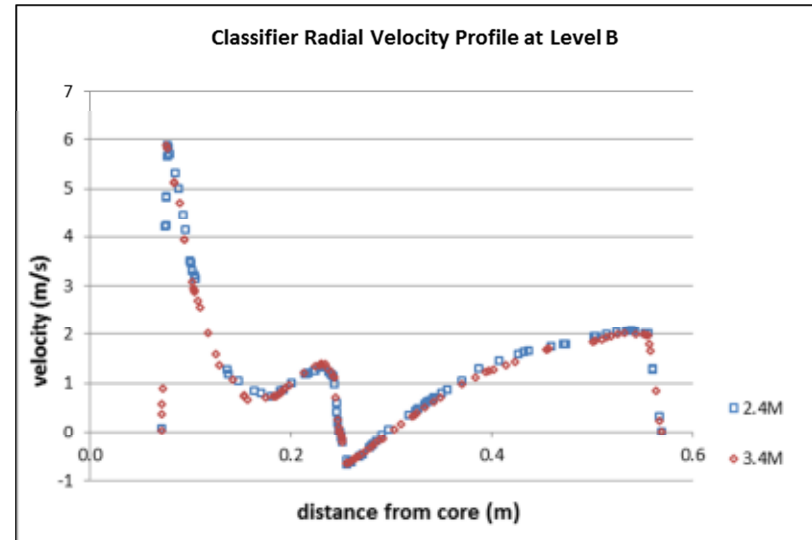
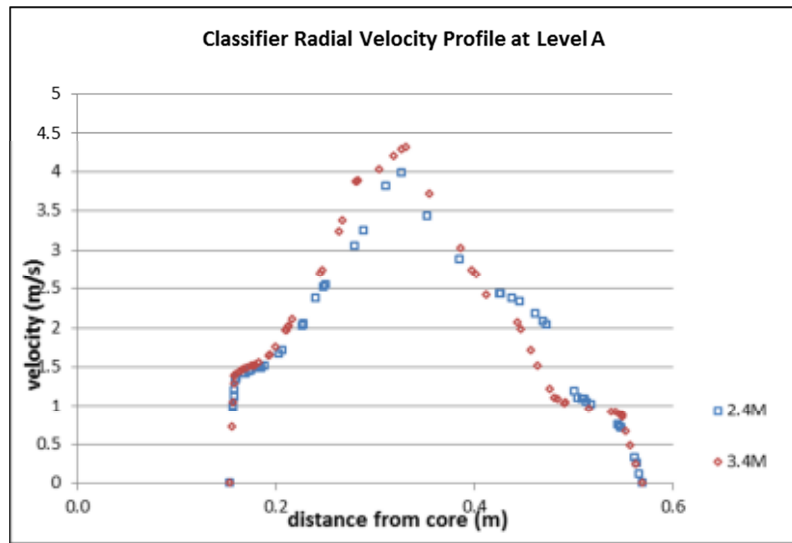


Figure 6.2: Radial velocity profile comparison between 2.4 million and 3.4 million mesh sizes

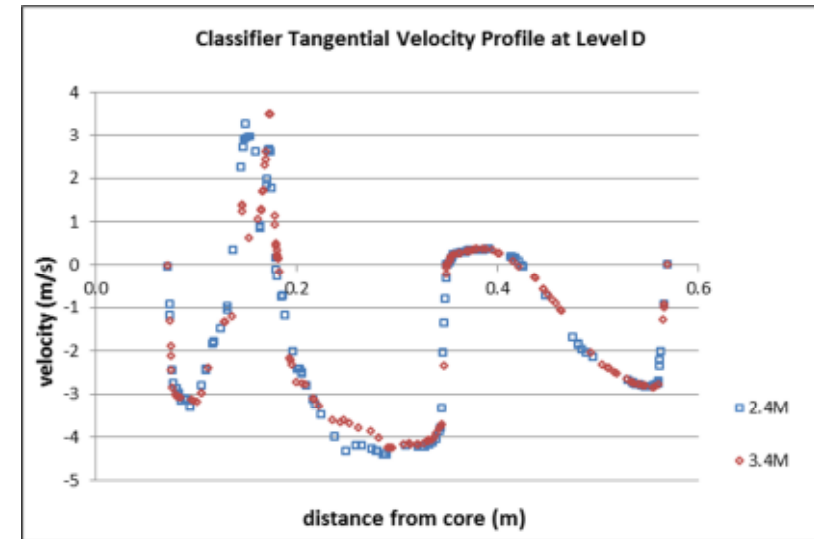
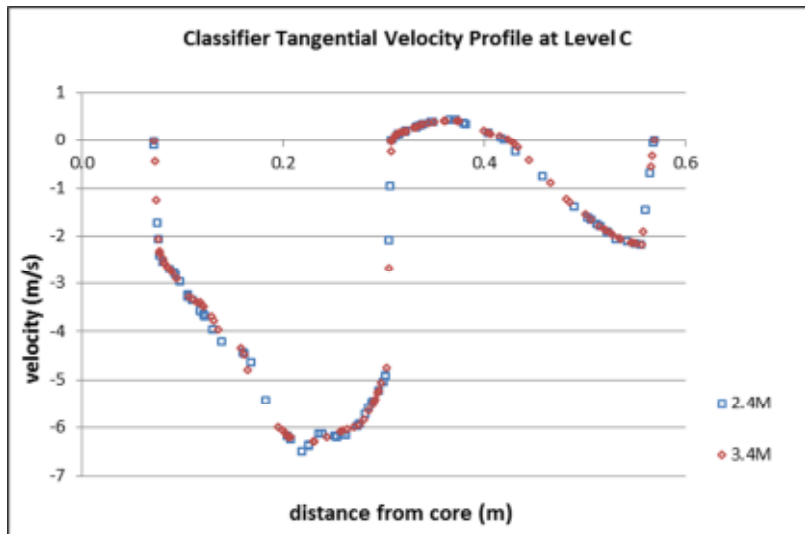
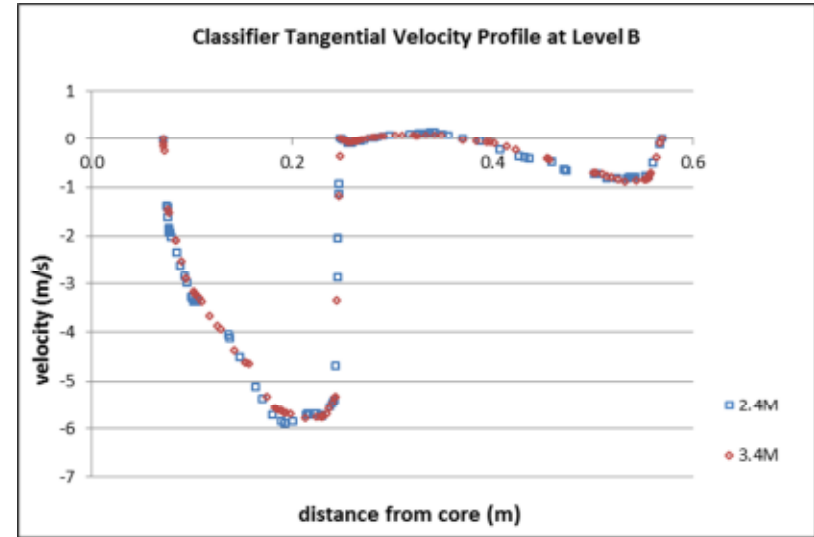
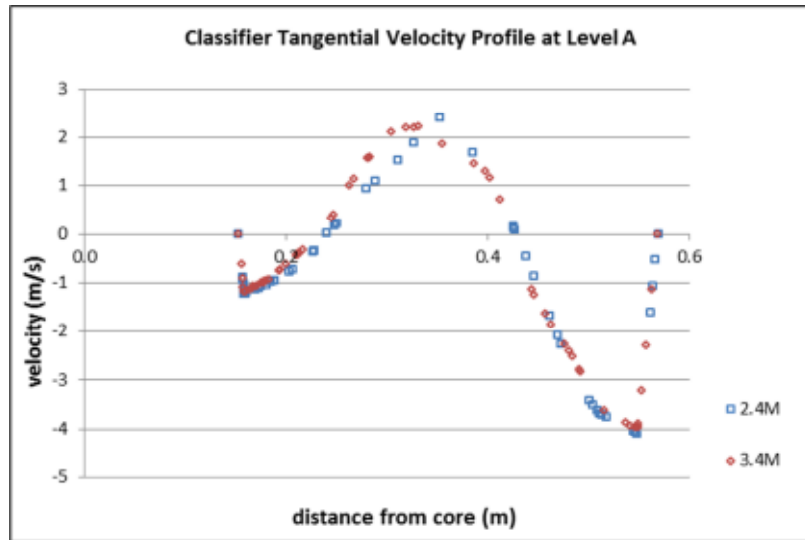


Figure 6.3: Tangential velocity profile comparison between 2.4 million and 3.4 million mesh sizes

6.2 Experimental Setup

The computational model used in this study was described in Chapter 4. When using CFD, it is important that the solution gained through computation relates to real-life situations within a certain margin of error. Computer simulations have to relate to real situations, otherwise the point of carrying out the computation is moot.

To validate the choice of models and schemes used in the CFD simulations completed for this thesis, a test case was run on the one-third scale rig, followed by a computational model of the same flow scenario and conditions. Once run, it was possible to see the correlation of air flow and particle behaviour between the experimental and the computational simulation. This test showed whether the CFD programme FLUENT could model, within acceptable limits.

Experiments were conducted for the air velocity distribution and particles distribution. The experiments were carried out for inlet velocity of 13m/s, 60° vane angle and at outlet position 1. As mentioned in Section 3.3.3, the motor speed was set at the controller. Through the calibration, it was found that a 20Hz on the display produced an air velocity of approximately 13m/s.

Experiments on particles' distribution were also carried out. The description of the particulate phase experiment was given in Section 3.6. Figure 3.23 shows the arrangement of the experiment conducted.

6.3 Validation of CFD

The validation of CFD is assessed through quantitative and qualitative methods. Comparison of both methods showed the differences and similarities that led to the conclusion of the method used.

6.3.1 Quantitative Validation

Quantitative validation was done by comparing the velocity distribution and behaviour. The difference was seen by comparing the values of the axial velocity, radial velocity and tangential velocity of the CFD method with the experiment. Percentage of error was also calculated to demonstrate the suitability of the method and also to show the CFD prediction to be true.

6.3.1.1 Velocity Flow Field

Velocities inside the classifier were also taken along Level A, Level B, Level C and Level D, as shown in Figure 6.4 for 60° vane angles. Measurements along Level A represent velocity profile at the area close to the inlet. Measurements along Level B and Level C show the velocity profile in the cone (separation area), while measurements along Level D demonstrated the velocity close to the guide vane and at the entrance of the vortex finder. For validation purposes, readings of CFD data were also taken at the same distance.

Figure 6.5 through to Figure 6.7 show the comparison between the CFD and experimental velocity components distributions for 60° vane angle along Level A, Level B, Level C and Level D respectively. The axial velocity profiles at different radial distances and axial heights in the classifier model are shown in Figure 6.5.

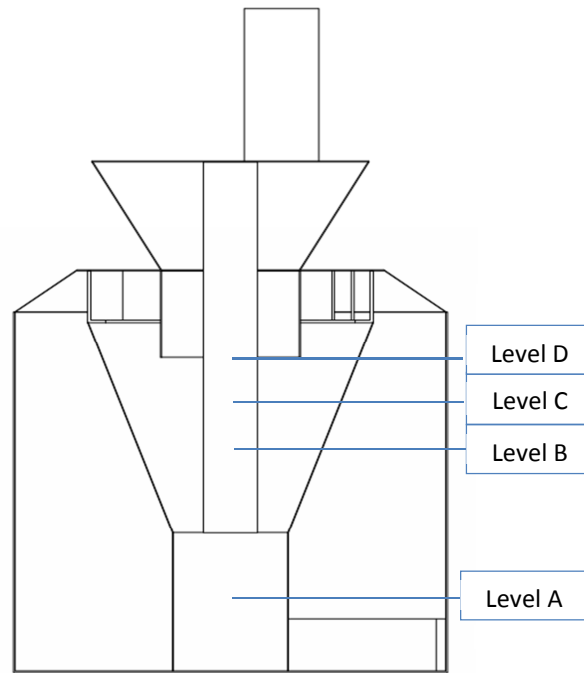


Figure 6.4: The measurement locations

Figure 6.6 shows the comparison of radial velocity for the experiment, Rke and RSM at different heights. Radial velocity is important in respect to the separation mechanisms, as it requires a difference in radial displacement. The centrifugal force field necessary for classification inside the system was generated by the tangential velocity component. The comparison of tangential velocity for the experiment, Rke and RSM at different heights is illustrated in Figure 6.7.

From the figures it can be observed that the velocities measured from the experiment were slightly higher compared to CFD. The largest deviation between the CFD and the experimental results are 19.96 and 1.12 at Level B RSM axial velocity component and Level A Rke radial velocity component respectively.

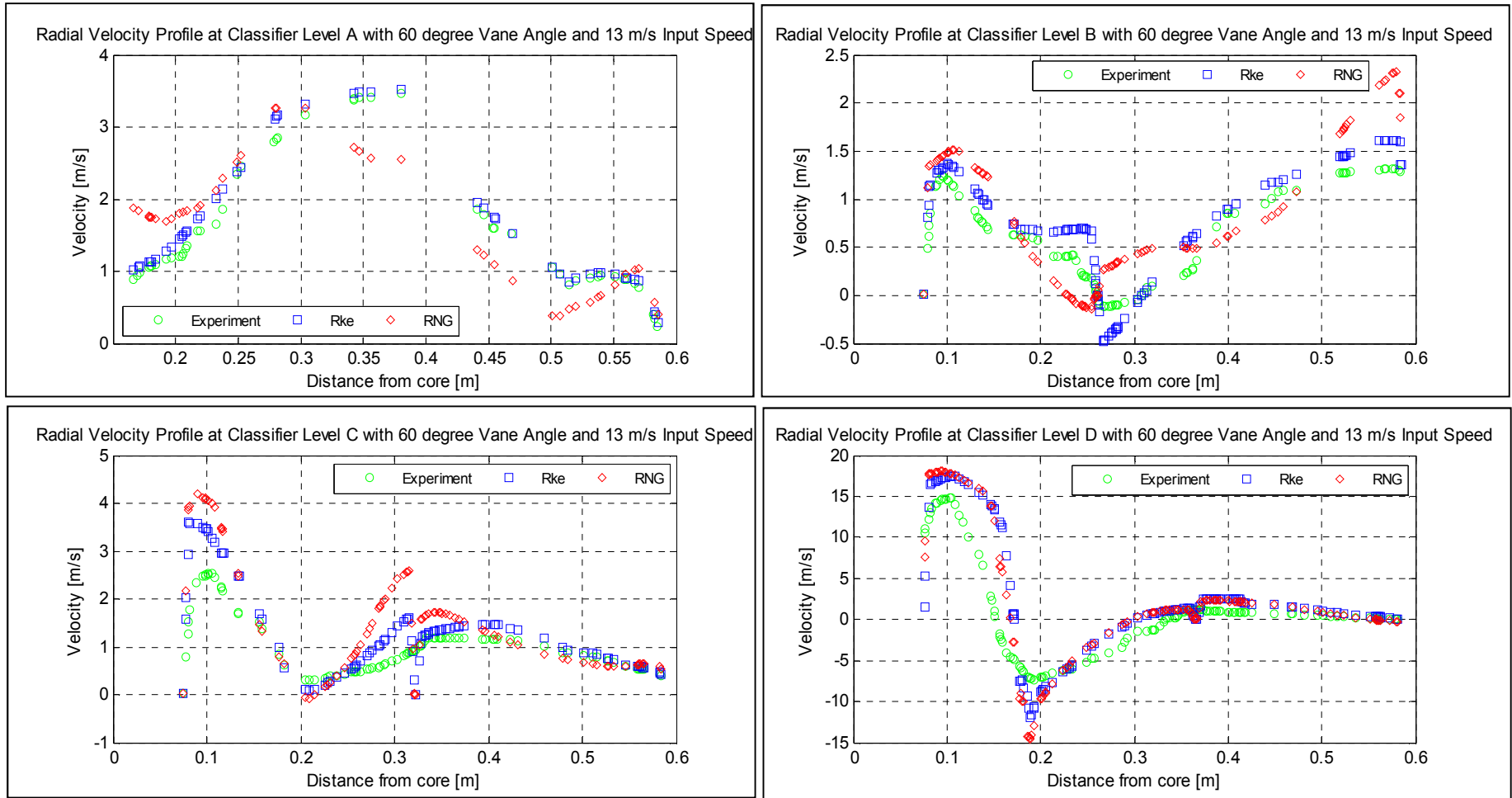


Figure 6.5: Comparison of the experiment, Rke and RSM axial velocity profiles at different heights in the classifier

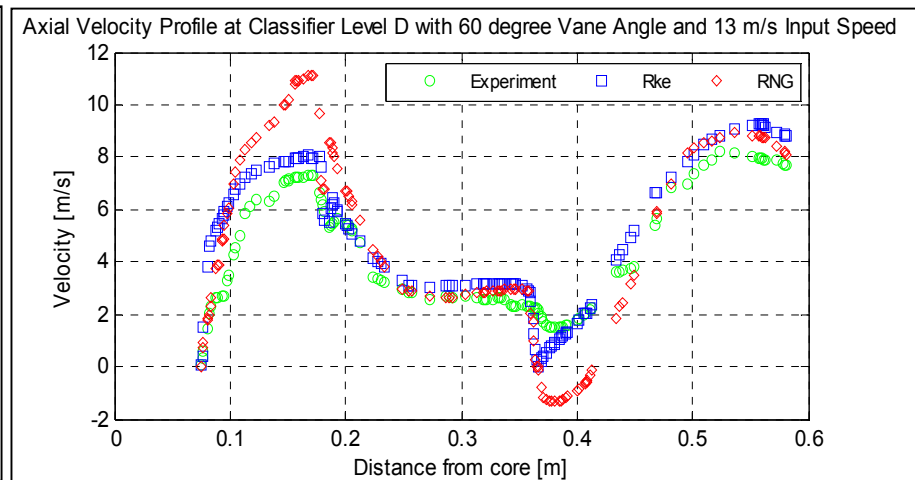
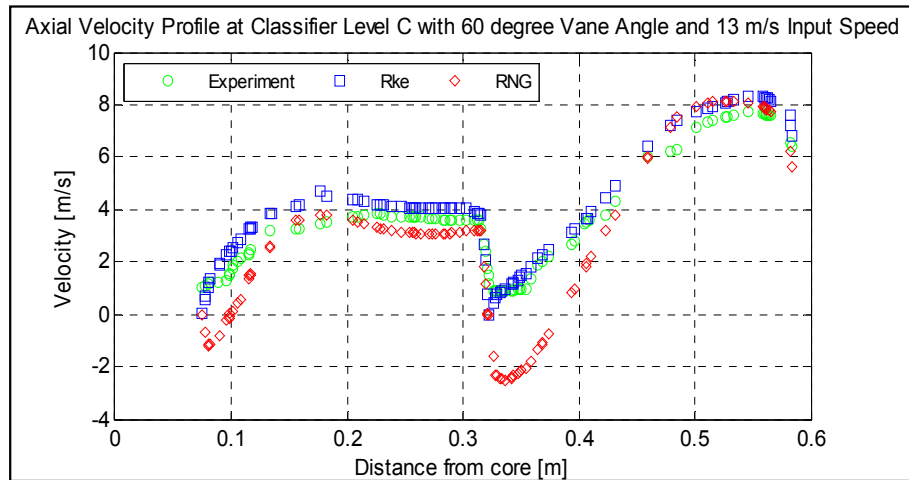
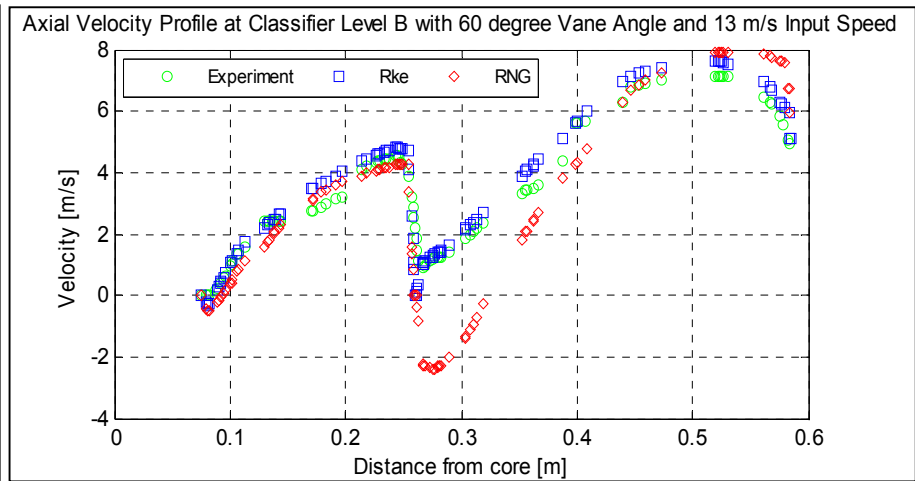
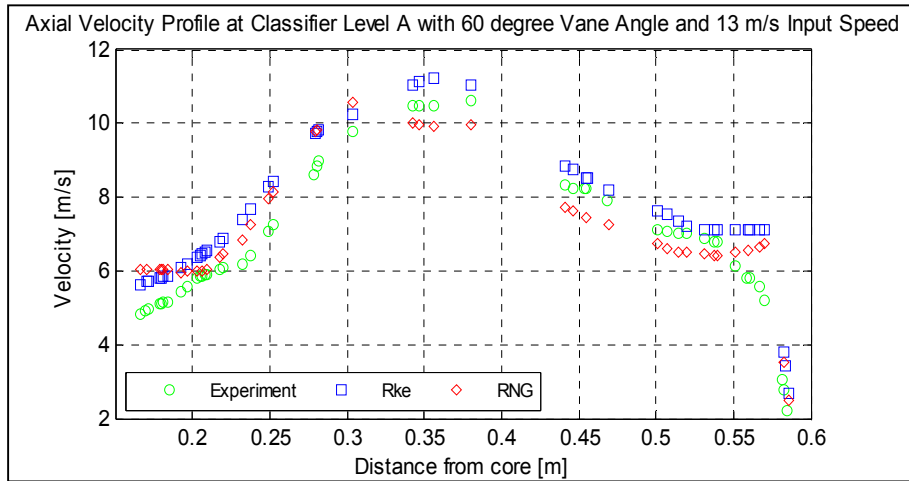


Figure 6.6: Comparison of the experiment, Rke and RSM radial velocity profiles at different heights inside the classifier

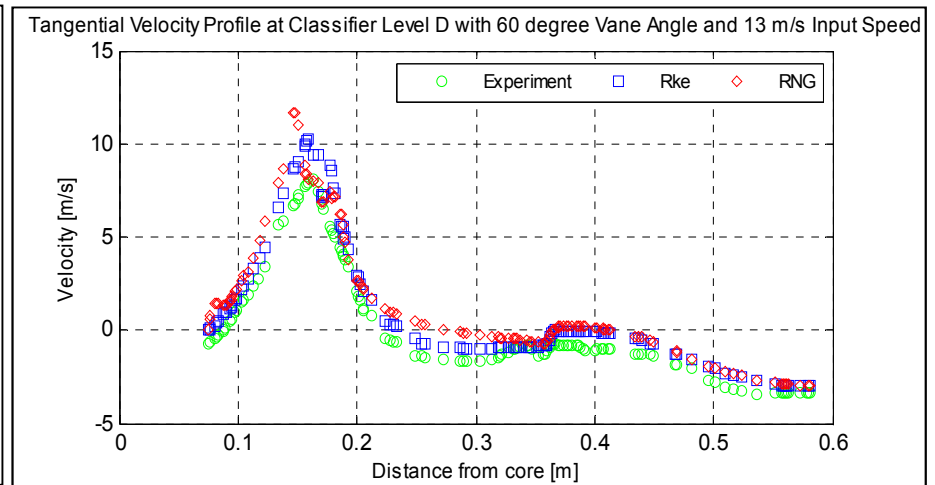
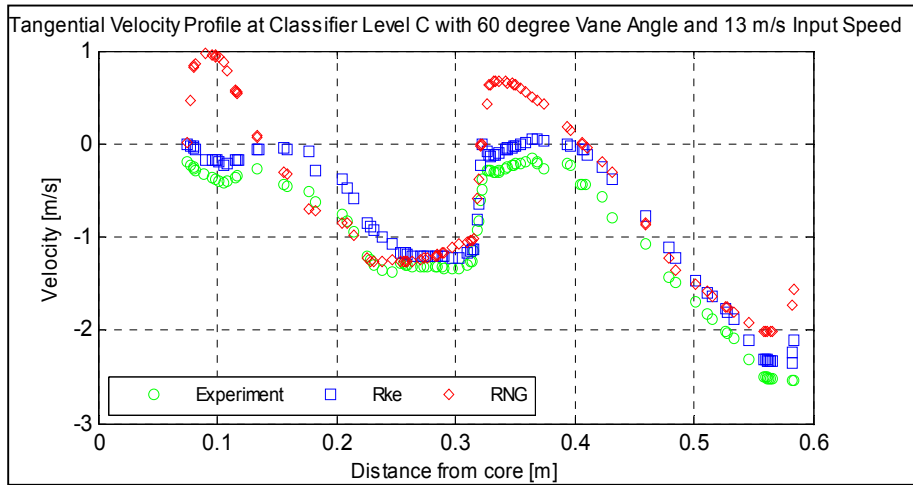
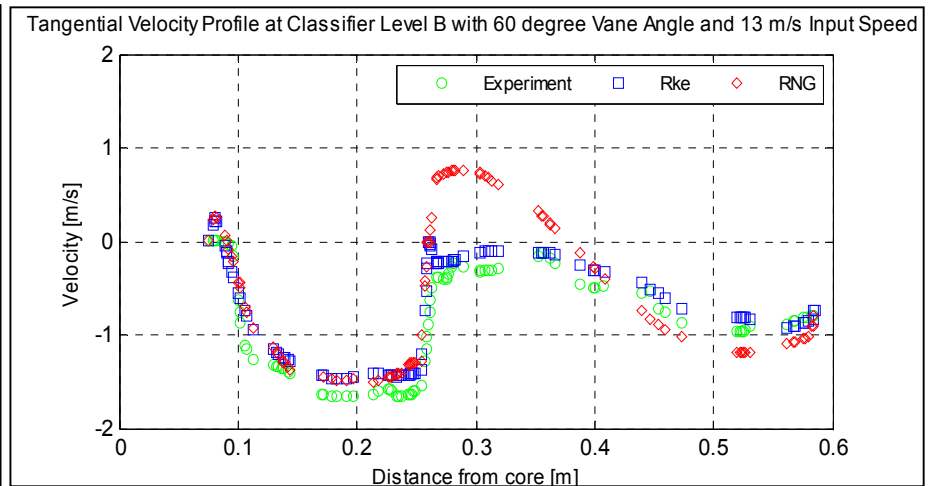
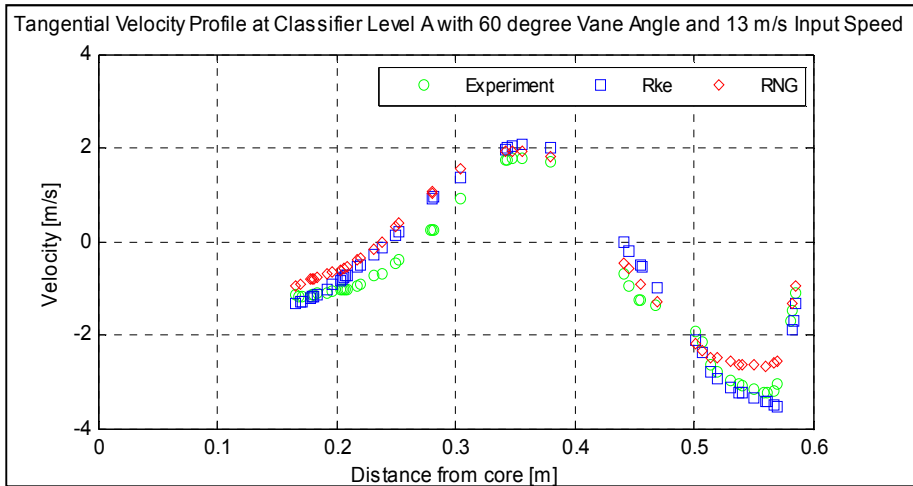


Figure 6.7: Comparison of the experiment, Rke and RSM tangential velocity profiles at different heights in the classifier

From these resulting outputs, it is evident that a number of turbulence models provide different results. Although some give distinct data compared to the experimental, the Rke k- ϵ and RSM do present reasonable flow patterns weighed against the experimental results. However, through close observation, the Rke k- ϵ was chosen as the most suitable model to give the closest results compared to the experimental.

These figures verify the satisfactorily qualitative agreement between the numerical and experimental data. However, accessing the discrepancies quantitatively is essential. The Root Mean Square (RMS) was used to determine the deviation between the experimental and numerical results. Consequently, the percentages of deviation (%) between the CFD and experimental results for each velocity component were calculated and are tabulated in Table 6.1. The percentages of deviation are compared to the experimental result. These components are named as cases 1 to 12 according to their sequence in the figures above.

Engineering is the art of coping with uncertainty and in exactitude. The percentages of deviation between experimental and numerical results as tabulated in Table 6.1 give an average of 5.34% discrepancy, which is reasonable in highly complex flow situations. Furthermore, since the current study uses a physical approach to arrive at the best geometrical configurations of the modelling, it is the qualitative nature of the results and the physics of it that are important. Therefore, due to the physical plausibility and reasonable deviations to the experiment, the chosen numerical approach is reliable and has been finally validated.

Table 6.1: CFD and experimental results for each velocity component

| No. | Measurement point and description | Percentage of deviation (%) | |
|-----|---|-----------------------------|-------|
| | | Rke | RSM |
| 1 | Axial Velocity at line A- area close to the inlet | 5.89 | 6.12 |
| 2 | Axial Velocity at line B- bottom part of the separation area | 6.00 | 19.96 |
| 3 | Axial Velocity at line C- upper part of the separation area | 6.56 | 18.52 |
| 4 | Axial Velocity at line D- area close to the guide vane and at the entrance of the turret | 5.15 | 14.52 |
| 5 | Radial Velocity at line A- area close to the inlet | 1.12 | 4.00 |
| 6 | Radial Velocity at line B- bottom part of the separation area | 2.67 | 4.63 |
| 7 | Radial Velocity at line C- upper part of the separation area | 5.84 | 9.84 |
| 8 | Radial Velocity at line D- area close to the guide vane and at the entrance of the turret | 9.43 | 5.17 |
| 9 | Tangential Velocity at line A- area close to the inlet | 2.91 | 3.35 |
| 10 | Tangential Velocity at line B- bottom part of the separation area | 2.74 | 6.27 |
| 11 | Tangential Velocity at line C- upper part of the separation area | 2.66 | 7.33 |
| 12 | Tangential Velocity at line D- area close to the guide vane and at the entrance of the turret | 13.05 | 16.87 |

6.3.1.2 Particle Distribution

The particle size distribution from the samples collected in the cyclone (experiment) and the samples at the outlet from CFD were measured. The sample from the experiment and the sample from CFD were compared. A similar trend was observed in the samples collected in the cyclone in comparison with the result from CFD.

Figure 6.8 and Figure 6.9 illustrate the cumulative volume and cumulative size distribution for the experimental and CFD results. Figure 6.10 shows particle size at 40, 50, 60, 70 and 80% of cumulative distribution for all tests. The results of both plots show that the measured sizes were not much different for the CFD and experimental results. This can be confirmed with the deviation percentage as illustrated in Table 6.2. The results show that both methods produce little difference in comparison with each other. It was recorded that the deviation for all methods were below 7%. This means that the CFD result has a good agreement with the result from the experiment.

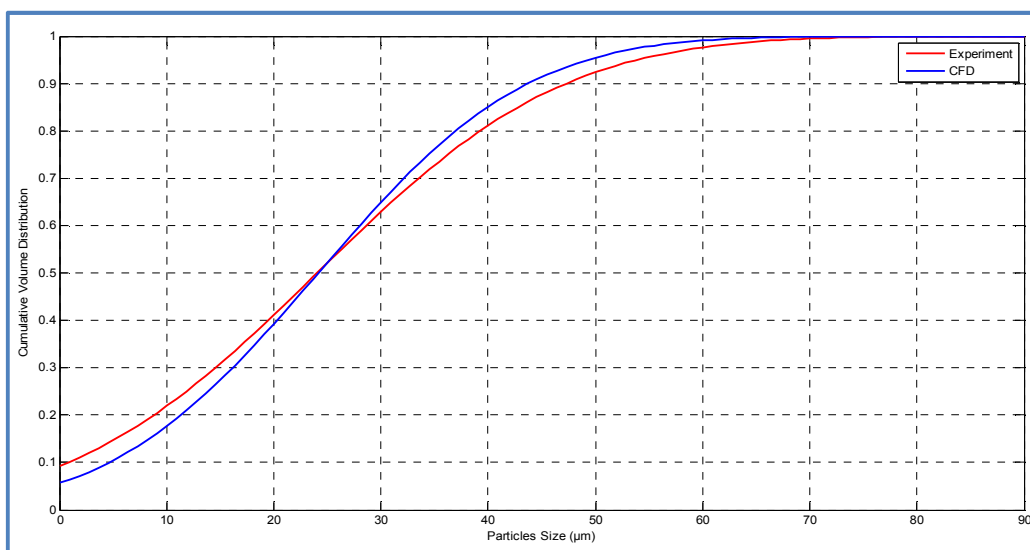


Figure 6.8: Particles cumulative volume distribution

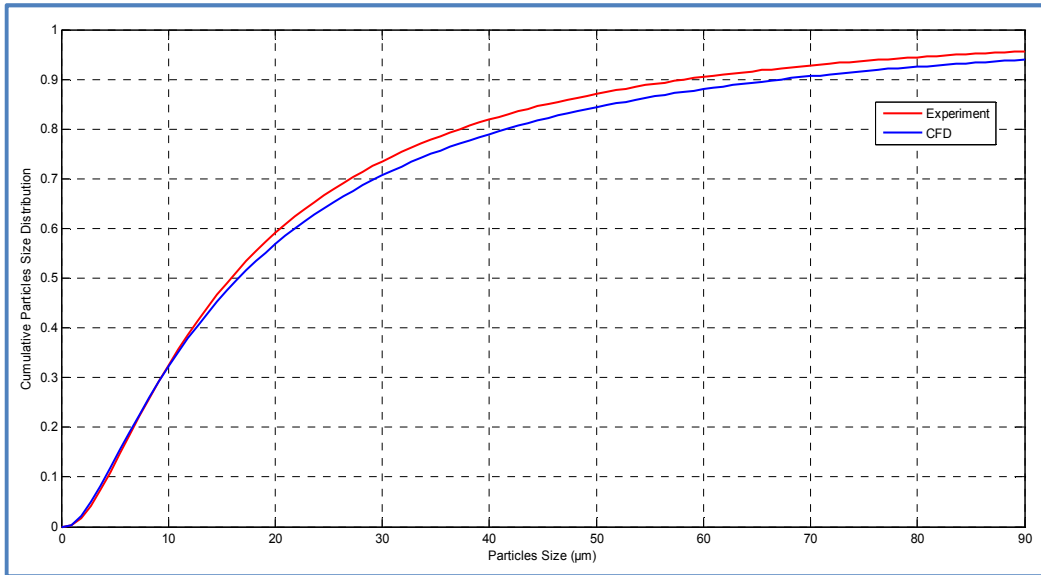


Figure 6.9: Particles cumulative size distribution

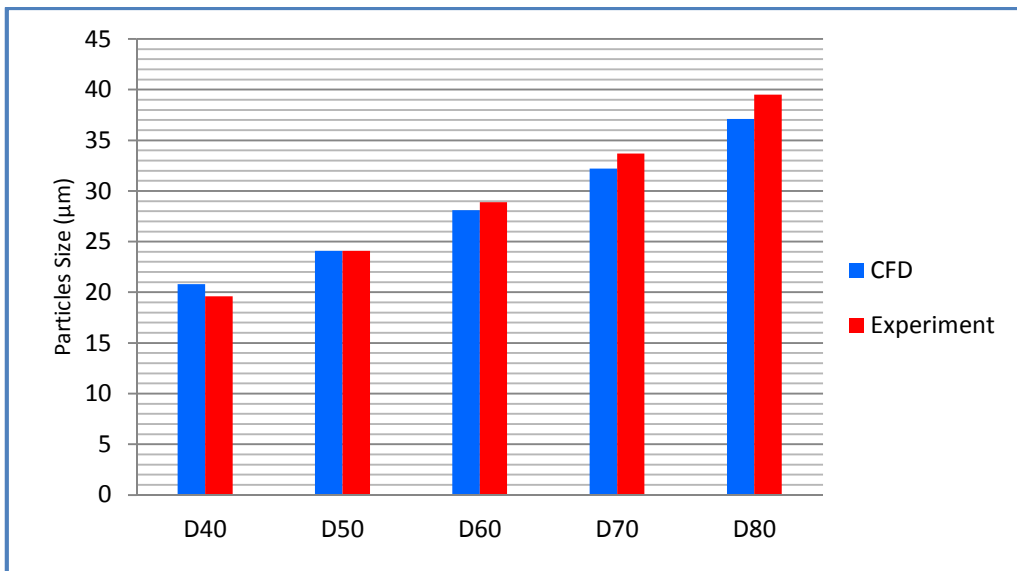


Figure 6.10: Particles size 40, 50, 60, 70 and 80 % of cumulative distribution

Table 6.2: Deviation result for experimental result and cfd

| Particles Size at 40, 50, 60, 70 and 80 of cumulative distribution | % of Deviation |
|--|----------------|
| D40 | 6.12 |
| D50 | 0 |
| D60 | 2.85 |
| D70 | 4.66 |
| D80 | 6.47 |

6.3.2 Flow Visualisation

Flow visualisation using tufts was performed inside the classifier model to demonstrate the flow patterns. Figure 6.11 illustrates the similarities in the velocity flow field between the simulations and experimental. The experimental flow visualisation is captured using tufts, a laser sheet and a camera. The inclination and wavering of the tuft affected by the swirling flow were observed from the horizontal direction. The image taken is at Level D (guide vane area). Similar flow patterns for both approaches were obtained, thus proving the reliability of the numerical methods applied in this study.

High-quality flow vectors, resulting in better concurrence, were acquired for the horizontal planes compared to the vertical one. Due to the limits of the viewing area, the vertical images are more difficult to capture. Furthermore, one of the cause factors was the fault signals obtained in the latter case, when the images

were captured through a Perspex thickness. Other problems, such as distortion and scratches on the Perspex, also affected the images taken.

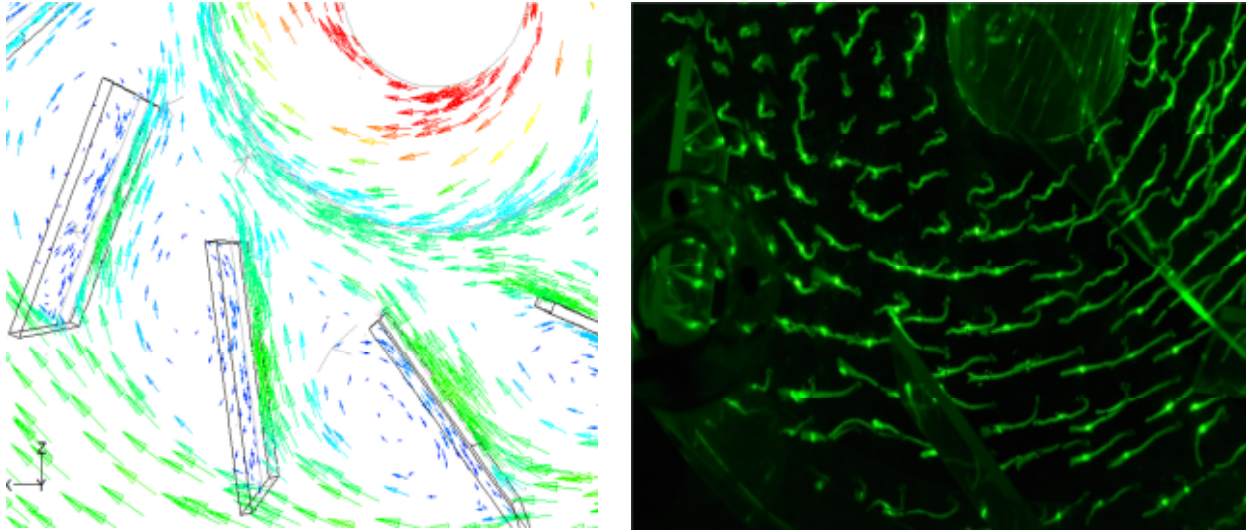


Figure 6.11: Air velocity flow field from the simulation and experimental visualisations

6.4 Conclusion

The validation test shows that CFD can be used to predict the flow behaviour and particles distribution of the classifier. Whilst the accuracy of some of the velocity component information is lacking, this is due to a failing in the CFD code. From the validation test it is believed that CFD can be used as a predictive tool for looking the parameters that need to be taken into account, which is important for the outcome of this project. CFD is valid for its purpose.

The chapter has shown how important validation is to CFD and that, without both validation and experienced or knowledgeable interpretations of the results, CFD is worthless as a tool. The CFD modelling satisfies its key purpose, as a predictive

tool for identifying parameters that need to be taken into account. CFD can then be used as a tool for relatively quick studies into prototyped devices without the need for costly construction of all initial ideas. The main use for the CFD will be to undertake preliminary studies and any parametric studies required in the scope of this work. For comparison of envisioned solutions, experimental testing will be used, given the poor correlation to actual velocity and particle distribution.

The pros and cons of the turbulence model, Realisable k - ϵ (Rke) model and Reynolds Stress Model (RSM)) have been elaborated. These models were compared to the experimental results in order to choose the best method. The Rke has been chosen as the most suitable model to give the closest results in comparison to the experimental. The deviation of the chosen methodology to the experimental data was then determined in order to arrive at the average discrepancy. The Root Mean Square (RMS) was used to determine the deviation, where an average of less than 6% discrepancy, which is reasonable in highly complex flow situations such as the present one. The comparison of particles' distribution acquired using both experimental and numerical approaches were then presented, giving on average deviation less than 7%, which implies good concurrence between both methods. Comparison of flow visualisations between the experimental and numerical approaches was shown in the last section. Similar flow patterns for both methods were obtained, thus proving the reliability of the numerical methodology applied in this study. The numerical results discussed in the previous chapter have therefore been validated.

CHAPTER SEVEN: CONCLUSIONS

In this thesis a thorough investigation into the effects of several parameters that control the performance of a coal classifier has been conducted. Because of the non-linearity of the system, Computational Fluid Dynamic (CFD) has been used to assist the investigation.

Although CFD is a useful tool and faster-working instrument for understanding a system, simulation alone is insufficient without any validation. Thus, within this research, validation of the CFD was done with experiments conducted on a one-third scale classifier, built in the laboratory. The experimental results were found to be agreeable with the CFD findings.

The investigations into the air flow and particle trajectories, as well as distribution within the model coal classifier, yielded the following conclusions:

- When the inlet velocity is high, the axial velocity outside the classifier's separation area is also high. Higher velocity enables larger particles to be raised to the top of the classifier.
- Higher inlet velocity contributes to higher radial velocity outside the separation area, however the tangential velocity is also high. In other words, although high radial velocities are able to move the particles to the core, high tangential velocities create greater centrifugal forces, which are

the resistance to motion towards the core.

- Small vane angles produce higher tangential velocities outside the separation area. Thus, the magnitude of the centrifugal force is also high. As a result, larger particles are pushed towards the classifier wall and only smaller particles are allowed into the separation area. Particle distribution analyses confirm the finding where a 60° vane angle is found to release more large-size particles than the 30° and 45° vane angles.
- Vane angles have no influence on axial velocities outside the separation area, however smaller vane angles develop very high axial velocities inside the separation area. Higher axial velocities inside the separation area help the particles move more quickly towards the turret and the outlet. Air distribution analysis confirms the finding where it was discovered that the resident time of particles of the same size for 30° vane angle was less compared to the 45° and 60°.
- Varying the outlet position has minimal or no effect on the classifier performance.

7.1 Contribution to Knowledge

The work undertaken in this thesis represents a contribution to knowledge based on its originality and thrust. The aim was not only an understanding of the ad hoc mechanism of particulate stratification currently used in power plants classifiers, but also to isolate the controlling parameters so that a bespoke classification system can be devised. The following conclusions are made:

- (i) The research study has documented extensive information on the effect and influence of important classifier parameters on the air flow and particle distributions. This information is critical in providing a better understanding on the behaviour of the classifier.
- (ii) The study has provided a better understanding of the classifier non-linear behaviour and the swirling flow systems prevailing within. It has shown, because of its non-linearity, that it is not possible from the parameters examined to have a set of conditions that are suitable for all classifier applications. An even more in-depth parametrical study needs to be performed. However, through CFD analysis, it is possible to optimise the classifier performance for a specific requirement with a set of parameters. Thus, the study has provided a methodology on how this can be achieved.
- (iii) Through this research a look-up table that relates the classifier performance and the appropriate classifier parameters settings has been constructed. The construction of the look-up table is novel, and to date no such table has been produced for classifier application. The look-up table will be very useful in assisting optimum design of classifiers and operation of dynamic classifiers.

7.2 Future Directions

- (i) Further CFD analyses, which include further variations of vane angles and inlet velocity conditions, could help to complete the look-up table.

Several other look-up tables for other types of classifier arrangement will also be useful.

- (ii) Due to the time constraints, the current study only focused on a single classifier outlet with various outlet positions. The study of the effects of having multiple outlets or various outlet sizes should also be considered in the future. Multiple outlet classifiers are now employed in most North American power plants.
- (iii) Furthermore, combinations of other parameters, such as coal properties, could also be included in the study.

REFERENCES

Aroussi, A. (2006), Pulverized Fuel Balancing In Power Stations, *Journal of Flow Visualization & Image Processing*, vol. 13, pp. 1–28.

Akilli H., Levy E. and Sahin B. (2001), Gas-Solid Flow Behaviour In A Horizontal Pipe After A 90° Vertical-to-Horizontal Elbow, *Powder Technology*, Volume 116, 43-52.

American Institute of Chemical Engineers (AIChE) (1993), *AIChE Equipment Testing Procedure. Particle Size Classifiers*, 2nd ed. AIChE, New York, pp. 1–64.

Barth, T. J. and Jespersen, D. C., (1989), The Design and Application of Upwind Schemes on Unstructured Meshes, *American Institute of Aeronautics and Astronautics*, Washington, D. C.

Bemin, A.C. (2005), *Simulation of the Two Phase Flow in a Lab Coal Pulverizer*, Springer-Verlag.

Bernardo, S. (2006), 3-D Computational Fluid Dynamics for Gas and Gas-Particle Flows in A Cyclone with Different Inlet Section Angles, *Powder Technology* 162. 190 – 200.

Bhasker, C. (2002), Numerical Simulation of Turbulent Flow in Complex Geometries Used in Power Plants, *Advances in Engineering Software*, 33, pp. 71-83.

Buell (undated), *Introduction to Air Classification*, Fisher-Klosterman Inc.

Department of Energy and Climate Change (DECC) (2011), *UK Energy Brief 2011*, National Statistics Publication, London.

Department of Trade and Industry (DTI) (2007), *Meeting the Energy Challenge*, DTI White Paper on Energy, UK.

FOSSIL FUEL (2011), *Coal*, <http://fossil-fuel.co.uk/coal-frequently-asked-questions>, [Accessed: 4 May 2011]

Galk, J., Peukert, W. and Krahen, J. (1999), Industrial Classification in a New Impeller Wheel Classifier, *Powder Technology*, Vol. 105, 186-189.

Giddings, D., Aroussi, A., Azzopardi, B. and Pickering, S. (2003), *Bulk Effect of Particles in a One-Quarter Scale Rig of a Coal Fired Power Station Coal Delivery Unit*, Proc. CFD, Vancouver Canada.

Giddings, D., Aroussi, A., Pickering, S.J and Mozaffari, E. (2004), A ¼ Scale Test Facility for PF Transport in Power Station Pipelines, *FUEL*, Volume 83, 2195-2204.

Rumpf, H. (1975), *Particle Technology*, Chapman and Hall.

Hampartsoumian, E., Foloyan, O.O., Nimmo, W. and Gibbs, B.M. (2003), Optimisation of NO_x Reduction in Advanced Coal Reburning Systems and the Effect of Coal Type, *FUEL* 82, 373-384.

Hoffmann, A. C. and Stein, L. E. (2002), *Gas Cyclone and Swirl Tubes-Principles*, Berlin, Springer-Verlag

Holman, J.P. (2001), *Experimental Methods for Engineers*, 7th. Ed. Boston: McGraw-Hill.

International Energy Agency (IEA) (2008), *World Energy Outlook 2008*, IEA OECD/IEA, Paris, France.

International Energy Agency (IEA) (2007), *Profiles: Clean Coal Technologies for a Carbon-Constrained World*, IEA Clean Coal Centre, UK.

International Energy Agency (IEA) (2003a), *Improving Efficiencies of Coal-fired Power Plants in Developing Countries*, IEA Clean Coal Centre, London.

International Energy Agency (IEA) (2003b), *Clean Coal Technologies Roadmaps*, IEA Clean Coal Centre, London.

Karagoz, I. and Kaya, F. (2007), CFD Investigation of the Flow and Heat Transfer Characteristics in a Tangential Inlet Cyclone, *International Communications in Heat and Mass Transfer* 34, 1119 – 1126.

Karunakumari, L., Eswaraiah, C., Jayanti, S. and Narayanan, S. S. (2005), Experimental And Numerical Study of a Rotating Wheel Air Classifier, *AIChE Journal*, Volume 51, Issue 3, pp. 776-790.

Kimball J. (2011), *The Carbon Cycle*, <http://users.rcn.com/jkimball.ma.ultranet/BiologyPages/C/CarbonCycle.html>, [Accessed: 4 May 2011)

Kolacz, J. (2002), Investigating Flow Conditions in Dynamic Air Classification, *Mineral Engineering*, 15, pp. 131-138.

Lee, J.W. (2006), Effect of The Cylinder Shape of a Long-Coned Cyclone on the Stable Flow-Field Establishment, *Powder Technology* 165, 30 – 38.

Ljus, C., Johansson, B. and Almstedt, A. E. (2002), Turbulence Modification by Particles in a Horizontal Pipe Flow, *International Journal of Multiphase Flow*, Volume 28, 1075-1090.

MacPhail, J., Ballentyne, T.M.C. and King, J.L. (1983), *Assessment of the Effectiveness of Various P.F. Rope Destructor Devices on the Henfren P.F. Splitting Facility*, Babcock Report, Number (03)/82/51.

Massey, B.S (1989), *Mechanics of Fluids*, (6th Edition), Van Nostrand Reinhold (International) Co. Ltd.

Menter, F., Hemstrom, B., Henriksson, M., Karlsson, R., Latrobe, A., Martin, A., Muhlbauer, P., Scheuerer, M., Smith, B., Takacs, T. and Willemsen, S. (2002), *CFD Best Practice Guidelines for CFD Code Validation for Reactor-Safety Applications*, Report EVOL-ECORA-D01, Contract No. FIKS-CT-2001-00154.

Harding, N.S. (2003), *Optimizing Pulveriser and Riffle Performance*, Electric Power Research Institute Inc.

Nardi, J.A., United States Patent, Patent No: 5957300, *Classifier Vane for Coal Mills*, Sure Alloy Steel Corporation.

NEED (2011), *Coal*, http://www.need.org/needpdf/infobook_activities/SecInfo/CoalS.pdf, [Accessed: 4 May 2011]

Ogawa, A. (1984), *Separation of Particles from Air and Gases, Volume II*. CRC Press Inc., Boca Raton, Florida, USA.

Parham, J., and Easson, W. (2003), Flow Visualisation and Velocity Measurement in a Vertical Spindle Coal Mill Classifier, *Fuel*, Volume 82, Issues 15-17, pp. 2115-2123.

Patankar, S.V. (1980), *Numerical Heat Transfer and Fluid Flow*, Hemisphere Publishing Corporation, New York

Piepho, R.R. and Dougan, R. (1999), United States Patent, Patent No: 5884776, *Dynamic Classifier with Hollow Shaft Drive Motor*, The Babcock & Wilcox Company.

Shah, K.V., Vuthaluru, R. and Vuthaluru, H.B., (2009), CFD Based Investigations in Optimization of Coal Performance: Effect of Classifier Vane Settings, *Fuel Processing Technology*, Volume 90, pp. 1135-1141.

Shapiro, M. and Galperin, V. (2005), Air Classification of Solid Particles: A Review, *Chemical Engineering and Processing*, 44, pp. 279–285.

Sommerfeld, M. (2002), *Kinetic Simulations of Analysing the Wall Collision Process of Non-Spherical Particles*, Proc. ASME FEDSM, Montreal, Canada.

Sommerfeld, M. (2001), Validation of a Stochastic Lagrangian Modelling Approach for Inter-Particle Collisions in Homogenous Isotropic Turbulence, *International Journal of Multiphase Flow*. Volume 27, 1829-1858.

Sommerfeld, M. (1999), *Modelling and Numerical Calculation of Turbulent Gas-Solid Flows with the Euler/Lagrange Approach*, KONA 16, pp. 194-205

St. Cyr, C. (2009), *The MPS Coal Pulveriser with a Dynamic Classifier*, Babcock Power Inc.

Storm, R.F. and Storm, S.K. (2007), *To Optimized Performance, Begin at the Pulverizers*, Storm Technologies Inc.

Thompson, J. F. (1985), *Numerical Grid Generation*, New York: North-Holland.

Trozzi, N.K. (1984), United States Patent, Patent No: 4450071, *Adjustable Particle Classifier*, Foster Wheeler Energy Corporation.

Versteeg, H.K. and Malalasekera, W. (1995), *An Introduction to Computational Fluid Dynamics*, Harlow: Pearson Education Limited.

Vuthaluru, H.B., Pareek, V.K. and Vuthaluru, R. (2005), Multiphase Flow Simulation of a Simplified Coal Pulveriser, *Fuel Processing Technology*, Volume 86, pp. 1195-1205.

Wark, R.E. (1999), United States Patent, Patent No: 5873156, *Coal Pulverizer and Method of Improving Flow Therein*, Sure Alloy Steel Corp.

World Energy Council (WEC) (2007), *Deciding the Future: Energy Policy Scenarios to 2050*, Executive Summary World Engineering Council.

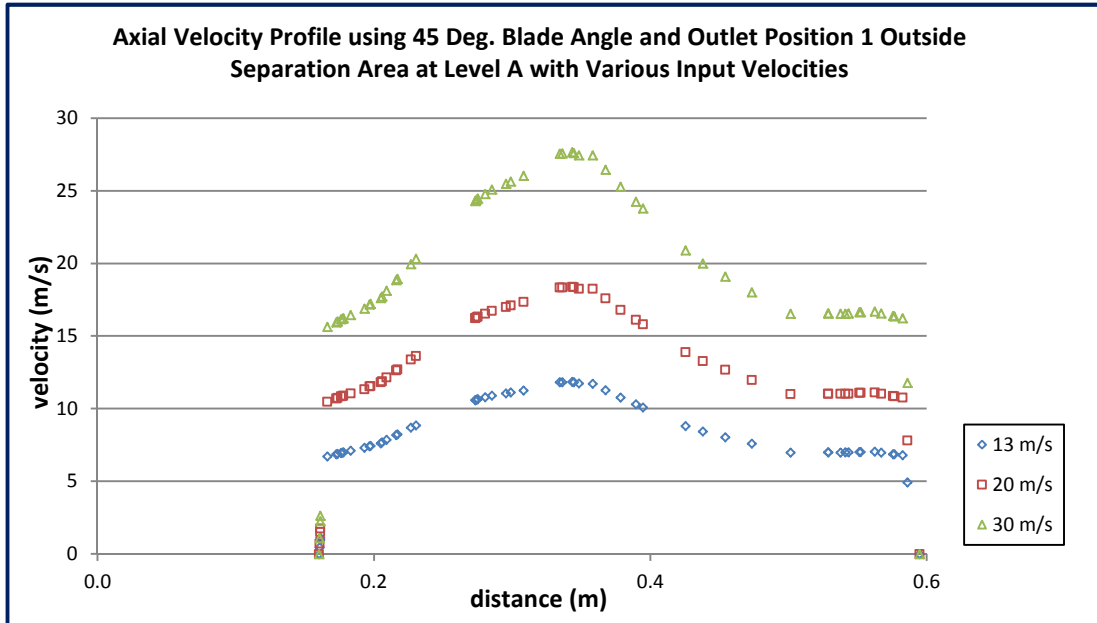
World Coal Institute (WCI) (2005), *The Coal Resource: A Comprehensive Overview Of Coal*, World Coal Institution Publication, London.

Yoshida, H., United States Patent, Patent No: 5657877, *Rotary Classifier for a Roller Mill*, Mitsubishi, Japan, 1997

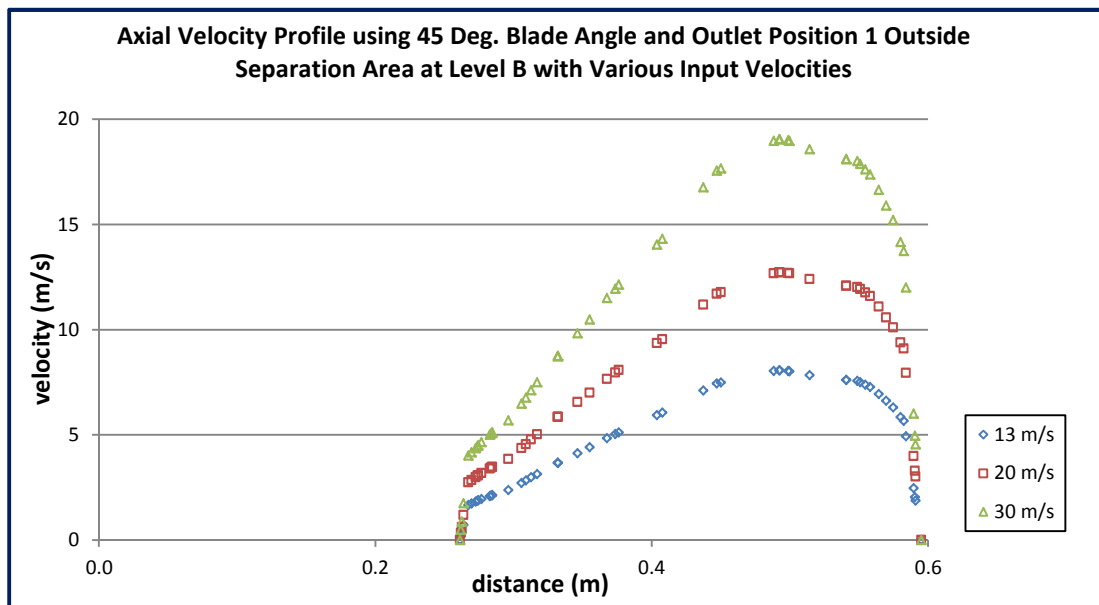
APPENDIX I

Effects of Varying Input Velocity Outside Separation Area for 45° and 60° Vane

Angle



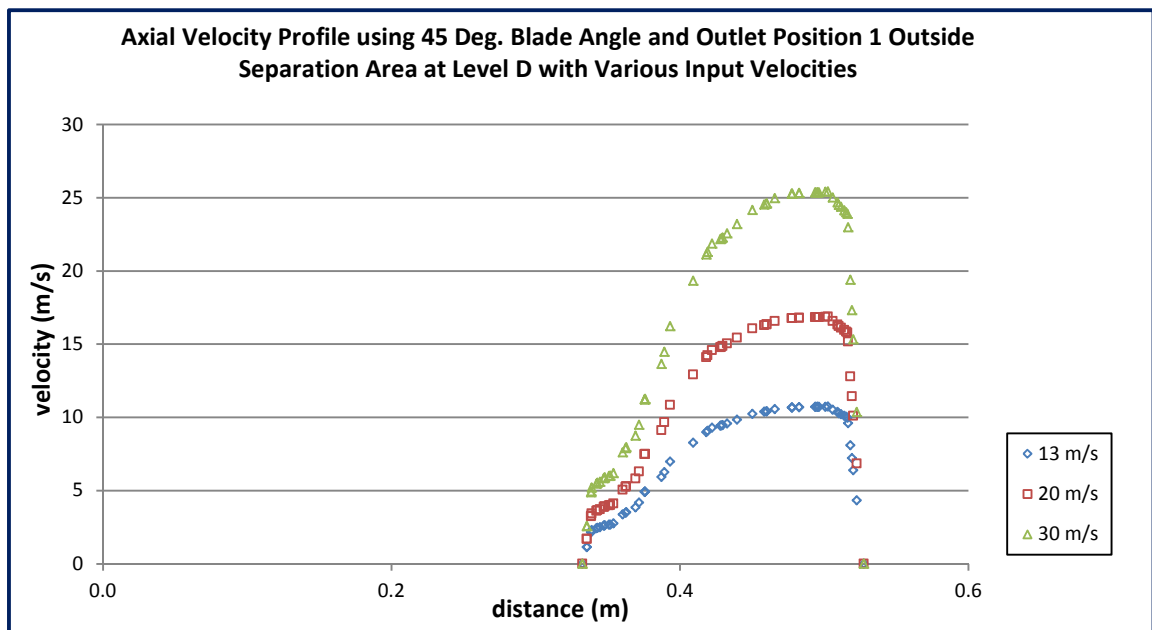
Axial velocity profile outside separation area at Level A for various input velocities
(45 degrees vane angle)



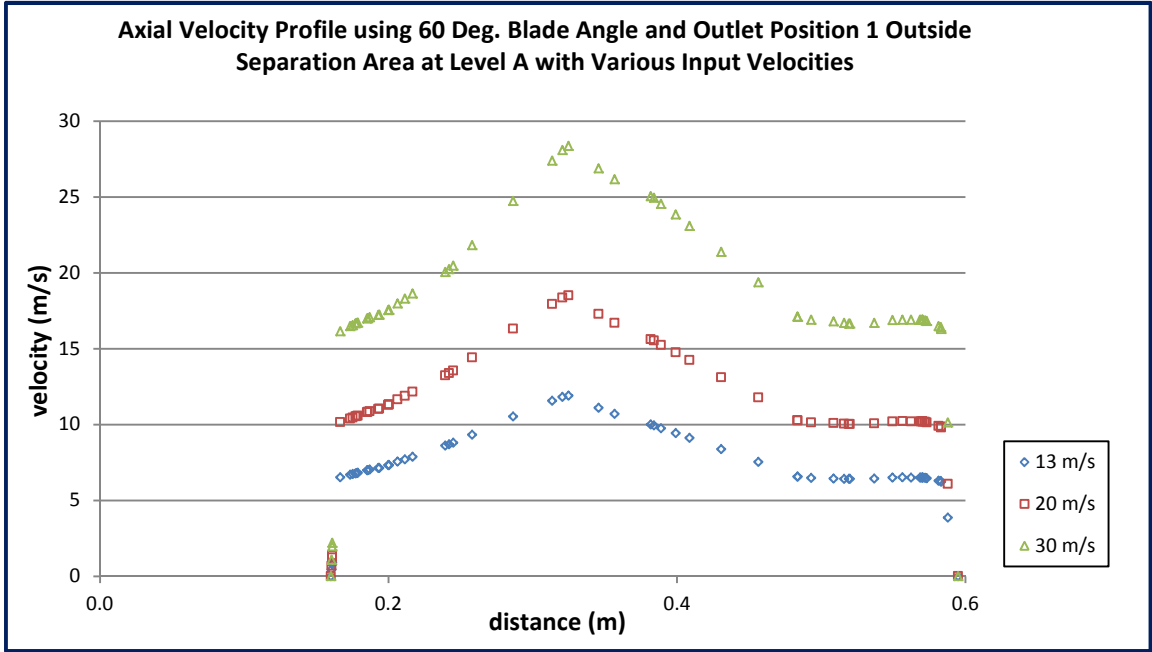
Axial velocity profile outside separation area at Level B for various input velocities
(45 degrees vane angle)



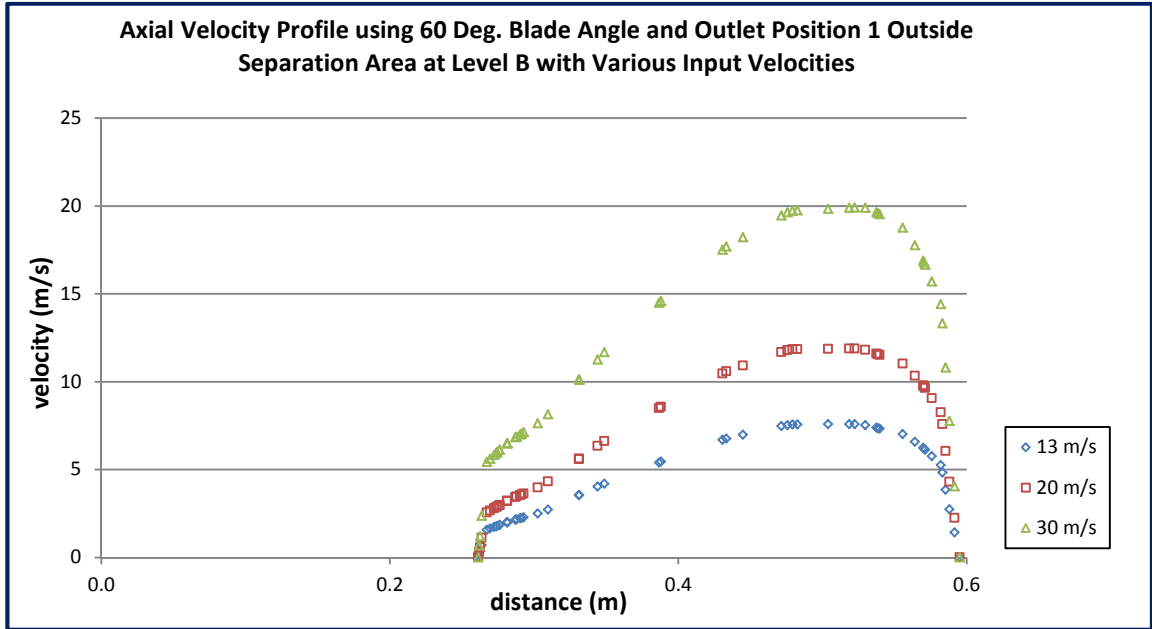
Axial velocity profile outside separation area at Level C for various input velocities
(45 degrees vane angle)



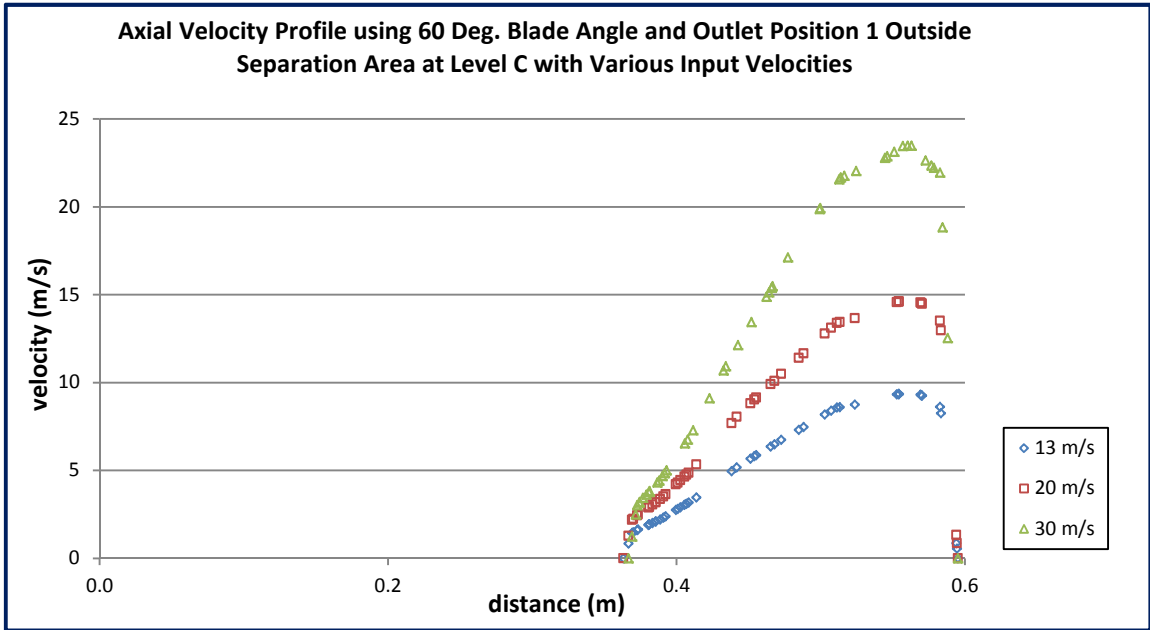
Axial velocity profile outside separation area at Level D for various input velocities
(45 degrees vane angle)



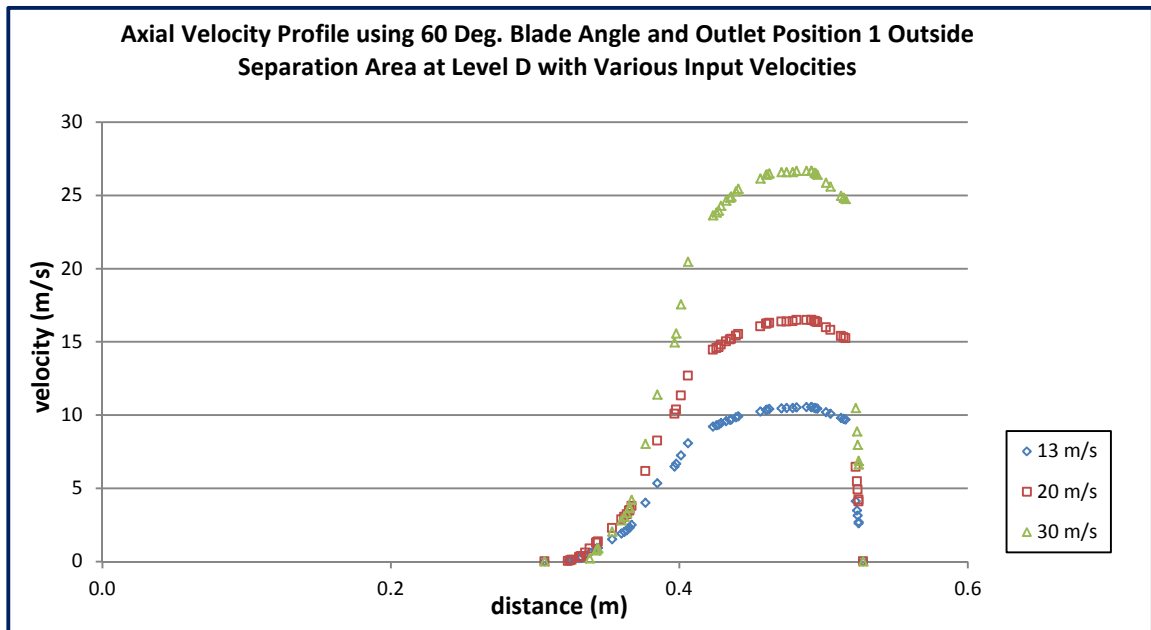
Axial velocity profile outside separation area at Level A for various input velocities
(60 degrees vane angle)



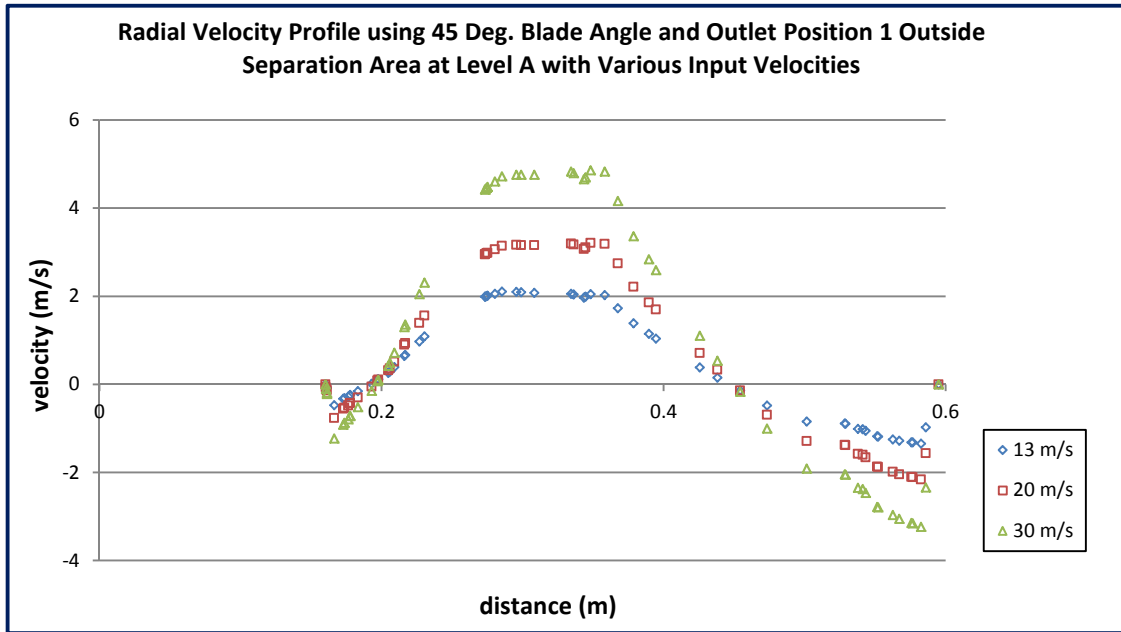
Axial velocity profile outside separation area at Level B for various input velocities
(60 degrees vane angle)



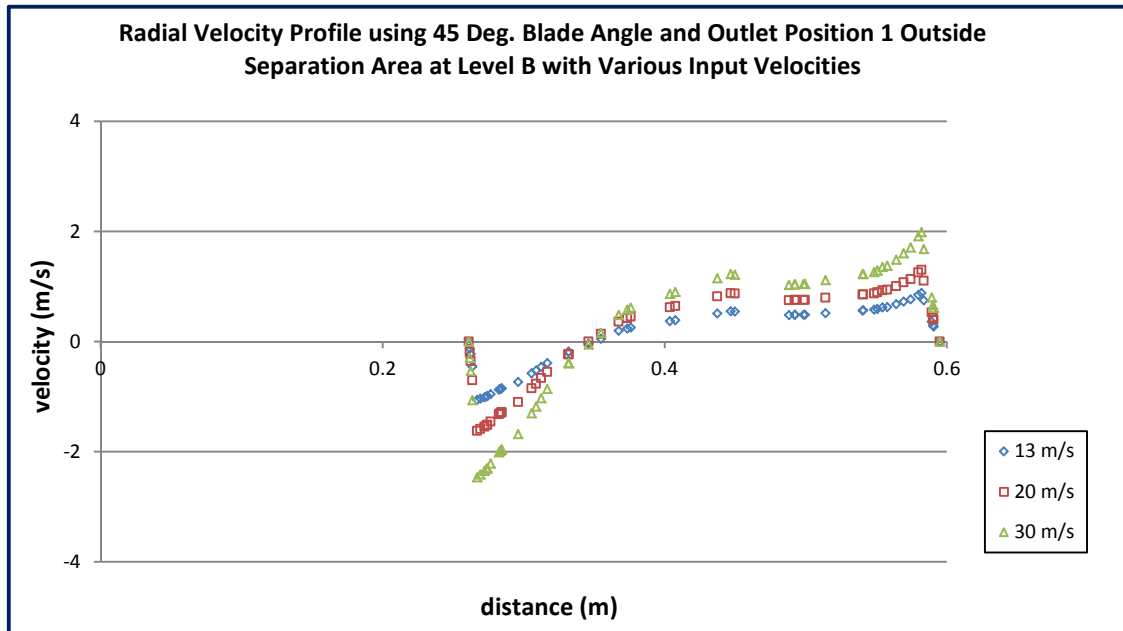
Axial velocity profile outside separation area at Level C for various input velocities
(60 degrees vane angle)



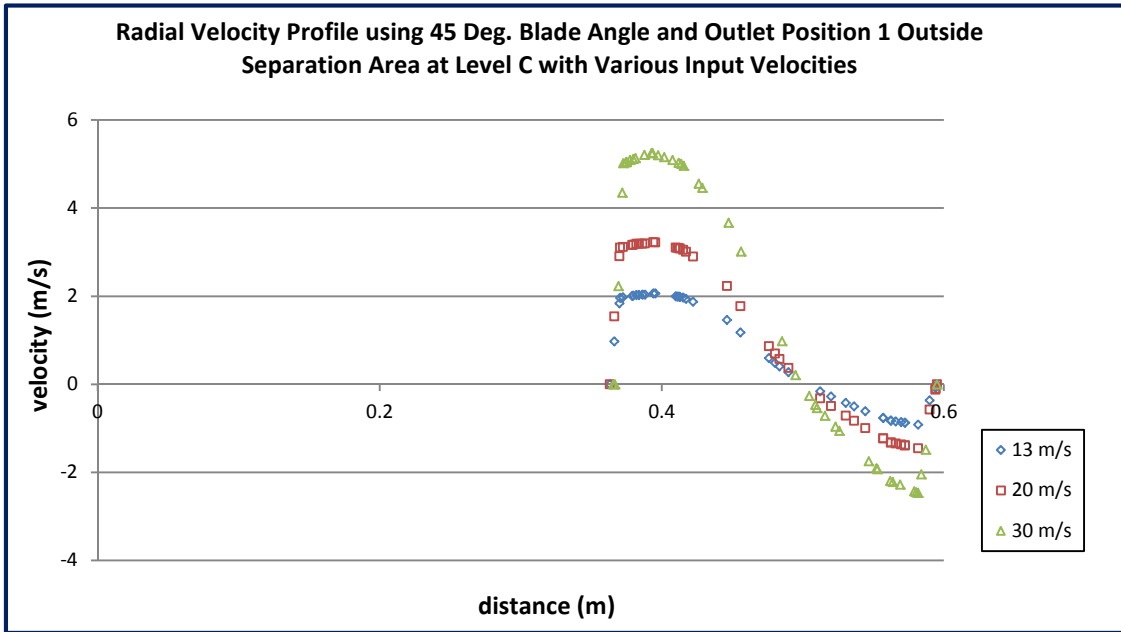
Axial velocity profile outside separation area at Level D for various input velocities
(60 degrees vane angle)



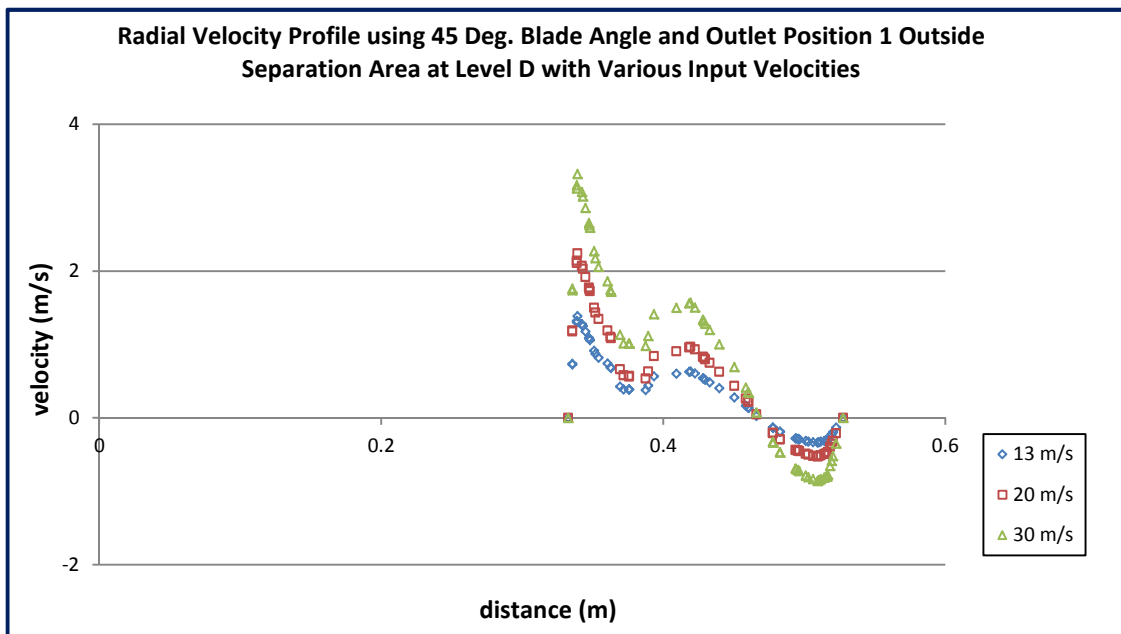
Radial velocity profile outside separation area at Level A for various input velocities
(45 degrees vane angle)



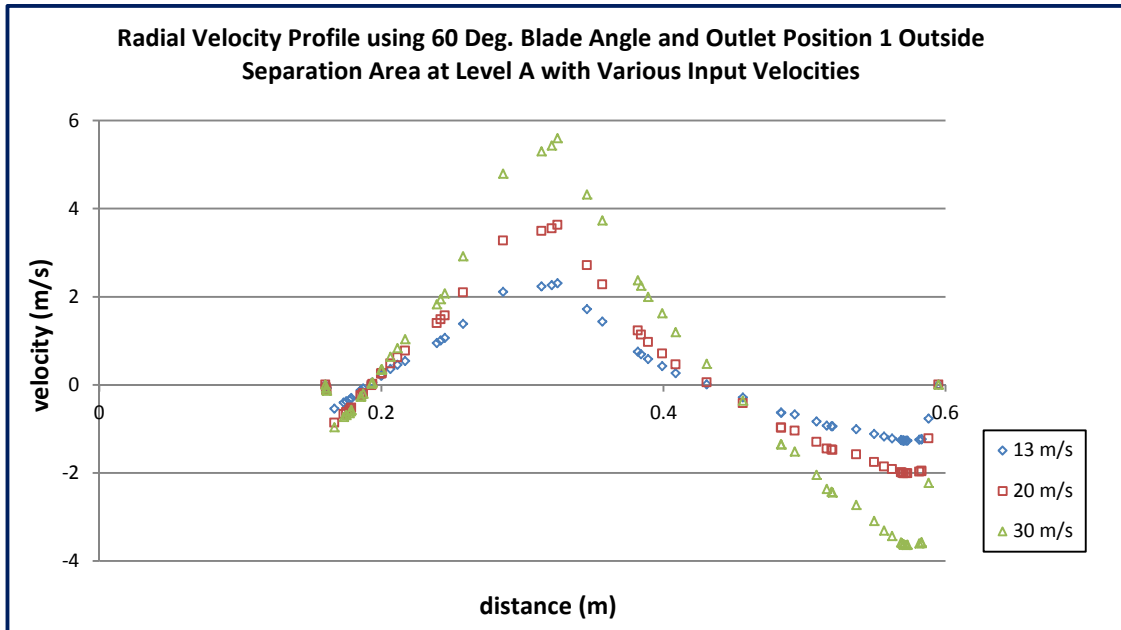
Radial velocity profile outside separation area at Level B for various input velocities
(45 degrees vane angle)



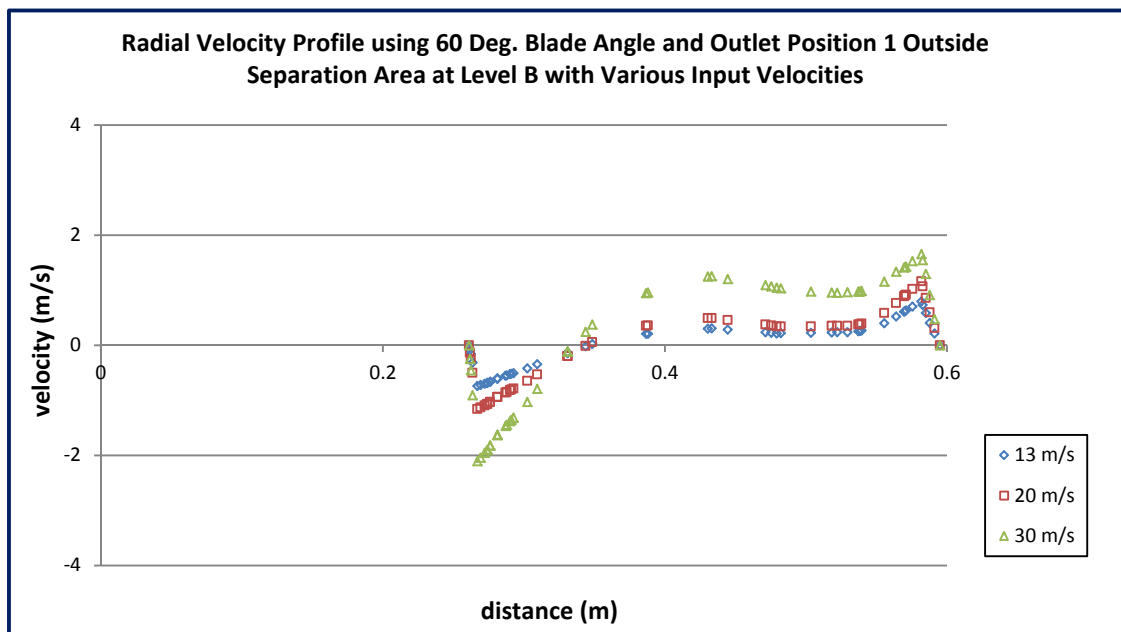
Radial velocity profile outside separation area at Level C for various input velocities
(45 degrees vane angle)



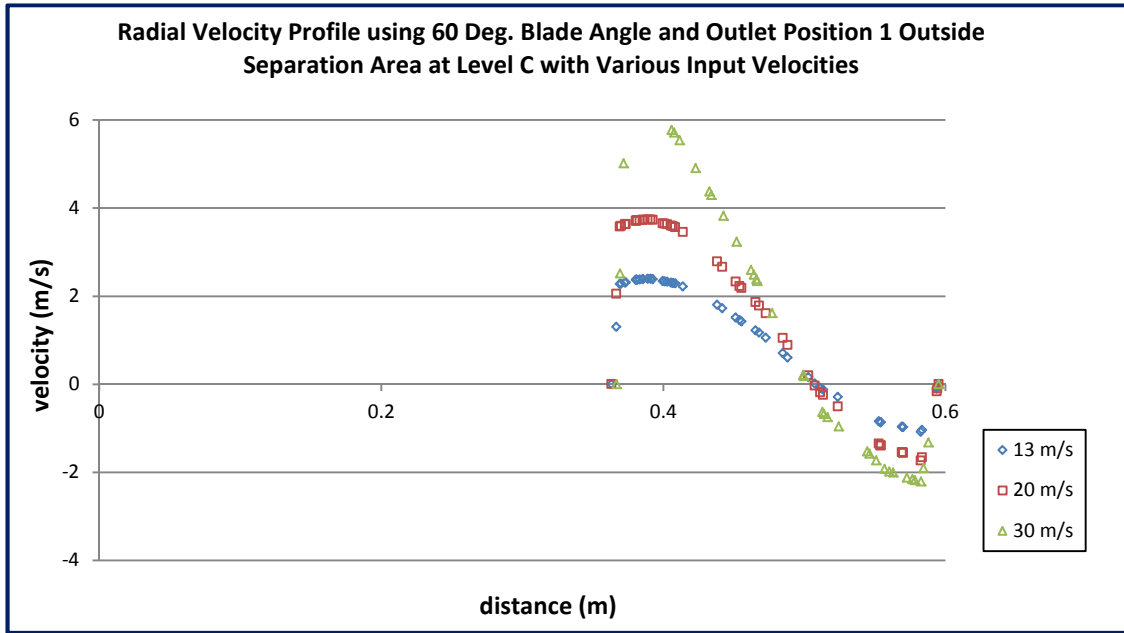
Radial velocity profile outside separation area at Level D for various input velocities
(45 degrees vane angle)



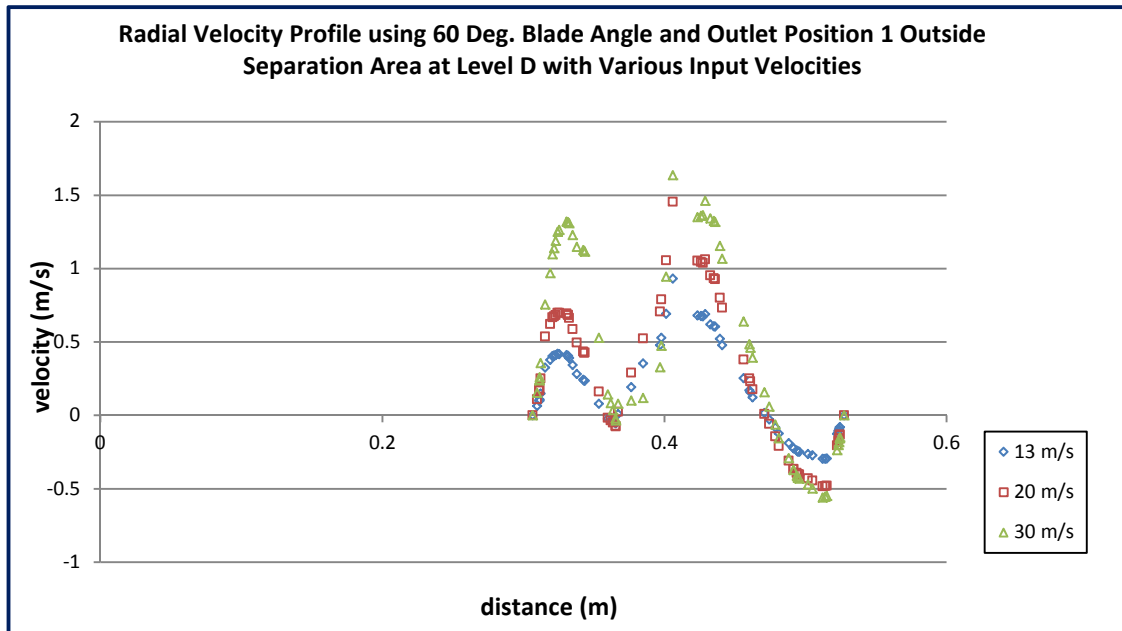
Radial velocity profile outside separation area at Level A for various input velocities
(60 degrees vane angle)



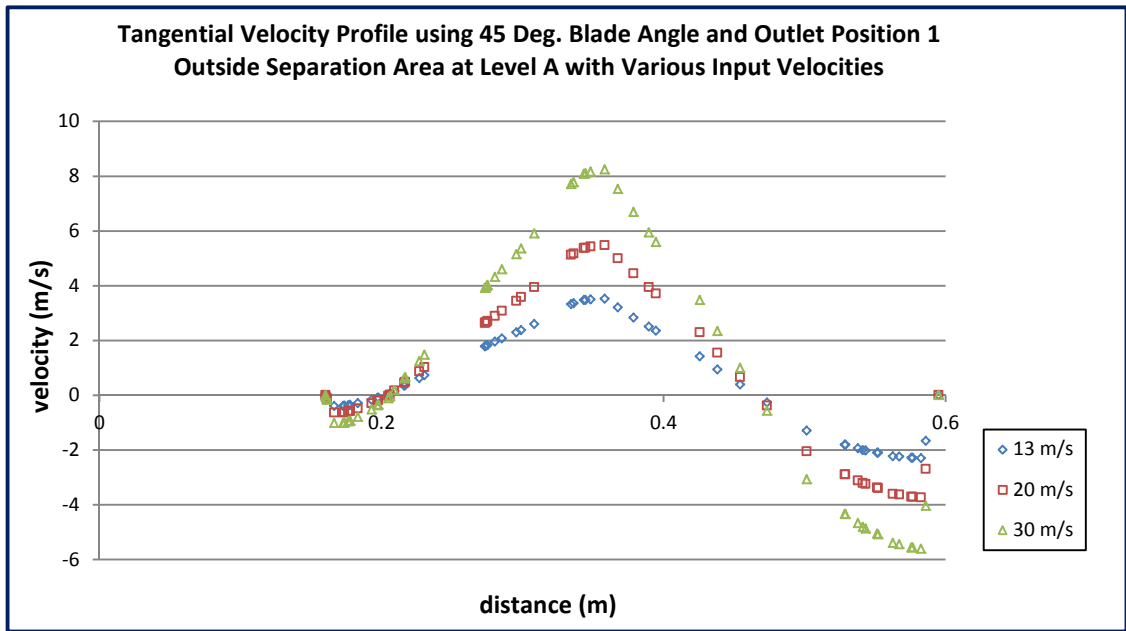
Radial velocity profile outside separation area at Level B for various input velocities
(60 degrees vane angle)



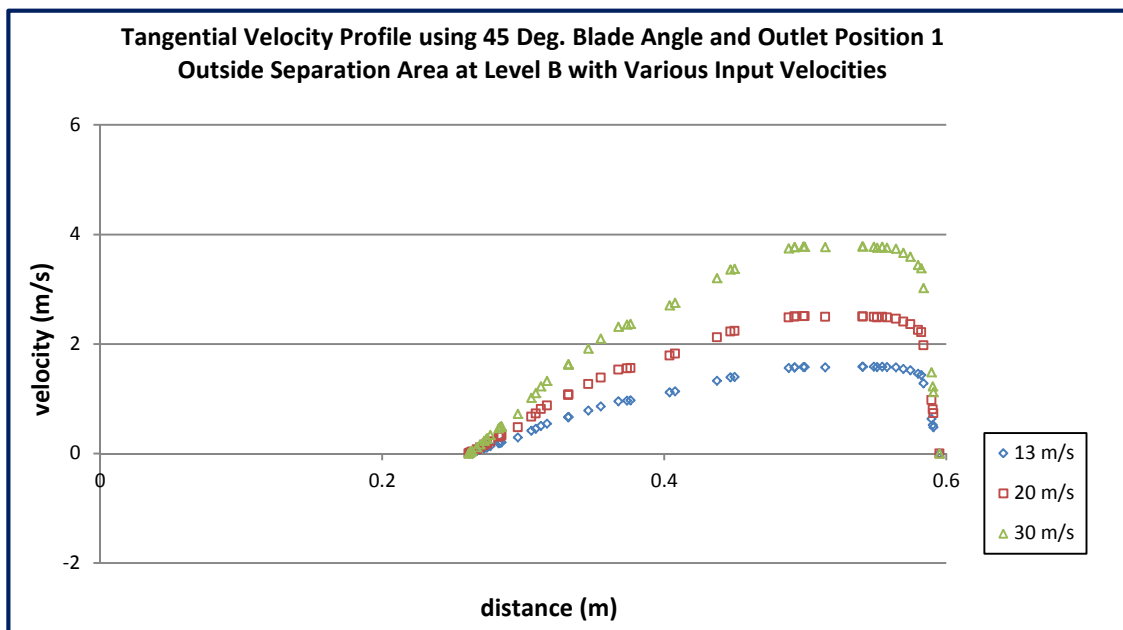
Radial velocity profile outside separation area at Level C for various input velocities
(60 degrees vane angle)



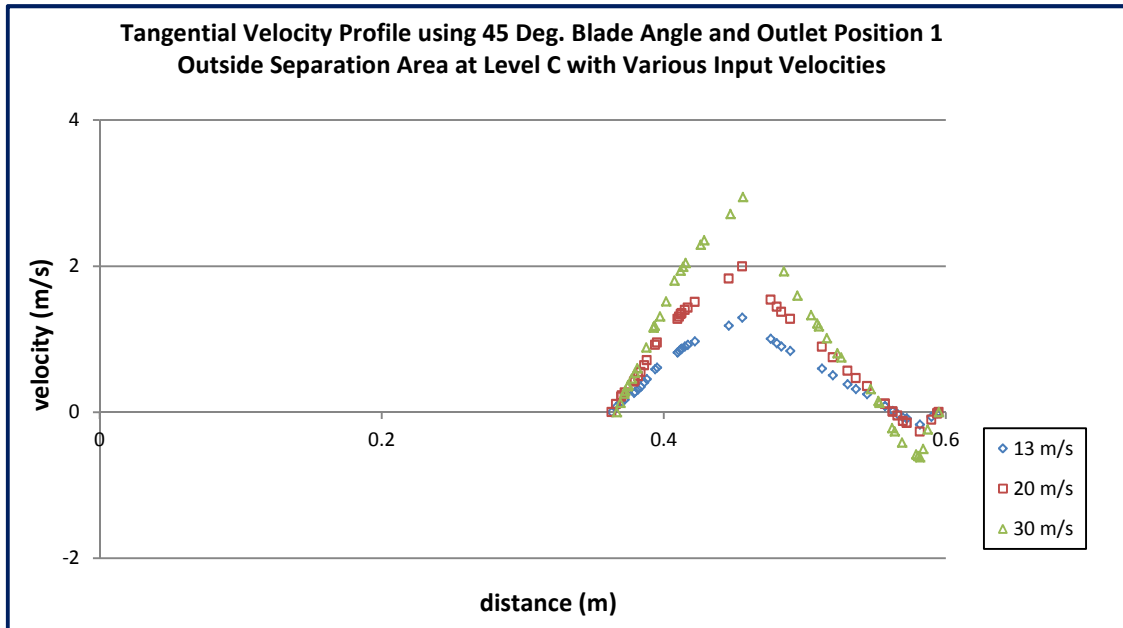
Radial velocity profile outside separation area at Level D for various input velocities
(60 degrees vane angle)



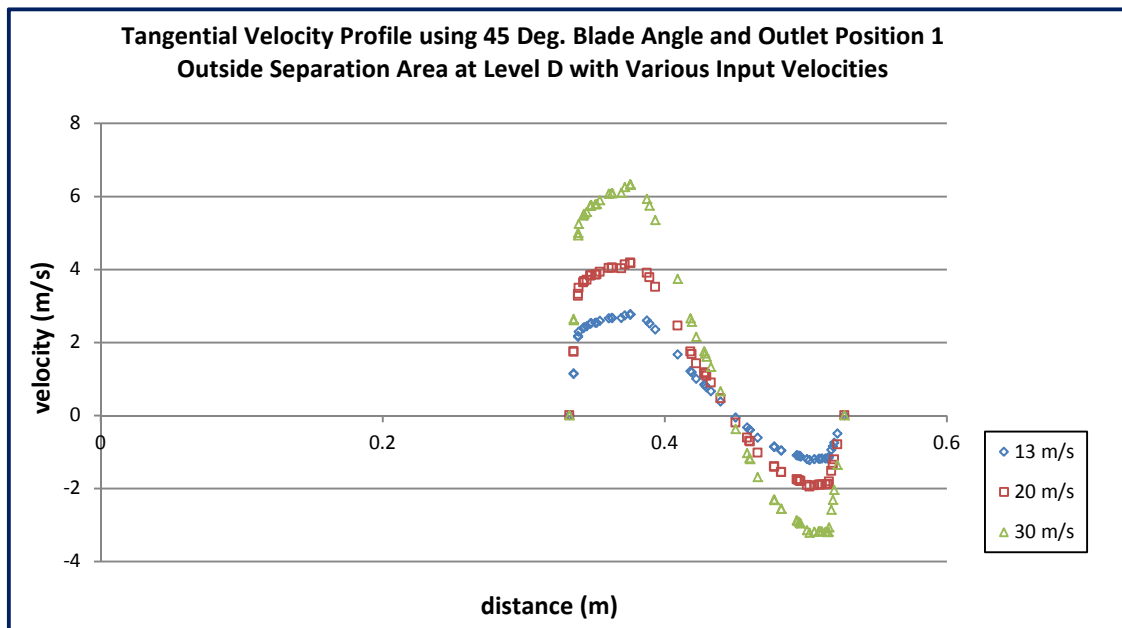
Tangential velocity profile outside separation area at Level A for various input velocities (45 degrees vane angle)



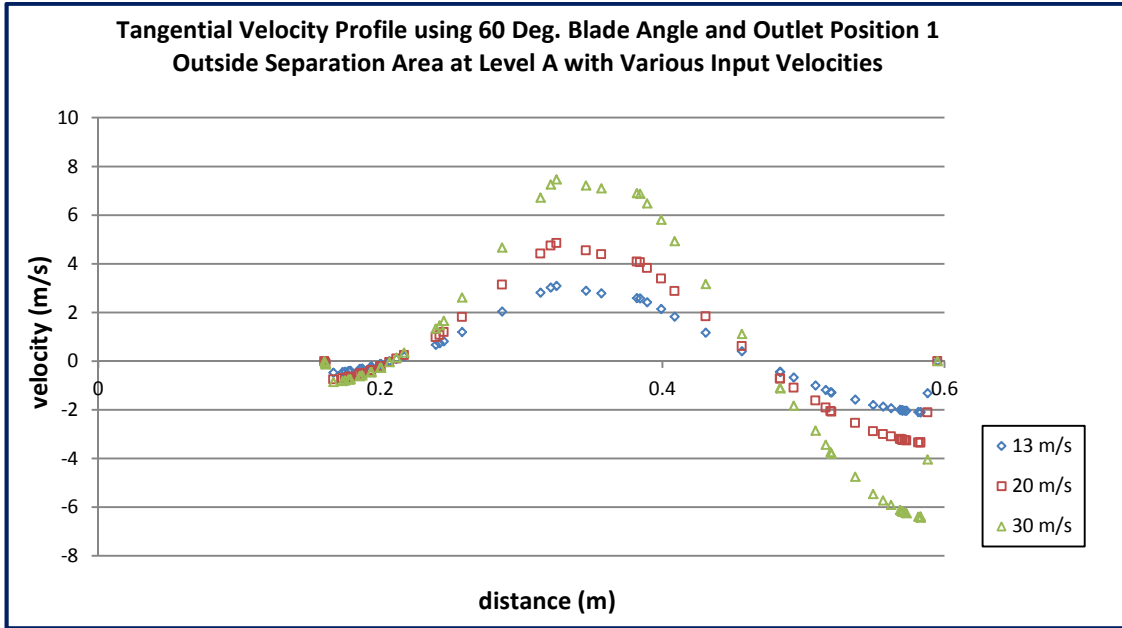
Tangential velocity profile outside separation area at Level B for various input velocities (45 degrees vane angle)



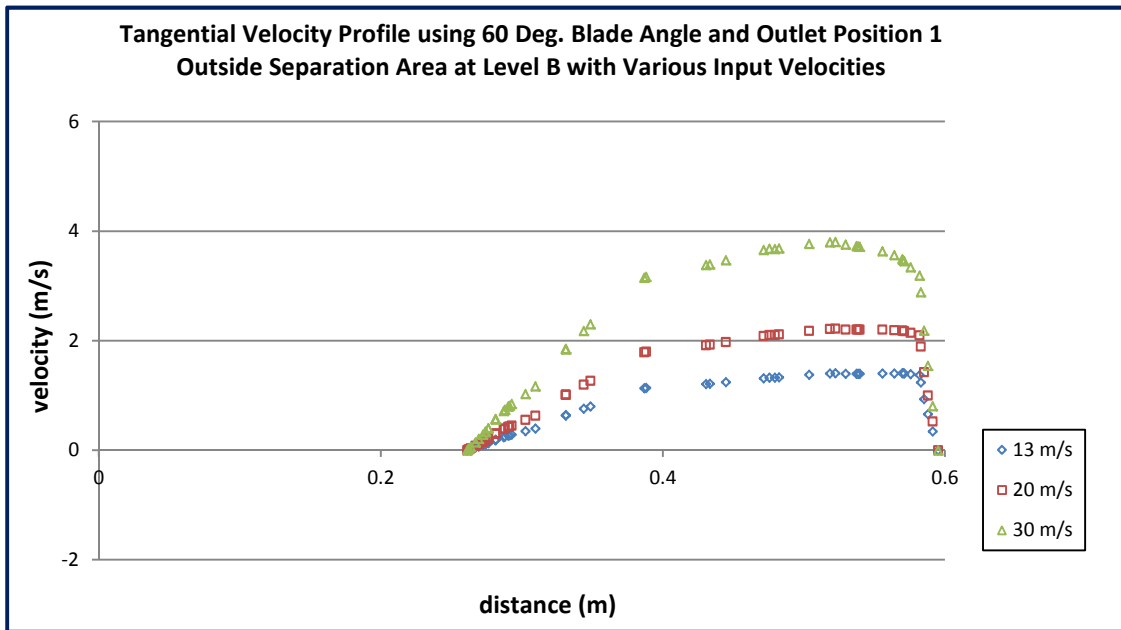
Tangential velocity profile outside separation area at Level C for various input velocities (45 degrees vane angle)



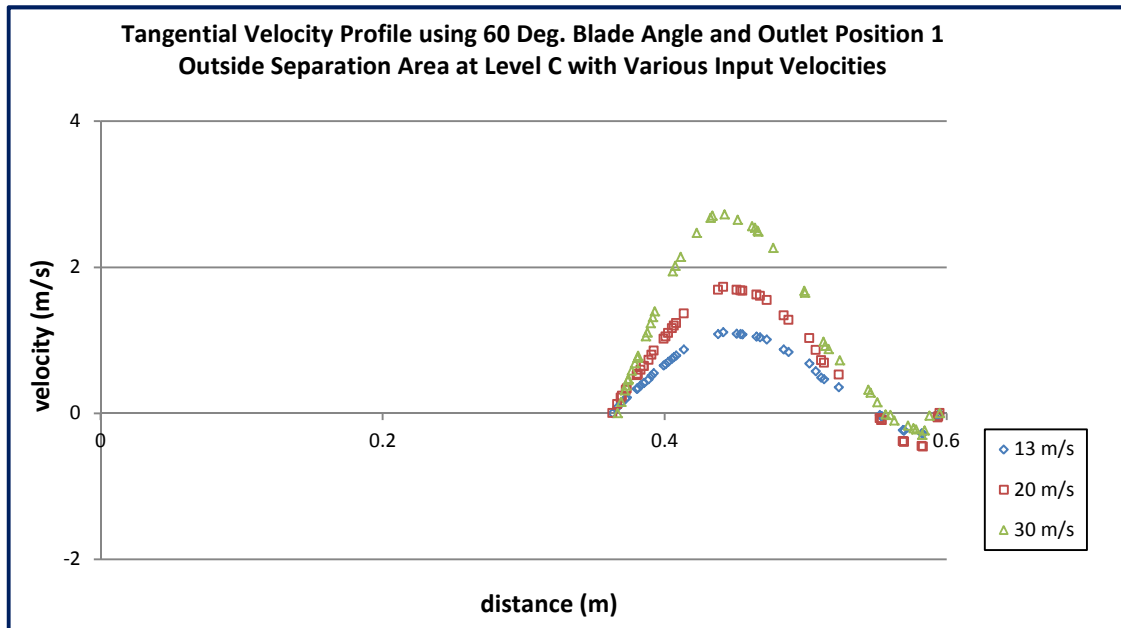
Tangential velocity profile outside separation area at Level D for various input velocities (45 degrees vane angle)



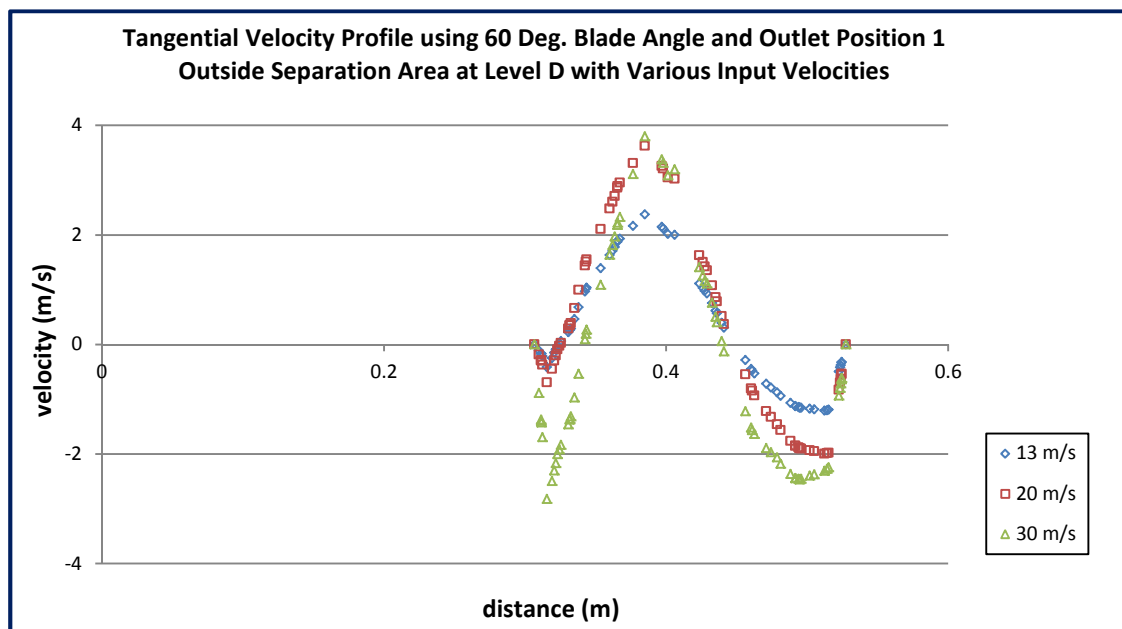
Tangential velocity profile outside separation area at Level A for various input velocities (60 degrees vane angle)



Tangential velocity profile outside separation area at Level B for various input velocities (60 degrees vane angle)



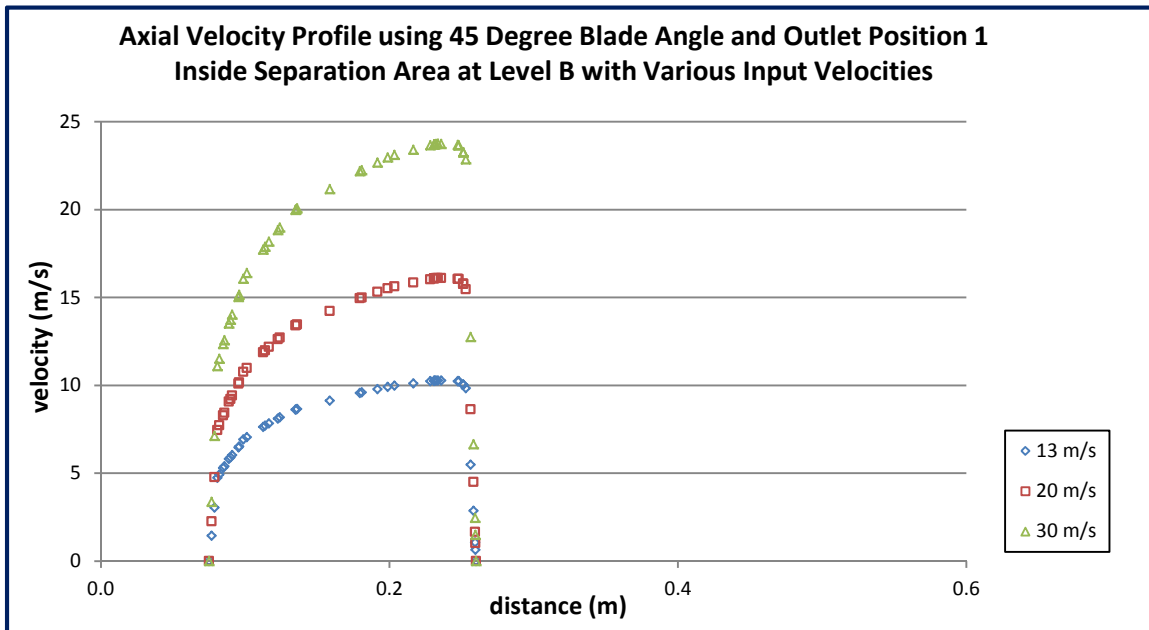
Tangential velocity profile outside separation area at Level C for various input velocities (60 degrees vane angle)



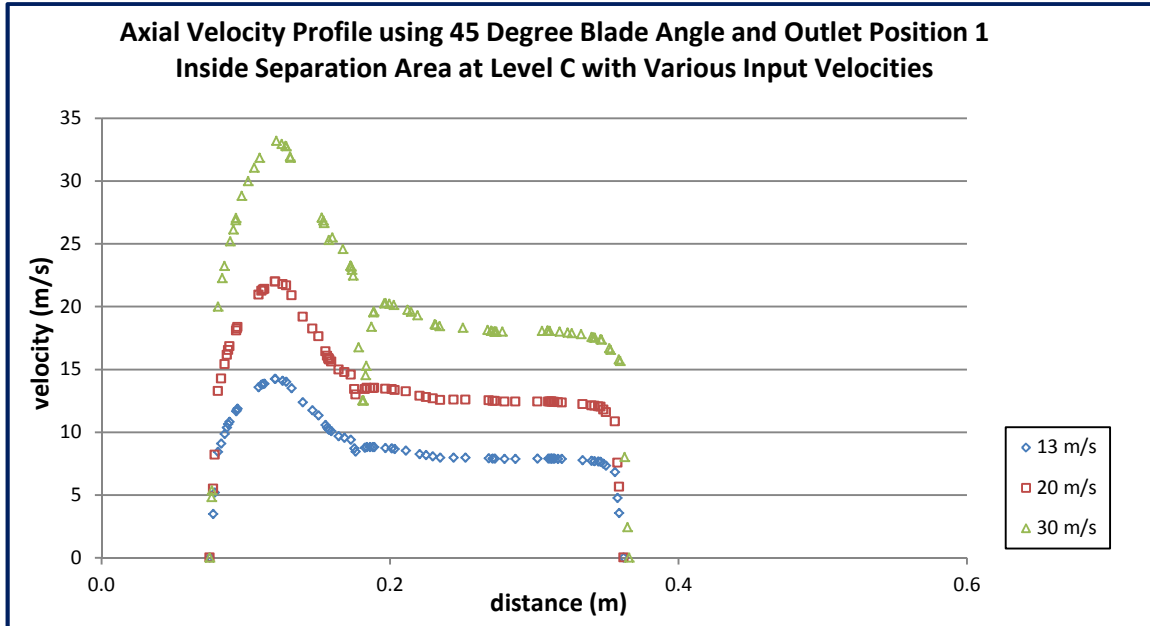
Tangential velocity profile outside separation area at Level D for various input velocities (60 degrees vane angle)

APPENDIX II

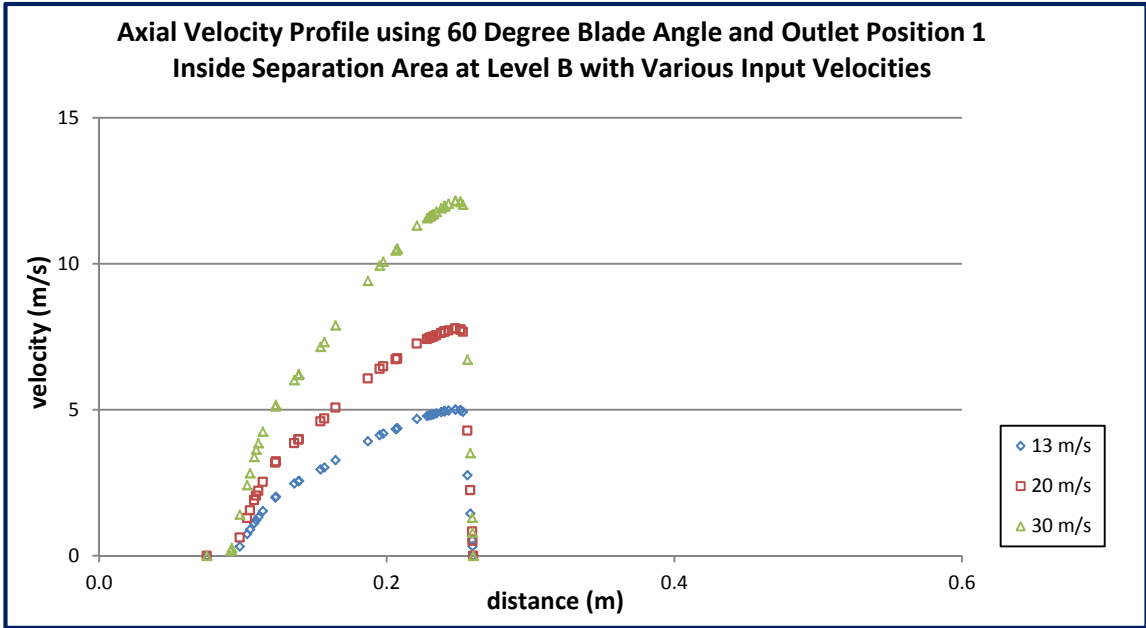
Effects of Varying Input Velocity Inside Separation Area and Vortex Finder for 45°
and 60° Vane Angles



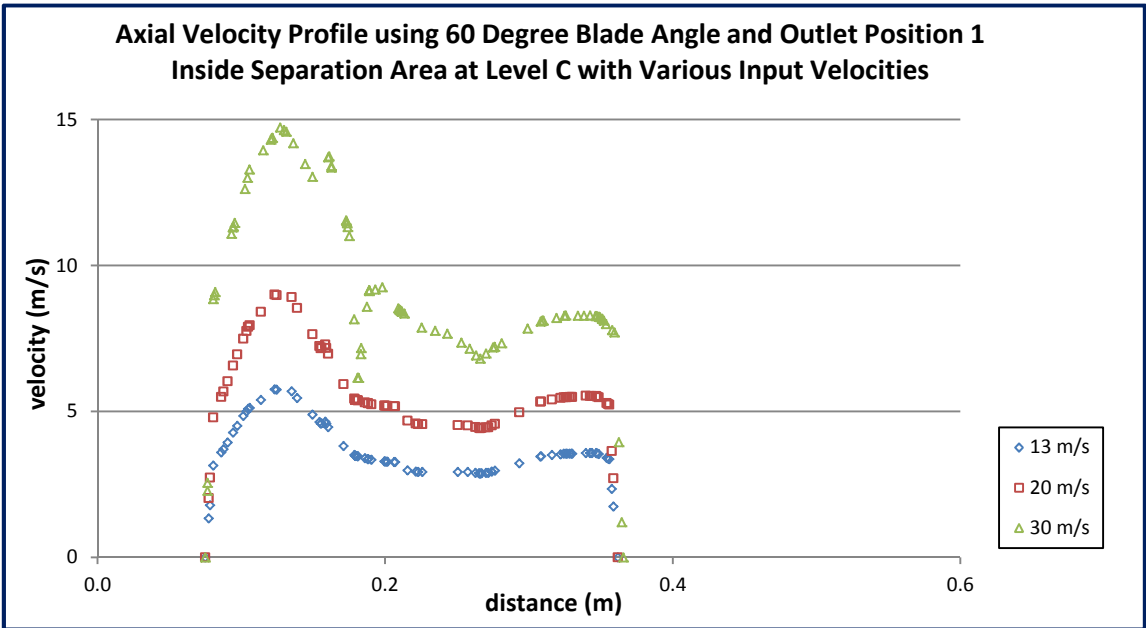
Axial velocity profile inside separation area at Level B for various input velocities
(45 degrees vane angle)



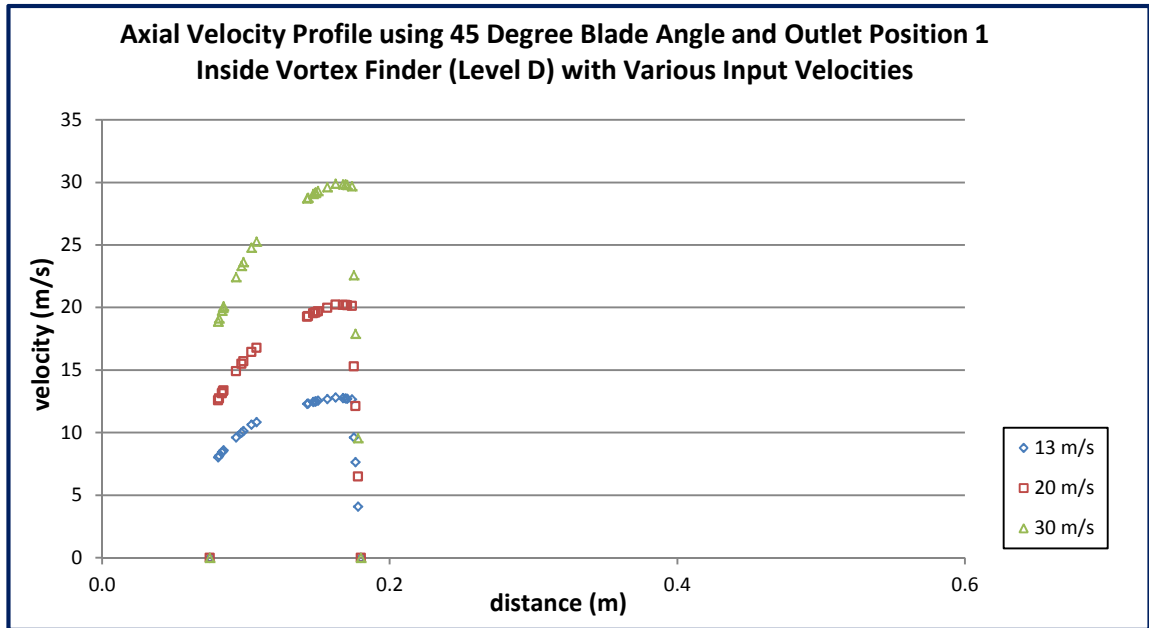
Axial velocity profile inside separation area at Level C for various input velocities
(45 degrees vane angle)



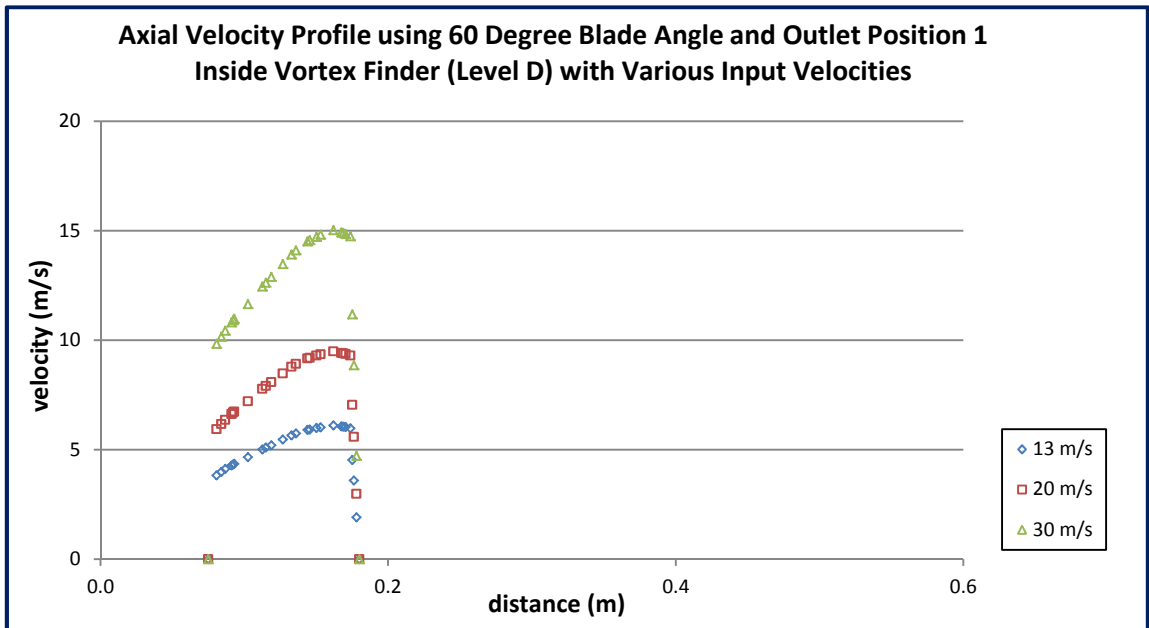
Axial velocity profile inside separation area at Level B for various input velocities
(60 degrees vane angle)



Axial velocity profile inside separation area at Level C for various input velocities
(60 degrees vane angle)



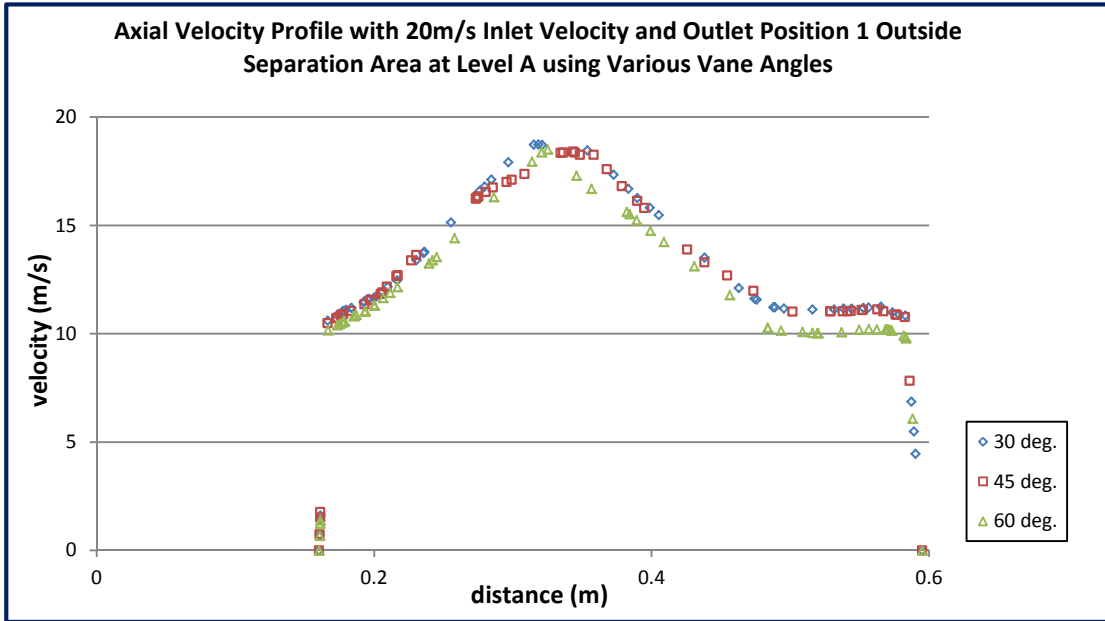
Axial velocity profile inside vortex finder (Level D) for various input velocities with outlet Position 1 (45 degrees vane angle)



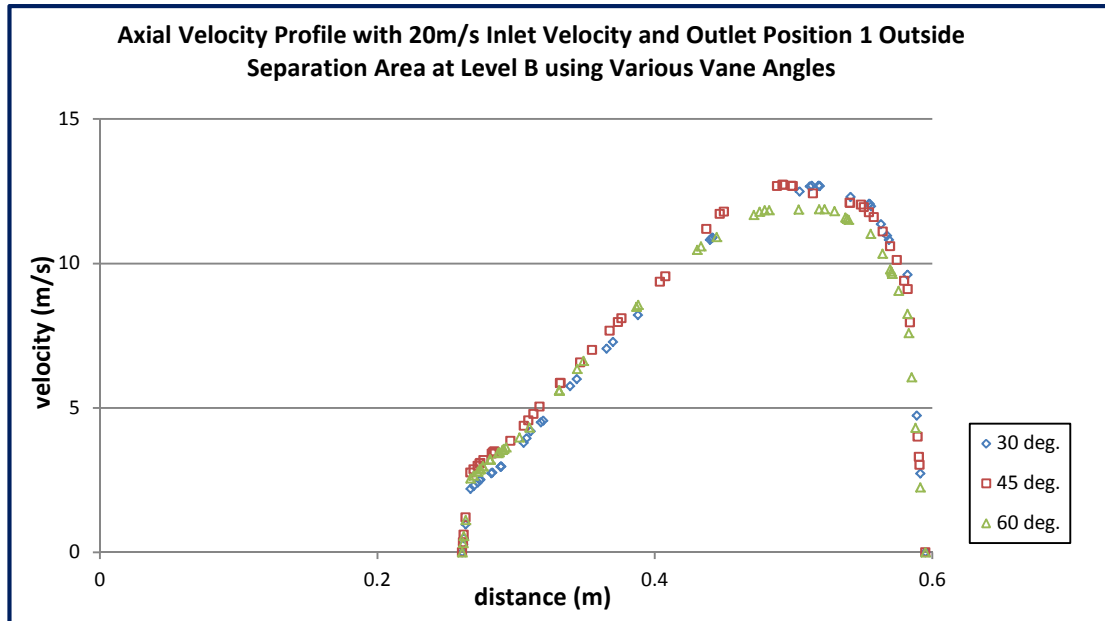
Axial velocity profile inside vortex finder (Level D) for various input velocities with outlet Position 1 (60 degrees vane angle)

APPENDIX III

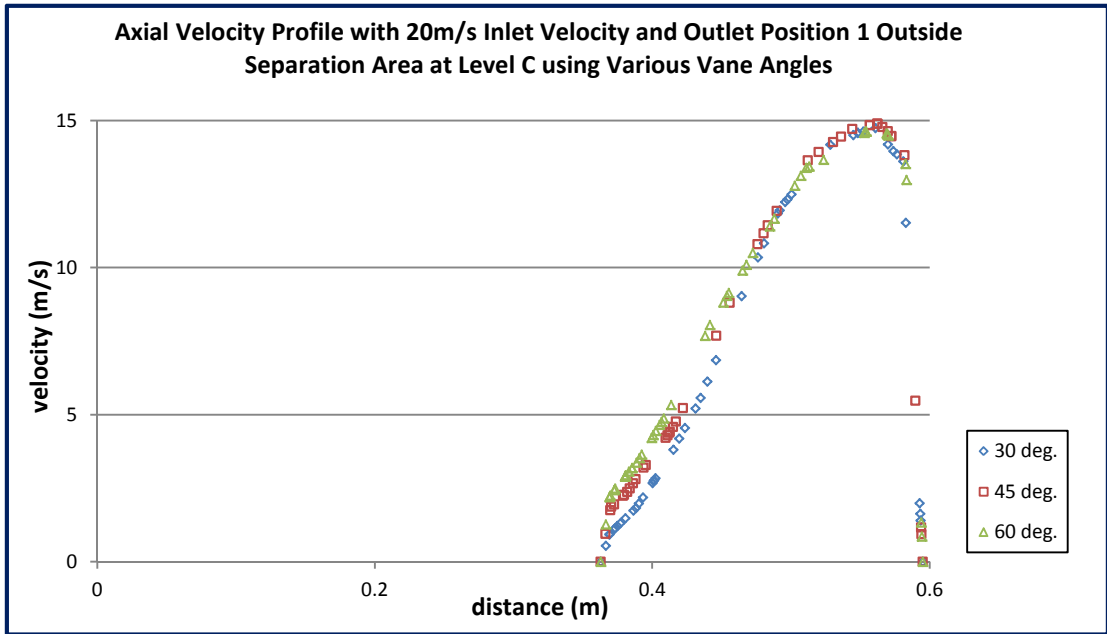
Effects of Varying Vane Angle Outside Separation Area for 20m/s and 30m/s Inlet
Velocities



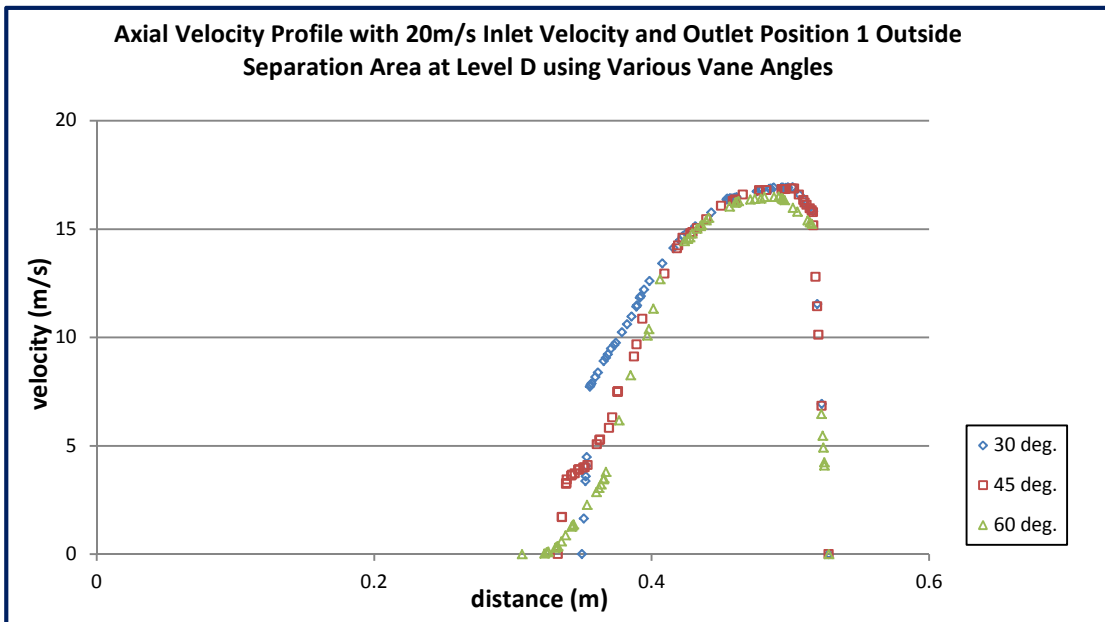
Axial velocity profile outside separation area at Level A for various vane angles
(20m/s inlet velocity)



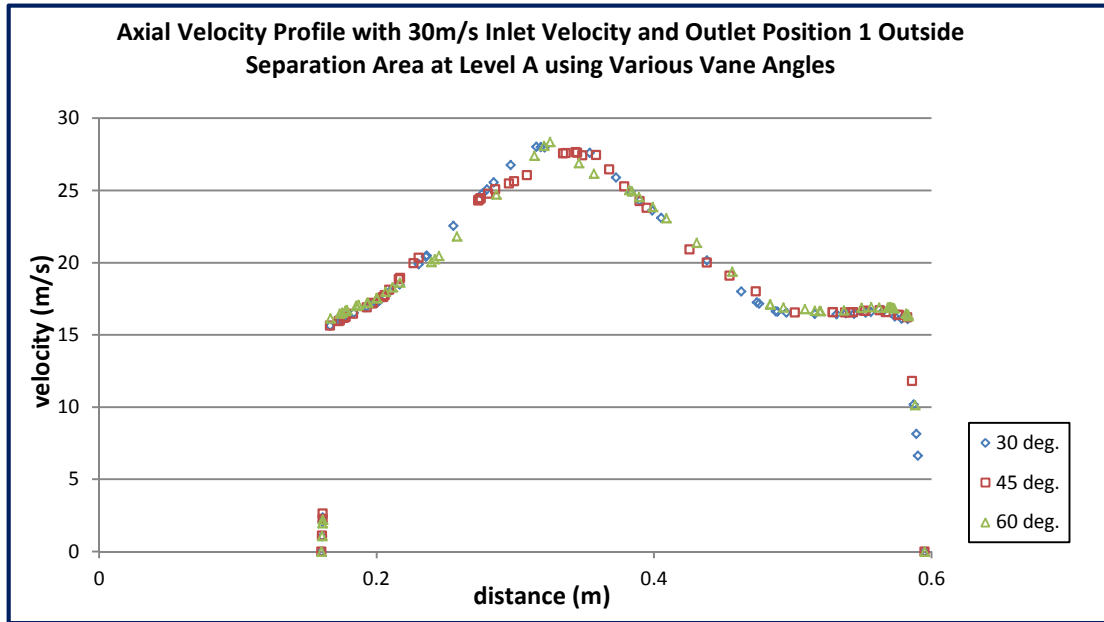
Axial velocity profile outside separation area at Level B for various vane angles
(20m/s inlet velocity)



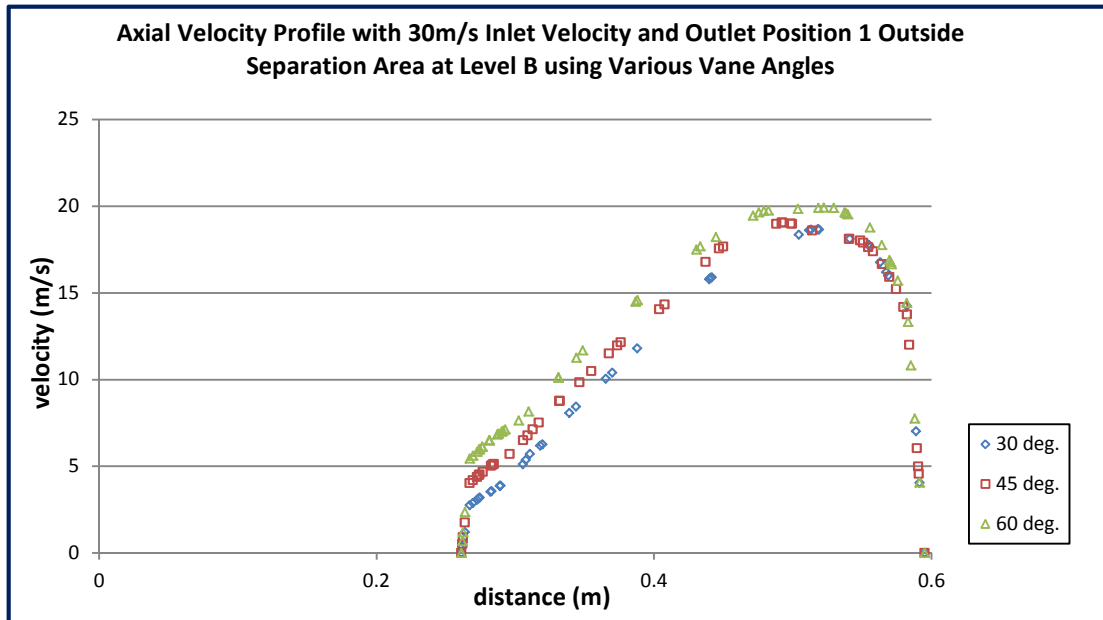
Axial velocity profile outside separation area at Level C for various vane angles
(20m/s inlet velocity)



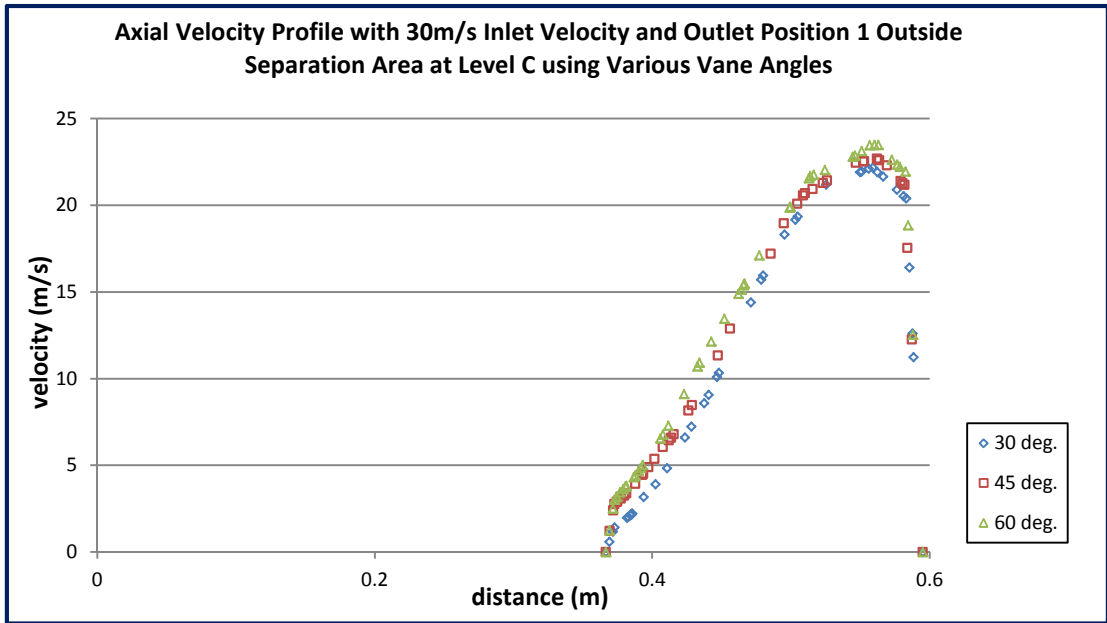
Axial velocity profile outside separation area at Level D for various vane angles
(20m/s inlet velocity)



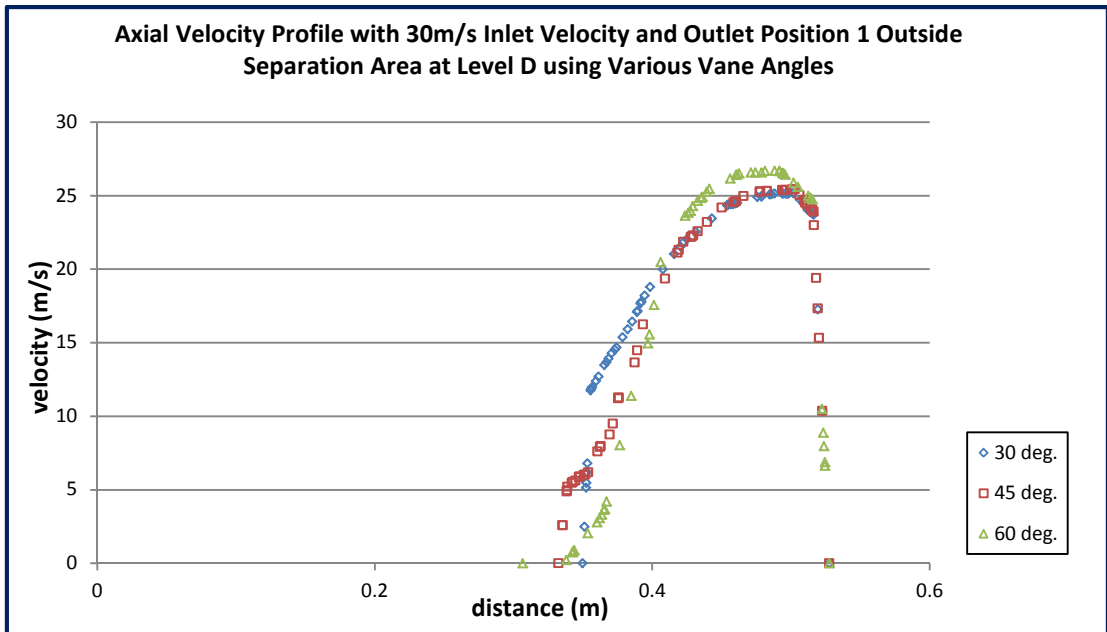
Axial velocity profile outside separation area at Level A for various vane angles
(30m/s inlet velocity)



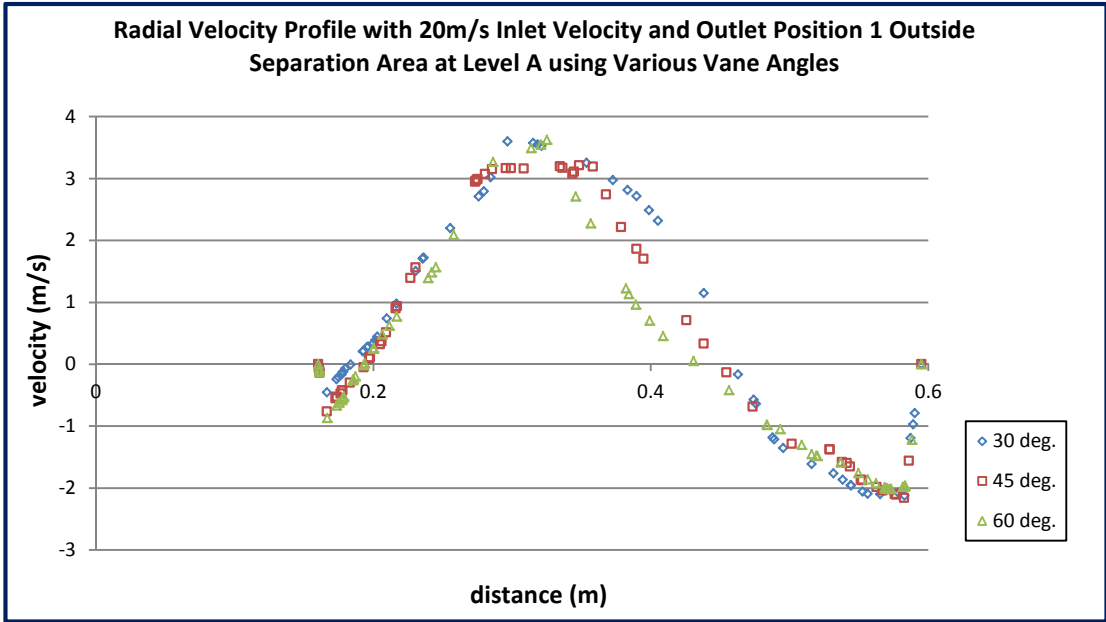
Axial velocity profile outside separation area at Level B for various vane angles
(30m/s inlet velocity)



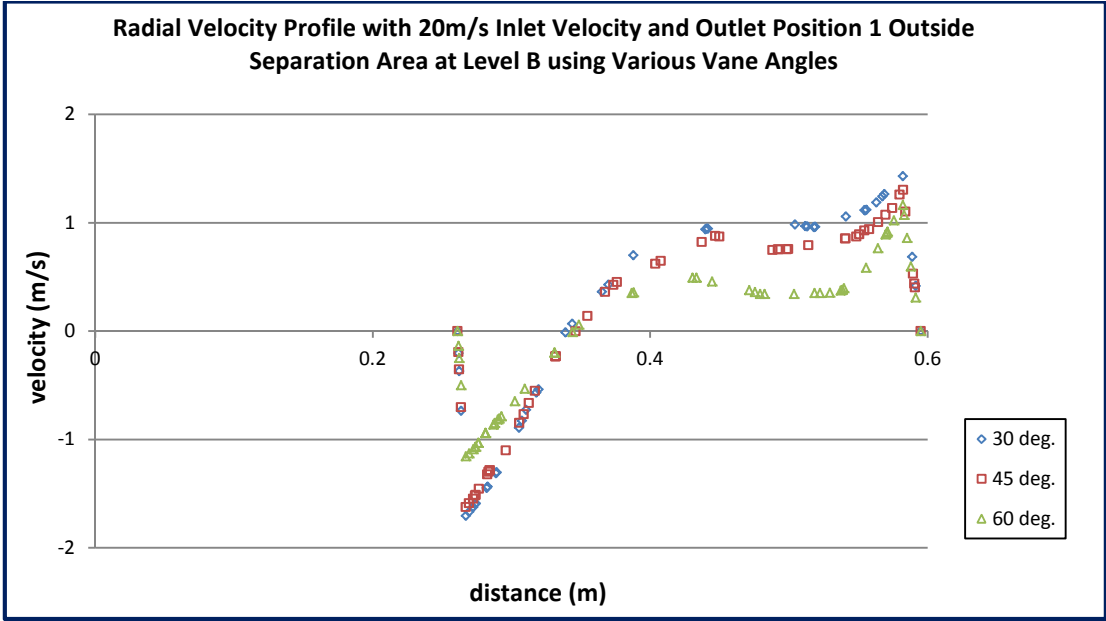
Axial velocity profile outside separation area at Level C for various vane angles
(30m/s inlet velocity)



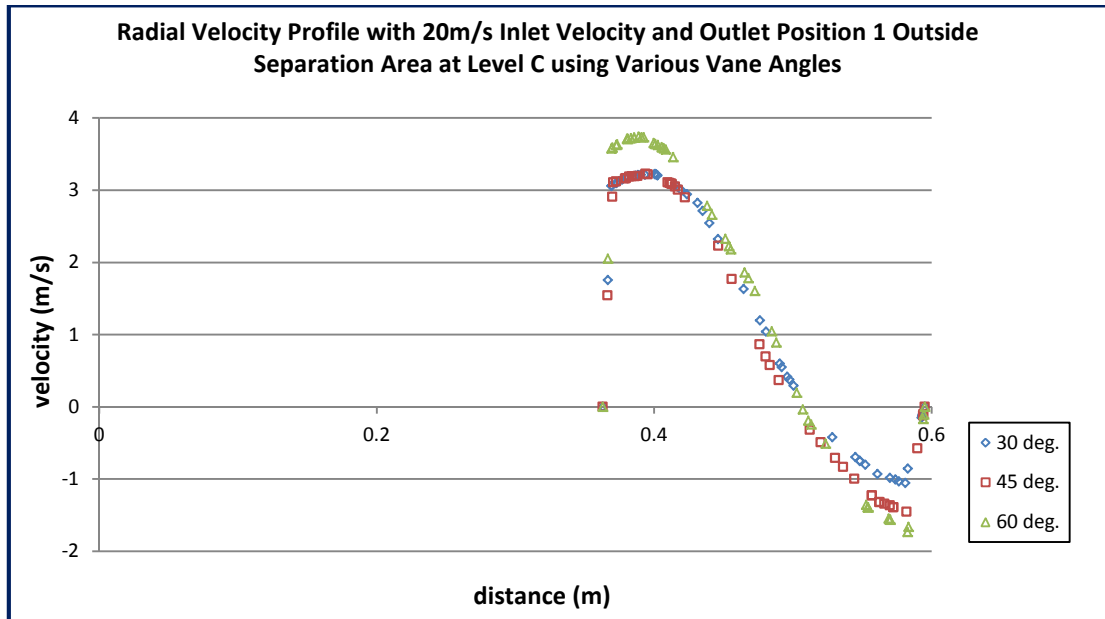
Axial velocity profile outside separation area at Level D for various vane angles
(30m/s inlet velocity)



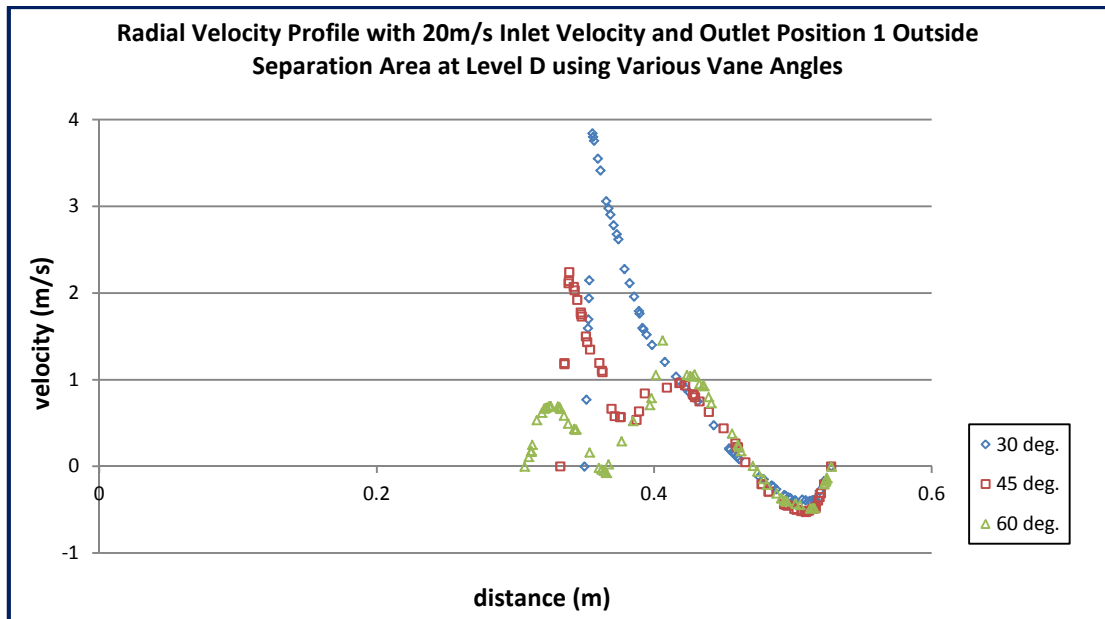
Radial velocity profile outside separation area at Level A for various vane angles
(20m/s inlet velocity)



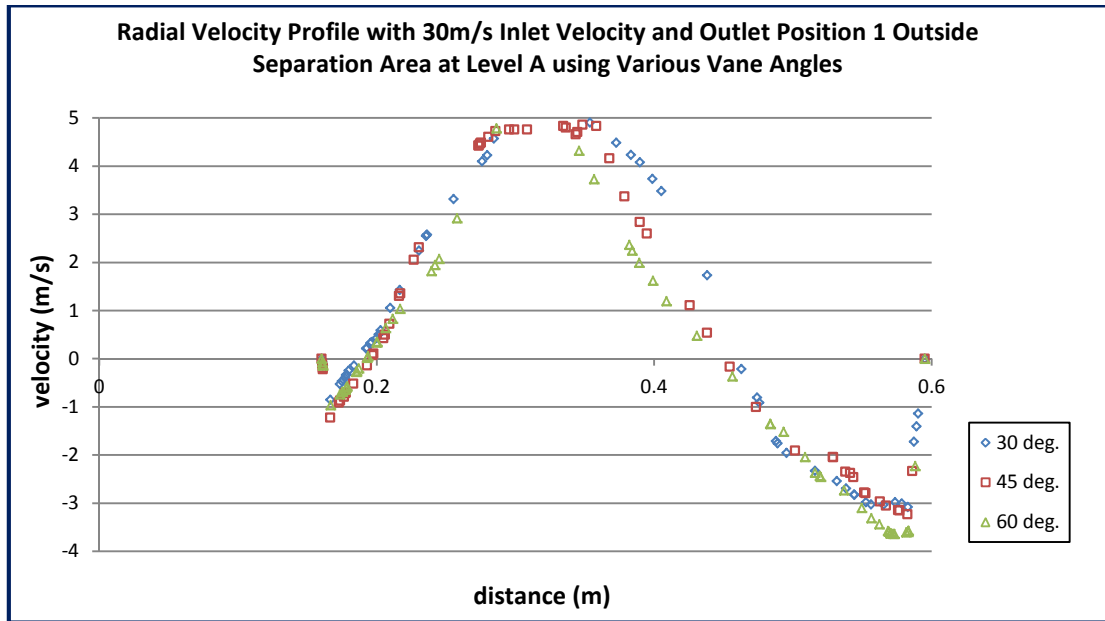
Radial velocity profile outside separation area at Level B for various vane angles
(20m/s inlet velocity)



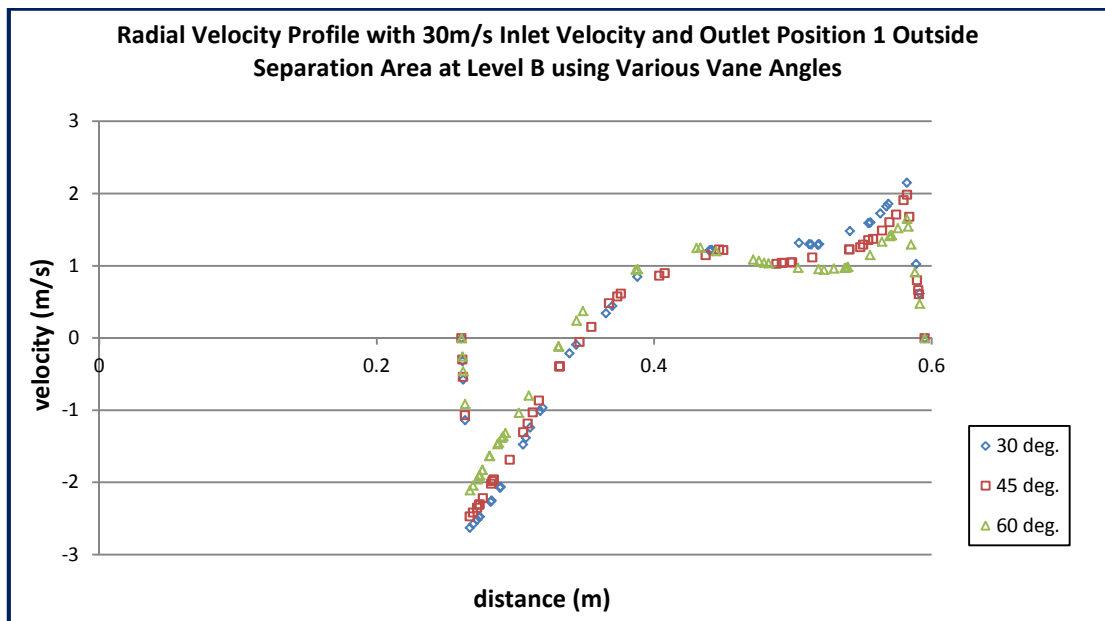
Radial velocity profile outside separation area at Level C for various vane angles
(20m/s inlet velocity)



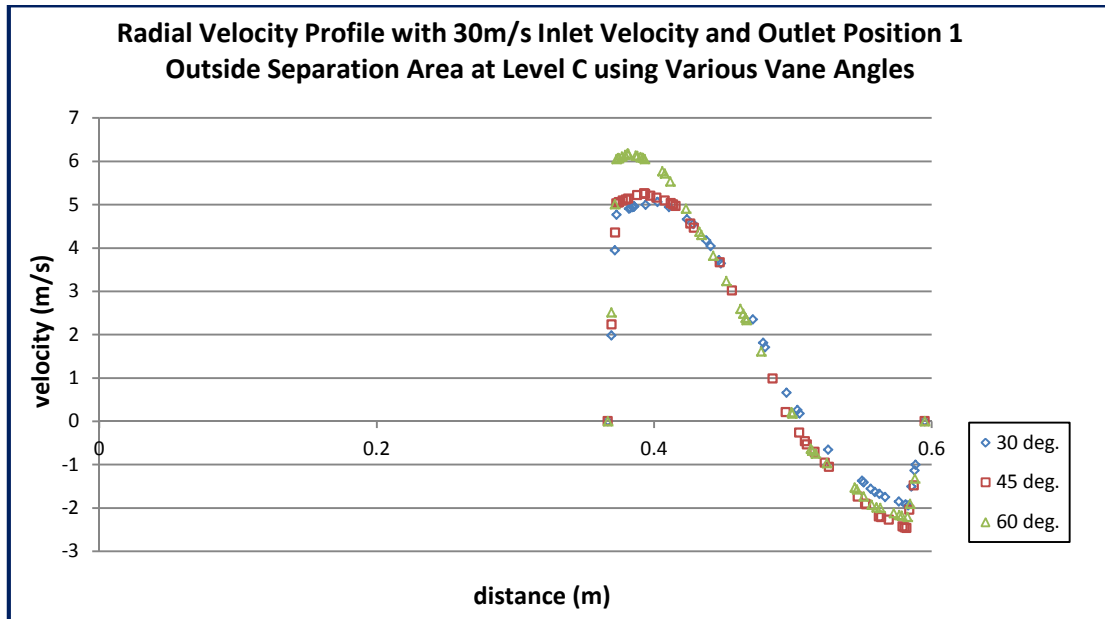
Radial velocity profile outside separation area at Level D for various vane angles
(20m/s inlet velocity)



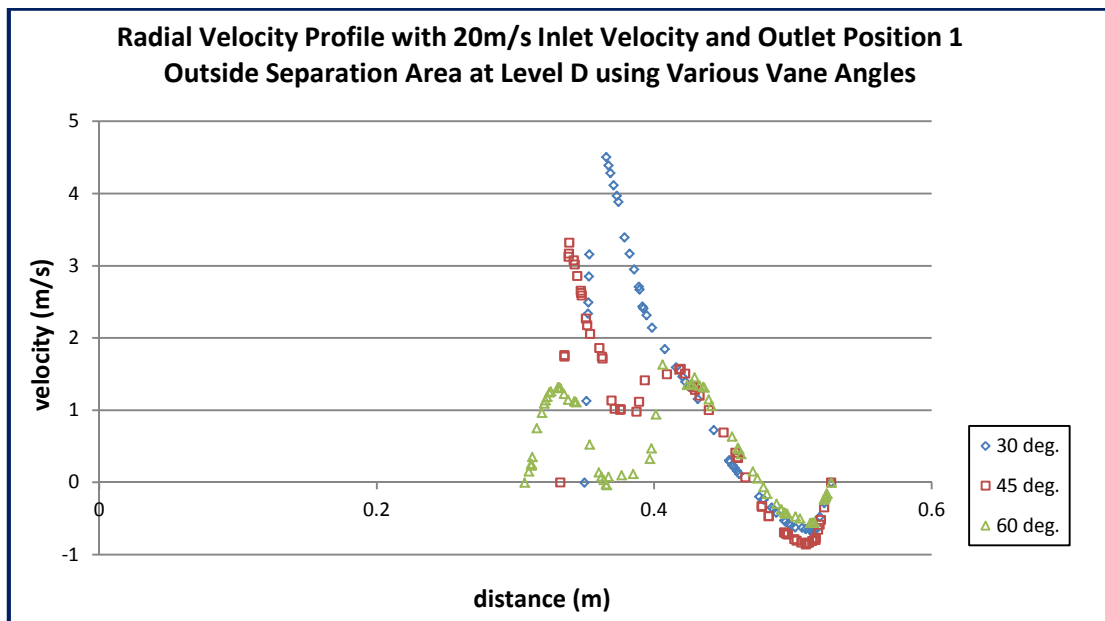
Radial velocity profile outside separation area at Level A for various vane angles
(30m/s inlet velocity)



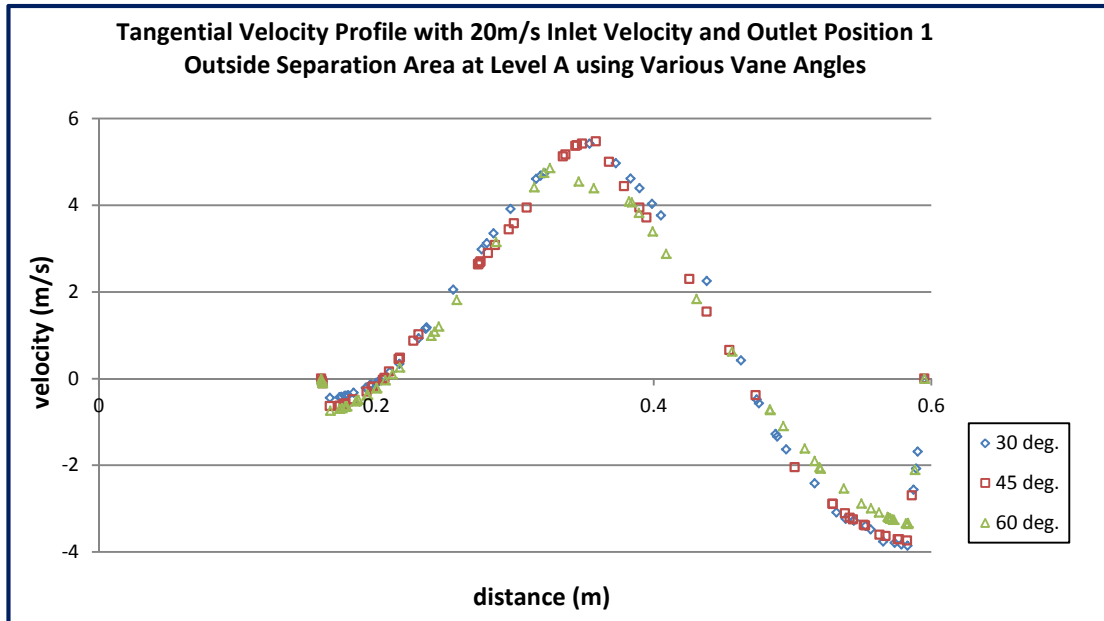
Radial velocity profile outside separation area at Level B for various vane angles
(30m/s inlet velocity)



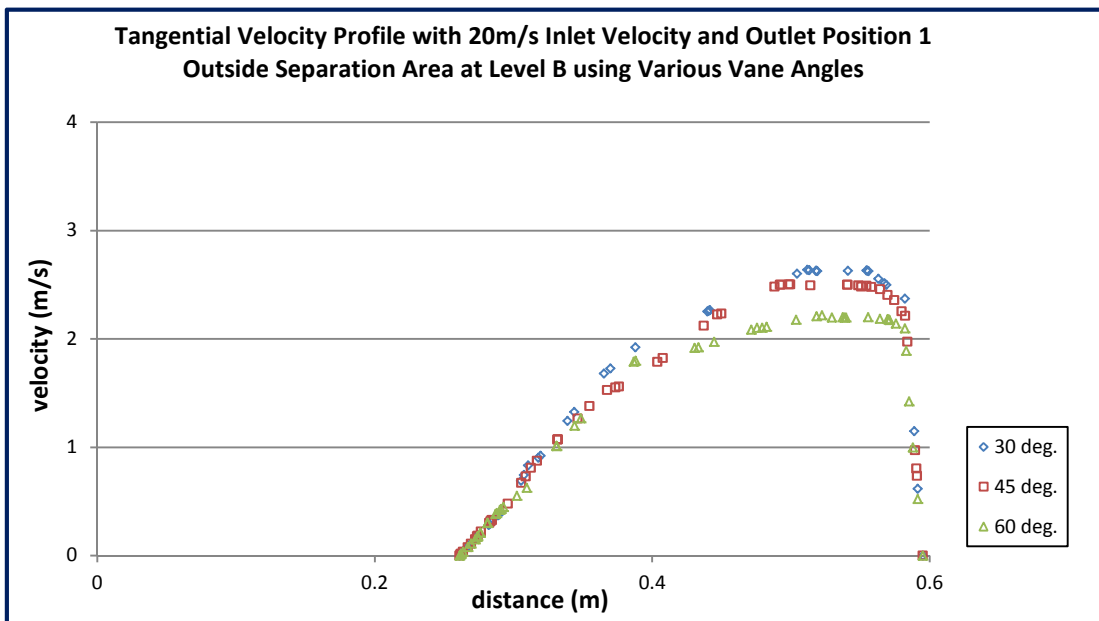
Radial velocity profile outside separation area at Level C for various vane angles
(30m/s inlet velocity)



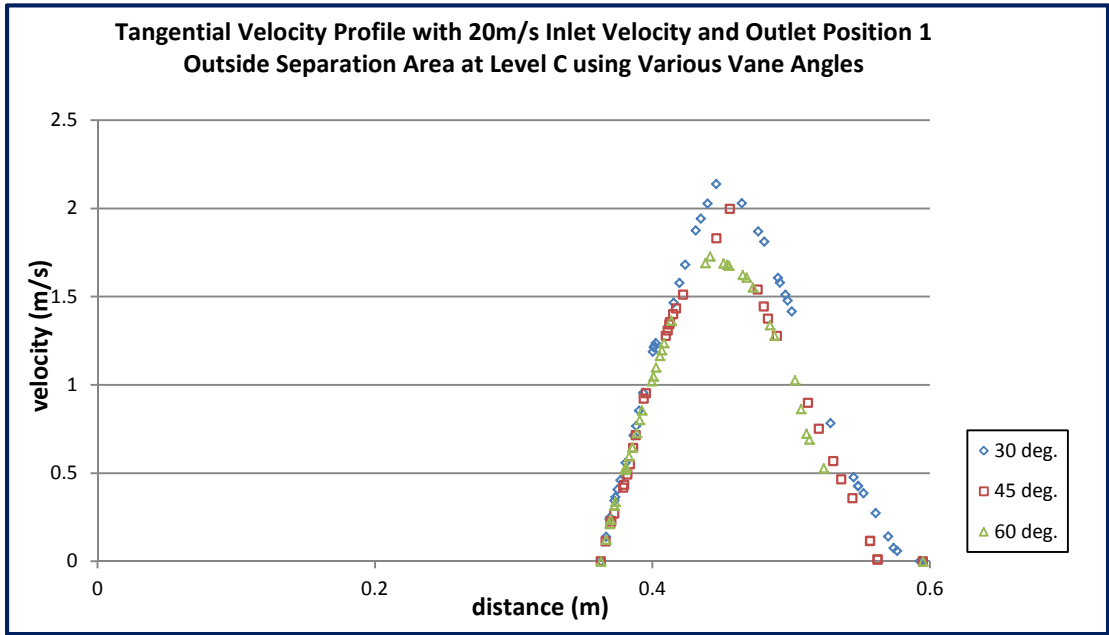
Radial velocity profile outside separation area at Level D for various vane angles
(30m/s inlet velocity)



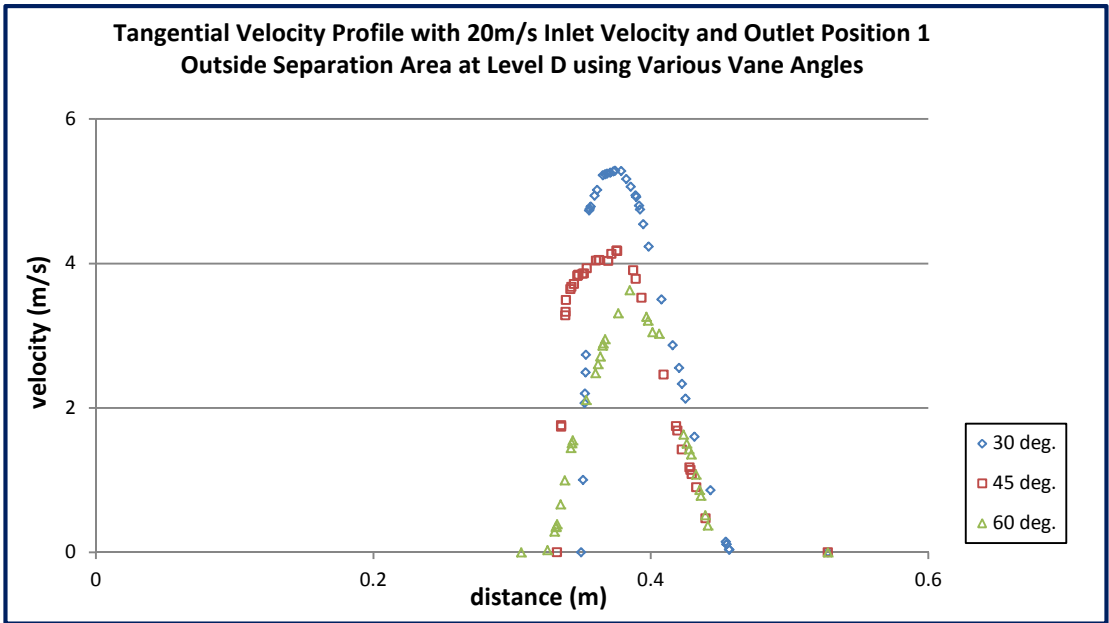
Tangential velocity profile outside separation area at Level A for various vane angles
(20m/s inlet velocity)



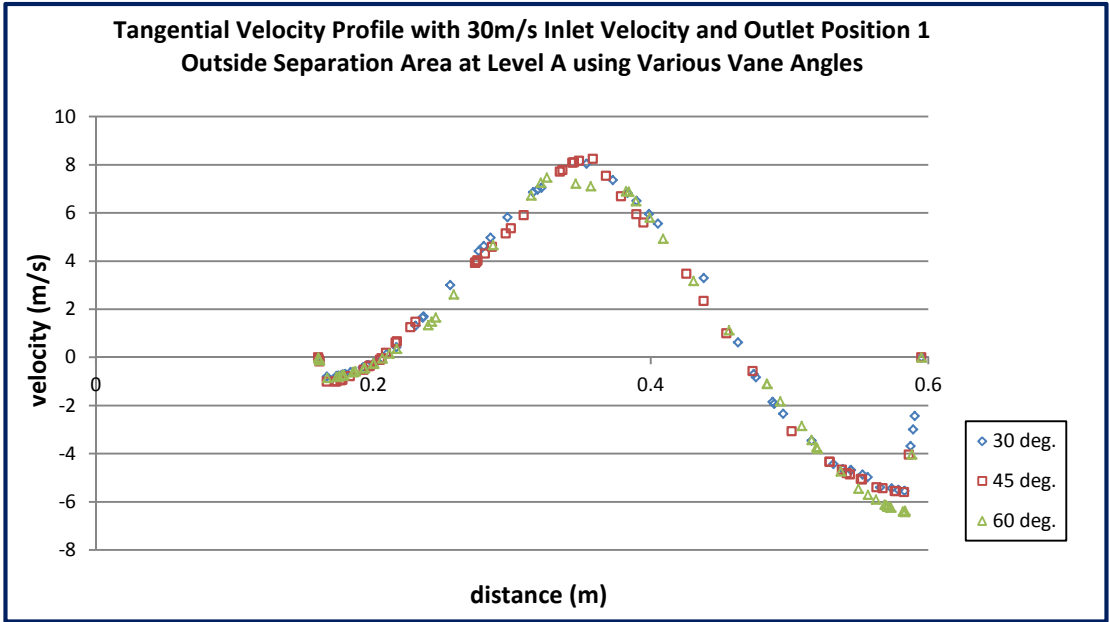
Tangential velocity profile outside separation area at Level B for various vane angles
(20m/s inlet velocity)



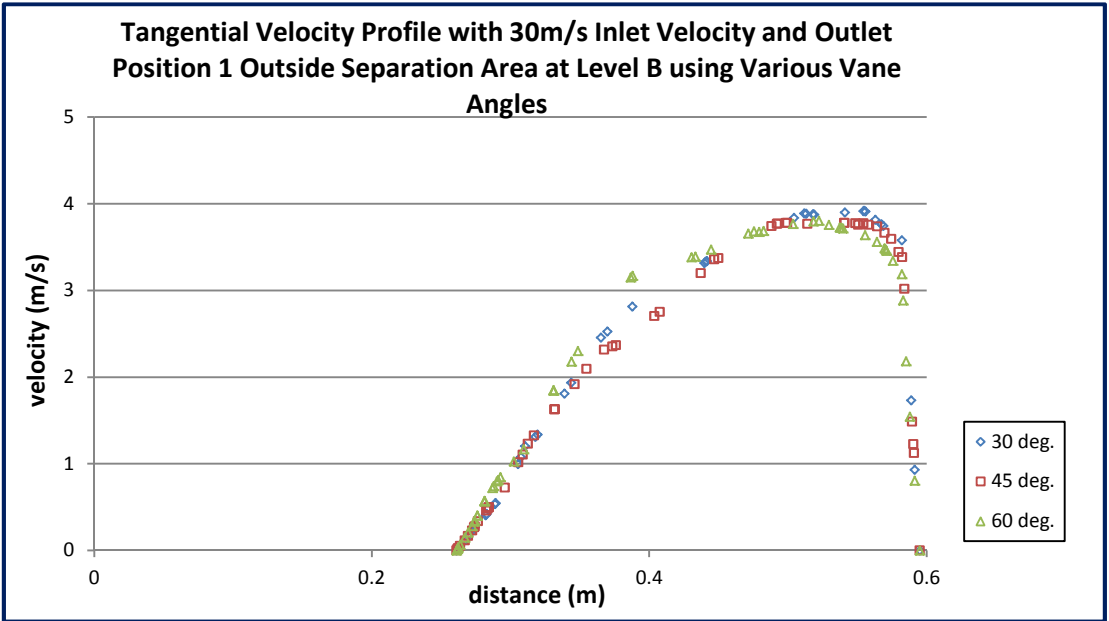
Tangential velocity profile outside separation area at Level C for various vane angles (20m/s inlet velocity)



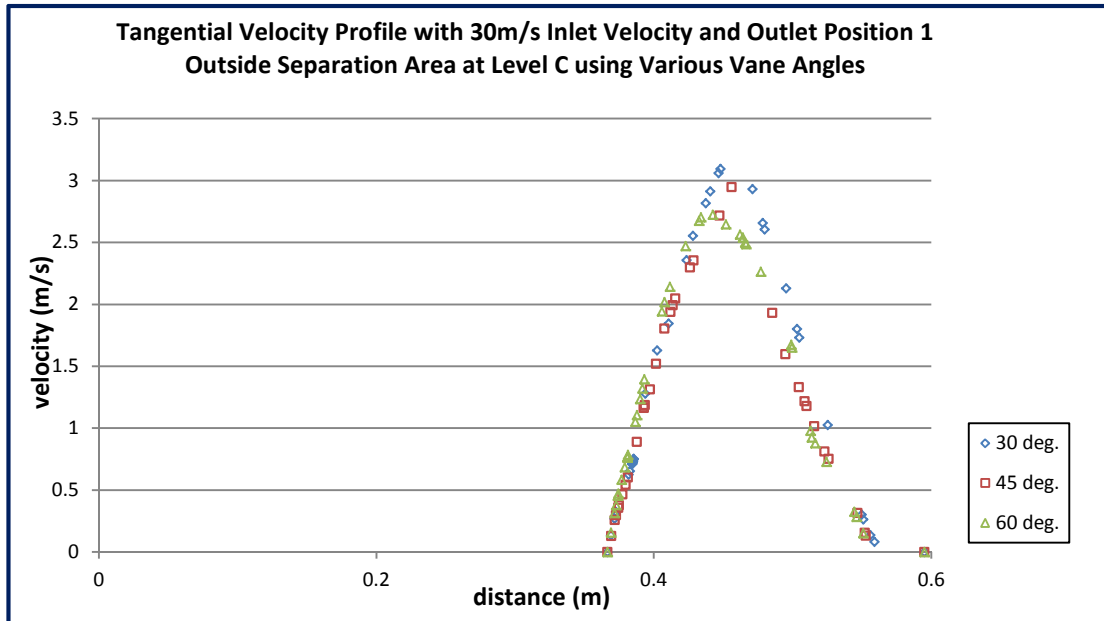
Tangential velocity profile outside separation area at Level D for various vane angles (20m/s inlet velocity)



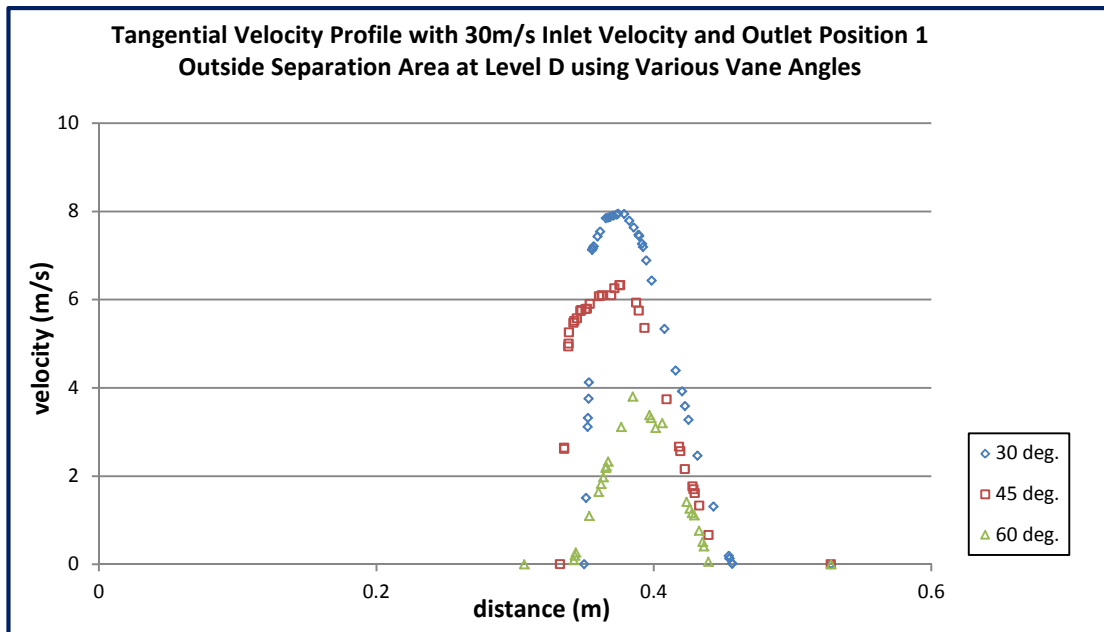
Tangential velocity profile outside separation area at Level A for various vane angles
(30m/s inlet velocity)



Tangential velocity profile outside separation area at Level B for various vane angles
(30m/s inlet velocity)



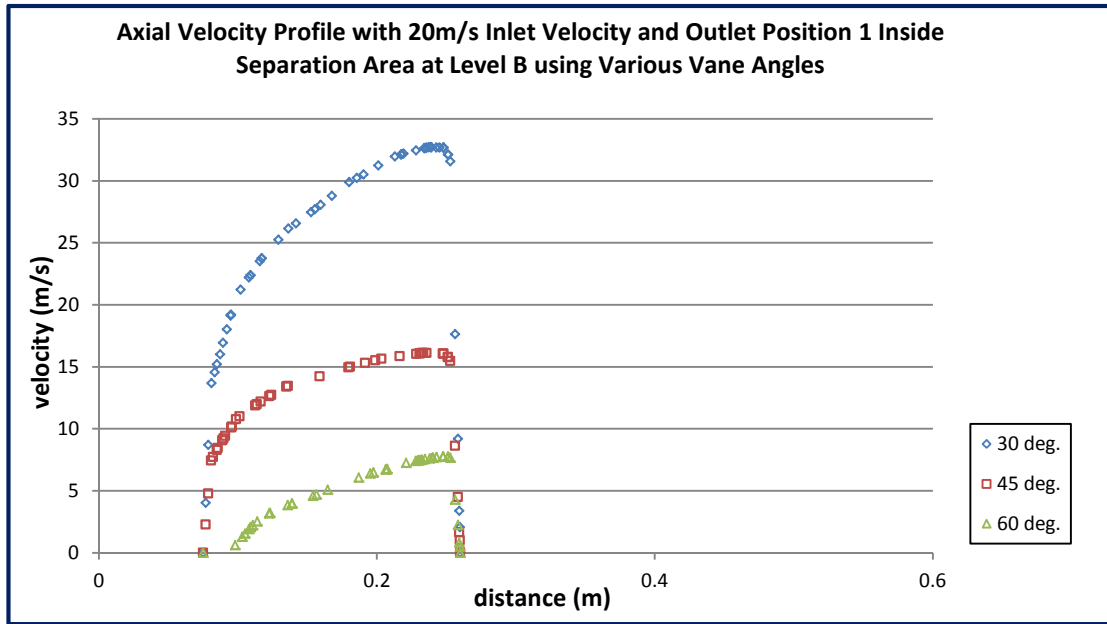
Tangential velocity profile outside separation area at Level C for various vane angles
(30m/s inlet velocity)



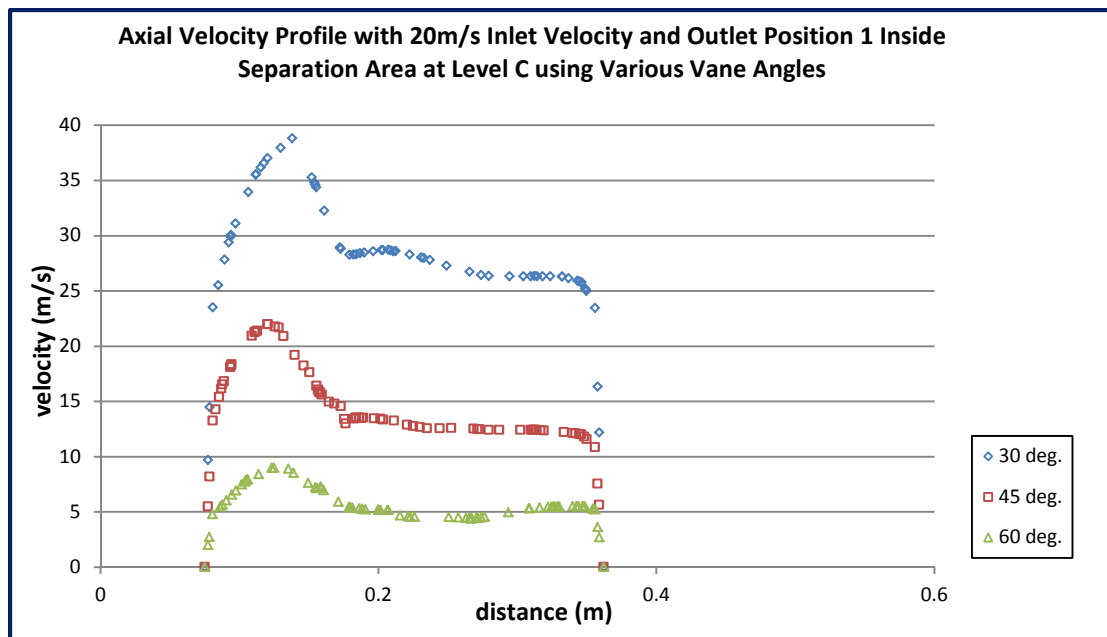
Tangential velocity profile outside separation area at Level D for various vane angles
(30m/s inlet velocity)

APPENDIX IV

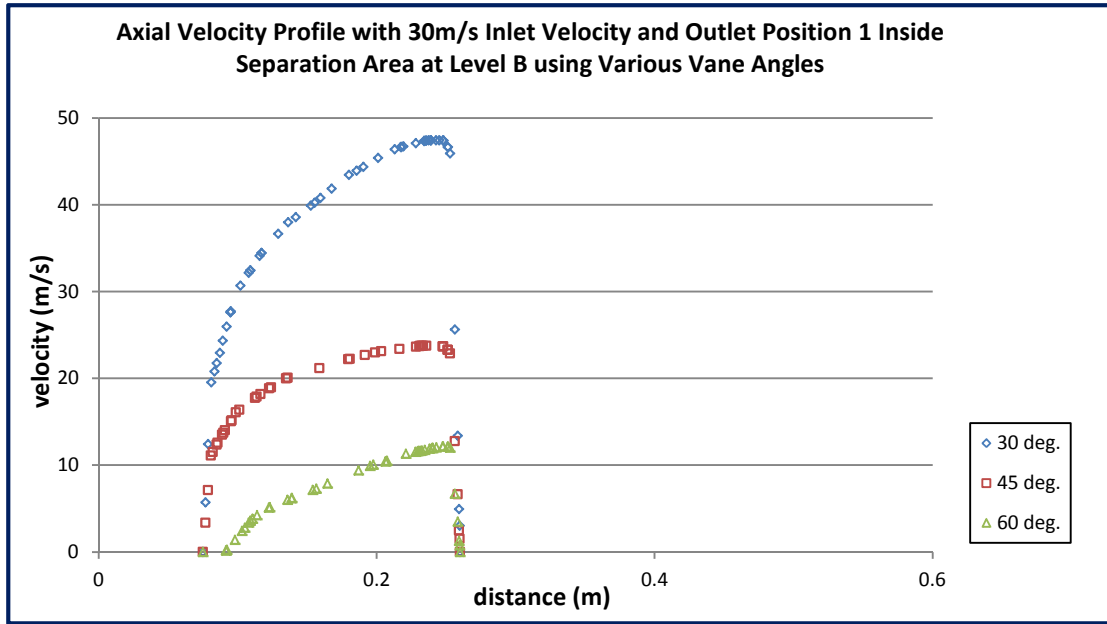
Effects of Varying Vane Angle Inside Separation Area and Vortex Finder for 20m/s
and 30m/s Inlet Velocities



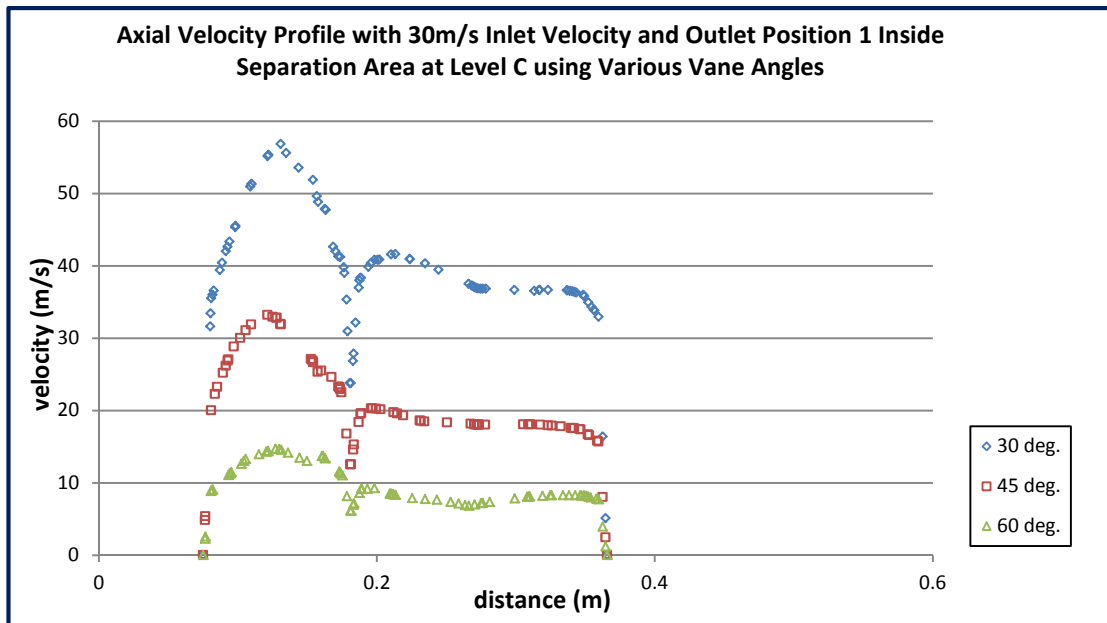
Axial velocity profile inside separation area at Level B for various vane angles
(20m/s inlet velocity)



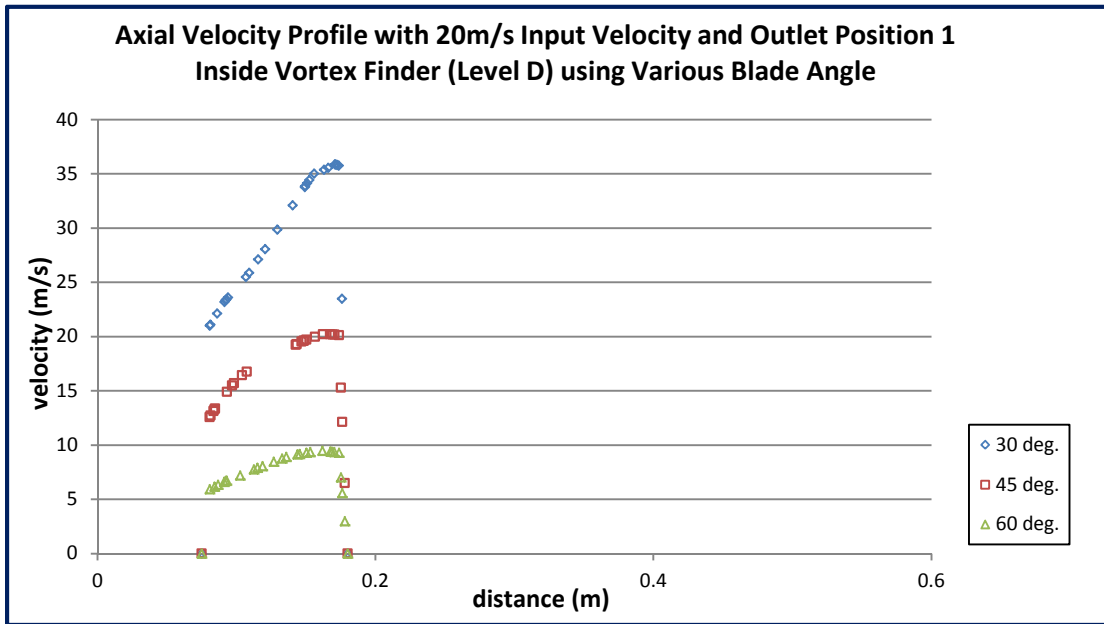
Axial velocity profile inside separation area at Level C for various vane angles
(20m/s inlet velocity)



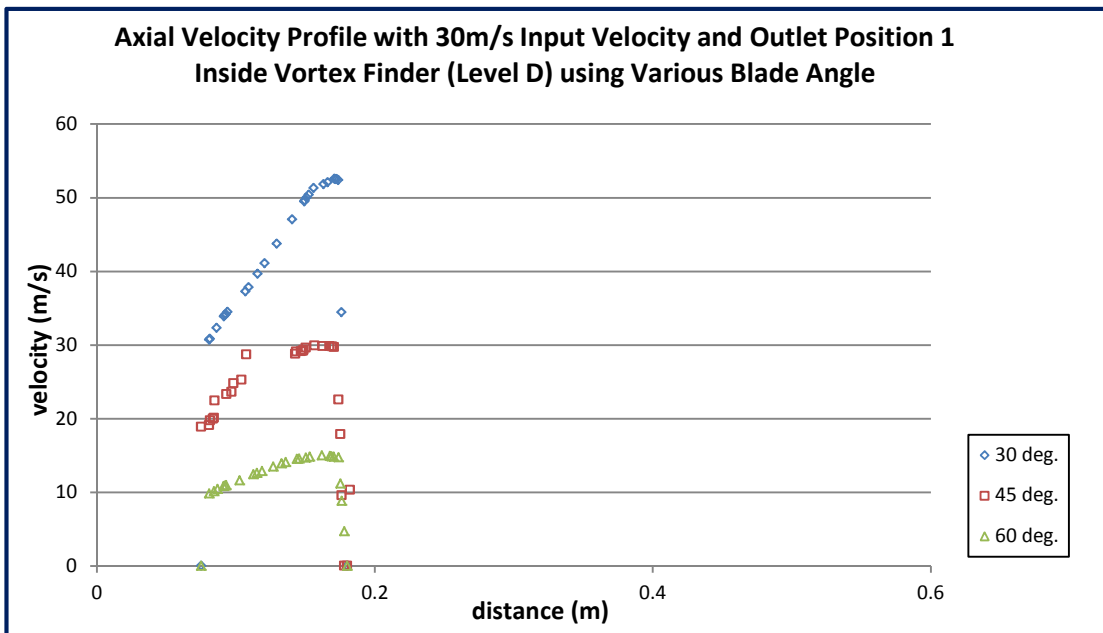
Axial velocity profile inside separation area at Level B for various vane angles
(30m/s inlet velocity)



Axial velocity profile inside separation area at Level C for various vane angles
(30m/s inlet velocity)



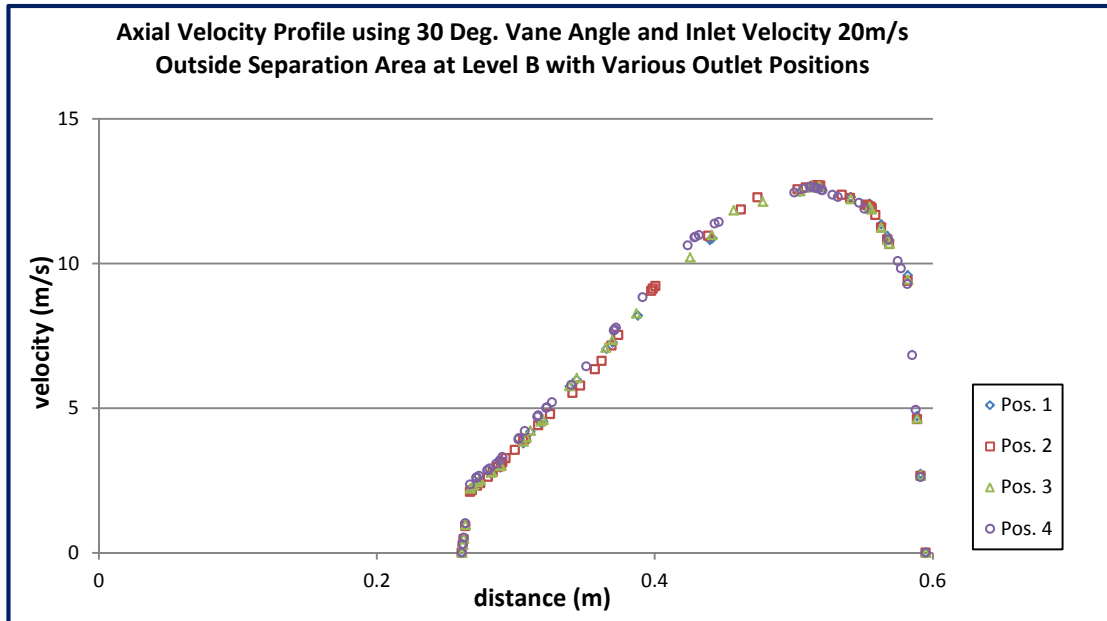
Axial velocity profile inside vortex finder (Level D) for various vane angles with outlet Position 1 (20m/s inlet velocity)



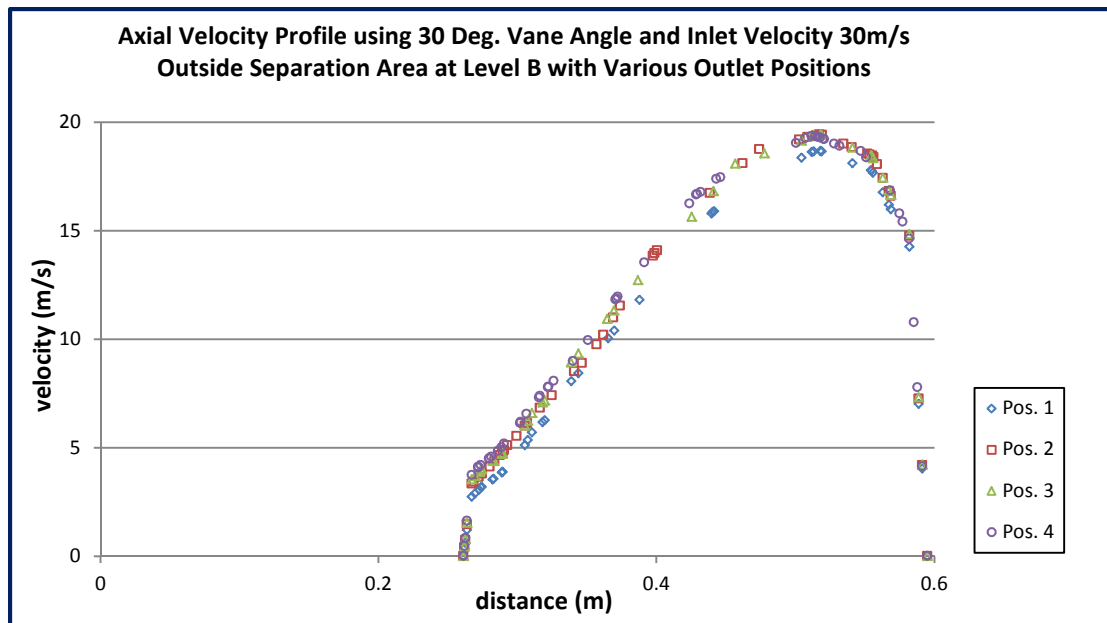
Axial velocity profile inside vortex finder (Level D) for various vane angles with outlet Position 1 (30m/s inlet velocity)

APPENDIX V

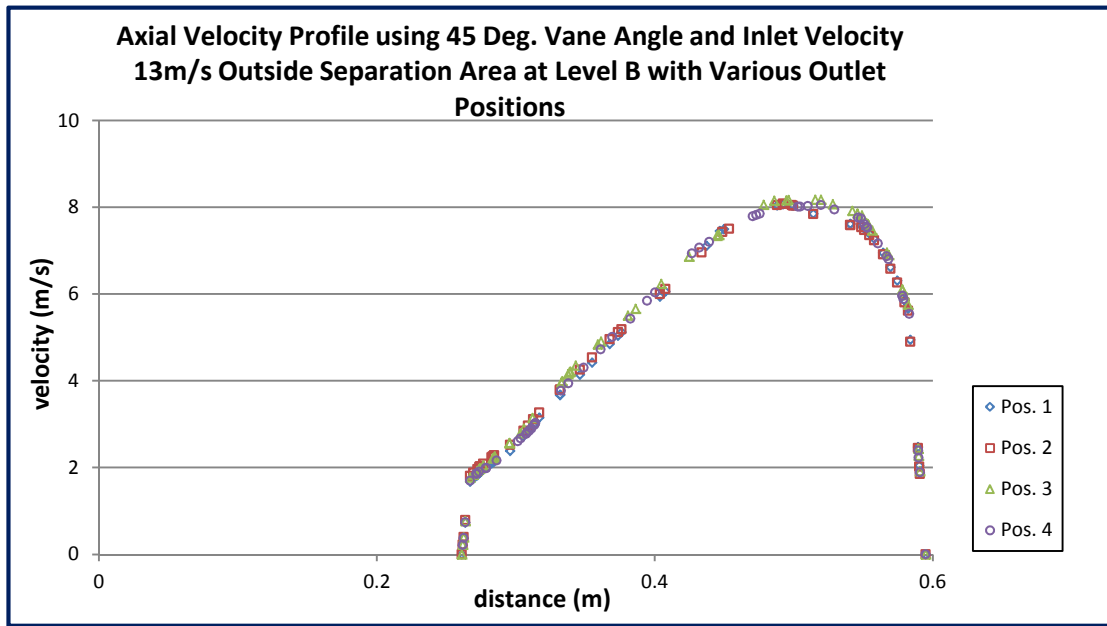
Effects of Varying Outlet Position Outside Separation Area



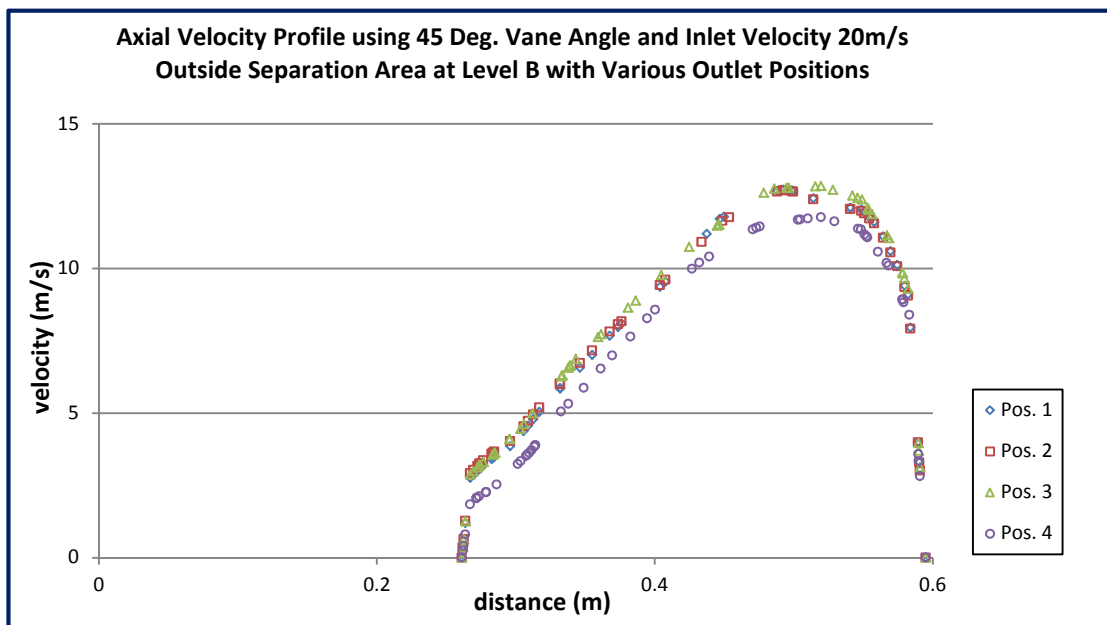
Axial velocity profile outside separation area at Level B for various outlet positions
(30 degrees vane angle, 20m/s inlet velocity)



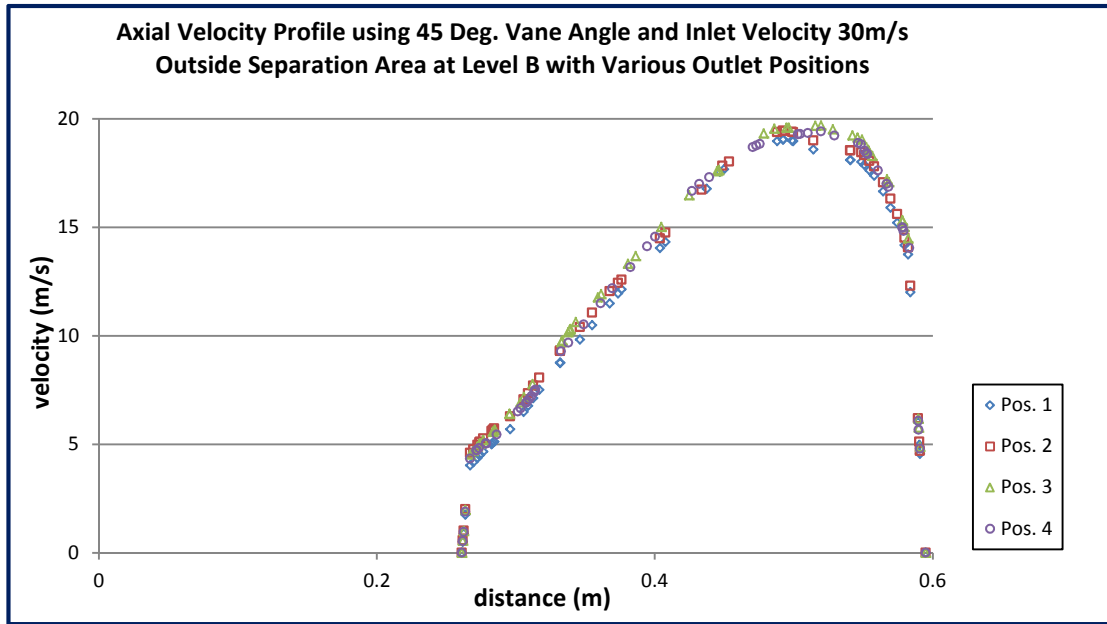
Axial velocity profile outside separation area at Level B for various outlet positions
(30 degrees vane angle, 30m/s inlet velocity)



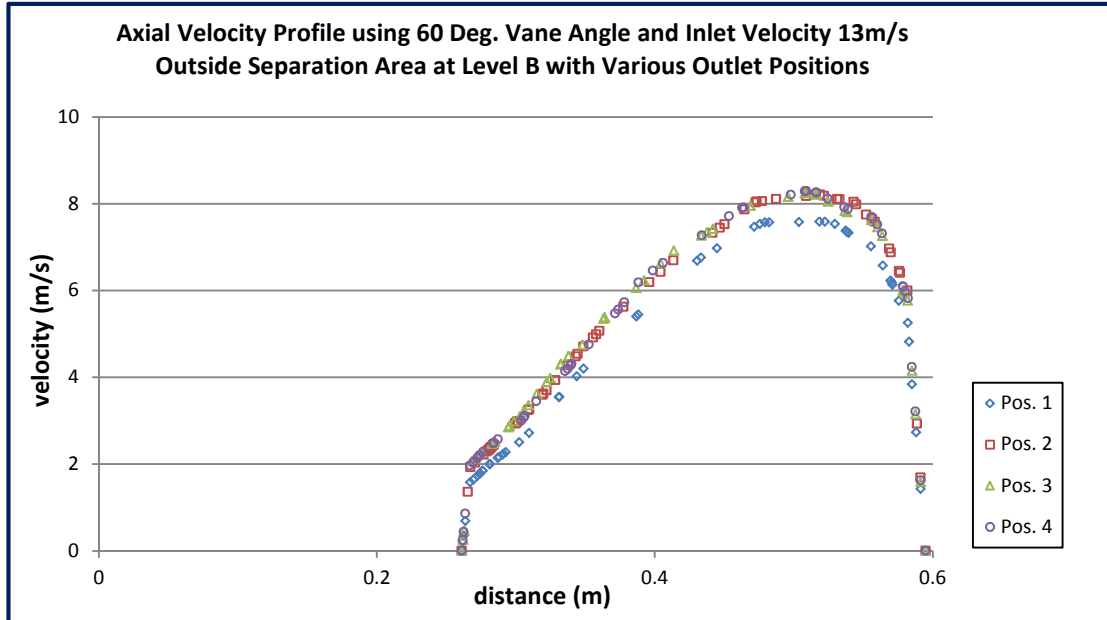
Axial velocity profile outside separation area at Level B for various outlet positions
(45 degrees vane angle, 13m/s inlet velocity)



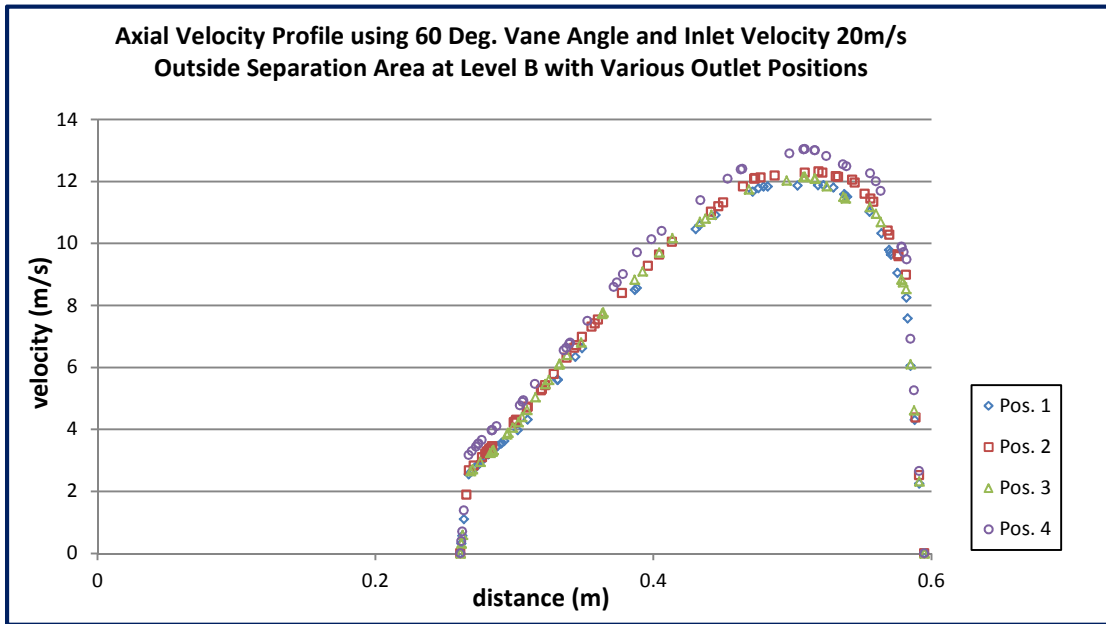
Axial velocity profile outside separation area at Level B for various outlet positions
(45 degrees vane angle, 20m/s inlet velocity)



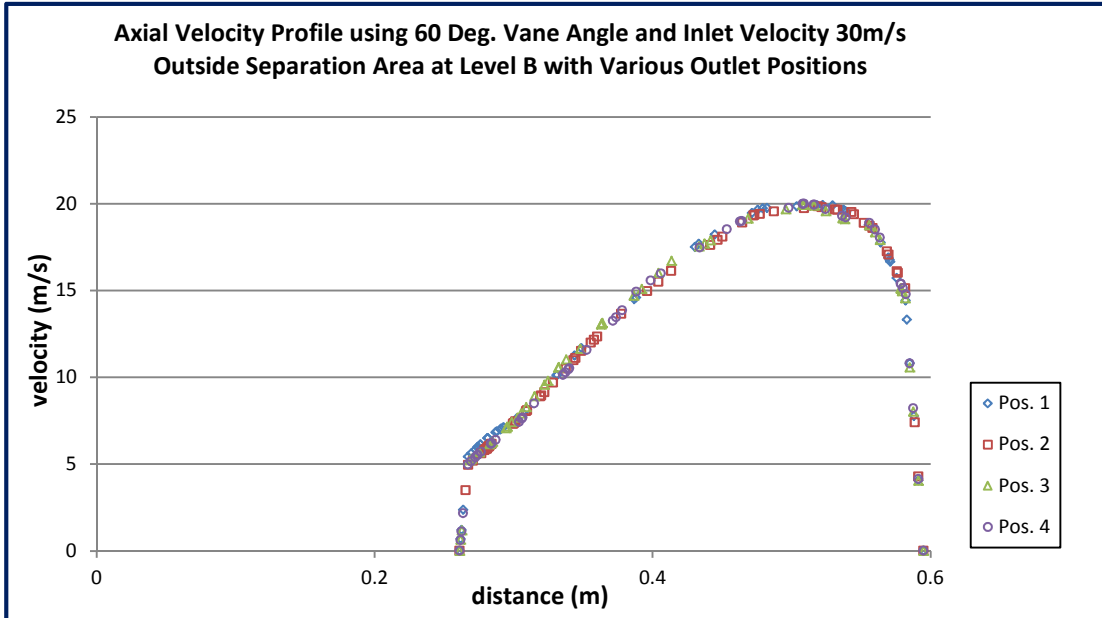
Axial velocity profile outside separation area at Level B for various outlet positions
(45 degrees vane angle, 30m/s inlet velocity)



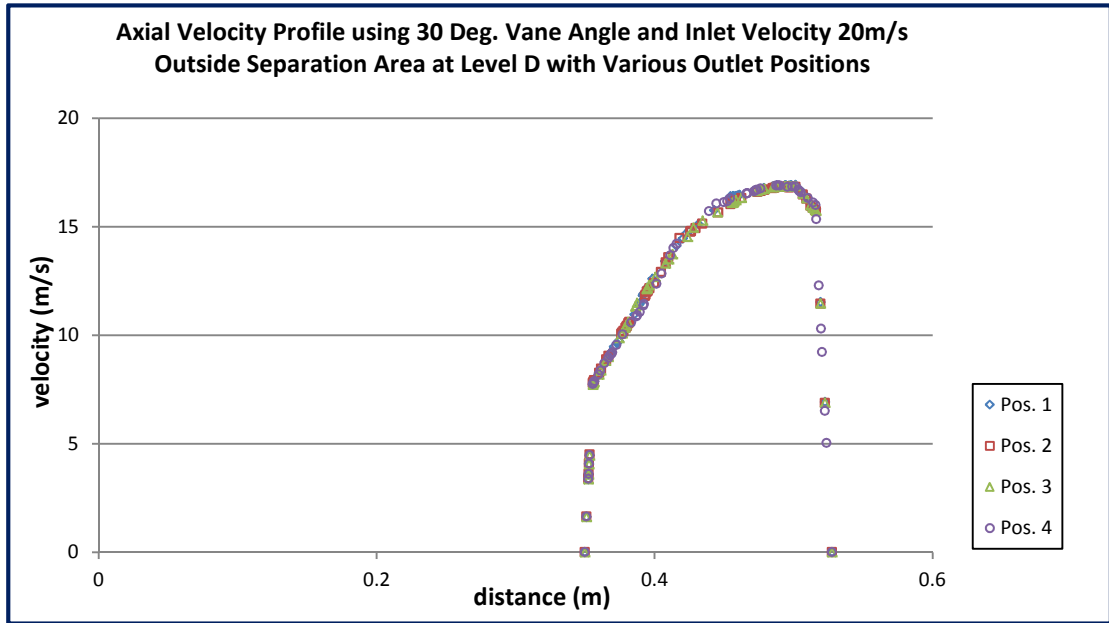
Axial velocity profile outside separation area at Level B for various outlet positions
(60 degrees vane angle, 13m/s inlet velocity)



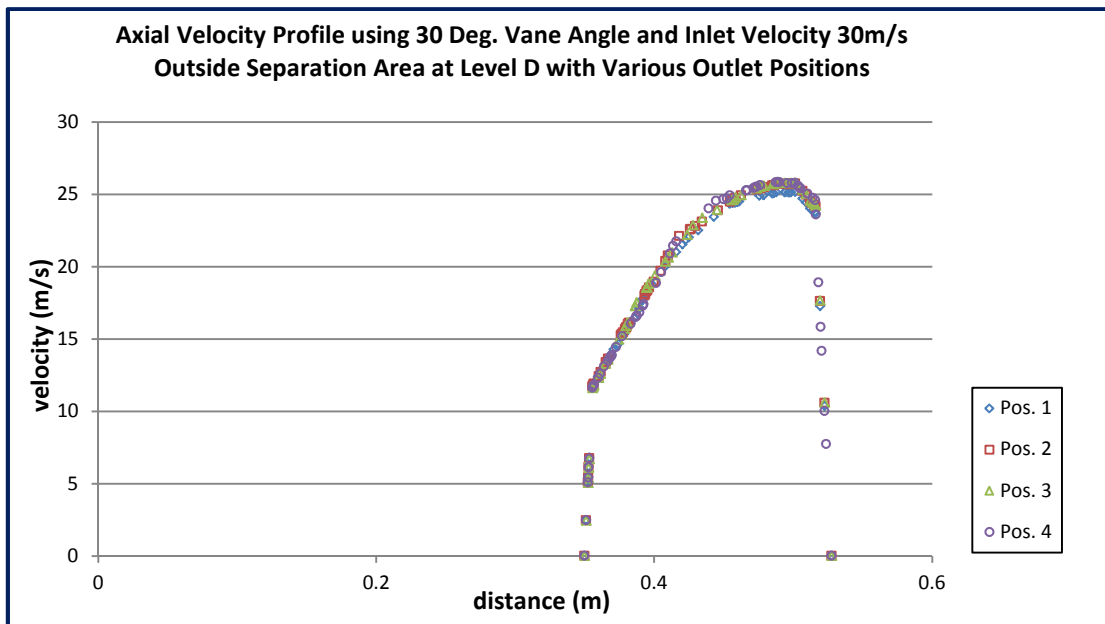
Axial velocity profile outside separation area at Level B for various outlet positions
(60 degrees vane angle, 20m/s inlet velocity)



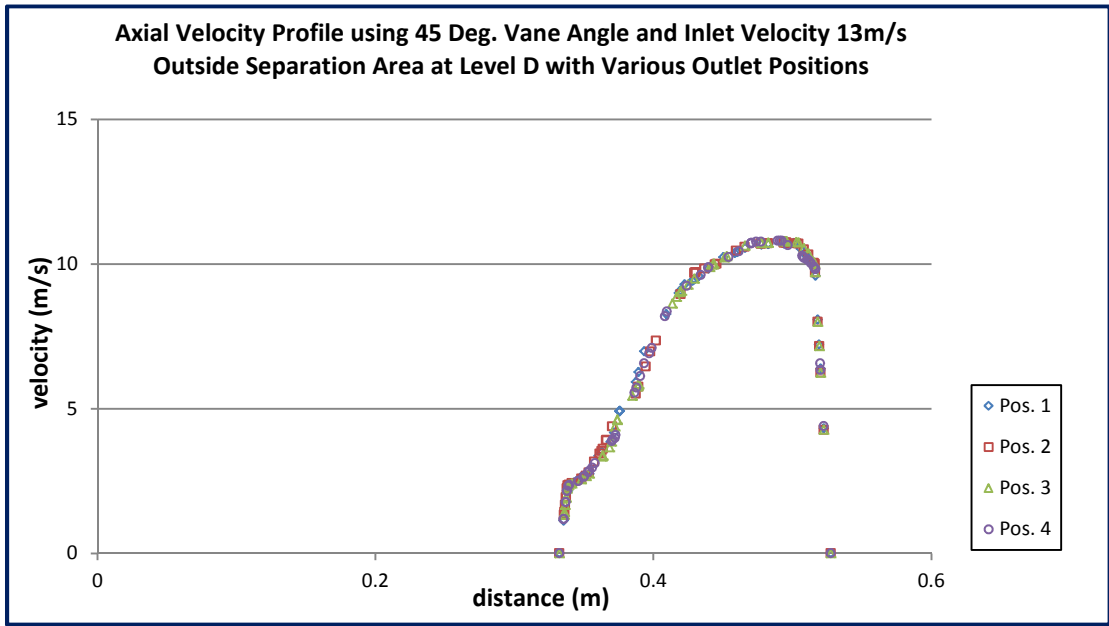
Axial velocity profile outside separation area at Level B for various outlet positions
(60 degrees vane angle, 30m/s inlet velocity)



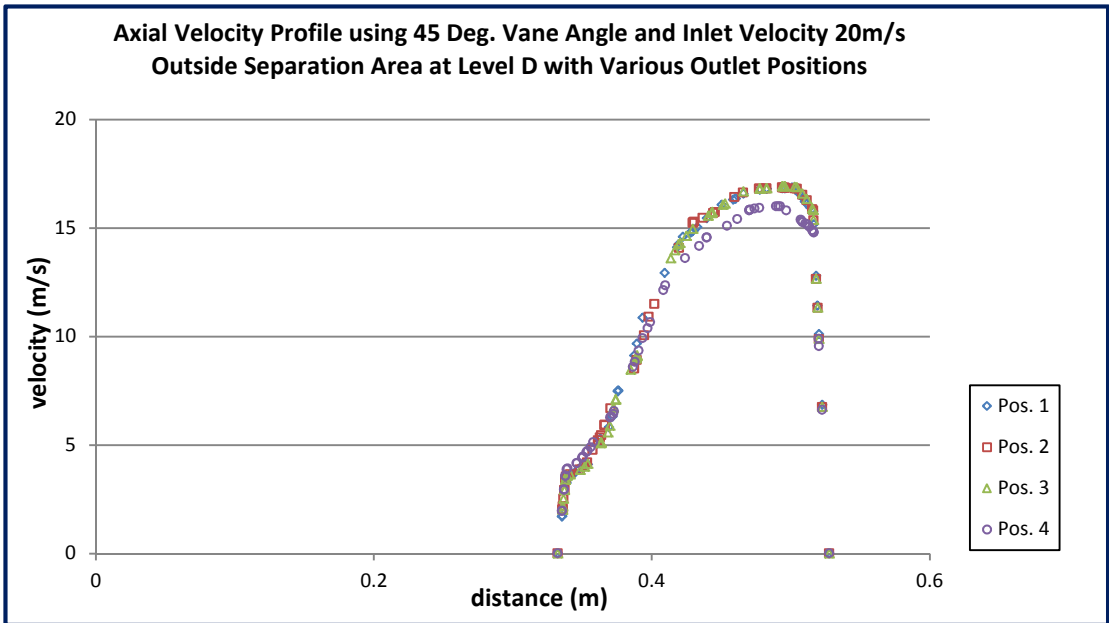
Axial velocity profile outside separation area at Level D for various outlet positions
(30 degrees vane angle, 20m/s inlet velocity)



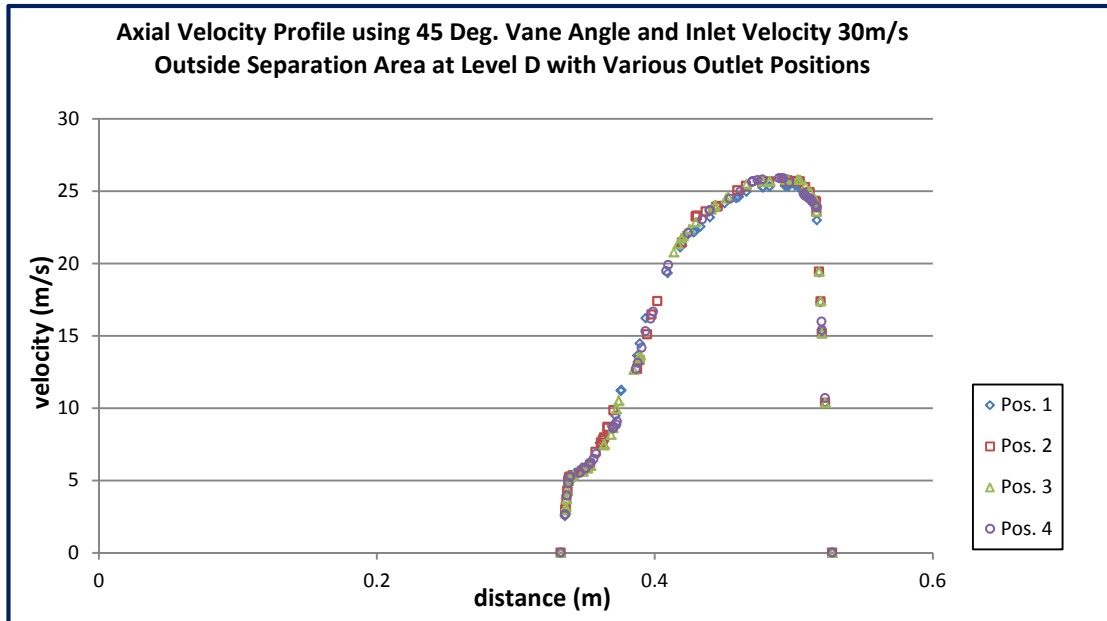
Axial velocity profile outside separation area at Level D for various outlet positions
(30 degrees vane angle, 30m/s inlet velocity)



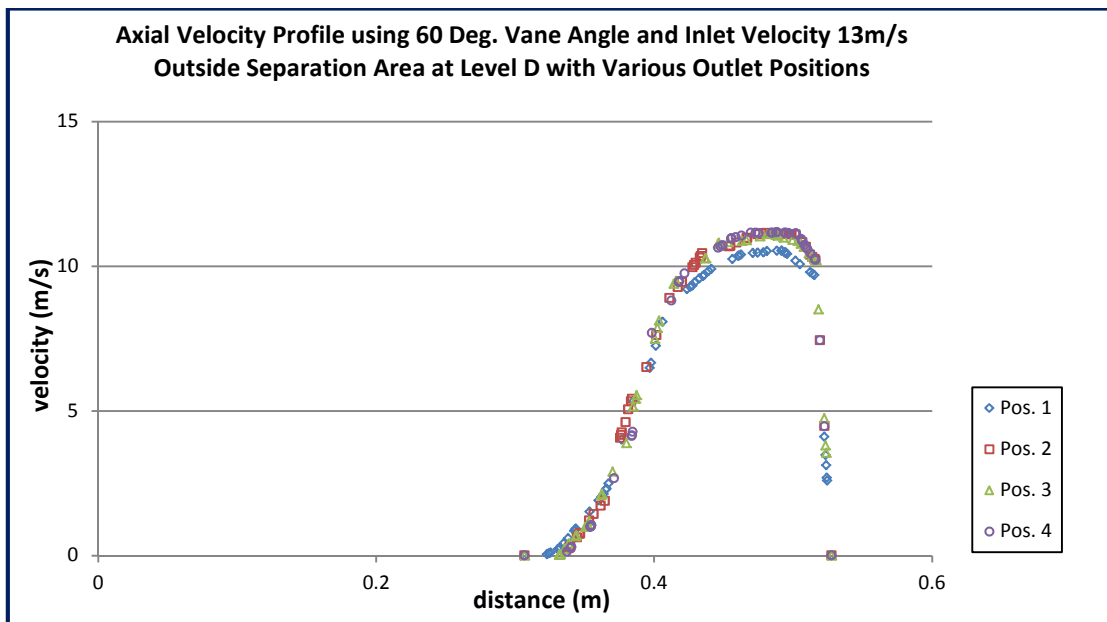
Axial velocity profile outside separation area at Level D for various outlet positions
(45 degrees vane angle, 13m/s inlet velocity)



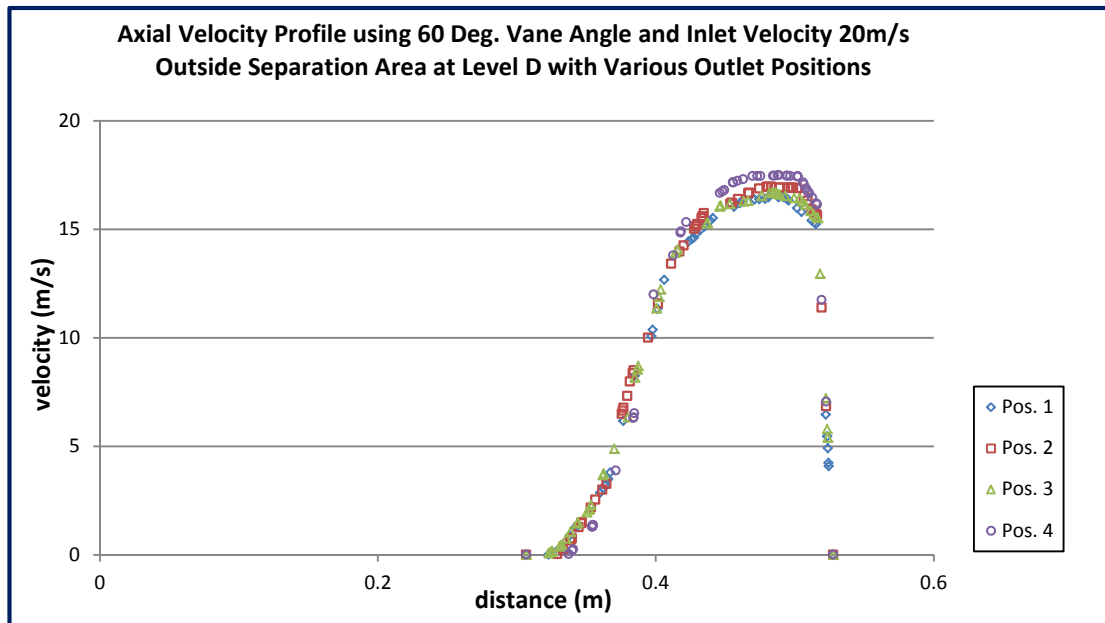
Axial velocity profile outside separation area at Level D for various outlet positions
(45 degrees vane angle, 20m/s inlet velocity)



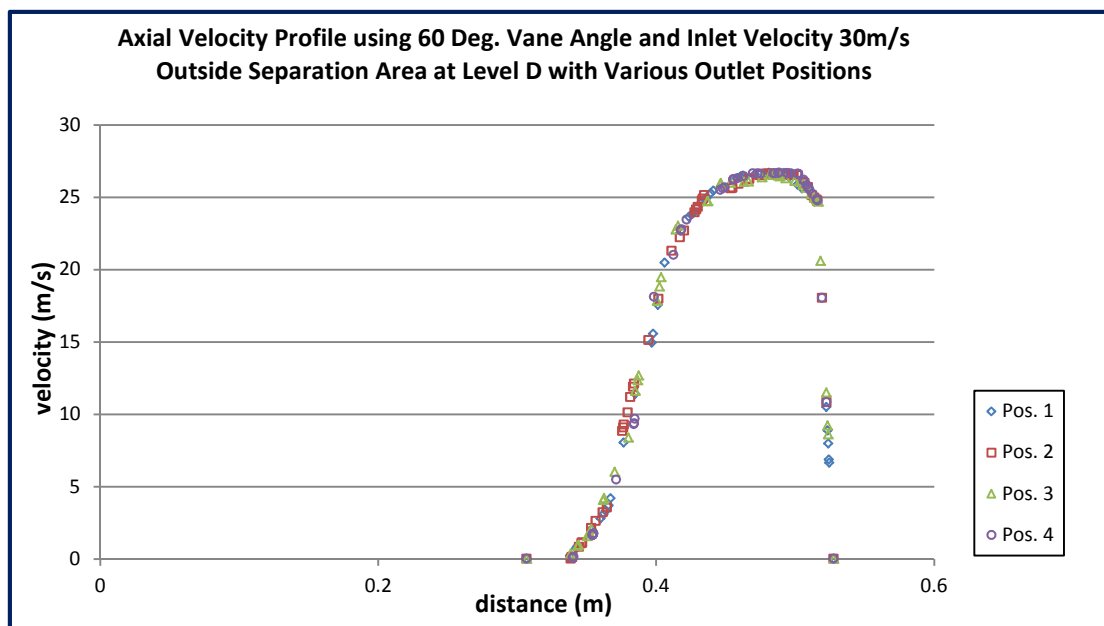
Axial velocity profile outside separation area at Level D for various outlet positions
(45 degrees vane angle, 30m/s inlet velocity)



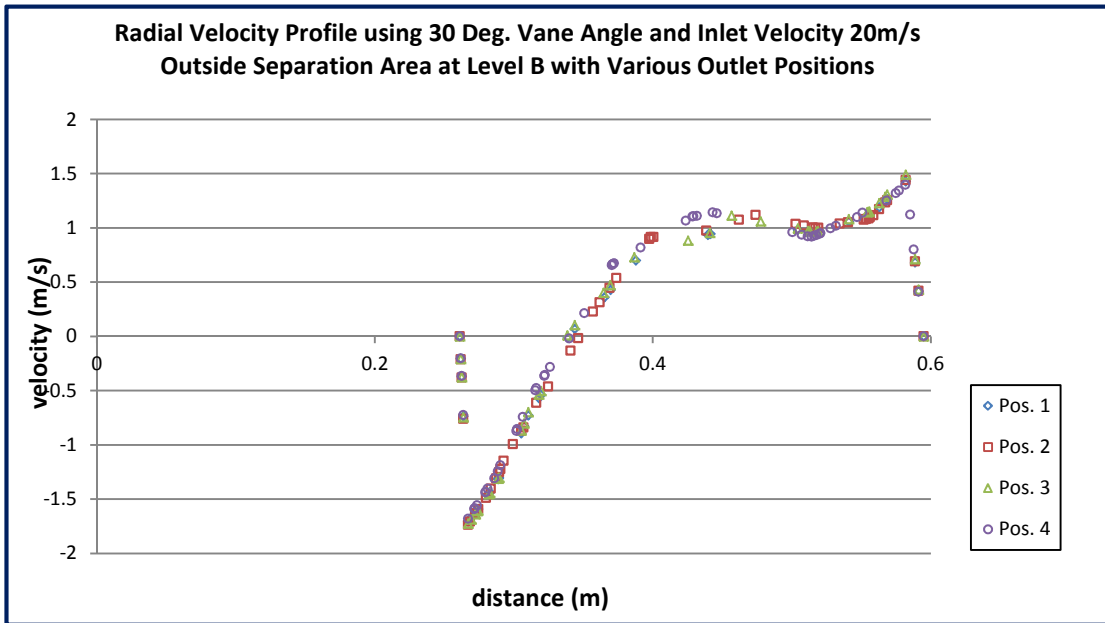
Axial velocity profile outside separation area at Level D for various outlet positions
(60 degrees vane angle, 13m/s inlet velocity)



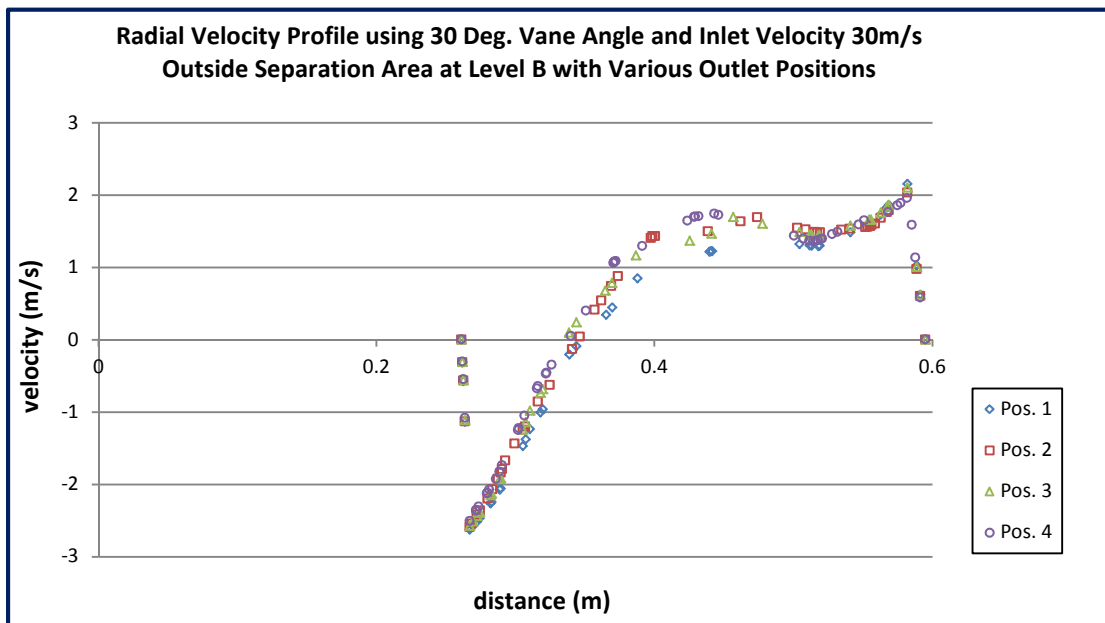
Axial velocity profile outside separation area at Level D for various outlet positions
(60 degrees vane angle, 20m/s inlet velocity)



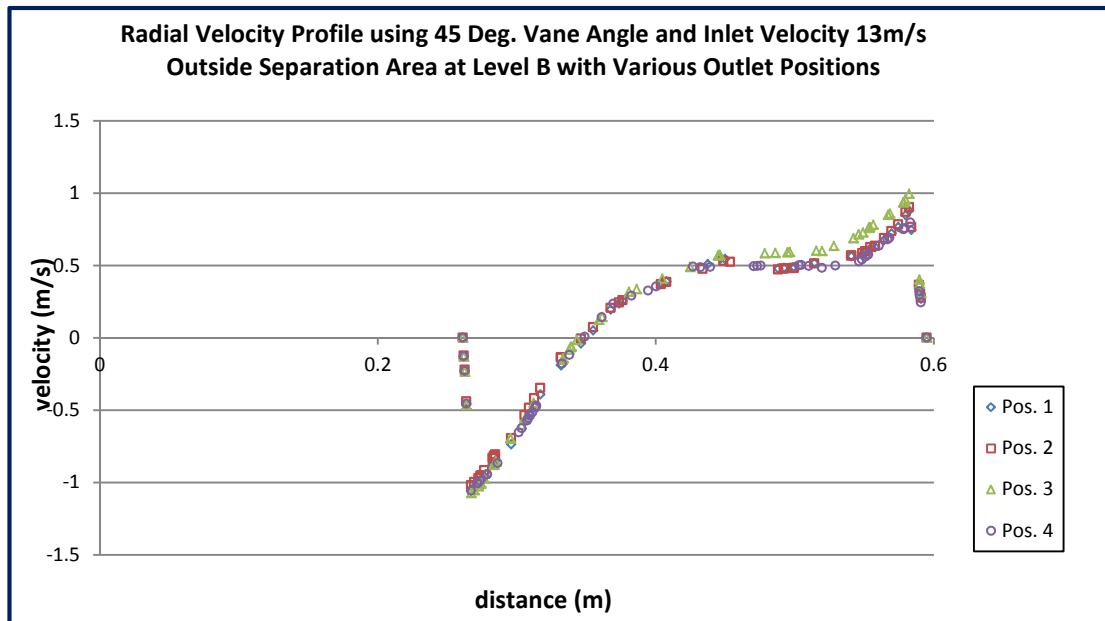
Axial velocity profile outside separation area at Level D for various outlet positions
(60 degrees vane angle, 30m/s inlet velocity)



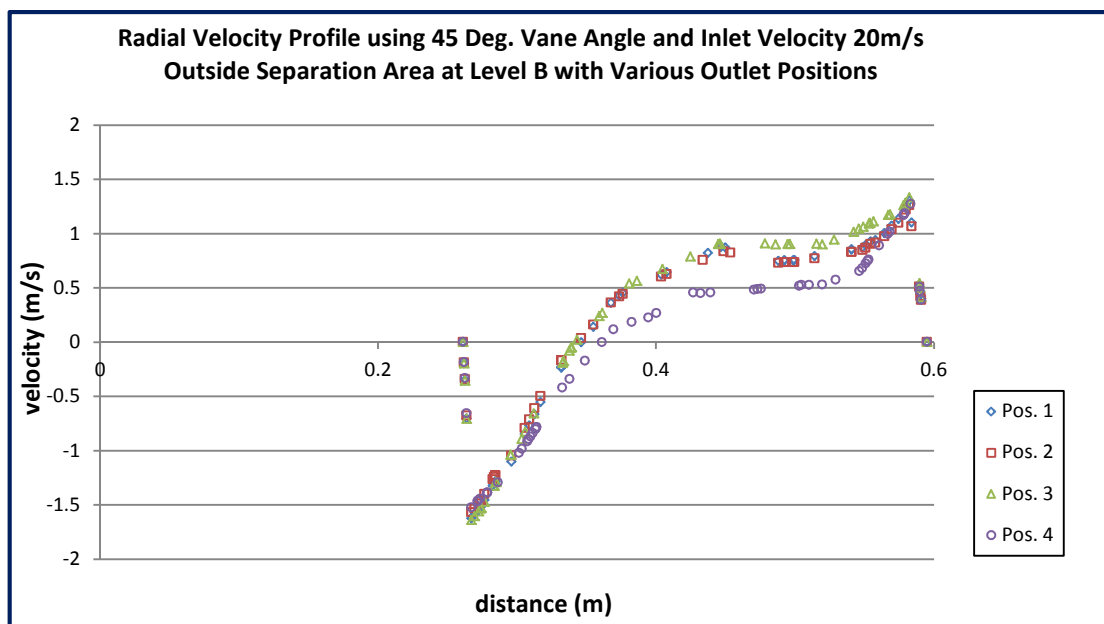
Radial velocity profile outside separation area at Level B for various outlet positions
(30 degrees vane angle, 20m/s inlet velocity)



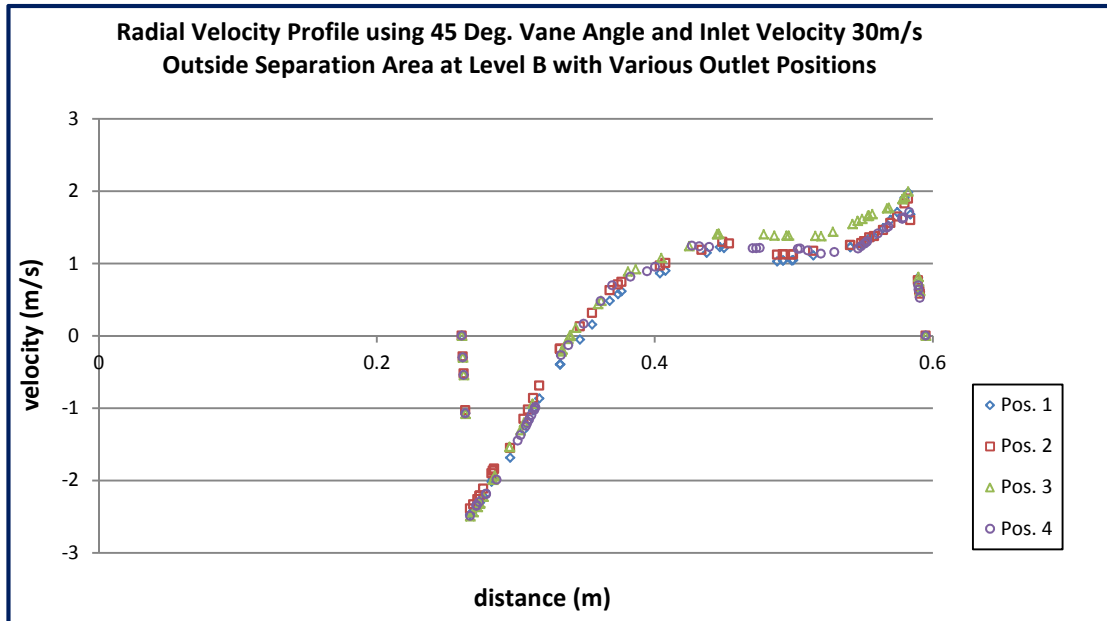
Radial velocity profile outside separation area at Level B for various outlet positions
(30 degrees vane angle, 30m/s inlet velocity)



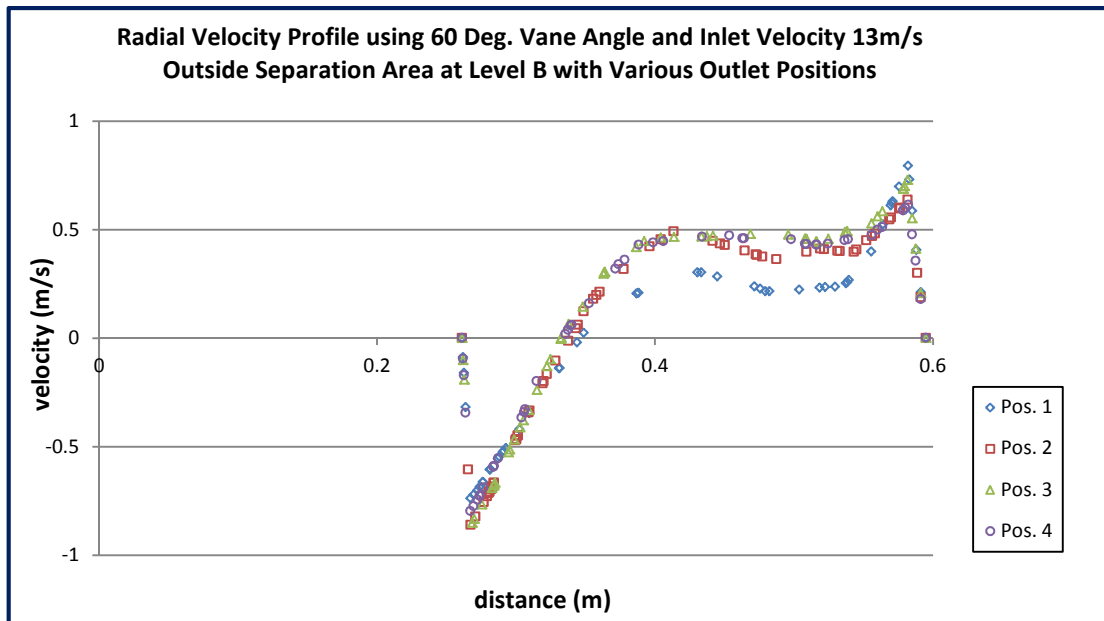
Radial velocity profile outside separation area at Level B for various outlet positions (45 degrees vane angle, 13m/s inlet velocity)



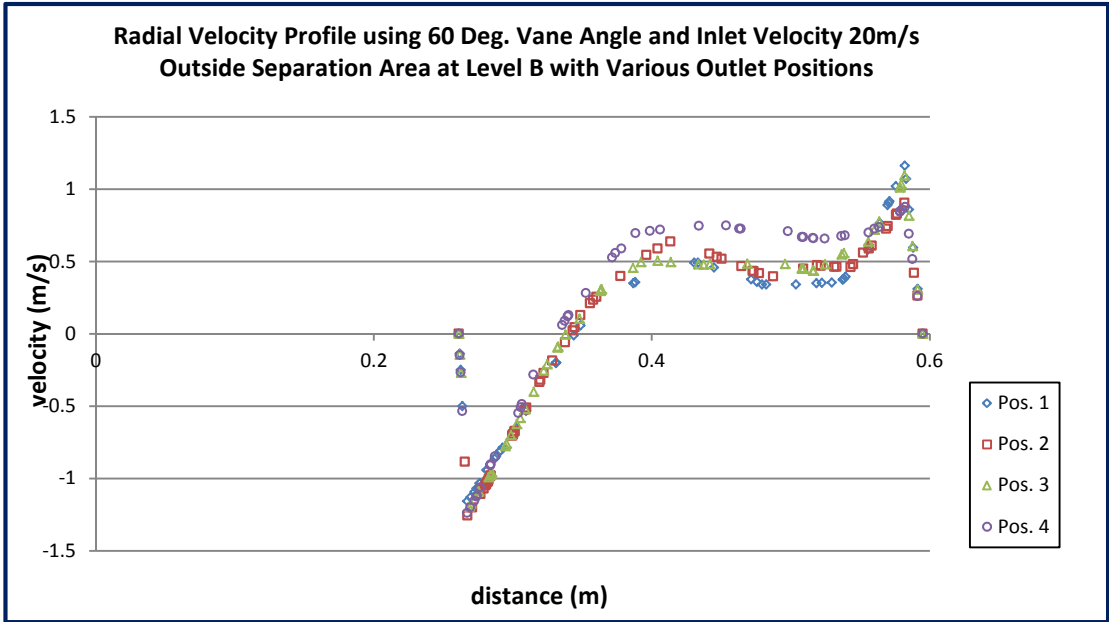
Radial velocity profile outside separation area at Level B for various outlet positions (45 degrees vane angle, 20m/s inlet velocity)



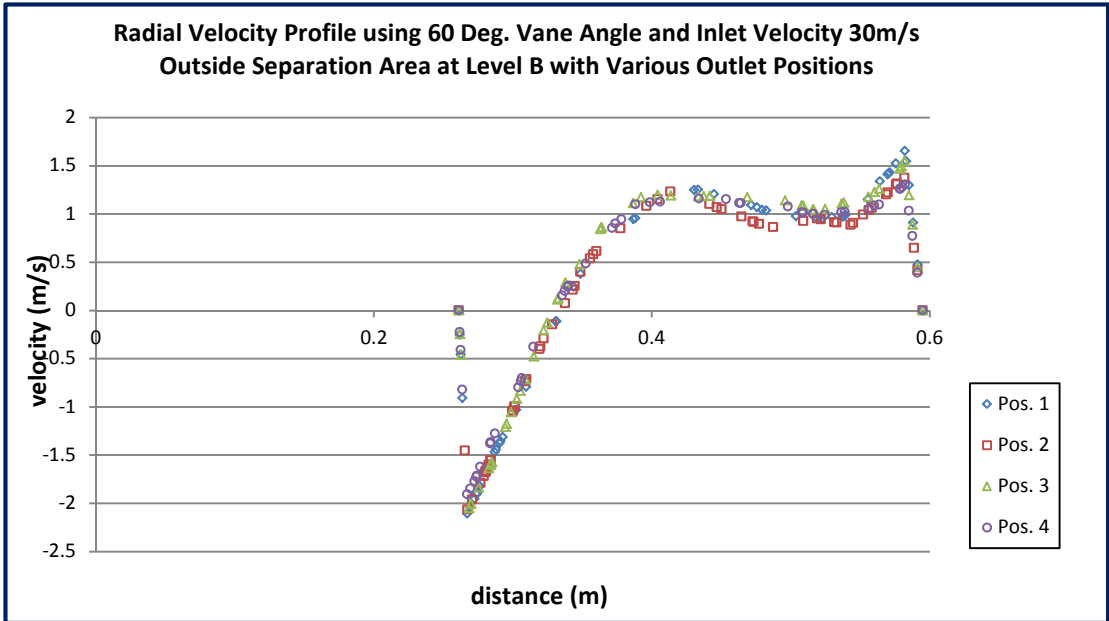
Radial velocity profile outside separation area at Level B for various outlet positions
(45 degrees vane angle, 30m/s inlet velocity)



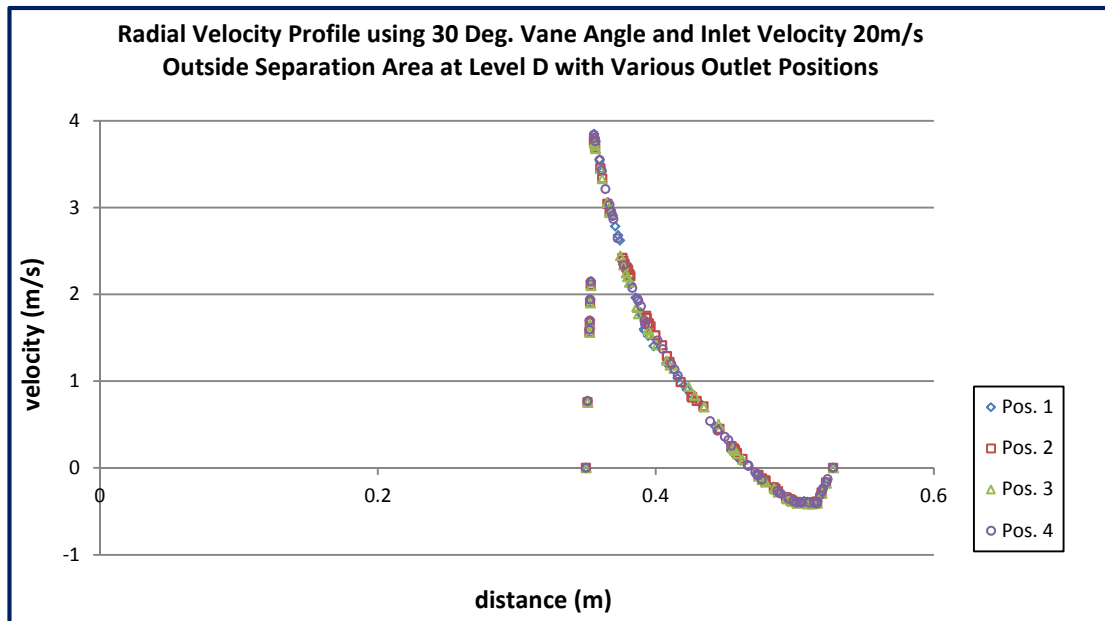
Radial velocity profile outside separation area at Level B for various outlet positions
(60 degrees vane angle, 13m/s inlet velocity)



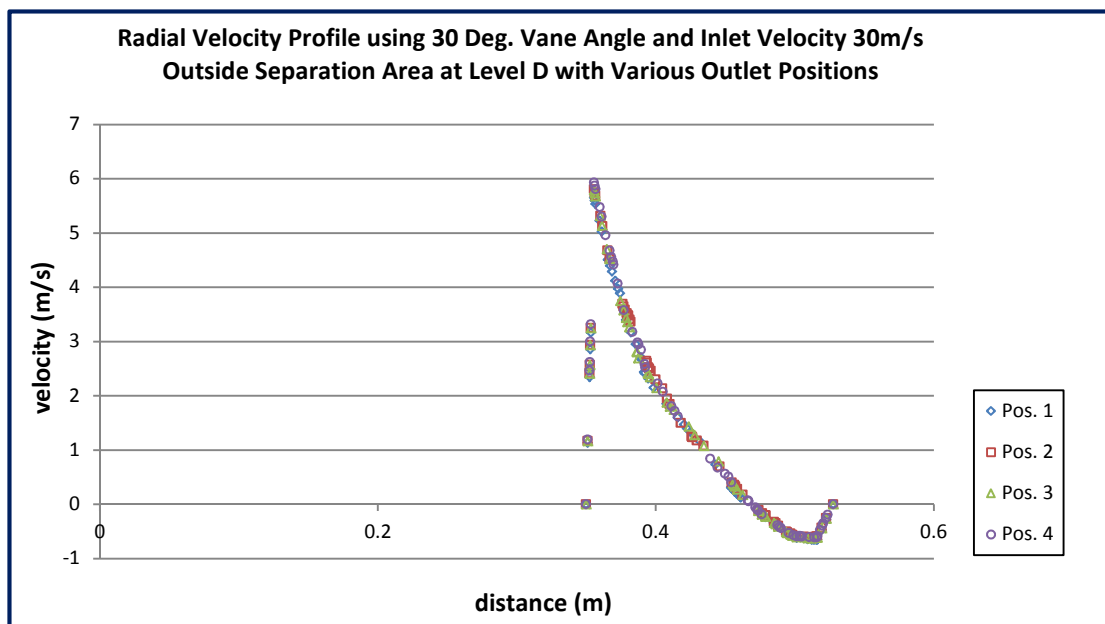
Radial velocity profile outside separation area at Level B for various outlet positions (60 degrees vane angle, 20m/s inlet velocity)



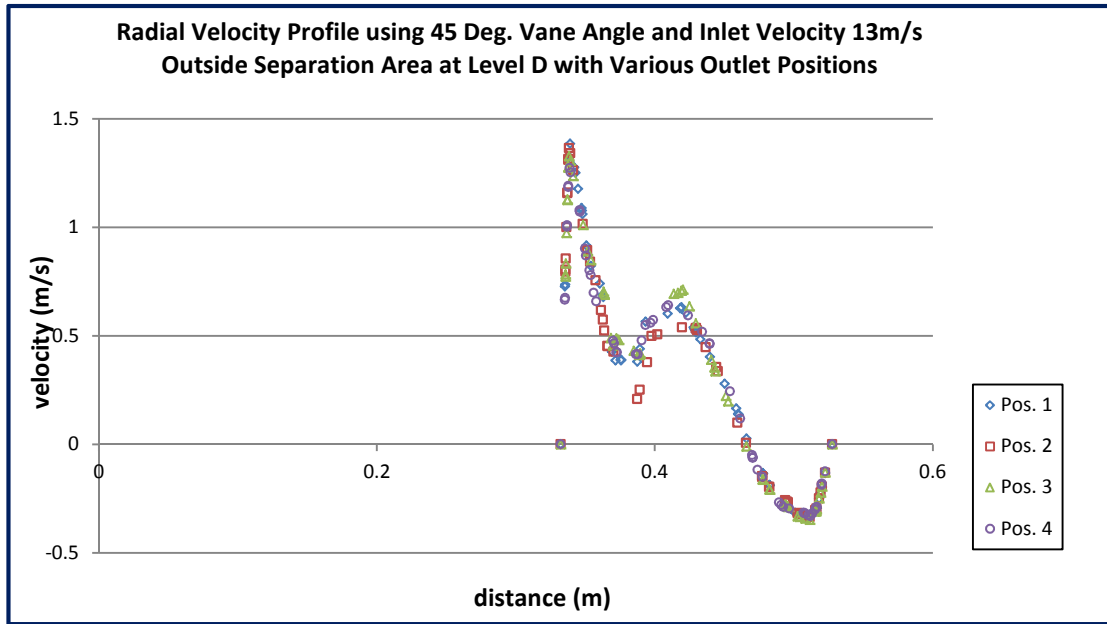
Radial velocity profile outside separation area at Level B for various outlet positions (60 degrees vane angle, 30m/s inlet velocity)



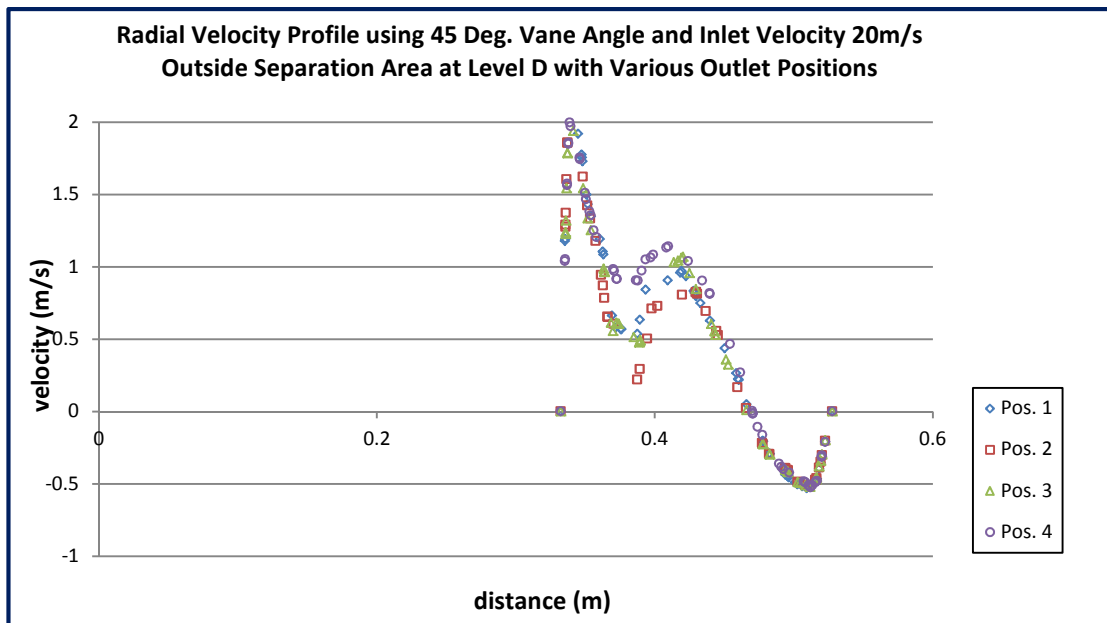
Radial velocity profile outside separation area at Level D for various outlet positions
(30 degrees vane angle, 20m/s inlet velocity)



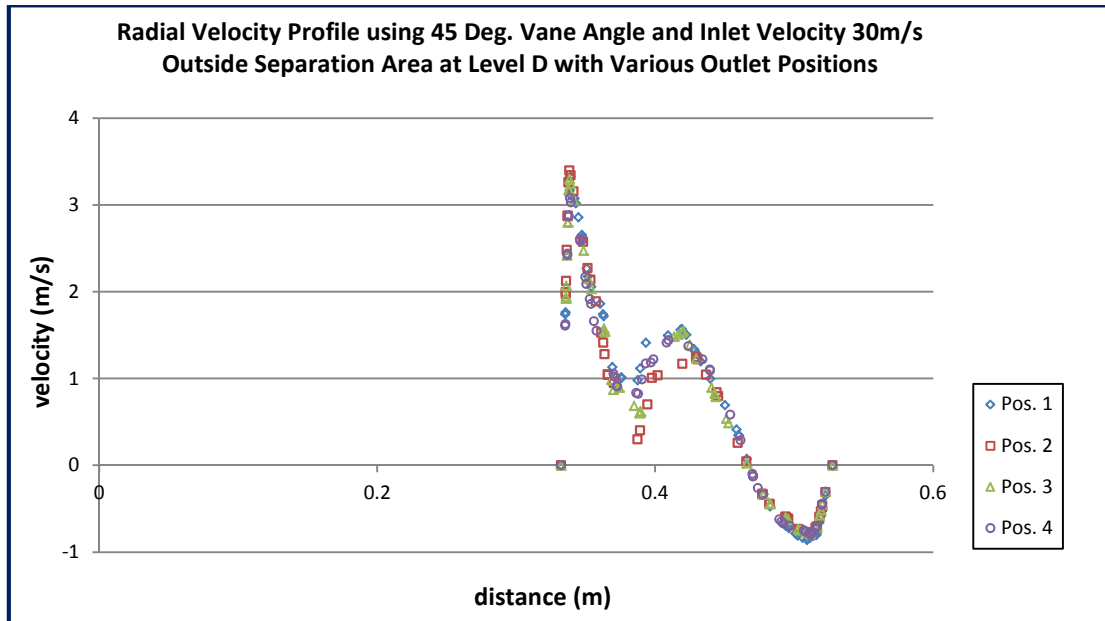
Radial velocity profile outside separation area at Level D for various outlet positions
(30 degrees vane angle, 30m/s inlet velocity)



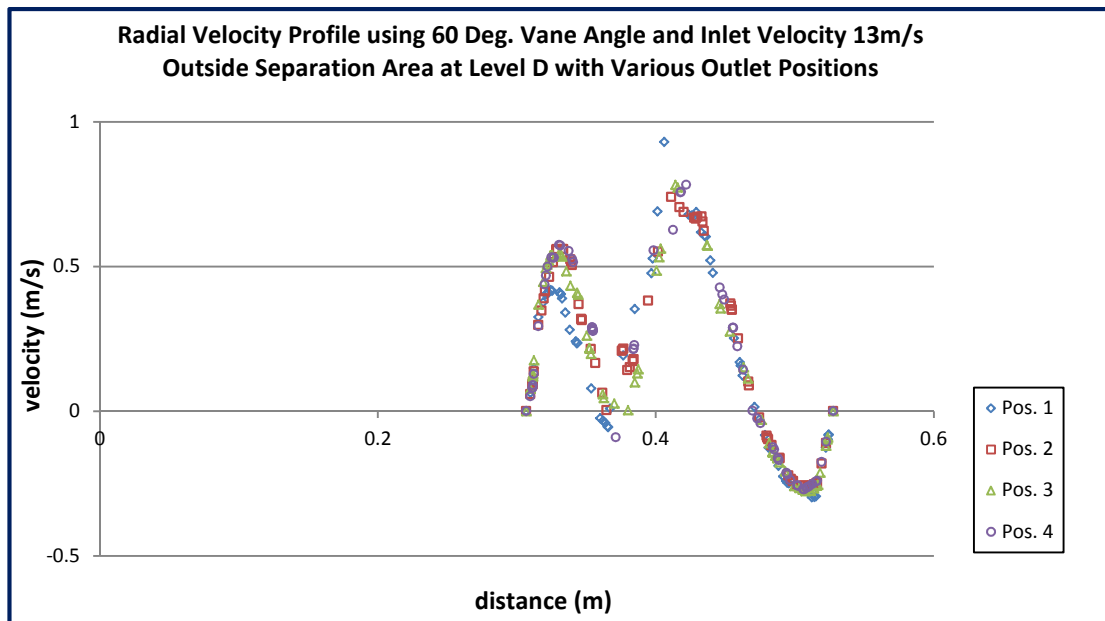
Radial velocity profile outside separation area at Level D for various outlet positions
(45 degrees vane angle, 13m/s inlet velocity)



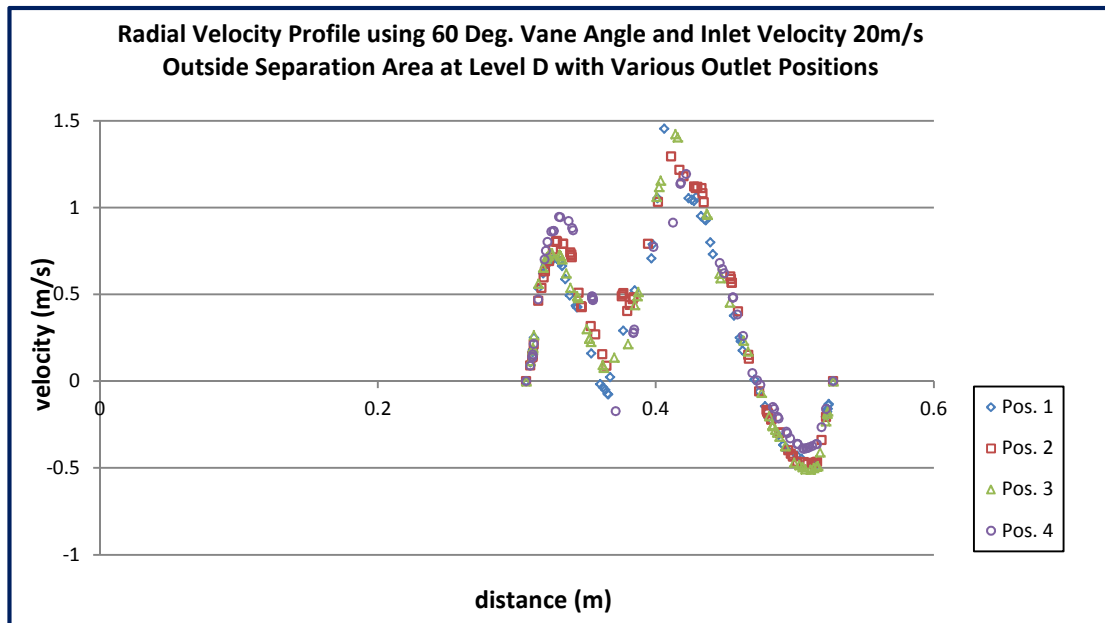
Radial velocity profile outside separation area at Level D for various outlet positions
(45 degrees vane angle, 20m/s inlet velocity)



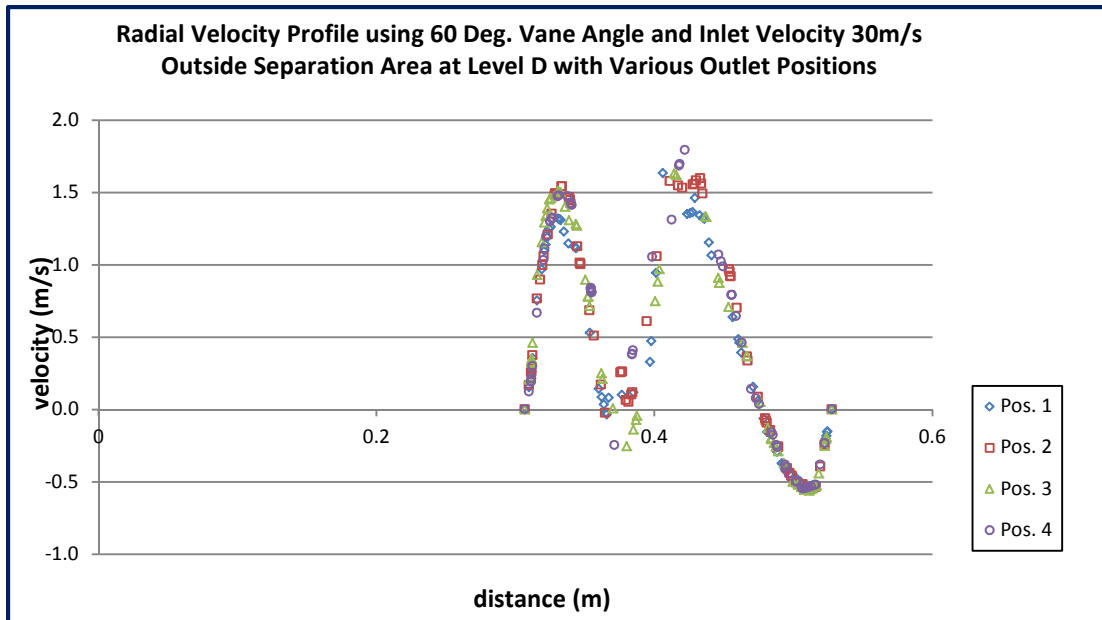
Radial velocity profile outside separation area at Level D for various outlet positions (45 degrees vane angle, 30m/s inlet velocity)



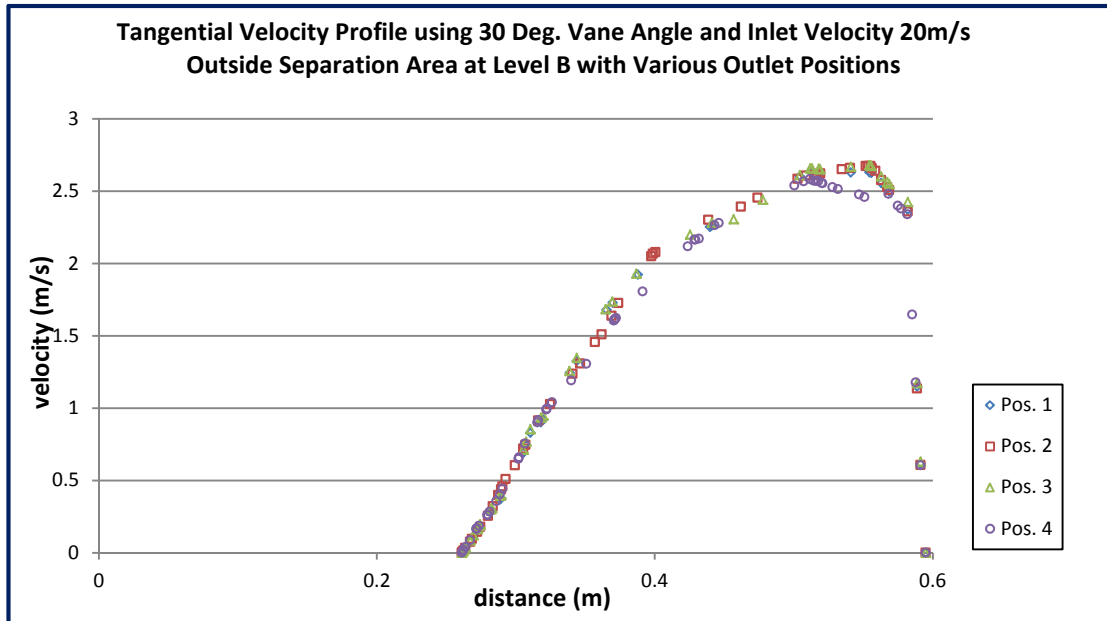
Radial velocity profile outside separation area at Level D for various outlet positions (60 degrees vane angle, 13m/s inlet velocity)



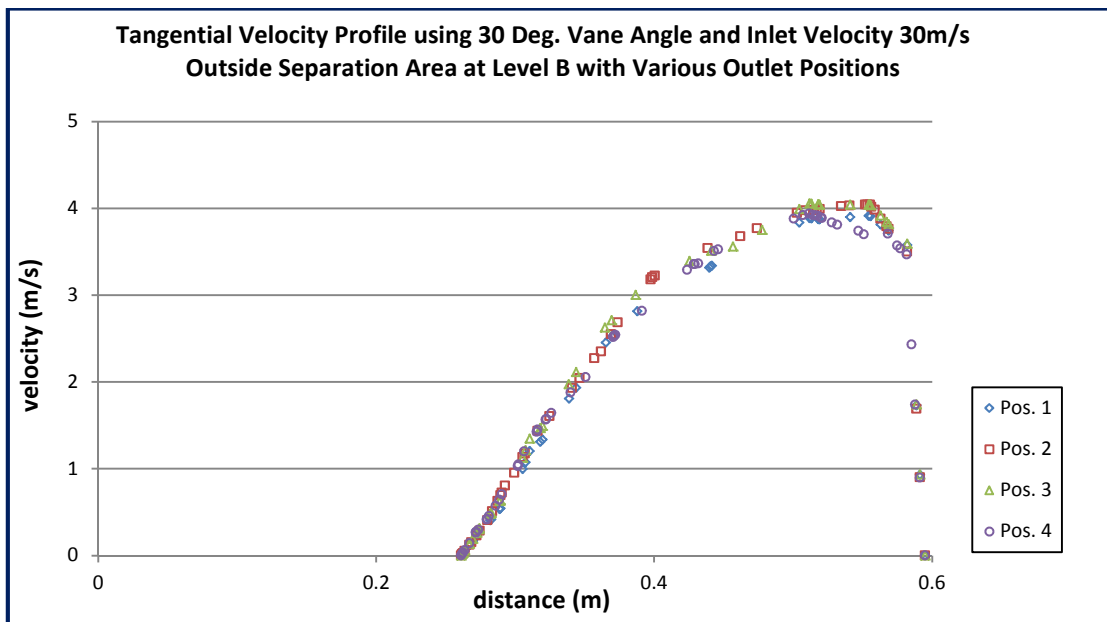
Radial velocity profile outside separation area at Level D for various outlet positions
(60 degrees vane angle, 20m/s inlet velocity)



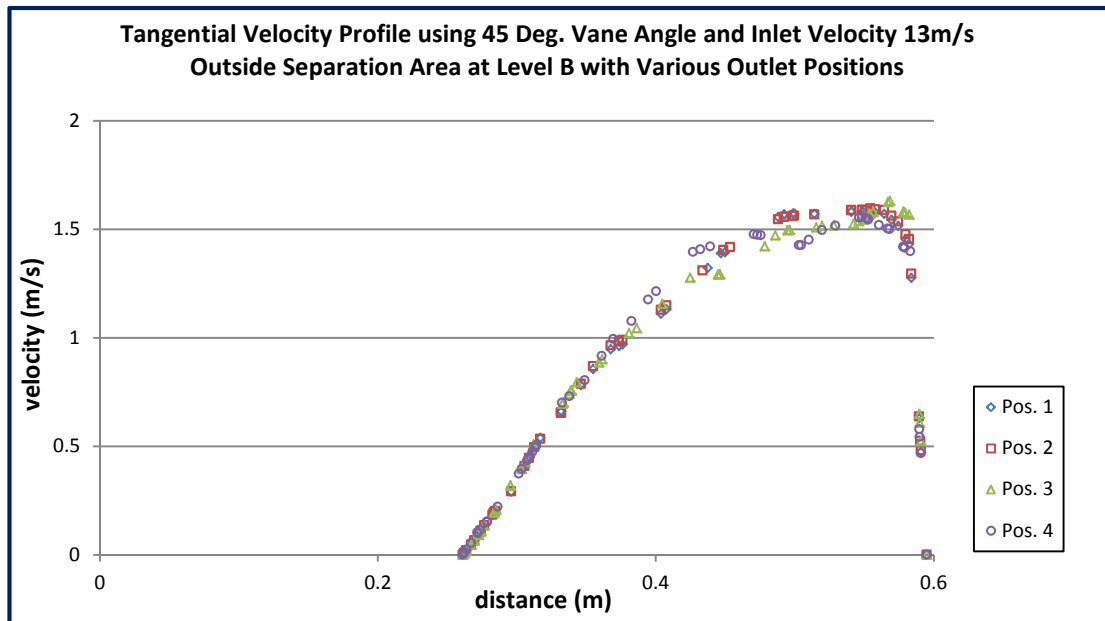
Radial velocity profile outside separation area at Level D for various outlet positions
(60 degrees vane angle, 30m/s inlet velocity)



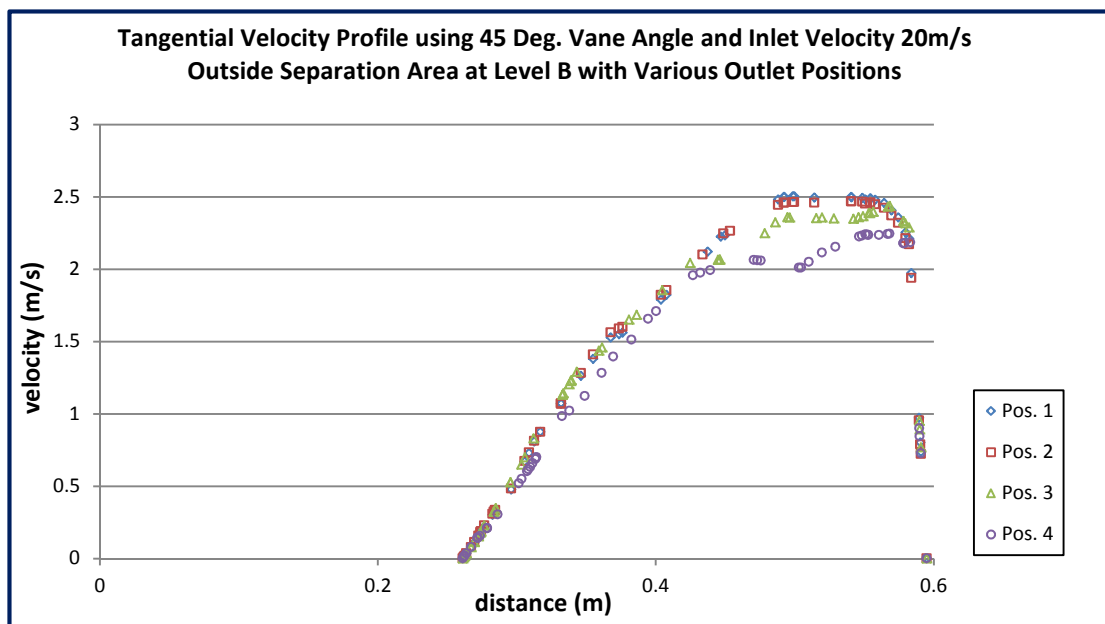
Tangential velocity profile outside separation area at Level B for various outlet positions (30 degrees vane angle, 20m/s inlet velocity)



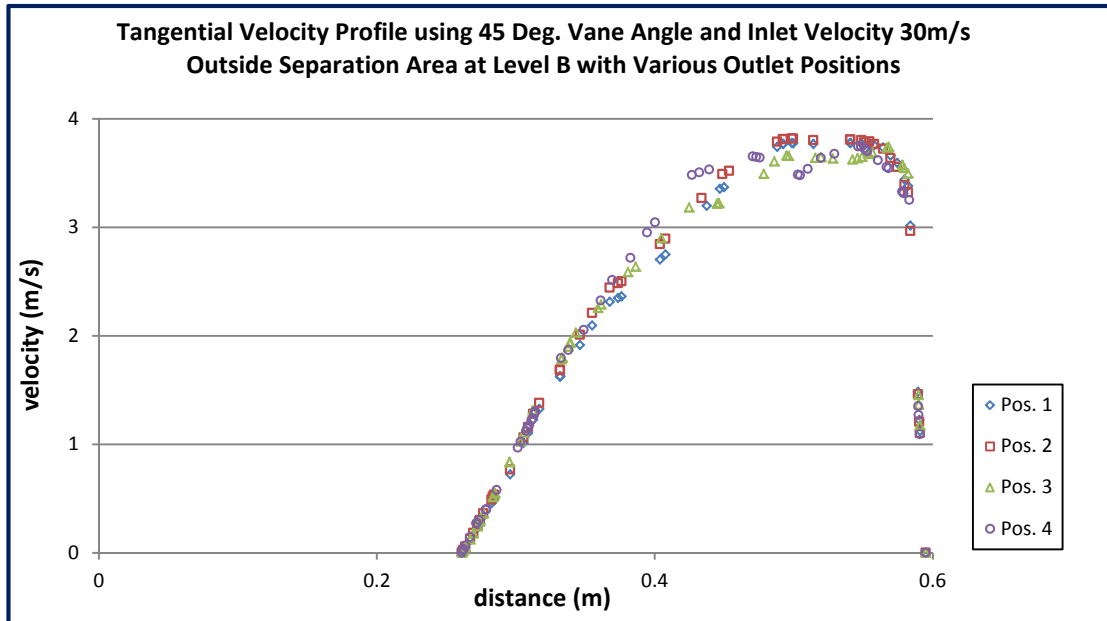
Tangential velocity profile outside separation area at Level B for various outlet positions (30 degrees vane angle, 30m/s inlet velocity)



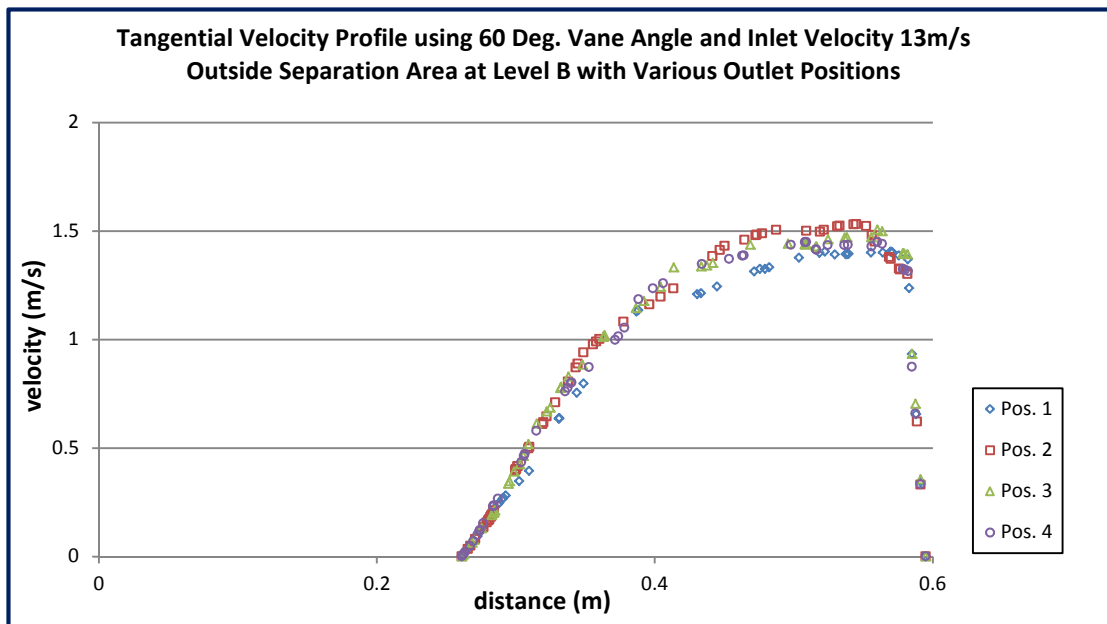
Tangential velocity profile outside separation area at Level B for various outlet positions (45 degrees vane angle, 13m/s inlet velocity)



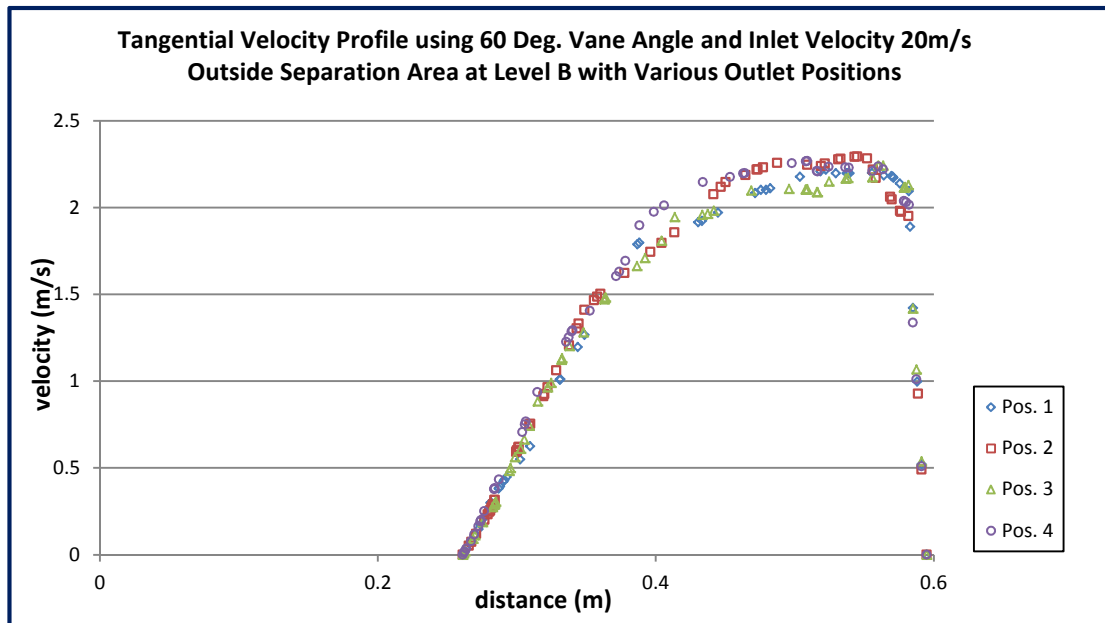
Tangential velocity profile outside separation area at Level B for various outlet positions (45 degrees vane angle, 20m/s inlet velocity)



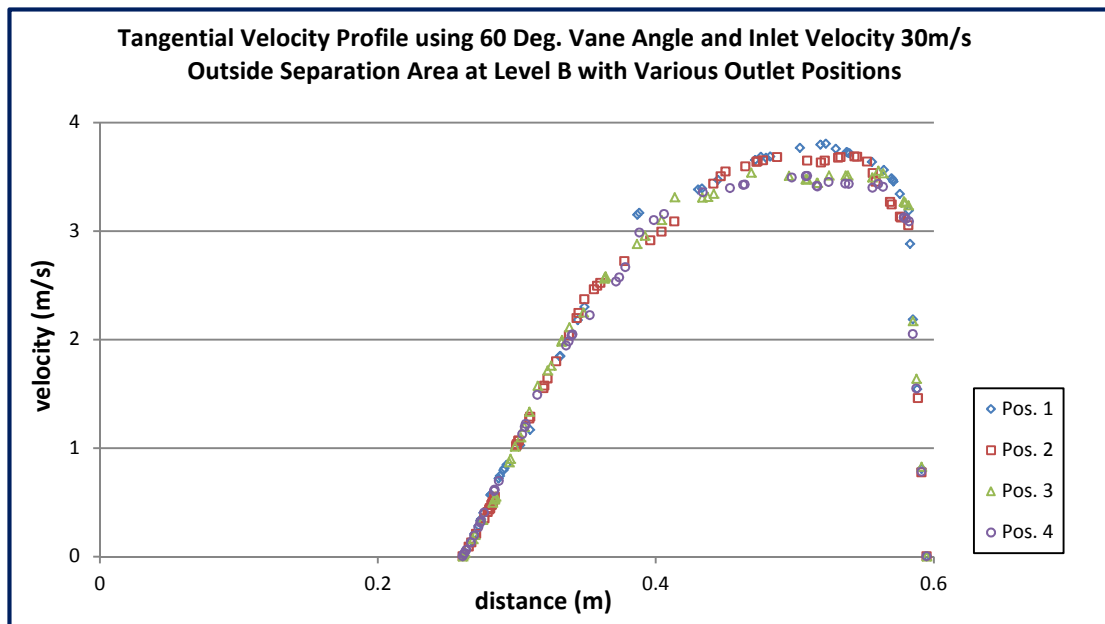
Tangential velocity profile outside separation area at Level B for various outlet positions (45 degrees vane angle, 30m/s inlet velocity)



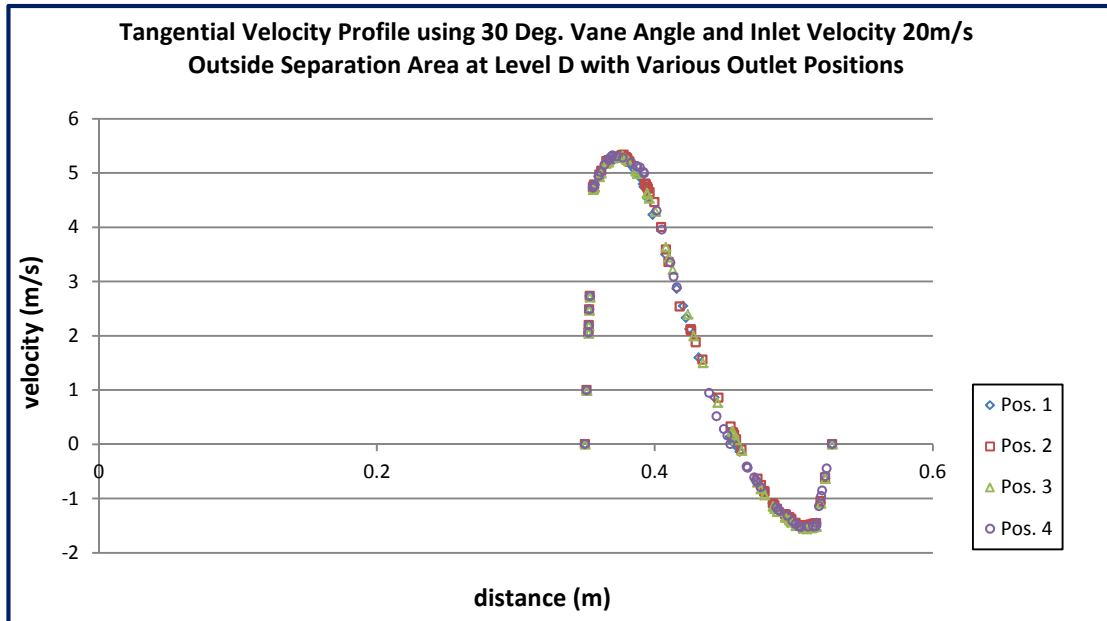
Tangential velocity profile outside separation area at Level B for various outlet positions (60 degrees vane angle, 13m/s inlet velocity)



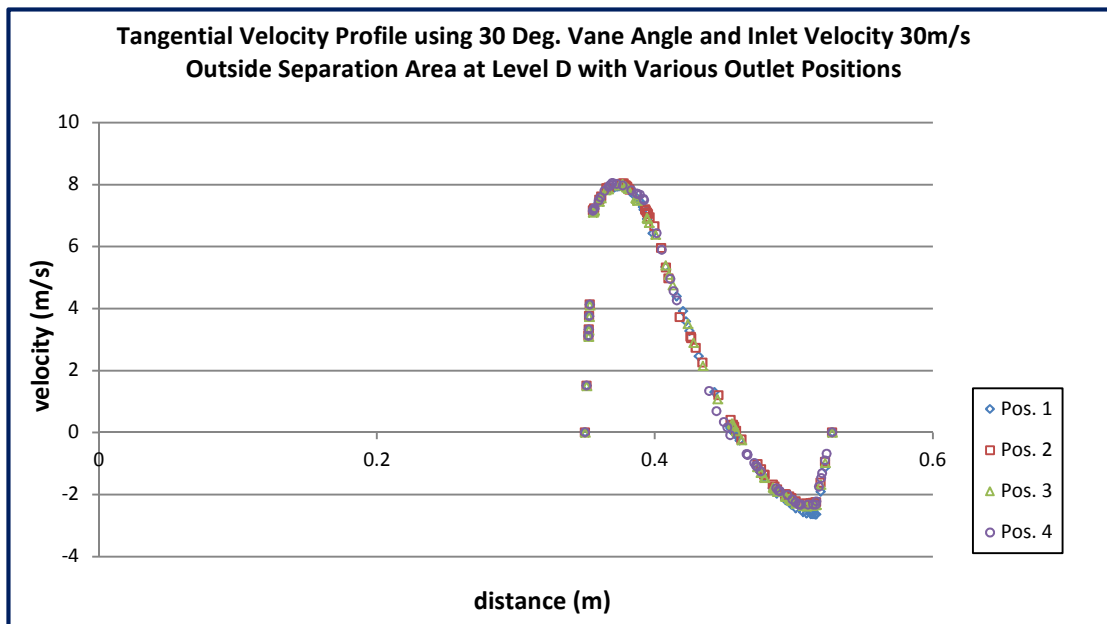
Tangential velocity profile outside separation area at Level B for various outlet positions (60 degrees vane angle, 20m/s inlet velocity)



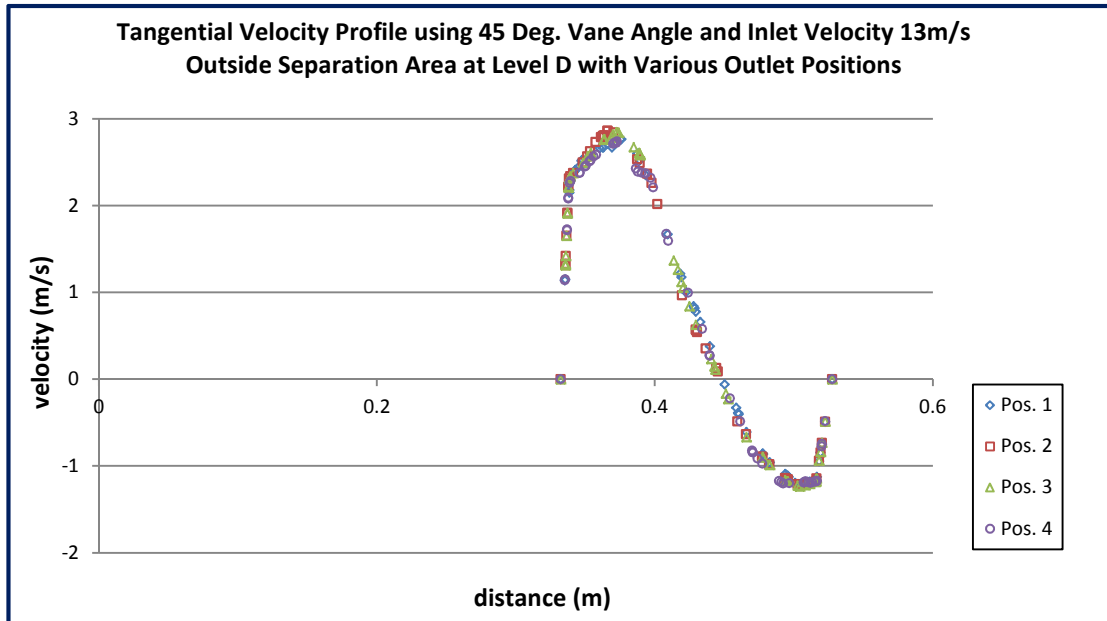
Tangential velocity profile outside separation area at Level B for various outlet positions (60 degrees vane angle, 30m/s inlet velocity)



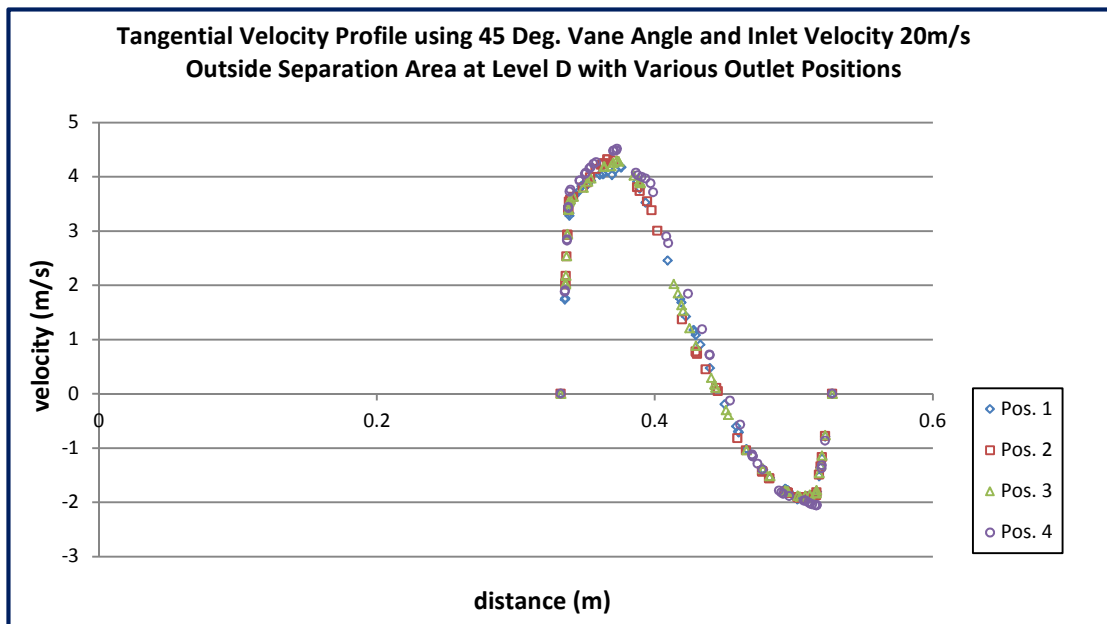
Tangential velocity profile outside separation area at Level D for various outlet positions (30 degrees vane angle, 20m/s inlet velocity)



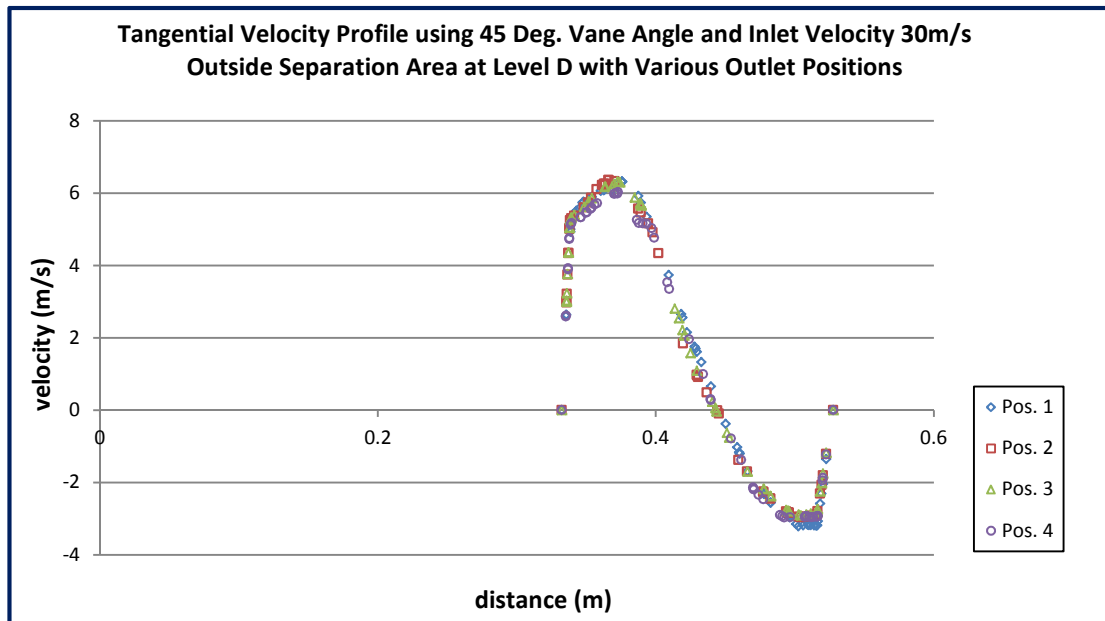
Tangential velocity profile outside separation area at Level D for various outlet positions (30 degrees vane angle, 30m/s inlet velocity)



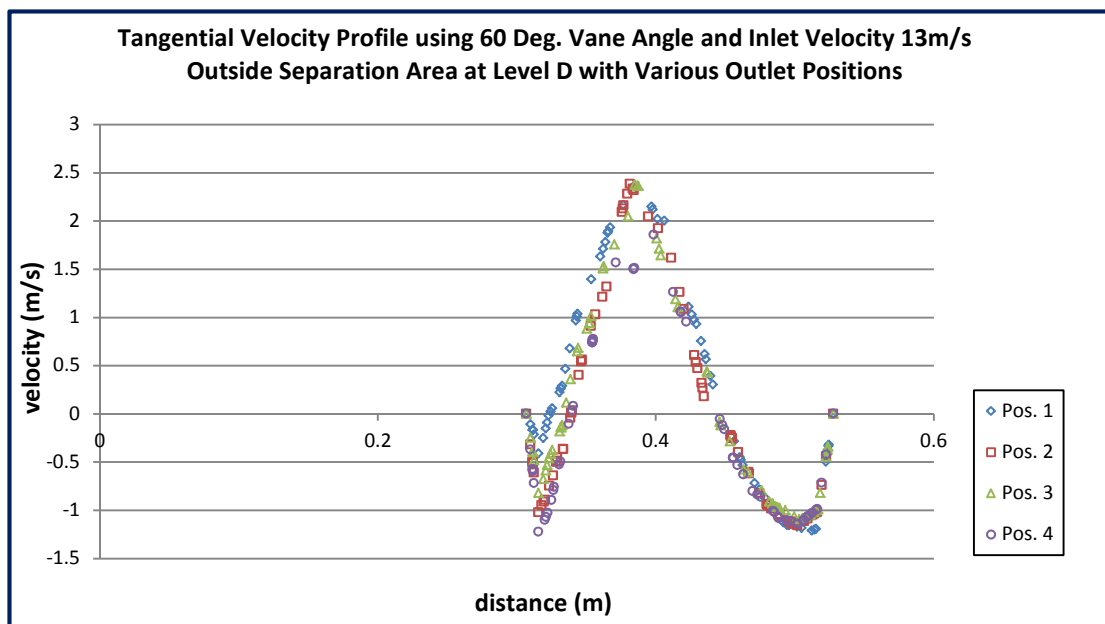
Tangential velocity profile outside separation area at Level D for various outlet positions (45 degrees vane angle, 13m/s inlet velocity)



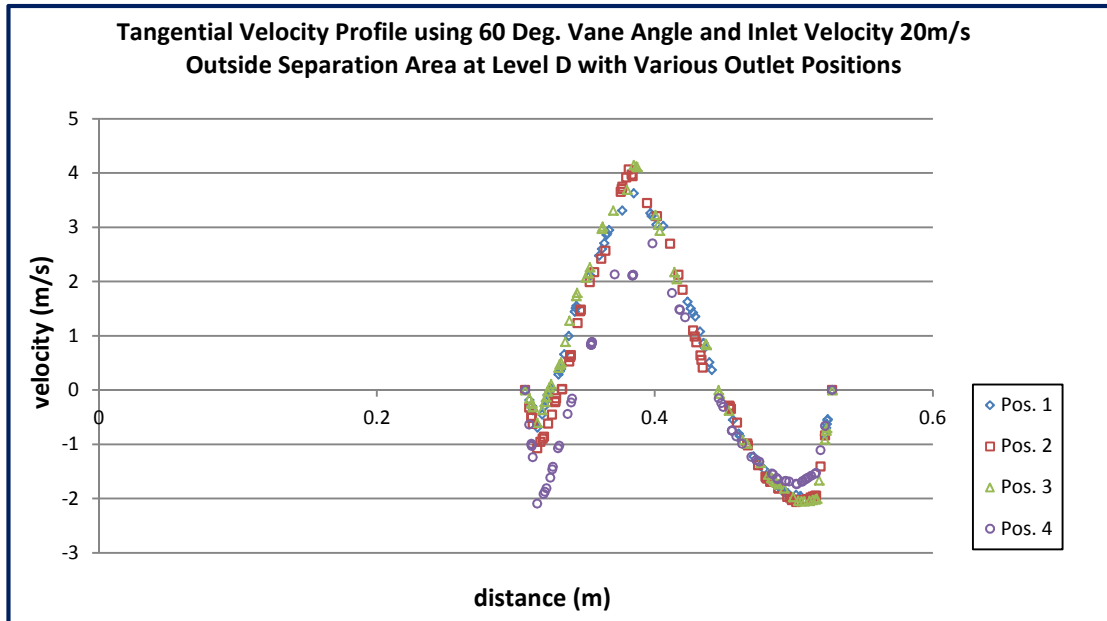
Tangential velocity profile outside separation area at Level D for various outlet positions (45 degrees vane angle, 20m/s inlet velocity)



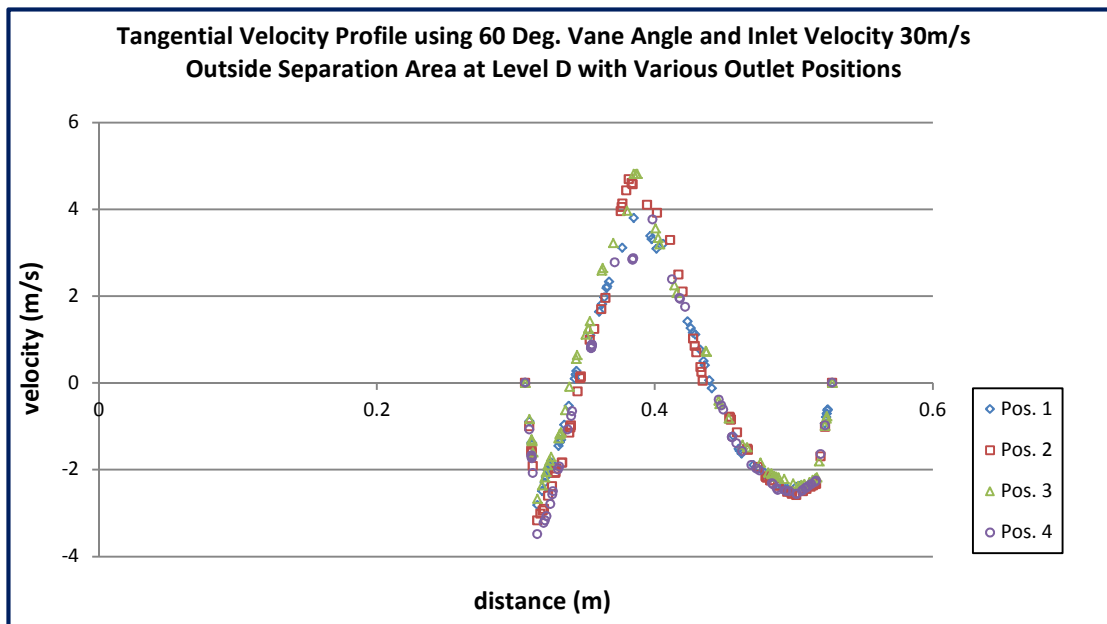
Tangential velocity profile outside separation area at Level D for various outlet positions (45 degrees vane angle, 30m/s inlet velocity)



Tangential velocity profile outside separation area at Level D for various outlet positions (60 degrees vane angle, 13m/s inlet velocity)



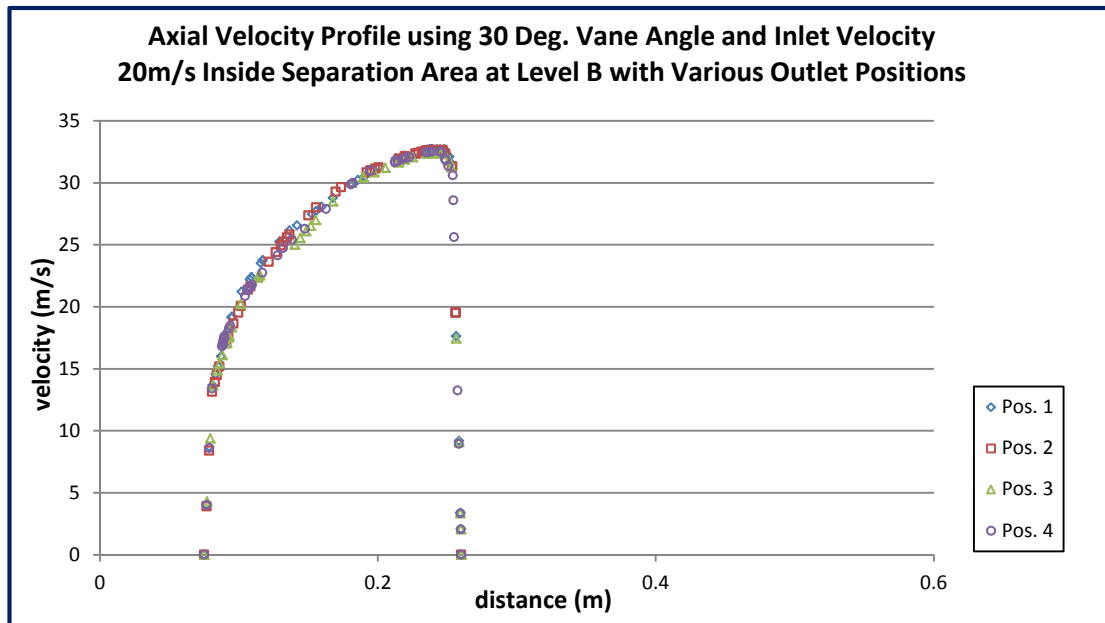
Tangential velocity profile outside separation area at Level D for various outlet positions (60 degrees vane angle, 20m/s inlet velocity)



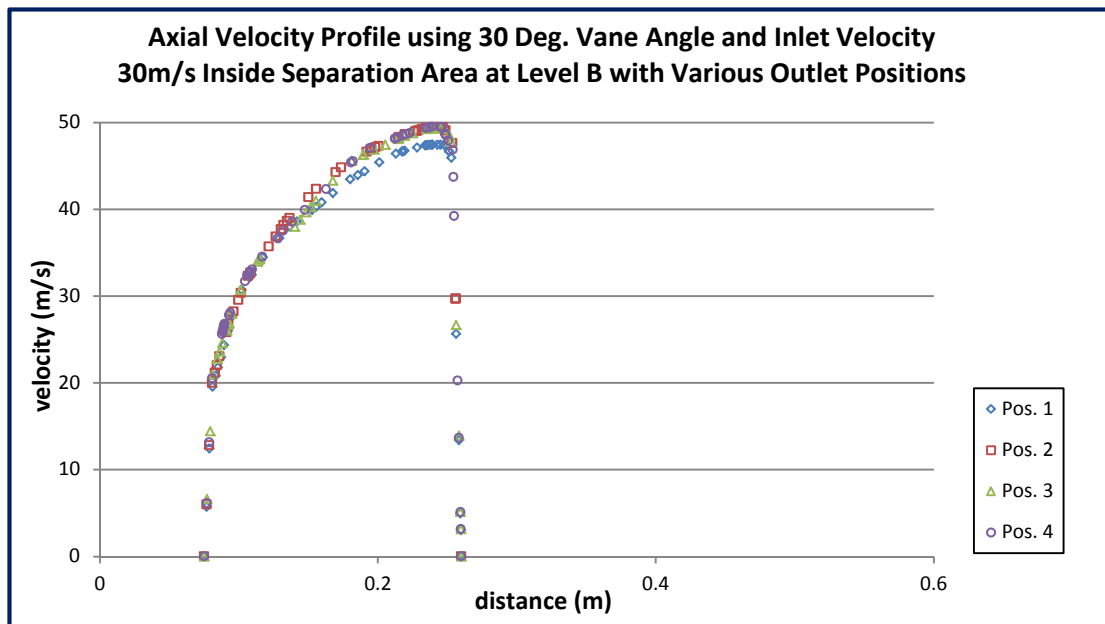
Tangential velocity profile outside separation area at Level D for various outlet positions (60 degrees vane angle, 30m/s inlet velocity)

APPENDIX VI

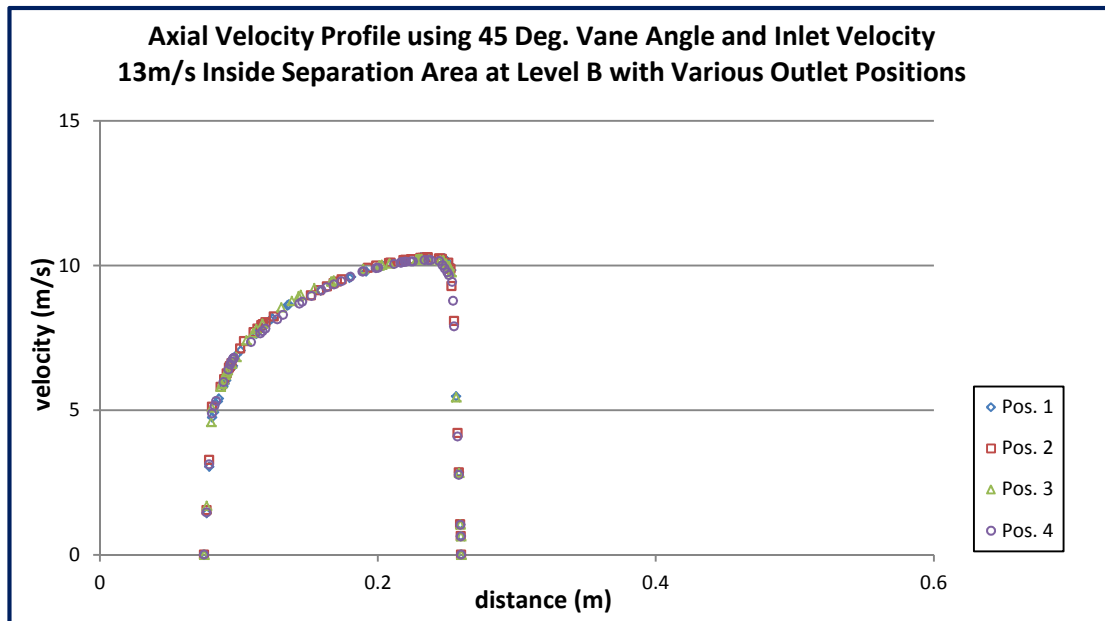
Effects of Varying Outlet Position Inside Separation Area and Vortex Finder



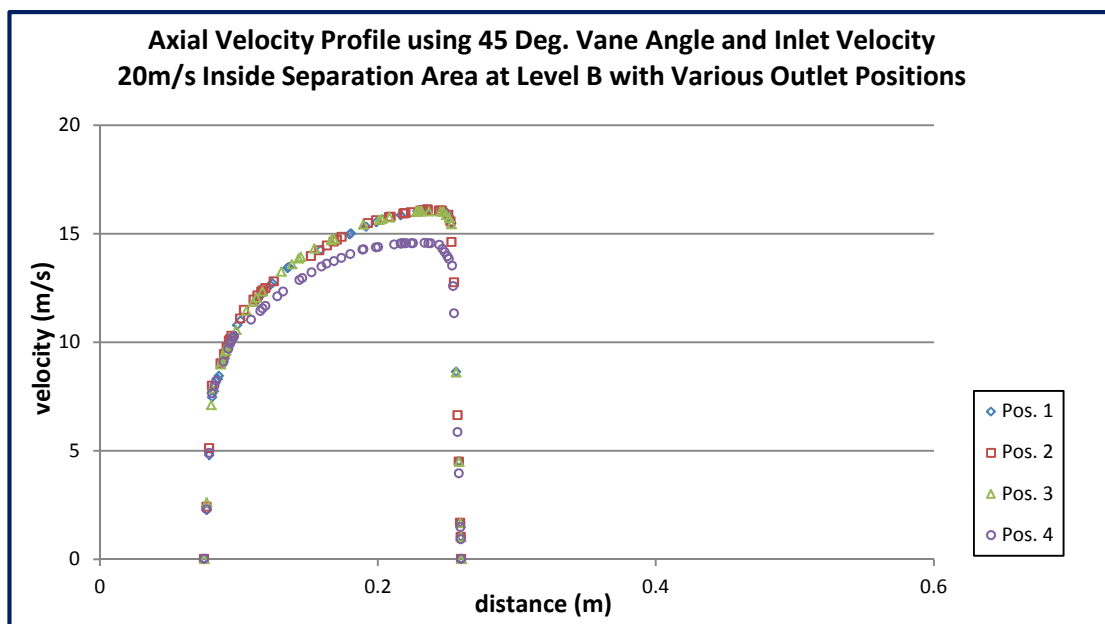
Axial velocity profile inside separation area at Level B for various outlet positions
(30 degrees vane angle, 20m/s inlet velocity)



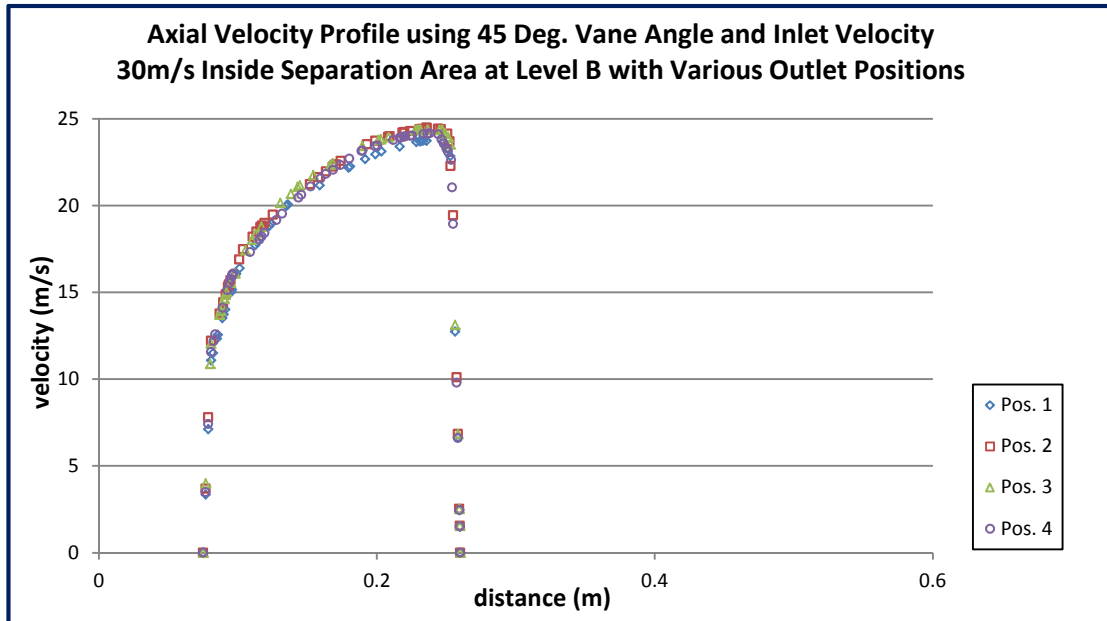
Axial velocity profile inside separation area at Level B for various outlet positions
(30 degrees vane angle, 30m/s inlet velocity)



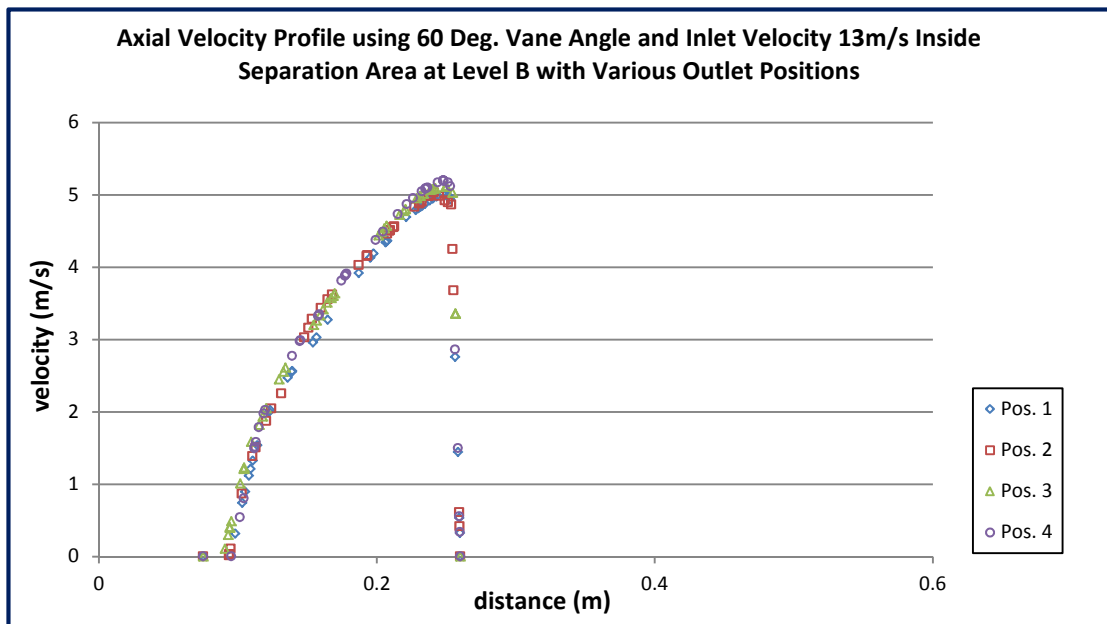
Axial velocity profile inside separation area at Level B for various outlet positions
(45 degrees vane angle, 13m/s inlet velocity)



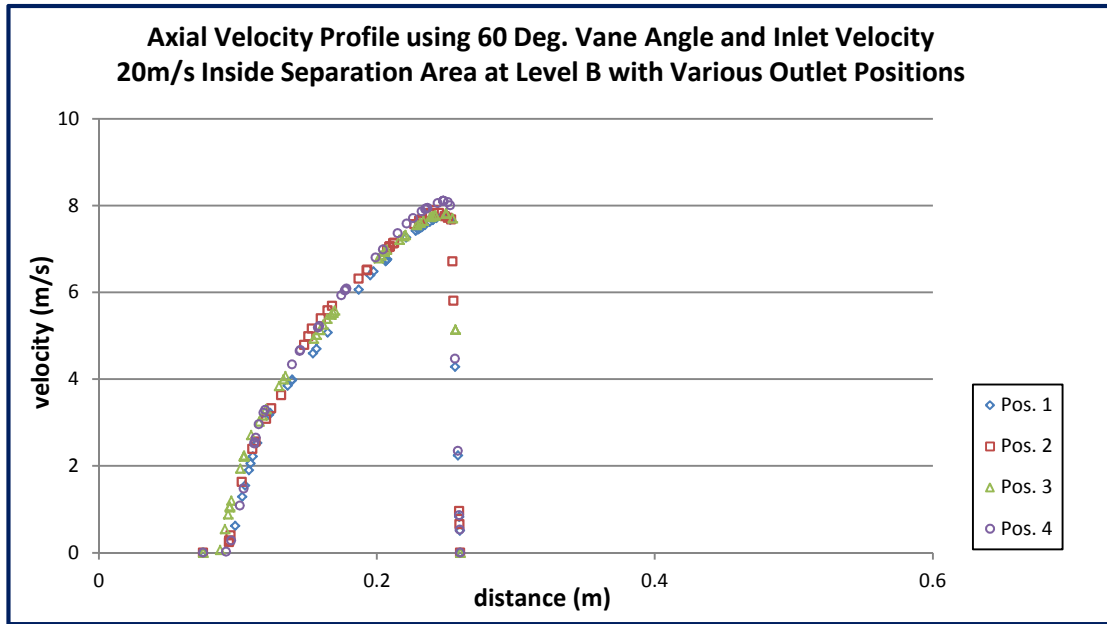
Axial velocity profile inside separation area at Level B for various outlet positions
(45 degrees vane angle, 20m/s inlet velocity)



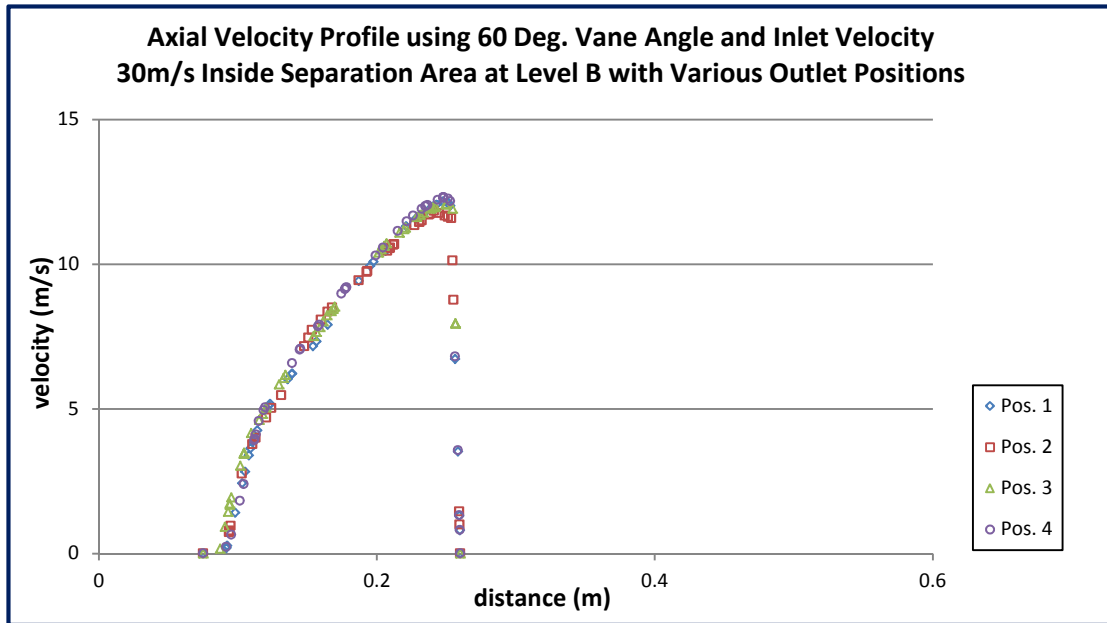
Axial velocity profile inside separation area at Level B for various outlet positions
(45 degrees vane angle, 30m/s inlet velocity)



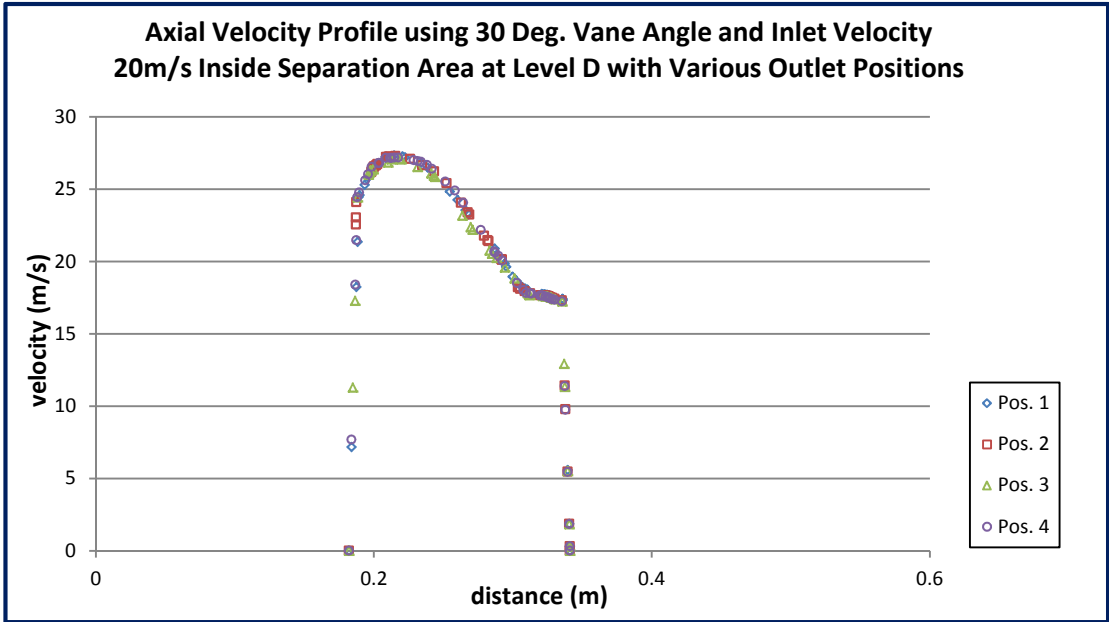
Axial velocity profile inside separation area at Level B for various outlet positions
(60 degrees vane angle, 13m/s inlet velocity)



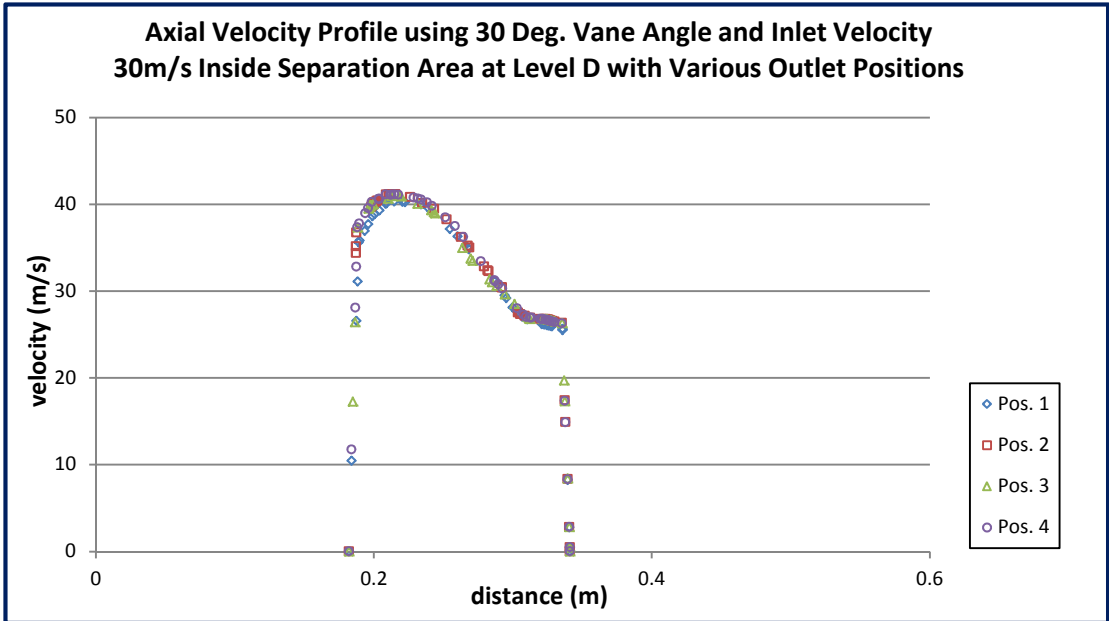
Axial velocity profile inside separation area at Level B for various outlet positions
(60 degrees vane angle, 20m/s inlet velocity)



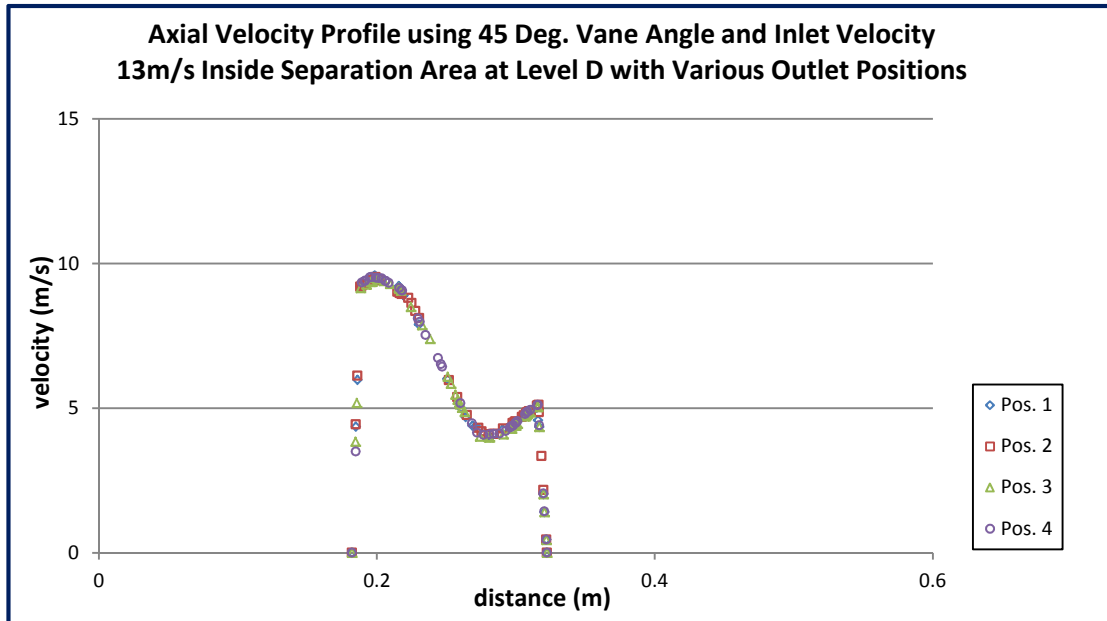
Axial velocity profile inside separation area at Level B for various outlet positions
(60 degrees vane angle, 30m/s inlet velocity)



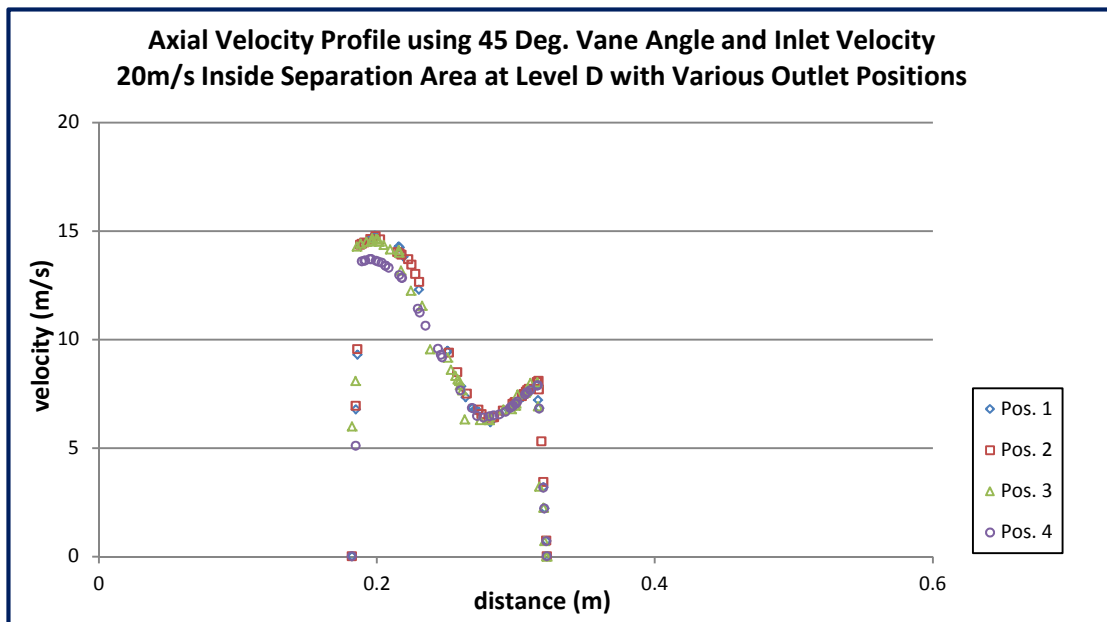
Axial velocity profile inside separation area at Level D for various outlet positions
(30 degrees vane angle, 20m/s inlet velocity)



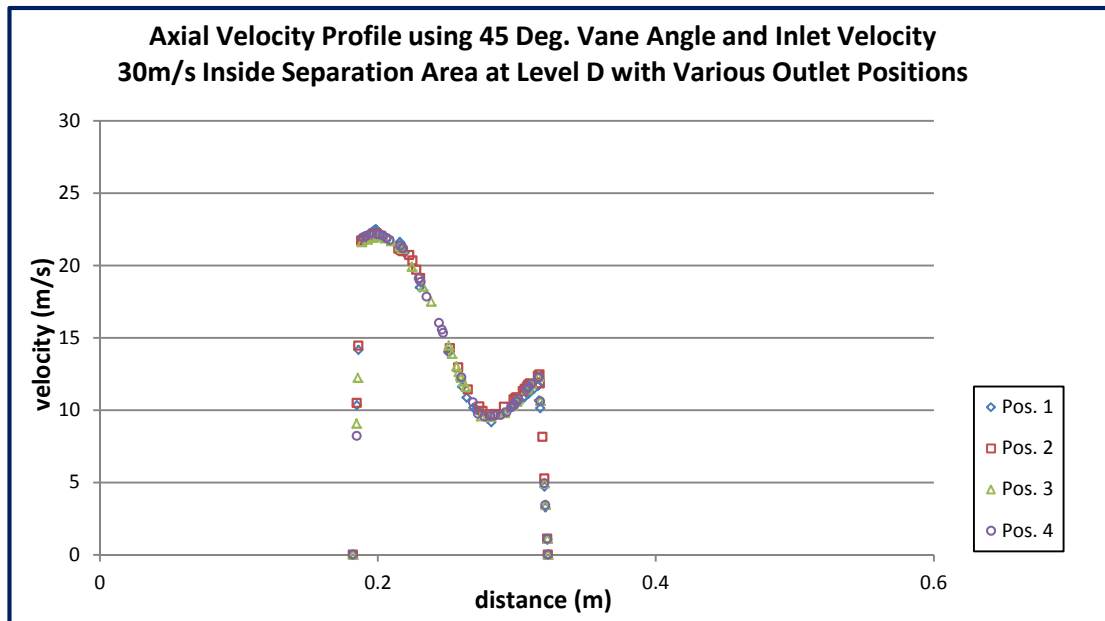
Axial velocity profile inside separation area at Level D for various outlet positions
(30 degrees vane angle, 30m/s inlet velocity)



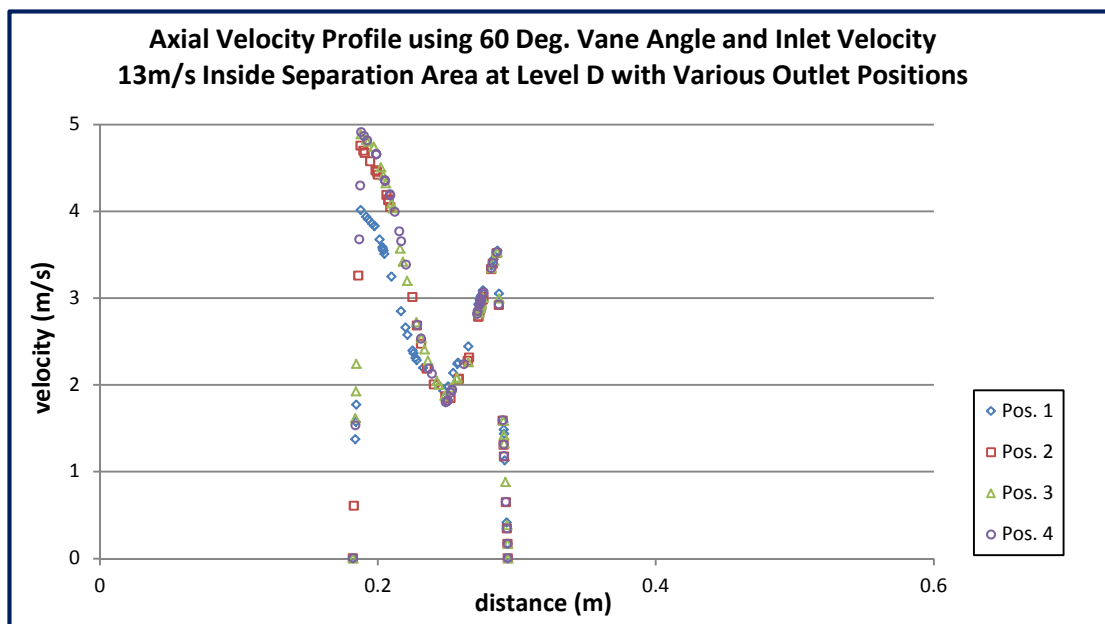
Axial velocity profile inside separation area at Level D for various outlet positions
(45 degrees vane angle, 13m/s inlet velocity)



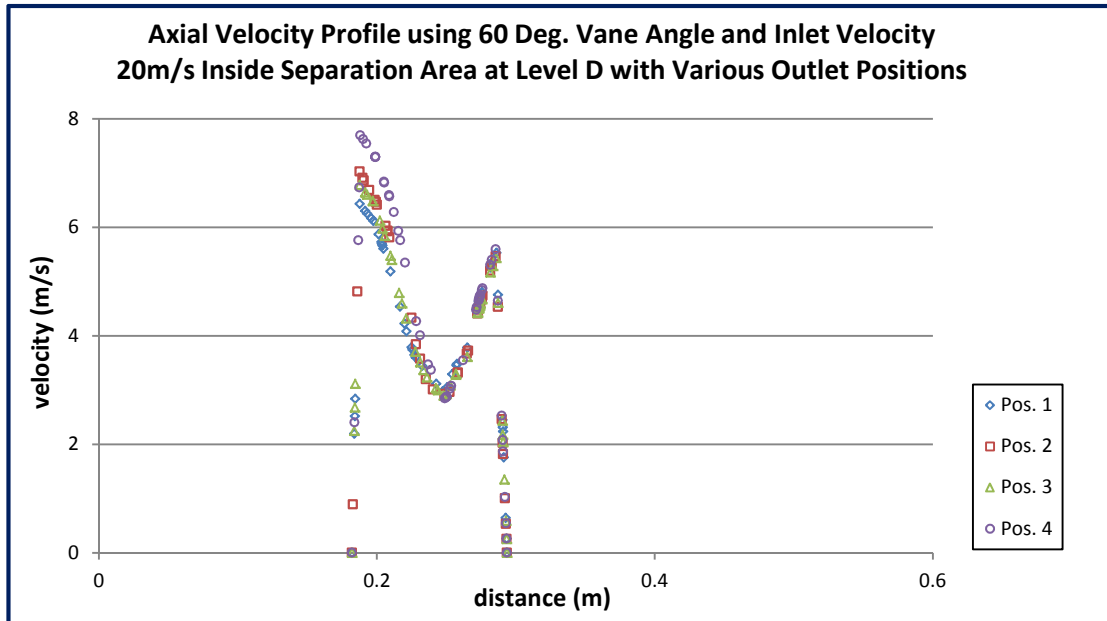
Axial velocity profile inside separation area at Level D for various outlet positions
(45 degrees vane angle, 20m/s inlet velocity)



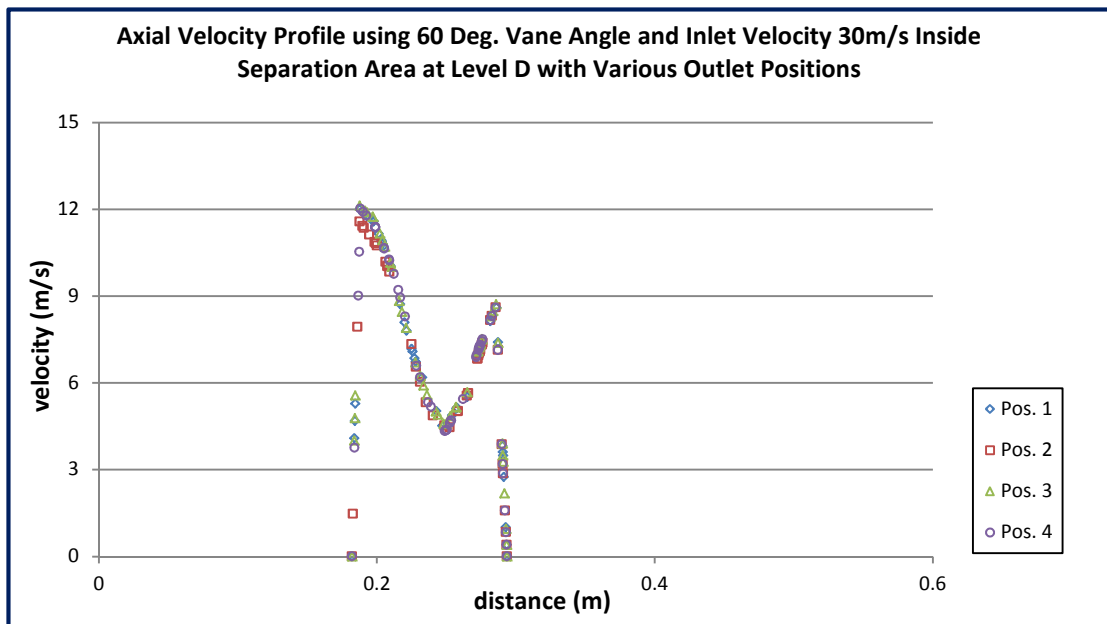
Axial velocity profile inside separation area at Level D for various outlet positions
(45 degrees vane angle, 30m/s inlet velocity)



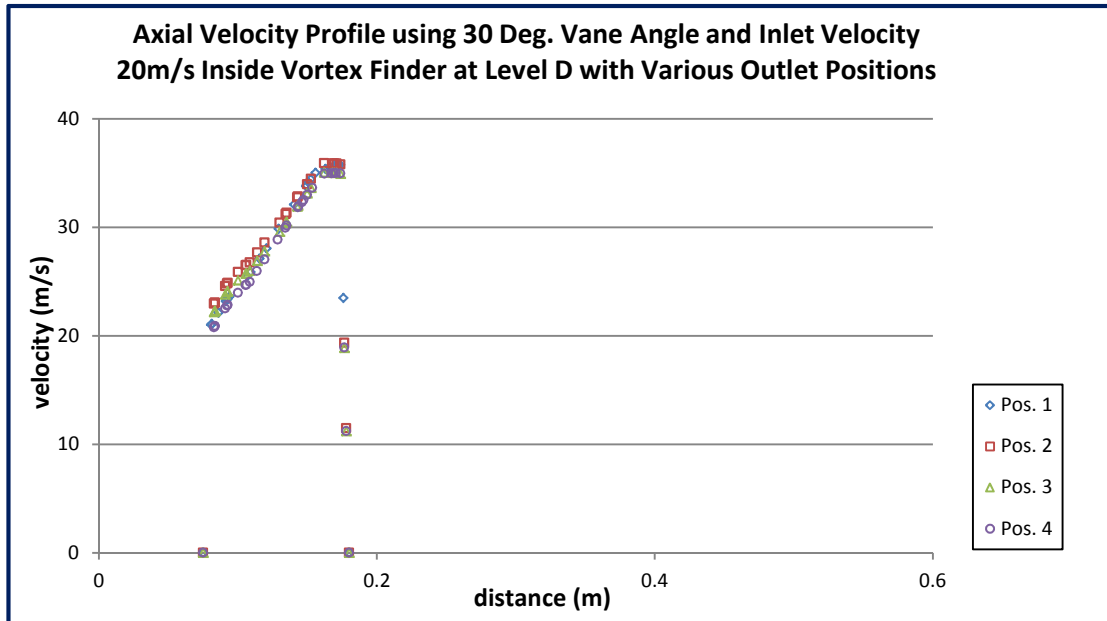
Axial velocity profile inside separation area at Level D for various outlet positions
(60 degrees vane angle, 13m/s inlet velocity)



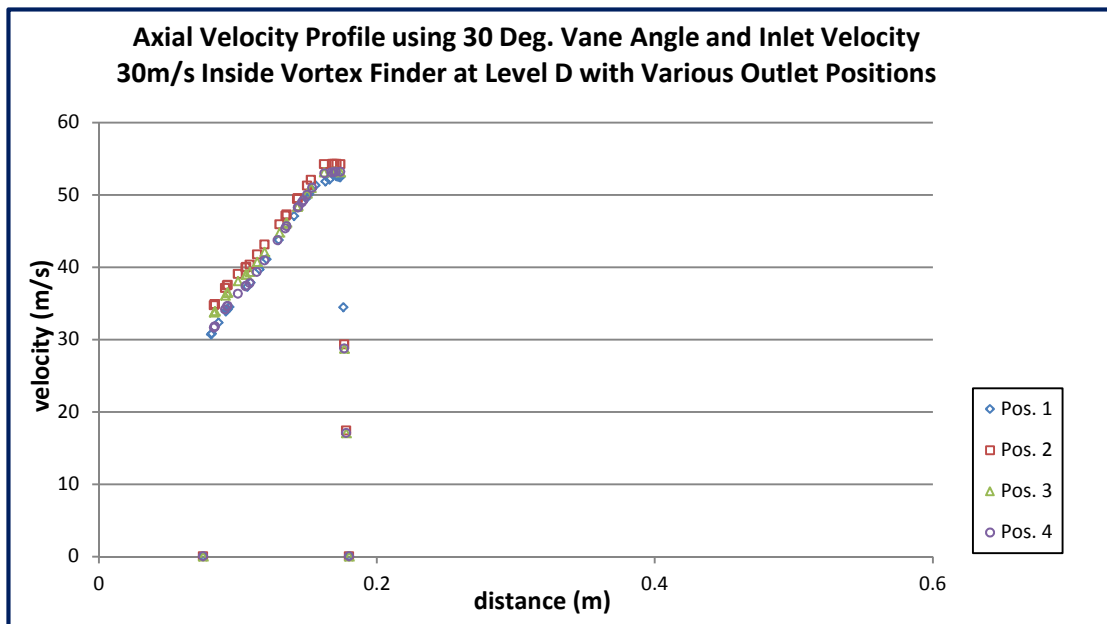
Axial velocity profile inside separation area at Level D for various outlet positions
(60 degrees vane angle, 20m/s inlet velocity)



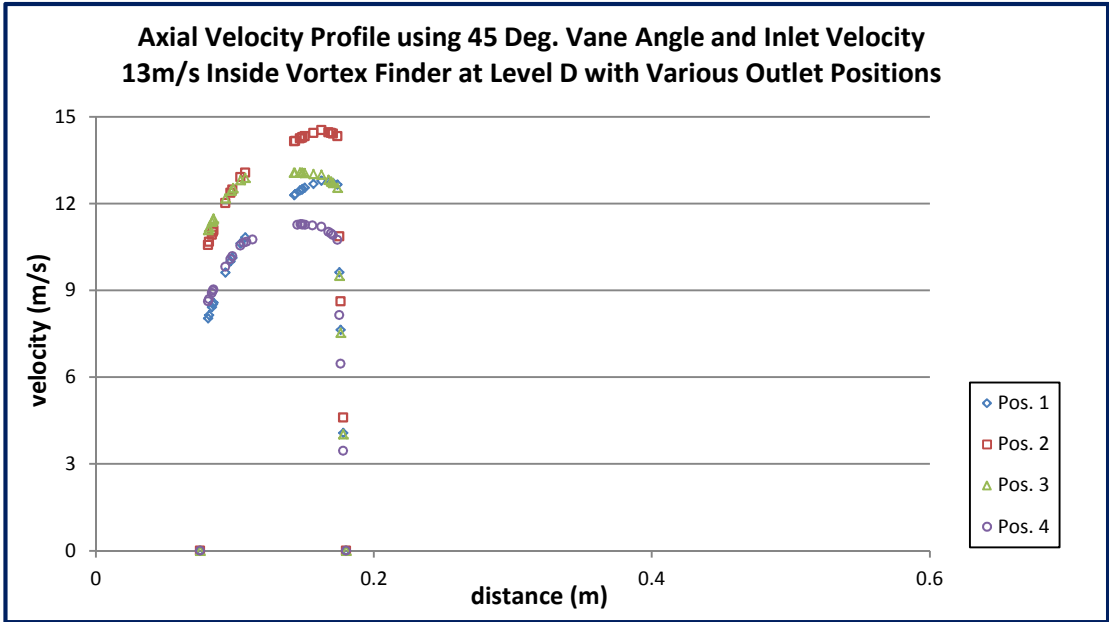
Axial velocity profile inside separation area at Level D for various outlet positions
(60 degrees vane angle, 30m/s inlet velocity)



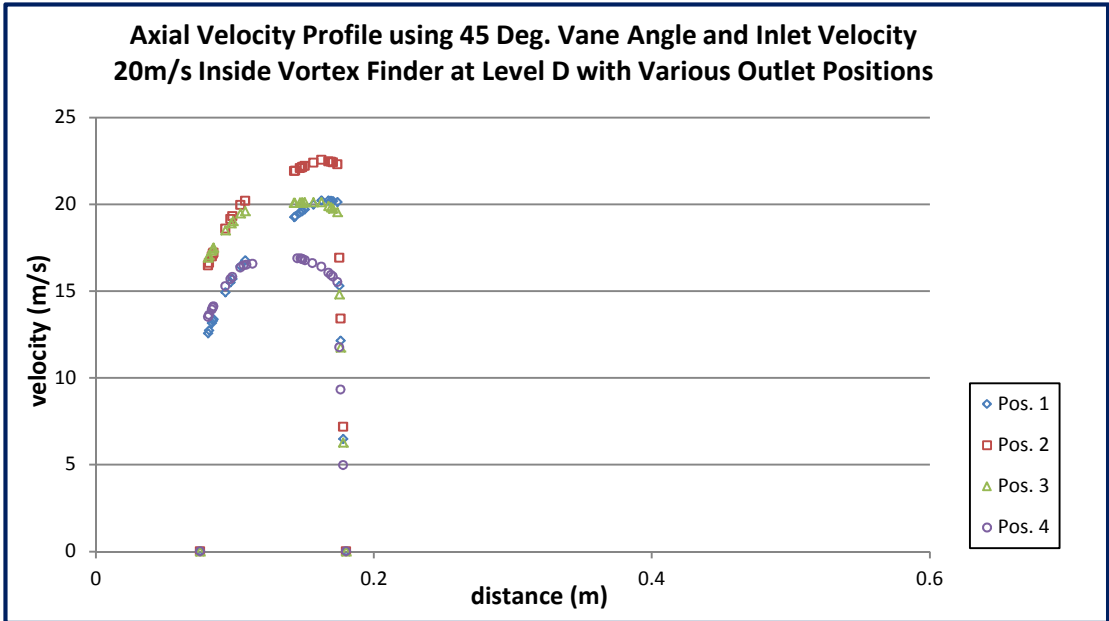
Axial velocity profile inside vortex finder at Level D for various outlet positions
(30 degrees vane angle, 20m/s inlet velocity)



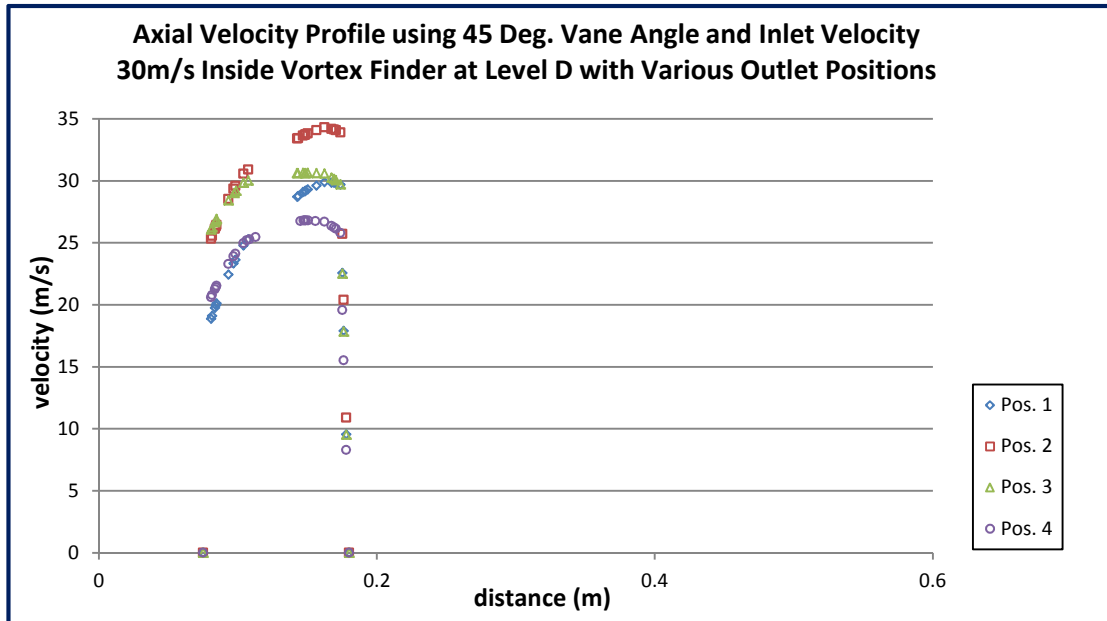
Axial velocity profile inside vortex finder at Level D for various outlet positions
(30 degrees vane angle, 30m/s inlet velocity)



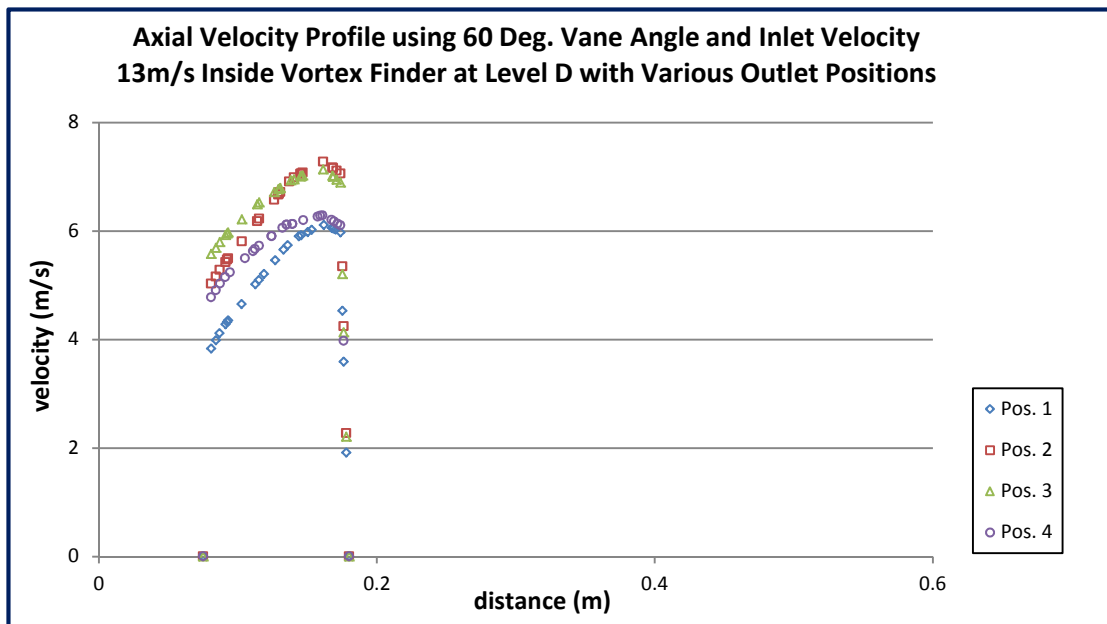
Axial velocity profile inside vortex finder at Level D for various outlet positions
(45 degrees vane angle, 13m/s inlet velocity)



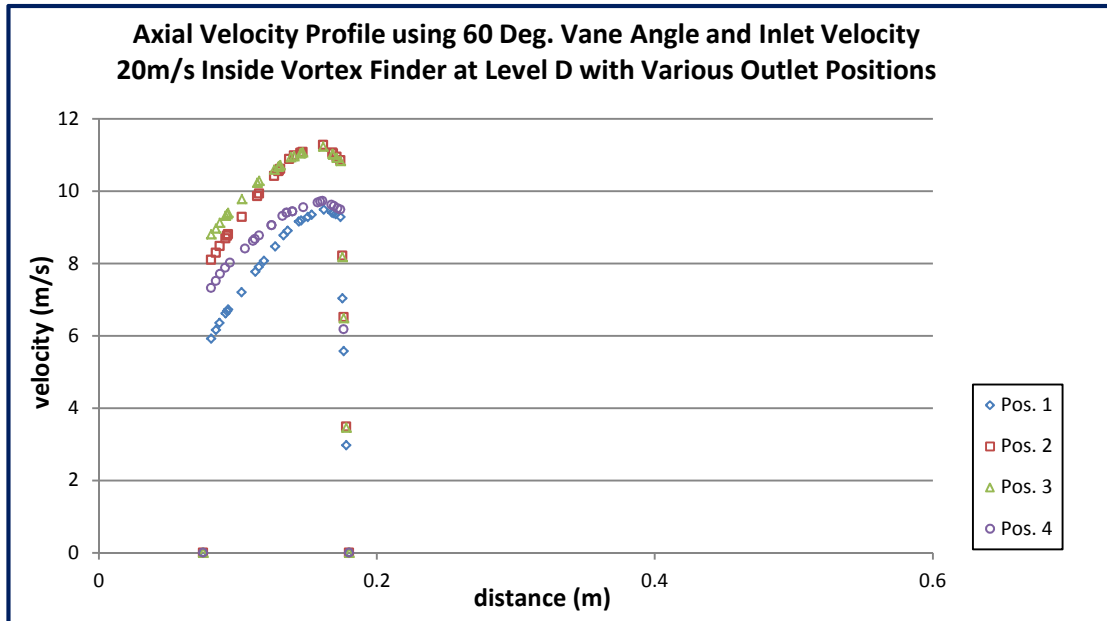
Axial velocity profile inside vortex finder at Level D for various outlet positions
(45 degrees vane angle, 20m/s inlet velocity)



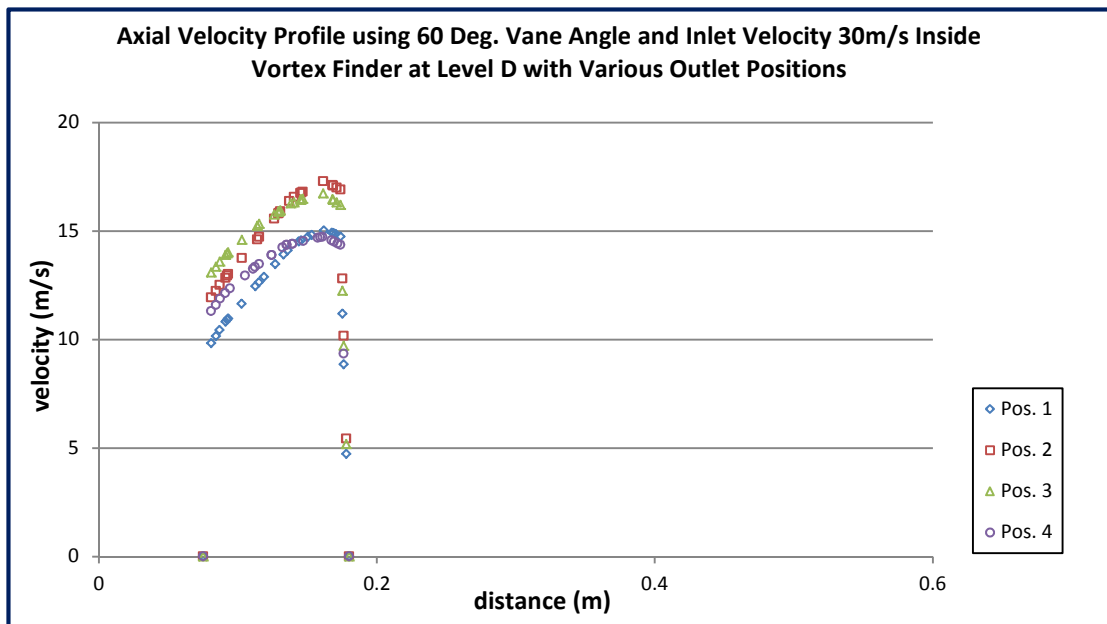
Axial velocity profile inside vortex finder at Level D for various outlet positions
(45 degrees vane angle, 30m/s inlet velocity)



Axial velocity profile inside vortex finder at Level D for various outlet positions
(60 degrees vane angle, 13m/s inlet velocity)



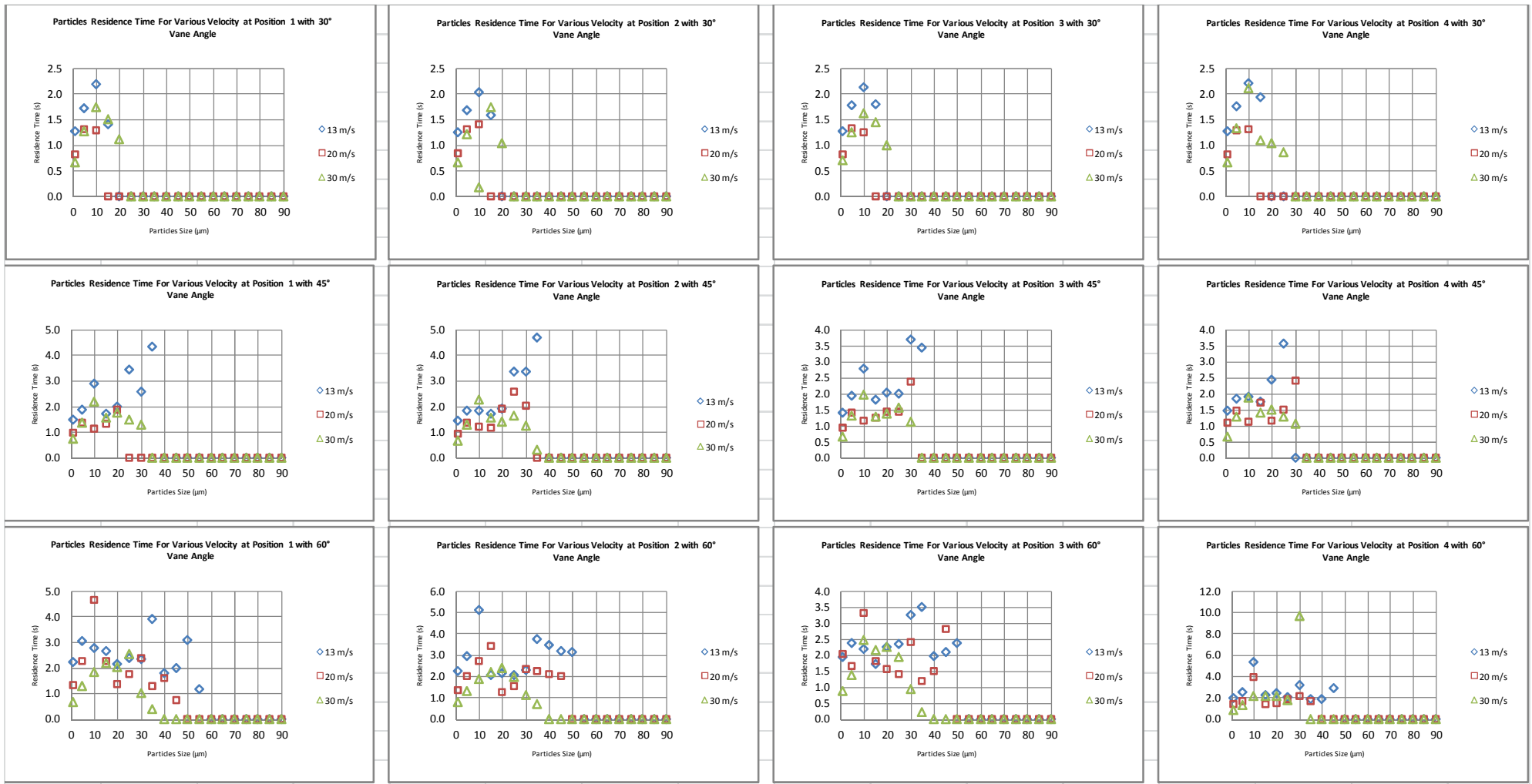
Axial velocity profile inside vortex finder at Level D for various outlet positions
(60 degrees vane angle, 20m/s inlet velocity)



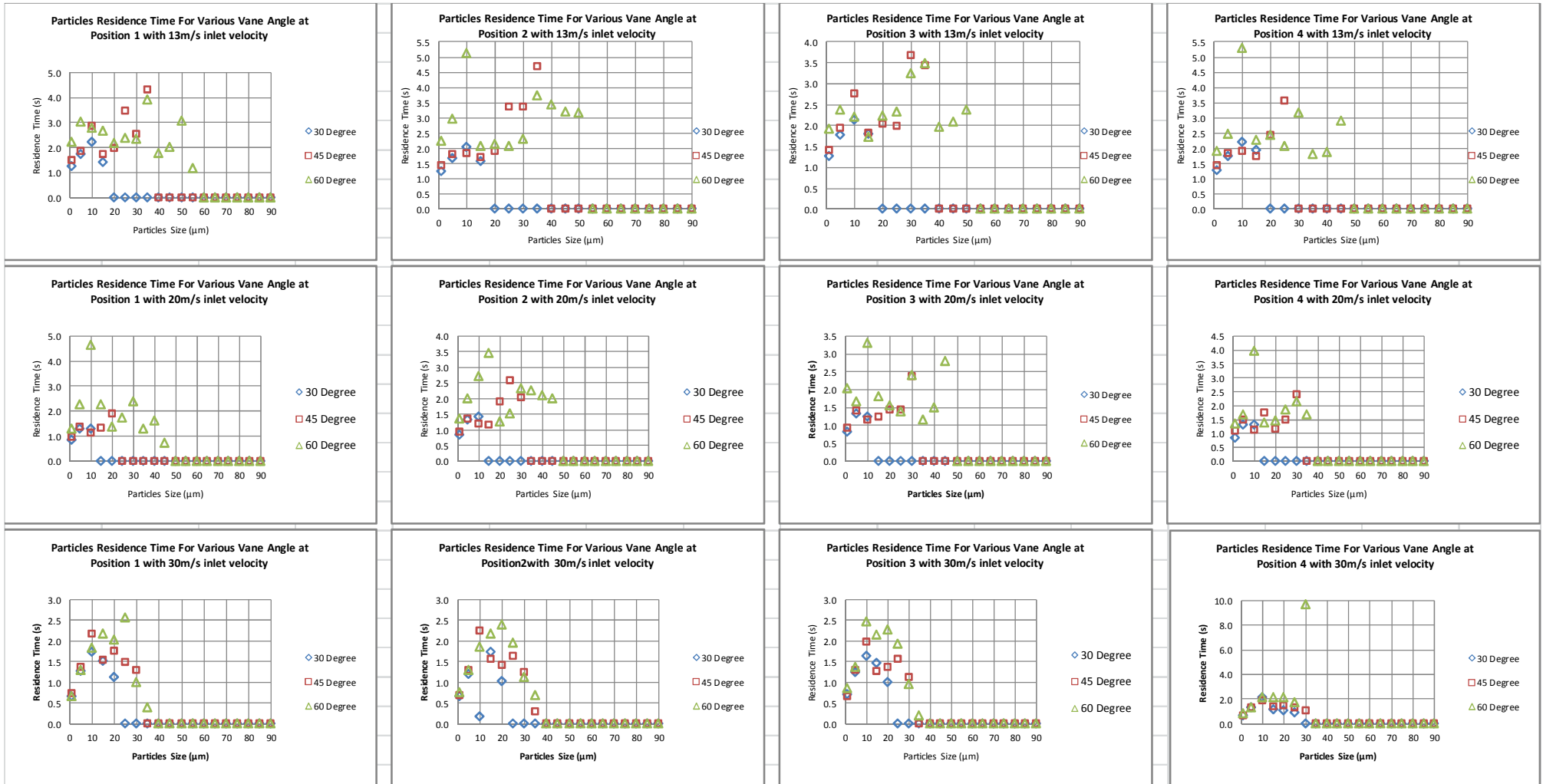
Axial velocity profile inside vortex finder at Level D for various outlet positions
(60 degrees vane angle, 30m/s inlet velocity)

APPENDIX VII

Effects of Varying Inlet Velocity and Vane Angle



Residence time for various velocity with 30°, 45° and 60° vane angle at outlet position 1, 2, 3 and 4



The effect of vane angle on particles residence time at outlet position 1, 2, 3 and 4 with 13 m/s, 20m/s and 30 m/s inlet velocity